

ENGINEERING DESIGN OF NANOFIBRE WOUND DRESSINGS

by

Victor Ka Lun Leung

B.ASc, The University of British Columbia, 2009

A THESIS SUBMITTED IN PARTIAL FULFILLMENT OF
THE REQUIREMENTS FOR THE DEGREE OF

DOCTOR OF PHILOSOPHY

in

The Faculty of Graduate and Postdoctoral Studies
(Materials Engineering)

THE UNIVERSITY OF BRITISH COLUMBIA
(Vancouver)

December 2014

© Victor Ka Lun Leung, 2014

Abstract

This research aimed to develop a nanofibrous carrier design process for hydrophilic, small-molecule drugs for controlled wound healing. Kynurenine was used as representative example, as it presented challenges with its size and structure necessitating significant optimization to reach release target. The objective of the design is thus to facilitate controlled healing via addressing hypotheses on carrier material compatibility, release control through process or material modification, and fabrication of continuous structures.

The design process began with material selection, which identified poly(vinyl alcohol) (PVA) as the candidate carrier. Experimental verification via drug-polymer interaction characterization suggested that kynurenine formed a solution with PVA, and was encapsulated within PVA nanofibres, implying drug release is diffusion-controlled. The characterization process provided more insightful understanding of drug release mechanism compared to data fitting to empirical models performed in existing literatures.

Release assays showed complete kynurenine release from PVA within five hours. In subsequent optimization studies, three methods to control release from nanofibres were proposed. First, material parameters such as molecular weight, electrospinning concentration and drug dosage were shown to be a suitable fine-control mechanism. The second method was matrix modification via heat treatment, which changed the burst release behavior, although drug entrapment was observed. The third method was a composite approach in which the drug-

polymer system was encased in the more hydrophobic poly(lactic-co-glycolic acid) (PLGA), which significantly reduced burst release, and extended the release period to over 120 hours.

Applicability of the PVA kynurenine carrier, planar dressings and braided sutures were explored, which could become useful for a variety of wounds. For planar dressings, the proposed design showed tensile properties within the range of various commercial dressing products and thus was considered robust for handling and application to open acute and chronic wounds. For sutures, process modification in 3D braiding was introduced to significantly increase tensile strength, which could help create robust wound closure devices for patients prone to scarring.

The outcomes of this study demonstrated customization of drug release and structural properties of wound dressing materials to suit various open wounds, to provide a platform for supporting the expanding therapeutic functionalities in next generation wound dressings.

Preface

The research described in this dissertation is based heavily on a project funded by the Collaborative Health Research Projects program under the Natural Science and Engineering Research Council and the Canadian Institute of Health Research, entitled “Development and application of nanofibres releasing anti-fibrogenic factors for treating dermal fibrosis”. The anti-fibrogenic drug that was the driving force of the project, kynurenine, was used in this dissertation as a representing example on how an effective drug carrying wound dressing material can be developed based on a specific therapeutic agent. Several design steps described in this dissertation were original in order to establish a universally applicable process for different types of therapeutic agents.

The funded project that led to this dissertation was also collaboration between the Department of Materials Engineering and the BC Professional Firefighters Burn and Wound Healing Laboratory at the University of British Columbia. It should be noted that the research described in this dissertation focused on material aspects of wound dressing design, including material selection, fabrication, characterization, and optimization. The therapeutic aspects of the kynurenine, such as its activity after being released from nanofibres, cell and animal studies results, are the subject of a separate doctoral dissertation and thus outside of the scope of this dissertation. Therefore, all the work described in this thesis is the work of this candidate. Although cell studies on MMP expression and animal studies on drug response using kynurenine have been performed in the course of the funded project, they were not described in this dissertation as the candidate did not participate in this part of the study.

Parts of this dissertation are also based on published work or prepared manuscripts that will be submitted by the author for publication. The background and literature review section contained modified excerpt of the following publication:

- Leung, V. and Ko, F. (2011). "Biomedical applications of nanofibers." Polymers for Advanced Technologies **22**(3): 350-365.

Chapter 2 of this dissertation is based on the material selection, fabrication, and characterization aspect of a prepared manuscript entitled "Electrospun Kynurenine Carrier for Wound Healing Applications" that will be submitted for publication.

Chapter 3 of this dissertation is partially based on a manuscript draft entitled "Nanofiber-based Composites for Anti-Scarring Wound Dressing", which will be submitted for publication pending animal testing results from collaborators at the BC Firefighters Burn and Wound Healing Laboratory.

While Chapter 4 describes studies in fabricating planar wound dressing and braided sutures based on the optimal drug carrier design, the suture aspect of the chapter was based on a prepared manuscript entitled "Braided Electrospun Sutures for Wound Closure Applications".

Table of Contents

Abstract.....	ii
Preface.....	iv
Table of Contents.....	vi
List of Tables.....	ix
List of Figures.....	x
List of Abbreviations.....	xiii
List of Symbols.....	xiv
Acknowledgement.....	xvi
1 Introduction.....	1
1.1 Background and Literature Review.....	1
1.1.1 Tissue Repair.....	1
1.1.2 Structure of the Skin.....	2
1.1.3 Types of Wounds.....	4
1.1.4 The Wound Healing Process.....	4
1.1.5 Current Technology for Skin Repair.....	7
1.1.6 Polymer Nanofibres as Wound Dressings.....	11
1.1.7 Material Selection for Electrospinning Tissue Scaffolds.....	20
1.1.8 Nanofibres for Drug Delivery in Wound Dressings Applications.....	24
1.1.9 Fibroproliferative Disorders and Current Treatment.....	28
1.1.10 Antifibrogenic Drugs and its Use in Scaffolds.....	33
1.1.11 Nanofibre for Controlled Drug Delivery.....	37
1.1.12 Factors Controlling Drug Release.....	47
1.2 Knowledge Gap and Research Scope.....	52
1.3 Project Objectives.....	58
2 Matrix Selection for Kynurenine-Loaded Nanofibre Scaffold.....	61
2.1 Introduction.....	61
2.2 Methods.....	64
2.2.1 Solubility Calculation.....	64

2.2.2	Electrospinning	65
2.2.3	Drug Release Assay	66
2.2.4	Characterization	68
2.2.5	Thermal Analysis	71
2.3	Results	72
2.3.1	Solubility Calculations	72
2.3.2	Electrospinning	73
2.3.3	Kynurenine Release	79
2.3.4	Nanofibre Characterization	89
2.3.5	Thermal Analysis	96
2.4	Discussion	98
2.5	Conclusion	105
3	Matrix Modification for Controlling Kynurenine Release	108
3.1	Introduction	108
3.2	Materials and Methods	111
3.2.1	Materials	111
3.2.2	Electrospinning Procedure	112
3.2.3	PVA-Kynurenine Fibre Modification	112
3.2.4	PLGA Protective Shell Incorporation	113
3.2.5	Fibre Characterization	116
3.3	Results	117
3.3.1	Modification of PVA-Kynurenine Fibre Membranes	117
3.3.2	Multilayered Structure with Fibrous Shell	124
3.3.3	Dip-Coated Structure with Non-Porous PLGA Shell	128
3.4	Discussion	137
3.5	Conclusion	143
4	Carrier Design Fabrication into Practical Dressing Materials	147
4.1	Introduction	147
4.2	Materials and Methods	152
4.2.1	Materials	152
4.2.2	Dressing Fabrication	152
4.2.3	Suture Fabrication	153

4.2.4 Characterization	155
4.3 Results	159
4.3.1 Dressings.....	159
4.3.2 Sutures.....	161
4.4 Discussion.....	171
4.5 Conclusion	177
5 Summarizing Discussion, Conclusion and Recommendations.....	181
5.1 Summarizing Discussion	181
5.2 Conclusion	189
5.3 Recommendations and Future Work.....	194
References	201
Appendix 1 Matrix Material Selection via Theoretical Approach.....	219
Background	219
Method	219
Appendix 2 Determining Closeness of Fit to Empirical Drug Release Models	223
Background	223
Method	223
Sample Calculation	225

List of Tables

Table 1: Release comparison between four anti-inflammatory drugs from PVA nanofibres.....	50
Table 2: Plotting method for kynurenine release data for determining fit with empirical release models.....	67
Table 3: Summary of the three types of PVA used in electrospinning.....	74
Table 4: Fibre Diameters and standard deviations observed on PVA electrospun at different concentrations, average of 50 observations were presented.....	76
Table 5: Comparing release data fitness to empirical models, based on different PVA grades..	81
Table 6: Effect of nanofibre diameter and drug loading on kynurenine release from PVA 18-88 nanofibres.....	83
Table 7: Release kinetics dependence on material parameters.....	100
Table 8: Release mechanisms and corresponding coefficients for each crosslinked sample ...	123
Table 9: PLGA dip-coating solution properties, resultant sample thickness, and effect on release kinetics	133
Table 10: Tensile properties comparison between PLGA dressing shell, kynurenine-loaded fibres as-electrospun and after dip coating, and commercially available wound products.....	160
Table 11: Summary of tensile properties of aligned and dip-coated sutures.....	170
Table 12: Summary of factors impacting kynurenine release kinetics	186

List of Figures

Figure 1: Structure of Skin. Image obtained with permission from (Metcalf and Ferguson 2007).	2
Figure 2: Epithelialization at the wound site during the proliferation stage. Image obtained with permission from (Epstein 1999), Copyright Massachusetts Medical Society	6
Figure 3: Simple electrospinning setup showing the essential aspects of an electrospinning system.....	13
Figure 4: Examples of randomly oriented and aligned nanofibres	17
Figure 5: Representation of skin regeneration and fibroproliferative disorders using an analogy of building fences. Image obtained with permission from (Tredget, Nedelec et al. 1997).	29
Figure 6: Molecular structure of kynurenine.....	35
Figure 7: Clinical appearance of rabbit ear scars that was (a) untreated, (b) treated with CMC carrier only and (c) treated with CMC loaded with kynurenine. Image obtained with permission from (Li, Kilani et al. 2013).....	36
Figure 8: Examples of ideal release behaviors for different applications	38
Figure 9: Schematic representation of the drug concentration vs. distance profile at pseudo-steady-state. Image obtained with permission from (Siepmann and Peppas 2011)	42
Figure 10: Graphical representation of theoretical release profiles for (a) surface desorption controlled release with , (b) square root of time diffusion release, (c) mixed diffusion-swelling release with $n = 0.7$, and (d) swelling or erosion controlled zero order release.....	46
Figure 11: Summary of drugs studied as part of nanofibre controlled drug delivery systems	55
Figure 12: Nanofibre wound dressing development flowchart	60
Figure 13: Chemical structure of partially hydrolyzed PVA, in which n is the fraction of PVA hydrolyzed and m is the residual ($m = 1 - n$).....	74
Figure 14: Structure of PLGA, containing n mol% of lactic acid and m mol% of glycolic acid.....	75
Figure 15: PVA concentration and degree of hydrolysis effect on kynurenine-loaded electrospun fibre morphology for a) PVA 8-88, b) PVA 18-88, c) PVA 40-88 and d) 20-98. SEM images were taken at 5000X magnification	77
Figure 16: Effect of drug concentration at a) 0.5 wt%, b) 2.0 wt%, and c) 7.5 wt% (to overall electrospinning solution) on fibre morphology. SEM images were taken at 5000X magnification	78
Figure 17: SEM Image (5000X) of kynurenine-loaded PLGA fibres	79
Figure 18: Kynurenine release from PVA electrospun fibres from different polymer grades	80
Figure 19: Effect of fibre diameter on K_{tr} . All samples are based on 10 wt% polymer loading.....	84
Figure 20: Release behavior from PLGA in comparison with PVA 18-88	85
Figure 21: Shelf life comparison between kynurenine in PVA fibre, film and solution	87
Figure 22: SEM images (5000X) of fibres after soaking in PBS for 15 minutes for (a) 18-88 PVA, (b) 40-88 PVA, (c) 20-98 PVA, and (d) PLGA	88

Figure 23: SEM images (1000X) of fibres after soaking in PBS for 1 hour for (a) 18-88 PVA, (b) 40-88 PVA, (c) 20-98 PVA, and (d) PLGA	89
Figure 24: ToF-SIMS spectra of kynurenine	90
Figure 25: ToF-SIMS spectra (zoomed into the 115 – 125 amu range) for electrospun PVA with kynurenine, and control samples including kynurenine powder, blank PVA fibres, PVA cast film with kynurenine, and dried solution obtained during the release assay.	91
Figure 26: FTIR Spectra of as-electrospun PVA and PVA nanofibres with various kynurenine loading. Spectrum of kynurenine powder was also shown as a reference	93
Figure 27: XRD spectra of PVA nanofibres with and without kynurenine loaded, with spectrum of kynurenine powder included as reference.....	95
Figure 28: DSC Thermograms comparing as-electrospun PVA nanofibres and PVA nanofibres with different kynurenine loading	96
Figure 29: MMP expression comparison between untreated fibroblast cells (Control) and those treated with blank nanofibres (Blank NF), kynurenine (kyn), and kynurenine-loaded nanofibres (Kyn-Incorporated NF).....	105
Figure 30: Graphical representation of the multilayer concept proposed in this thesis. The schematic on the left shows PVA/kynurenine nanofibres covered by PLGA nanofibre layers, whereas the schematic on the right shows PVA/kynurenine nanofibres dip-coated with PLGA	111
Figure 31: Kynurenine-loaded PVA on PLGA fibres in the fabrication of PLGA/PVA multi-layered fibrous structure	114
Figure 32: General representation of the dip-coating process.....	116
Figure 33: PVA fibre morphology comparison between fibres as-spun and after heat treatment at temperatures ranging from 75 - 175°C for two hours.....	119
Figure 34: Nanofibre morphology of heat treated PVA after soaking in PBS solutions for 15 minutes	120
Figure 35: Nanofibre morphology of heat treated PVA after soaking in PBS solutions for 1 hour	121
Figure 36: Nanofibre morphology change on PVA heat treated at 175°C up to 8 hours.....	121
Figure 37: Effect of PVA heat treatment temperature on kynurenine release	122
Figure 38: Kynurenine stability over the range of heat treatment temperatures	123
Figure 39: SEM image of the multilayered nanofibre after cold fracture, with (a) showing the separation between the PVA-kynurenine centre and the PLGA envelope from the edge, and (b) showing the two layers farther from the edge.....	125
Figure 40: SEM Images (2000X) on the multilayered nanofibres, with (a) focusing on the middle layer and (b) focusing on the top layer.....	125
Figure 41: Cross-sections of PVA-kynurenine with PLGA nanofibrous shell after soaking in PBS for (a) 4 hours and (b) 24 hours	126
Figure 42: Kynurenine release from PVA nanofibres with electrospun layers of PLGA as envelopes. The effect of the amount of PLGA electrospun on each side was also shown	127
Figure 43: Effect of coat drying temperature on kynurenine release	130
Figure 44: Effect of clamping dip-coated PVA while drying on kynurenine release	131
Figure 45: Single and double PLGA dip-coating and effect on kynurenine release	132
Figure 46: Effect of coating concentration on kynurenine release	134

Figure 47: Effect of lactic acid content in PLGA on wetting angle on coated nanofibres.....	135
Figure 48: Kynurenine release from PLGA coated samples with different lactic acid content in the coatings.....	136
Figure 49: Kynurenine release dosage vs. time for PLGA dip-coated kynurenine-PVA.....	141
Figure 50: (A) 3D Hexagonal Braider used in the fabrication of nanofibre-based hybrid sutures, with a schematic of the rotating yarn carrier shown in (B).....	155
Figure 51: Suture retention test setup.....	158
Figure 52: Laser confocal microscopy of the cross-section of the dressing design consisting of a PLGA nanofibrous shell around a PLGA dipcoated PVA core.	159
Figure 53: SEM micrograph (5000X magnification) of nanofibres (A) as-electrospun and (B) twisted into yarns.....	161
Figure 54: Yarn diameter controlled by PVA deposition volume	162
Figure 55: Comparison between (a) Lukens® Silk 0 Commercial Suture and (b) the braided electrospun PVA suture.....	164
Figure 56: SEM micrograph of a surface-reinforced braid containing three PVA nanofibre yarns and three YLI silk yarns.....	165
Figure 57: SEM image of the core-reinforced braid, with (A) showing the braid as-fabricated, while the braid shown in (B) was intentionally loosened to show the YLI silk core reinforcement	166
Figure 58: Tensile behavior comparison between sutures surface-reinforced with silk microfibrils	168
Figure 59: Tensile behavior comparison between sutures core-reinforced with silk microfibrils	169
Figure 60: PVA-kynurenine braids (a) before and (b) after dip-coating with PLGA solution.....	170
Figure 61: Kynurenine release from sutures vs. planar dressing, both coated with 10 wt% PLGA	171

List of Abbreviations

CEA	Cultured Epithelial Autograft
CMC	Carboxymethyl Cellulose
DSC	Differential Scanning Calorimetry
ECM	Extracellular Matrix
EGF	Epithelial Growth Factor
FGF	Fibroblast Growth Factor
FPD	Fibroproliferative Disorder
FTIR	Fourier-Transform Infrared
GAG	Glycosaminoglycan
IDO	Indoleamine 2, 3-Dioxygenase
IGF	Insulin-like Growth Factor
KGF	Keratinocyte Growth Factor
MMP	Matrix Metalloproteinase
PBS	Phosphate Buffered Saline
PCL	Poly(caprolactone)
PCLEEP	Poly(caprolactone-co-ethyl ethylene phosphate)
PDGF	Platelet-Derived Growth Factor
PLA/PLLA/PDLLA	Poly(lactic acid)/ Poly(L-lactic acid)/ Poly(DL-lactic acid)
PLGA	Poly(lactic-co-glycolic acid)
PMMA	Poly(methyl methacrylate)
PVA	Poly(vinyl alcohol)
PVAc	Poly(vinyl acetate)
PVP	Poly(vinyl pyrrolidone)
SEM	Scanning Electron Microscope
SRT	Square-Root-of-Time
TCH	Tetracycline Hydrochloride
TGF	Transforming Growth Factor
ToF-SIMS	Time of Flight – Secondary Ion Mass Spectroscopy
XRD	X-Ray Diffraction

List of Symbols

<u>Symbol</u>	<u>Definition</u>
Be	Berry's number
d	Nanofibre diameter
a	Empirical parameter for diameter calculation using Berry's Number
c	Empirical parameter for diameter calculation using Berry's Number
M_t	Mass of drugs released at time t
M_{d0}	Initial mass of drugs in matrix
M_∞	Mass of drugs released at infinite time
t	Time from matrix submersion in media
T_r	Characteristic time for surface desorption release model
α	Porosity factor for surface release model
D	Diffusion coefficient
C	Concentration
C_0	Initial drug concentration
C_s	Maximum drug soluble concentration
x	Drug linear position in matrix
h	Distance of from surface of matrix
K_H	Diffusion (SRT) model coefficient
K_1	Diffusion rate constant for power law model
K_2	Relaxation rate constant for power law model
K_M	Power law model combined diffusional and relaxational rate constant
n	Power law model rate exponent
k_0	Erosion rate constant for Hopfenberg model
m	Hopfenberg model geometry-dependent exponent
χ_{sp}	Flory-Huggins interaction parameter
δ	Holdenbrand-Scatchard solubility parameter
V_s	Molar volume of drug
R	Ideal gas constant
T	Temperature
δ_d	Dispersion bond force
δ_p	Polar bond force
δ_h	Hydrogen bond force
F_{di}	Molar dispersion constant
F_{pi}	Polar attraction constant
E_{hi}	Hydrogen bonding energy
R^2	Coefficient of determination
θ	Bragg angle for XRD

Φ	Crystallite size from Scherrer equation
λ	X-ray wavelength
β	Full width at half the maximum intensity of XRD peak
S	Dimensionless shape factor for Scherrer equation
σ	Stress
E	Young's modulus
ε	Strain
ρ	Density

Acknowledgement

This thesis and research would not have been possible without the support of many over the years. First, I would like to thank my supervisor Dr. Frank Ko, for his knowledge, care and support. He has been instrumental to my personal and professional growth from my undergraduate days. I would also like to thank Dr. Aziz Ghahary, for his kind support and suggestions to my research. I am grateful for the opportunity to work under Dr. Ko and Dr. Ghahary's supervision at the Advanced Fibrous Materials Laboratory and the BC Professional Firefighters Burn and Wound Healing Laboratory. I would also like to extend my gratitude to my supervisory committee members, Dr. Rizhi Wang and Dr. Goran Fernlund, for kindly spending time with my project and starting insightful discussions.

Several people have also been instrumental to completing this research, first to Dr. Heejae Yang for all his advice to many parts of my work. I am also grateful for the help of Malihe Pourmasjedi, Ryan Hartwell, and Sanam Salmi Elizei, with analyzing drug properties, of Dr. John Kim and Dr. Phil Wong for their expertise in ToF-SIMS, and also Dr. Kai Yu for his help with contact angle measurement. Thank you also to Saeromi Kim, Evelyn Frank, Daria Bietenbeck, and Christine Neusser for their support on the nanofibre suture aspect of this study. Special thanks my friends from the Advanced Fibrous Materials Laboratory as well as the Materials Engineering Joint Student Chapter, for all the help, the grinds, the gatherings, and all the fun. Thank you to all staff members in UBC Materials Engineering, for their support, kindness, and all the chats that made me feel right at home.

To my parents Aaron and Judy, brother Leo, and fiancé Millie - thank you for being with me, supporting and believing in me over the years. I am truly grateful to have you in my life.

1 Introduction

1.1 Background and Literature Review

To fully appreciate how a kynurenine releasing membrane may improve wound healing quality, it is important to explore current work on electrospun drug-releasing membranes and kynurenine-based therapies on animal models, which in turn require knowledge on the wound healing process. The first half of this chapter aims to provide a brief overview on the structure of skin and how it responds to wounds, followed by an overview of the current work on wound healing aids and scaffolds, including the recent contribution of the electrospinning technology. The second half of this chapter focuses on healing optimization through the use of drug-loaded materials, including discussions on material considerations, types of therapeutics used and methods for incorporation. The limitations in the current state of the art will be presented, which then open discussions on the potential for new drugs such as kynurenine. These discussions can then steer attention to how a kynurenine-loaded matrix can be formulated as well as possible routes for drug release control on electrospun nanofibres.

1.1.1 Tissue Repair

The skin is the largest organ of the human body. Acting as a barrier, the skin is responsible for protecting the body from bacteria and the environment, as well as retaining water and nutrients (Madison 2003). The skin also plays a critical role in providing senses, heat regulation, and fluid transport. It is thus important that any breach in this barrier be closed and regenerated to its original form. The most critical step in saving patients' lives is to provide protective means to

eliminate water loss and possible infection (Yannas and Burke 1980). After ensuring immediate survival, long-term wound care is another critical consideration in the treatment. While the skin is able to self-regenerate to some extent, more extensive injuries such as third degree burns will often lead to scarring or chronic open wounds, which are uncomfortable and may be lethal.

1.1.2 Structure of the Skin

Human skin is generally divided into two layers: the epidermis on the surface and the underlying dermis, shown in Figure 1, which are further divided into several sub-layers among themselves.

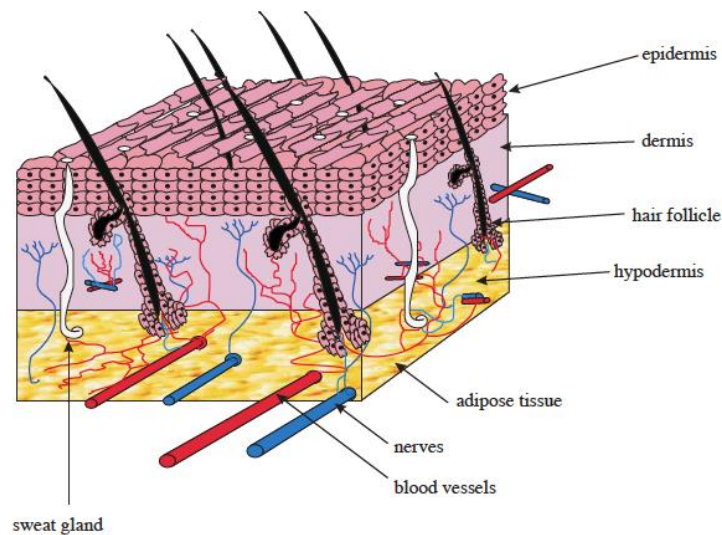


Figure 1: Structure of Skin. Image obtained with permission from (Metcalf and Ferguson 2007).

The epidermis contains five sub-layers, including stratum corneum on the outermost layer, stratum lucidum, stratum granulosum, stratum spinosum, and stratum germinativum (Kremer, Lang et al. 2000). The predominant cell type in the epidermis is keratinocyte, which makes up 95% of epidermal cells, with the remaining being Merkel cells, melanocytes, and Langerhans cells (Metcalf and Ferguson 2007). Keratinocyte life cycles begin as basal keratinocytes in the

stratum germinativum, also known as the basal layer, with nutrients provided by the underlying dermis. As the basal keratinocytes proliferate, some of the cells can migrate toward the upper layers, while differentiating into mature cell types (Schulz, Tompkins et al. 2000). As the basal cells migrate towards the stratum spinosum, keratinization begins in which the basal cells produce protein and begin to differentiate. At the stratum granulosum, keratinocyte cells differentiate into granular cells and produce keratohyalin (Compton, Butler et al. 1998). Upon migrating to the stratum lucidum and corneum, the protein keratin is produced as the cells become fully keratinized and undergo programmed cell death (Schulz, Tompkins et al. 2000). The dead packets of cells are then pushed towards the surface of the stratum corneum, forming a surface layer that can be removed and replaced by new packets of dead cells.

The dermis provides the structural integrity of the skin and is connected to the epidermis by a basement membrane. The dermis is subdivided into the papillary region and the underlying reticular region, with the main difference being that the reticular region contains denser tissue (Schulz, Tompkins et al. 2000). The dermis is composed of proteins such as collagen, elastin, fibronectin, and polysaccharides in glycosaminoglycans (GAG) (Mutsaers, Bishop et al. 1997). These materials collectively make up the extracellular matrix (ECM). In the ECM, collagen makes up 90% of the protein composition, and exists in fibrillar form as structural support for cells (Mutsaers, Bishop et al. 1997). Elastin, also existing in fibrillar form, provides the elasticity and extensibility in tissues. Fibronectin, on the other hand, helps attach cells to collagen fibres (Metcalf and Ferguson 2007). GAGs are a mix of polysaccharides usually attached to the ECM to form proteoglycans, which aids ECM structural stability by keeping its surrounding hydrated. The most common cell type in the dermis is fibroblast, which proliferates throughout the matrix and secret materials constituting the ECM. The dermis also contains blood vessels, which are essential in keeping fibroblast cells alive and providing nutrients for the keratinocytes at the

stratum germinativum above the basement membrane (Mutsaers, Bishop et al. 1997, Kremer, Lang et al. 2000).

1.1.3 Types of Wounds

There are different ways to classify wounds. One of the most common distinctions is between acute and chronic wounds. Acute wounds are those that can undergo a timely restoration of tissue function and integrity, in the absence of infection or complications (Bello and Phillips 2000). Examples of acute wounds include surgical incisions, small area burns, and blunt trauma. Chronic, or non-healing, wounds are those in which tissue functions could not be restored at all or in a timely manner. Examples of chronic wounds include infected surgical wounds, large area burns greater than 4 cm in size (Herndon, Barrow et al. 1989), as well as pressure, venous and diabetic ulcers. In terms of healing, the important requirement for acute wounds is protection against infections whereas in chronic wounds, there is an added requirement of healing promotion due to the lack of biological cues to initiate proper healing process.

Wounds can also be classified as open or closed. Open wounds are those in which the skin is breached, exposing the underlying tissue. All the acute and chronic wounds described above are open wounds. Closed wounds are those in which the skin remained intact but the underlying tissues are damaged, such as damages to muscles, blood vessels, and tendons.

1.1.4 The Wound Healing Process

As it is critical that skin defects are repaired, the body has developed a set of responses to skin trauma. Responses depend greatly on the depth of the wound, mainly because the epidermis is

able to regenerate whereas the dermis is not (Schulz, Tompkins et al. 2000). Injuries that breach only the epidermis are classified as first degree, whereas those that breach the dermis superficially are classified as second degree, and breach of near-full or full dermis is classified as third degree. Epidermal breaches can be repaired by the movement of basal keratinocytes from the wound edges to cover the wound site, followed by proliferation and apical migration, during which the cells would differentiate and deposit keratin (Schulz, Tompkins et al. 2000). The end result is a regenerated epidermis with the same properties as the original.

Responses to wounds that penetrate the dermis are more complicated, as the dermis cannot regenerate. Upon injury, the first stage in the healing process is homeostasis in which blood clot is formed in the wound site to provide temporary protection and a site for cell migration. In the inflammation stage that follows, cells such as neutrophils and monocytes migrate to the clot, via a variety of signaling molecules released by platelets and surrounding ECM, and clear the wound site of bacteria (Epstein 1999). The proliferation stage then begins when fibroblast cells enter the clot and produce proteins and GAGs to form a provisional ECM known as granulation tissue (Martin 1997). The fibroblast cells would differentiate into myofibroblasts, which attach to the surrounding dermis and pull it towards the granulation tissue in the contraction process (Martin 1997). If the surrounding dermis reaches close proximity to the granulation tissue, blood vessels are re-established in the provisional matrix (angiogenesis), and nutrient transport to the basal keratinocytes resumes, enabling the regeneration of the epidermis via the epithelialization process (Schulz, Tompkins et al. 2000). Figure 2 depicts the re-establishment of angiogenesis and epithelialization at the wound site.

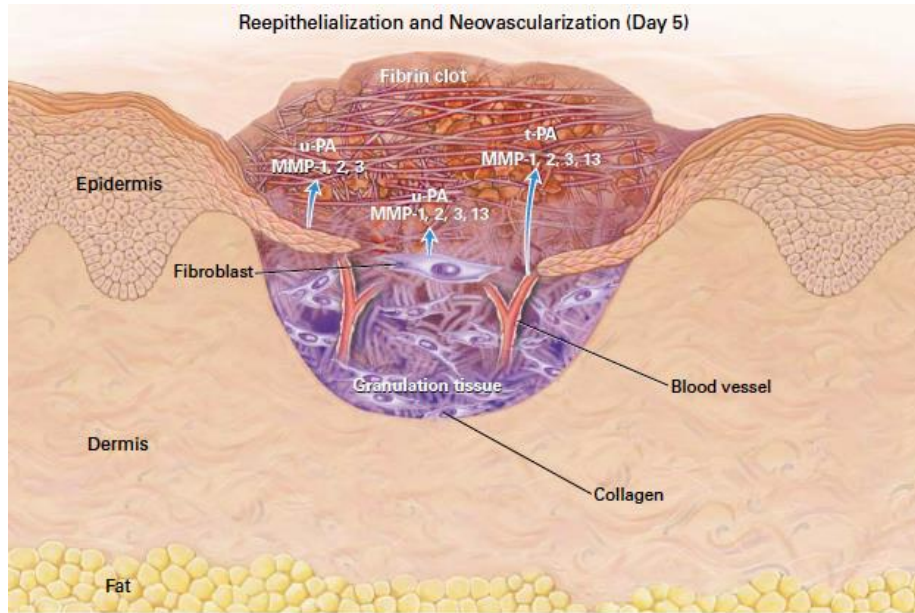


Figure 2: Epithelialization at the wound site during the proliferation stage. Image obtained with permission from (Epstein 1999), Copyright Massachusetts Medical Society

For second degree burns or split thickness injuries, healing can be achieved by contraction of the wound, but the dermis will become permanently thinner (Schulz, Tompkins et al. 2000). However, for full-thickness wounds such as third degree injuries and those that are larger than 4 cm in size, contraction is often insufficient (Herndon, Barrow et al. 1989). In this case, angiogenesis cannot be established and wound will remain unepithelialized, although the wound size will decrease due to contraction. In some cases wound closure can also be aided by scar tissue formation, caused by overproduction of ECM proteins by fibroblast cells. However, scarring often causes undesirable appearance and in extreme cases can lead to keloids formation (Tredget, Nedelec et al. 1997).

The wound healing process also involves a wide variety of signaling molecules, known as factors, that are responsible for different stages in the healing process, from attracting neutrophils during the inflammation stage, to controlling fibroblast differentiation (Mutsaers, Bishop et al. 1997). In fact, biochemists have yet to identify all the factors involved in wound

healing as well as to fully apprehend the role of those identified. While detailed understanding of the signaling molecules is beyond the scope of the current work, several factors that may be relevant include epithelial growth factor (EGF), transforming growth factor (TGF), fibroblast growth factor (FGF), keratinocyte growth factors (KGF), and antifibrogenic factor. EGF, FGF, and KGF are factors that control cell proliferation and differentiation, whereas antifibrogenic factors control the expression of ECM proteins during the healing process (Mutsaers, Bishop et al. 1997). The factors can attach to cells via receptor groups on the cells to perform their functions (Martin 1997).

However, activation of signaling molecules and their effectiveness depends greatly on many conditions such as the extent of the wound, and patient health. For example, certain cellular cues may not activate or may not be adequately carried out in patients suffering from poor blood circulation, infections, and diabetes (Falanga 2005, Guo and DiPietro 2010), causing the healing process to be inhibited at a certain stage, leading to chronic wounds.

1.1.5 Current Technology for Skin Repair

Despite having well-developed wound healing processes, the body's natural response is often inadequate in addressing extensive wounds and environments complicated by diseases. Accordingly, external wound healing aids have been used to supplement wound healing. In fact, recorded use of wound healing aids dates as far back as 1650 BC, using lint and honey (Herman 2002). While lint provided a fibrous substrate for cell adhesion and proliferation, honey served as a physical barrier for protection and antibiotic agent. More than three millennia later, in the 19th century, autograft and allograft were first used for wound healing and became widely accepted, although the skin transplant technique existed before that (Herman 2002). Both

techniques achieved successful results because of the structural similarity between the graft and the lost skin, which could promote angiogenesis and epithelialization. Also, as a structural support, grafts could also reduce wound contraction. While autograft involves applying onto the wound site healthy tissue from another part of the patient's body, allograft involves using the tissue from another human being. The use of autografts can eliminate allergic responses to the implanted skins due to their biological origin, but harvesting healthy tissues from the patient causes injuries at the donor site, which may cause new problems such as scarring (Supp and Boyce 2005). Allograft, on the other hand, eliminates problems associated with donor site morbidity, but immunogenic response or implant rejection may occur. In addition, allograft risks disease transmission, and therefore donors must be carefully screened. The first successful case of autograft with human patients was achieved by Bunger in 1823 when he repaired nasal defects by harvesting full-thickness skin from the thigh (Bunger 1823), whereas the first successful allograft procedure was performed by Reverdin in 1869 (Reverdin 1869). Within two years of the first allograft procedure, it was introduced by Pollock as a treatment for burn wounds (Pollock 1871). Since then several variations of allograft were developed. The next breakthrough occurred in the 1970s when Rheinwald and Green was able to culture keratinocytes (Rheinwald and Green 1975), which opened opportunities for what will be known as cellular skin repair products, with the first graft composed of keratinocyte sheets made available in 1979 (Herman 2002).

The cell culture technology eventually led to the introduction of cultured epithelial autografts (CEA) in the early 1980s (MacNeil 2007). CEA contains a small amount of skin from the patient's body, cut into a mesh structure and then combined with cells (Compton, Butler et al. 1998). By incorporating a cell-skin mixture, CEA allows coverage of larger wounds while reducing the requirement on the donor sites. In the same decade, a group of clinicians also sought to improve skin repair with a different approach that is later referred to as artificial skin.

Through a synthetic template mimicking skin structure, clinicians aimed to eliminate both the issues of donor site morbidity with autograft and disease transmission with allograft. One of the signature examples of artificial skin is Integra[®], developed by Yannas and Burke in the 1980s (Yannas and Burke 1980, Burke, Yannas et al. 1981, Jaksic and Burke 1987, Tompkins and Burke 1990, Schulz, Tompkins et al. 2000, MacNeil 2007, Metcalfe and Ferguson 2007). Integra[®] is composed of a silicone layer adhered onto a bovine collagen sponge, in which the bovine collagen layer facilitates angiogenesis and fibroblast migration, and the silicone protects the wound from water loss and the environment, much like the dermis and epidermis. Once the synthetic dermis becomes well vascularized, the silicone film would be removed and replaced with an epidermis autograft (Burke, Yannas et al. 1981, Jaksic and Burke 1987, Schulz, Tompkins et al. 2000). By incorporating a synthetic design, Integra[®] is able to promote wound closure and epithelialization, while reducing contraction and eliminating donor site morbidity. Although an epidermis autograft is used to replace the silicone layer, the epidermis at the donor site is able to self-regenerate and therefore will not lead to pain and scarring. While Integra[®] was under development, several other groups also explored the feasibility of cell incorporation into scaffolds, leading to a wide variety of cellular artificial skin products such as Apligraf[®] and OrCel[®] (Shevchenko, James et al. 2010). Both Apligraf[®] and OrCel[®] are based on a bovine collagen sponge, with fibroblasts and keratinocytes cultured inside to form a bilayer cellular structure. While both products showed reduced scarring and shortened healing time, viability of the cultured cells could not be maintained past two months (Shevchenko, James et al. 2010). However, many artificial skin products also suffered from the lack of defensive mechanism against bacteria, unlike autografts, requiring careful and lengthy decontamination procedures.

The drawbacks in using animal-derived materials mentioned above have led to interest in the use of natural or synthetic polymers in skin scaffolds other than collagen, with examples including alginate, chitosan, hyaluronic acid, poly(caprolactone) (PCL), poly(vinyl alcohol) (PVA),

poly (lactic acid) (PLA), and silk (Leung, Hartwell et al. 2012). The main advantages in using commercial polymers include reduced risk of disease transfer as well as cost. Many of these polymers, especially synthetic ones, are also easier and less costly to process as exotic solvents are often unnecessary (Ramakrishna, Fujihara et al. 2005). Furthermore, physical properties of synthetic polymer can be readily customized via control of molecular weight and mix ratio in the case of copolymers such as poly(lactic-co-glycolic acid).

In addition to material choices, different scaffold structures have also been explored, besides the sponge and film used in the artificial skin products. For example, hydrogels have become a popular form of temporary ECM for skin repair, due to its ease of application as a topical agent, and its ability to retain moisture (Rahmani-Neishaboor, Jallili et al. 2013). Alginate, chitosan, and PVA are widely used as hydrogels due to their swelling properties and biocompatibility (Ciofani, Raffa et al. , Luo, Kirker et al. 2000, Ribeiro, Barrias et al. 2004, Ruzica Jovanovic-Malinovska and Eleonora Winkelhausen 2006, Rahman-Neishaboor, Jackson et al. 2009). However, in applications in which structural integrity is required, hydrogel are often inadequate due to the lack of mechanical resistance against abrasion, pressure, and other physiological loading. Microspheres have also been explored in the recent years in applications involving drug delivery, as well as gene and cell therapy because of their ability to encapsulate therapeutic or active ingredients via emulsification techniques (Ulubayram, Cakar et al. 2001, Rahmani-Neishaboor, Hartwell et al. 2012). Being small particles, microspheres require a carrier, often a gel or cream, to remain on the wound surface. As a result, microsphere-based formulations may also lack structural integrity similar to hydrogel formulations. Fibres, on the other hand, are often used as scaffolds when integrity is required, as demonstrated in the work performed on alginate and silk (Vanstraelen 1992, Ko and Gandhi 2007, Leung, Yang et al. 2010). For skin scaffolds, fibres have high tensile strength, reaching the order of 10 MPa for skin scaffolds like BioFix and Resolut LT (Rho, Jeong et al. 2006). Another famous example of fibrous scaffold is Kaltostat, a

calcium alginate dressing known for its absorbability especially in exudative wounds since its introduction in the late 1980s (Vanstraelen 1992). Functionally, fibres are attractive because they have high aspect ratios, providing large surface area for cell activities. In addition, fibres can be continuous, thereby allowing fabrication of hierarchical structures such as wound pads and sutures.

The various forms that have been used in skin repair each have their own advantages, such as moisture retention, drug encapsulation and structural support, but none of them resemble the structure of the dermis in which the ECM is a nanofibrous composite containing mainly collagen (Leung and Ko 2011). However, when fabrication of thin, sub-micron sized polymer fibres became well-known in the late 1990's, these fibres have attracted much attention for potentially being the next frontier in tissue repair.

1.1.6 Polymer Nanofibres as Wound Dressings

Sub-micron fibres attract attention in skin repair due to its structural similarity to the nanofibrous ECM. In addition, with very high aspect ratios, thin fibres provide very high surface area for cell attachment, promoting improved cell coverage and timelier healing process. Like traditional fibrous dressings, sub-micron fibres are connective and can be fabricated into hierarchical structures (Leung and Ko 2010). Accordingly, recent research have focused on the feasibility of nanofibre use in tissue regeneration and have demonstrated superior results compared to their larger diameter counterparts, as will be discussed later in this section. Using the definition of nanomaterials by the National Science Foundation (NSF), thin fibres with less than 100 nm in diameter are considered nanofibres (Gibson, Lee et al. 2006). However, in existing literature and in the industry, the term nanofibre has been used to loosely define those with diameters

less than 1000 nm (Gibson, Lee et al. 2006). To remain consistency with literature, the term nanofibre will be used in this thesis to describe fibres with diameters less than 1000 nm.

There are several ways to fabricate nanofibres, such as drawing from a polymer solution with a micropipette tip, template synthesis using a nanoporous membrane, phase separation between a polymer solution and an incompatible solvent, self-assembly from smaller molecules, and electrospinning that draws fibres from polymer solutions using static repulsion (Ramakrishna, Fujihara et al. 2005, Kumbar, James et al. 2008). Electrospinning is the most commonly used due to its simplicity, low-cost, controllability and capability for mass production (Kumbar, James et al. 2008). The concept of electrospinning originates in the work by Boys in 1887 (Boys 1887) and in a patent by Cooley in 1902 (Cooley 1902), although at that time the technology was not considered important due to the lack of a means to collect continuous fibres. The work outlined by Formhals in his 1934 patent (Formhals 1934) highlighted for the first time the potential for practical use of the electrospinning technique. The Formhals patent describes mass production of textile fibres via electrospinning and a moving collector that can collect fibres in a continuous manner. The next breakthrough in electrospinning technology did not happen until more than half a century later, when the pioneering work by the Reneker group using various organic polymers was published in the 1990s (Ko, Laurencin et al. 1998, Li and Xia 2004), demonstrating feasibility in creating polymer nanofibres. Since then, the interest in synthesizing nanofibres from many polymers has increased exponentially, with applications spanning from structural to electrical, and to biomedical.

Electrospinning involves drawing jets from a polymer solution droplet by manipulating the balance between electrostatic repulsion and solution surface tension, via the steady increase of applied voltage. The basic setup for electrospinning, shown in Figure 3, includes a syringe with polymer solution, a needle through which the solution can exit, a high voltage power supply

capable of supplying up to 30 kV, a syringe pump, and a grounded collector.

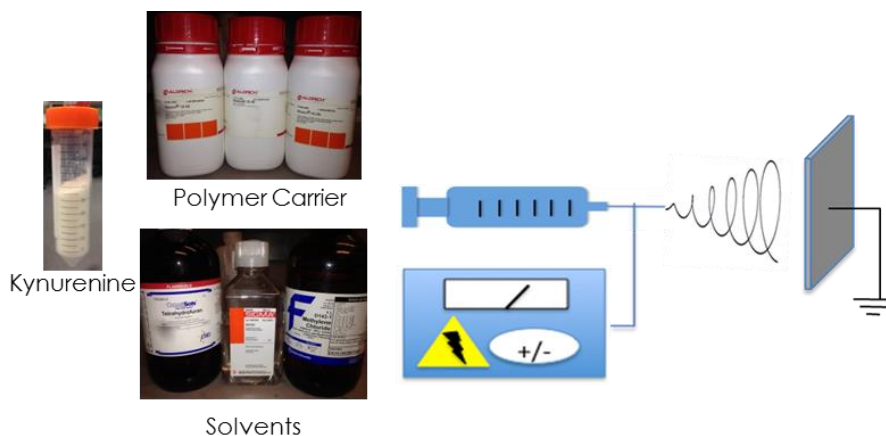


Figure 3: Simple electrospinning setup showing the essential aspects of an electrospinning system.

As a voltage is applied on the needle, charges are induced and are evenly distributed throughout the solution. The applied charge induces repulsion between molecules in the solution, which are held within the solution by surface tension. However, when the voltage overcomes surface tension, roughly in the range of 5 to 15 kV, polymer solution at the needle top can be deformed into a conical shape, known as the Taylor Cone, from which a jet can eventually be extracted (Ramakrishna, Fujihara et al. 2005). In the presence of a grounded collector, the jet will travel from the charged needle tip to the grounded collector under the influence of an electric field. Since there is electrostatic repulsion between the polymer molecules, the fibre jet will stretch as it travels (Ramakrishna, Fujihara et al. 2005). Furthermore, the fibre jet will undergo whipping motion due to bending instability and the interaction between the external electric field and the surface charge in the polymer molecules (Ramakrishna, Fujihara et al. 2005). This stretching and whipping motion further reduce fibre jet diameter, in addition to evaporating the solvent in the jet. When the fibre jet reaches the collector, a solvent-free layer of fibres is formed, with diameters that can range from tens of nanometers to tens of micrometers.

From a processing perspective, another benefit of the electrospinning technique is the control over fibre morphology, which can be influenced by electrospinning solution and processing parameters. Katti et al has conducted a detailed study on the effect of several solution and electrospinning parameters on the fibre morphology (Katti, Robinsin et al. 2005), although the work was more focused on drug-loaded nanofibres, which will be discussed in section 1.1.8.

In terms of the solution parameters, the polymer solution concentration is the most important parameter in determining the fibre diameter. The polymer solution concentration dictates three important solution properties: solution viscosity, surface tension, and charge density (Li and Xia 2004). The viscosity of a polymer solution originates from the entanglement of polymer chains. Less entanglement will lead to lower solution viscosity, and vice versa. Fibre diameter tends to increase with viscosity. However, if the solution viscosity is too low, typically below 50 mPa-s, fibre jet may break into droplets due to the lack of entanglement (Ramakrishna, Fujihara et al. 2005). On the other hand, if the viscosity is over 1000 – 2000 mPa-s, solution flow through the needle may become difficult and ultimately fibre formation will be hindered. The surface tension is the cohesive force between liquid molecules, and in electrospinning, the solution must be able to overcome the surface tension. To minimize surface area, surface tension tends to convert the solution jet into spherical droplet or droplets (Li and Xia 2004). A polymer solution with high viscosity will have a lower surface tension due to the increased interaction between solvent and polymer molecules, reducing the tendency for the solvent molecules to come together (Li and Xia 2004), whereas the opposite is true for a low viscosity polymer. Surface tension also prevents sudden changes in the shape of the fibre jet (Li and Xia 2004). The charge density in the polymer relate to the amount of charge carried by the polymer chains in the solution, and determine the extent of electrostatic repulsion experienced by the molecules during the electrospinning process (Baumgarten 1971). The relationship between polymer solution

concentration and electrospinning is best described by the Berry number, Be , defined as the product of the polymer intrinsic viscosity and its concentration. A dimensionless parameter, the Berry number can be used as a criteria in polymer selection for electrospinning, which has been demonstrated using various polymers including poly(lactic acid) (Gogotsi 2006), poly(acrylonitrile) (Yamashita, Ko et al. 2007), and poly(styrene-butadiene-styrene) (Gogotsi 2006). From previous studies on Berry number vs. fibre diameter relationships, four regions of the Berry number corresponding to different electrospinning regimes were identified. In region (I) at $Be < 1$, only polymer droplets can be formed due to insufficient polymer chain length or concentration for entanglement. In region (II) at Be between 1 and 2.7, the level of polymer entanglement becomes sufficient to form nanofibres, with diameter increasing with Be . Region (III), at Be between 2.7 and 4, marks a rapid increase in fibre diameter with Be due to the increasing amount of entanglement. As Be becomes greater than 4 in region (IV), fibre diameter no longer increases with Be and the high concentration may prevent successful electrospinning (Gogotsi 2006). In addition to aiding polymer and concentration selection, the Berry number is often used for expressing fibre diameter, following the relationship $d = aBe^c$, in which d is the fibre diameter, a and c are empirical constants determined experimentally (Gogotsi 2006).

In determining fibre diameter using the Berry number method, the solution concentration is the most significant free variable and that all electrospinning parameters must be constant in order to determine the empirical constants a and c . However, it must be noted that process parameters can also affect the nanofibre diameter, including voltage, solution feed rate, spinning distance, temperature and humidity. Voltage is an important parameter in electrospinning because the charges on the polymer molecules that form the fibre jet originate from the applied voltage. At voltages above 10 kV, the solution jet will be drawn at a faster rate and will experience a greater acceleration. Moreover, the greater acceleration causes the solvent in the solution to evaporate faster, reducing the fibre jet volume. These factors are in

favour of reducing fibre diameter. However, increased solution jet acceleration also reduces the flight time, or in other words, the jet will reach the collector quicker. A reduced flight time reduces the time available for the fibres to stretch, leading to a greater fibre diameter (Ramakrishna, Fujihara et al. 2005). Therefore, as the voltage increases, fibre diameter will decrease, but may increase once voltage increases past an optimum level. The balance in voltage is also important for the crystallinity of the polymer. In general, since a higher voltage causes a stronger stretch in the fibres, greater crystallinity can be achieved. However, a voltage that is too high reduces flight time, which gives the fibre less time to orient in an orderly fashion, reducing crystallinity.

The electrospinning solution feed rate is the rate at which the solution is supplied, and determines the amount of solution available for Taylor cone formation at a given moment. Since the Taylor cone must be kept at a certain size to be stable, a specific feed rate is required. Increasing the feed rate past this level will cause increase in fibre diameter since there is more solution supplied than that being withdrawn from the needle tip (Ramakrishna, Fujihara et al. 2005).

The spinning distance affects the flight time of the solution jet. When the distance is short, there is less time for the solvent in the solution to dry and for the jet to stretch, which can lead to an increase in fibre diameter. Also, as the distance between the needle tip and grounded target reduces, the electric field strength increases (Ramakrishna, Fujihara et al. 2005). The increase in electric field strength accelerates the jet, thus giving even less time for the jet to stretch and for solvent to evaporate. The effect of spinning distance on fibre morphology depends on the volatility of the solvent in the solution as well as the polymer concentration.

While solution and process parameters provide a large degree of control over fibre properties,

the electrospinning technique also offers a large degree of flexibility in material choice. The requirements for polymers to be electrospun include a minimum molecular weight of about 35,000 Daltons and linearity in polymer structure. The linearity requirements mean that electrospinning predominately involves thermoplastic polymers, although electrospun thermosets have also been reported in several studies (Ramakrishna, Fujihara et al. 2005, Reddy, Arinstein et al. 2009).

Another benefit of electrospinning over other fabrication approaches is the freedom in nanofibre placement and orientation. By adjusting the position and rotation of the fibre collector, nanofibre assemblies with different morphologies, orientations, density, and patterns can be fabricated. Figure 4 shows examples of randomly oriented and aligned nanofibres.

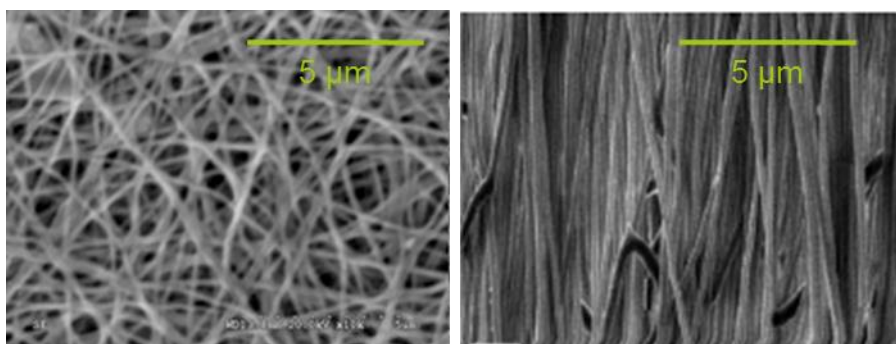


Figure 4: Examples of randomly oriented and aligned nanofibres

Fibre morphology has been studied previously via modeling and experimental work, with early models, based on Newton's second law, by Baumgartner, Fridrikh, and Rutledge (Fridrikh, Yu et al. 2003) focusing on the fibre jet formation, which has been summarized in the work by Wan et al (Park, Ito et al. 2010). In a more recent work, D'Amore et al demonstrated the use of an image-based algorithm for characterizing topography of electrospun poly(ester urethane) fibres, including diameter, intersection density, angle distribution and connectivity (D'Amore, Stella et al. 2010). In terms of experimental work, various groups have identified a range of process

parameters that affect fibre morphology and porosity, including voltage, spinning distance, solution flow rate, concentration and more.

Much of the earlier biomedical-related studies on nanofibres aimed to verify their effect on tissue regeneration, including the ECM-mimicking structure, adjustable fibre diameter and porosity, and large surface area. Ko et al. presented one of the first studies on cell interaction with nanofibres, outlining the effect of the increased surface area on the nanofibre scaffold compared to a microfibre one (Ko, Laurencin et al. 1998). Building on these early results, Ko and Gandhi further reported that fibroblast cell proliferation on *Bombyx mori* silk nanofibres were superior to that on microfibrils of the same silk, highlighting that cell activities on nanofibres are diameter-sensitive. In addition, Ko and Gandhi showed that cells adapt differently on the micro and nanofibre scaffolds (Ko and Gandhi 2007). While fibroblast cells were more crimped on the microfibrils, they were more spread on the nanofibre scaffold, resembling fibroblast morphology on native tissue. Besides silk, Ko et al also demonstrated that nanofibre scaffolds can be fabricated from native tissue proteins, such as collagen and elastin, while maintaining the cell activities on these materials (Li, Mondrinos et al. 2005). Scaffold interactions with cells such as fibroblasts, chondrocytes and mesenchymal stem cells (MSC) were also outlined in earlier studies by Li et al, showing positive initial results including comparable chondrogenesis between MSC in nanofibre scaffold and those in cell pellets and aggregates, as well as increased ECM production by chondrocytes on nanofibre scaffold compared to monolayer cultures on tissue culture plastics (Li, Tuli et al. 2005). In addition, Li et al also examined fibroblast interaction with a poly(lactic-co-glycolic acid) electrospun scaffold and suggested that the pore sizes, with the majority in the 25 – 100 μm range, are adequate for fibroblast migration (Li, Laurencin et al. 2002). Katti et al studied the effect of different electrospinning parameters on nanofibre architecture, and verified the feasibility of loading antibiotic drugs into the fibres without compromising morphology (Katti, Robinsin et al. 2005). More recently, studies on alginate

nanofibres also showed improved cell viability and proliferation compared to a commercial alginate-based microfibrinous dressing (Leung, Yang et al. 2010).

In addition to studies on general fibre architecture and comparison with other forms of scaffolds, several studies have also found that cell attachment and differentiation can be affected by controlling nanofibre orientation. For example, the earlier work by Li et al suggested that inducing controlled anisotropy in electrospun scaffolds affected organization of actin filaments from human MSC (Li, Mauck et al. 2007). Preliminary results from cell interaction with anisotropic nanofibre scaffolds prompted further investigations into their use on tissues in which directional properties are desired, such as cardiovascular and neural tissues, which are significant areas due to the lack of self-regeneration mechanisms and challenges associated with the small size-scale of these tissues. Lim et al (Lim, Liu et al. 2010) and Xie et al (Xie, Willerth et al. 2009) seeded neural and embryonic stem cells onto aligned poly(caprolactone) nanofibres and both reported elongation of the neural stem cells along fibre axis. In addition, when differentiation was initiated the cells exhibited a higher extent of neuronal differentiation markers compared to randomly oriented fibres. Similar results were also reported in the work by Mukhatyar et al, who reported that Schwann cell migration and neurite outgrowth on poly(acrylonitrile)-methacrylate nanofibres were superior to those on a smooth film (Mukhatyar, Salmerón-Sánchez et al. 2011), which the authors attributed to increased adsorption of fibronectin. Using the knowledge gained on interactions between cells and aligned fibres, Orlova et al demonstrated the ability to control architecture of cardiac tissue cultures by manipulating the positions of electrospun poly(methyl glutarimide) with cardiomyocytes seeded (Orlova, Magome et al. 2011). In addition to controlling architecture of cardiac tissue culture, Kurpinski et al also reported increased endothelial cell infiltration into aligned poly(L-lactic acid) nanofibres (Kurpinski, Stephenson et al. 2010), which may be helpful in fabricating scaffolds for blood vessels, which are often difficult to repair, especially with small diameter blood vessels.

Encouraging cell attachment and infiltration is only one of the potential uses for electrospun tissue repair scaffolds. In fact, there are also studies aimed at preventing cell and tissue adhesion, which is equally as important as tissue culturing because in many post-surgical cases, bacteria or scars may cause tissue adhesion that can lead to patient discomfort and reduced mobility. An example for preventing tissue adhesion is the demonstration by Yang et al who implanted an electrospun layer of poly(lactic acid)-poly(ethylene glycol) copolymer between the cecum and peritoneal wall defects in rats, and largely prevented cell and tissue adhesion on the fibre surface (Yang, Chen et al. 2009). Yang et al attributed their observed phenomenon to the enhanced hydrophilicity from the introduction of poly(ethylene glycol), which is more mobile in body fluid and facilitates liquid diffusion. Zong et al also reported reduction in abdominal adhesion by implanting an electrospun poly(lactic-co-glycolic acid) scaffold (Zong, Li et al. 2004).

1.1.7 Material Selection for Electrospinning Tissue Scaffolds

In medical applications such as wound repair, the main requirement is for the polymer to be biocompatible and not cause allergic or toxic response in the body. For applications such as burn dressing under a pressure garment, it is also desirable that the polymer is biodegradable. Polymers electrospun for tissue applications can be natural, synthetic, or combinations of both, depending on the desired functions.

Natural polymers can be derived from animals or plants, and therefore they are mostly biocompatible and many carry specific biological activity, such as antimicrobial and cell binding. In addition many natural polymers are renewable. Natural polymers that are common in electrospinning for tissue repair scaffolds include proteins such as collagen (Li, Mondrinos et al.

2005, Rho, Jeong et al. 2006, Newton, Mahajan et al. 2009), keratin (Li, Li et al. 2009), silk (Sukigara, Gandhi et al. 2003, Sukigara, Gandhi et al. 2004, Gandhi, Yang et al. 2009), and polysaccharides such as alginate (Leung and Ko 2010), hyaluronic acid (Ji, Ghosh et al. 2006), and chitosan (Desai, Kit et al. 2008, Chu, Shi et al. 2009). Several proteins that can be found in the native tissues, such as collagen and keratin, have superior cell affinity due to the presence of arginine-glycine-aspartic (RGD) sequences that can interact with integrin expressed by various cells. This enhanced cell affinity can be transferred to nanofibres via electrospinning, as verified by the studies by Li et al on keratin (Li, Li et al. 2009) and Rho et al. (Rho, Jeong et al. 2006). In addition Li et al compared human embryonic palatal mesenchymal (HEPM) cell proliferation on a range of substrates including electrospun fibres of ECM proteins such as collagen and elastin, and reported superior proliferation on these electrospun proteins compared to the tissue culture plate controls (Li, Mondrinos et al. 2005). Silk is another commonly used protein that has been found to support cell adhesion and differentiation in several studies, such as those by Mandal et al (Mandal and Kundu 2010) and Sukigara et al (Sukigara, Gandhi et al. 2003, Sukigara, Gandhi et al. 2004, Ayutsede, Gandhi et al. 2005, Gandhi, Yang et al. 2007). In addition to native proteins, polysaccharides also play a significant role in nanofibre scaffold fabrication. Alginate and chitosan, for example, can contribute to fluid absorbance and bacteria growth inhibition (Desai, Kit et al. 2008), respectively, enabling these polymers to be desirable candidates for various tissue scaffolds. In addition, the positive surface charge on chitosan nanofibres can be optimized for binding specific drugs or proteins. Hyaluronic acid is a polysaccharide that can be found in native ECM as part of the GAG, and possess binding capability with cells and other ECM proteins, which has been confirmed in the early study by Ji et al (Ji, Ghosh et al. 2006). Recently, Hsu et al also reported that by incorporating hyaluronic acid onto an electrospun collagen scaffold, the expression ratio of tissue inhibitors of metalloproteinases (TIMP) to matrix metalloproteinases (MMP) is

successfully reduced (Hsu, Hung et al. 2010), which have implications in scar prevention for wound healing.

While the biological properties of natural polymers continued to fuel interest in electrospinning them for tissue scaffolds, much effort has also been on synthetic polymer nanofibres due to their often superior and customizable mechanical properties. Examples of synthetic polymers commonly used for tissue applications include PCL (Bölgen, Vargel et al. 2007, Gandhi, Srikar et al. 2009), poly(L-lactic acid) or poly(DL-lactic acid) (PLLA or PDLLA) (Yang, Murugan et al. 2005, Li, Li et al. 2009, Liu and Ma 2010), poly(glycolic acid) (PGA) , poly(vinyl alcohol) (PVA) (Zeng, Aigner et al. 2005, Asran, Henning et al. 2010), and Poly(caprolactone-co-ethyl ethylene phosphate) (PCLEEP) (Chua, Lim et al. 2005). While the synthetic polymers do not serve functional purposes, unlike their natural counterparts, they are less costly to fabricate, as they do not require lengthy decontamination processes or exotic solvents. In fact, materials based on aliphatic polymers such as PCL, PLA, and PGA are the most common types of synthetic polymers used due to their low cost and reproducibility in manufacturing, in addition to their biocompatibility. Properties of synthetic polymers are controllable via its molecular properties. For example, PVA, synthesized from the hydrolysis of poly(vinyl acetate) (PVAc), can have varying crystallinity, and degradation rate depending on the degree of hydrolysis and molecular weight (Park, Ito et al. 2010, Peresin, Habibi et al. 2010). In addition, polymers such as PLA and PGA can be combined to form PLGA copolymer, with properties that can be controlled through the LA to GA ratio (Li, Laurencin et al. 2002, Duan, Yuan et al. 2006, Shin, Lee et al. 2006). Li et al compared the structural properties of several electrospun synthetic polymers, and reported that while electrospun PLLA and PCL formed compliant scaffolds, PGA and PLGA formed the stiffest ones, although both PGA and PLGA were more degradable in aqueous environments (Li, Cooper Jr et al. 2006). Moreover, Li et al showed that PLLA and PCL scaffolds exhibited faster cell proliferation compared to PGA and PLGA.

Knowing the properties of polymers commonly used in electrospinning, it is possible to select an appropriate material or combinations for scaffold design such that the most suitable properties can be incorporated. In addition to biocompatibility and functional properties, biodegradability is also an important aspect in scaffold design. For specific tissues biodegradability should be controlled for optimal treatment. For example, for wound healing, the scaffold must remain intact as cells populate, but not excessively persistent that formation of new ECM is obstructed.

Scaffold degradation usually involves several stages. First, fibres will uptake body fluids from surroundings, followed by cleavage of polymer bonds into shorter chains (Göpferich 1996). The process then continues until the polymer chains become sufficiently short to be dissolved in the surrounding media. As dissolution occurs, the scaffold loses mass, leading to changes in dimensions. In natural polymers such as silk, in vivo degradation can be catalyzed by enzymes. In enzymatic degradation, enzymes are adsorbed on the scaffold surface, followed by digestion of the matrix until it returns to its corresponding amino acids which will then be absorbed in the body (Cao and Wang 2009). Hydrophilic polymers usually degrade at a much faster rate in aqueous environments, whereas hydrophobic ones such as PLA and PCL are marginally degradable. In addition, studies by Chew et al also established PCLEEP as a marginally degradable polymer, being less degradable than PCL (Chew, Wen et al. 2005). In an attempt to more closely simulate degradation conditions in the body, Li et al characterized the degradation of an electrospun PLGA scaffold under tensile load, and reported that tensile strength and stiffness of scaffolds under load tend to increase initially in the degradation media, followed by a sharp decline that is faster than scaffolds not under load (Li, Feng et al. 2010). The findings by Li et al is important because in many situations nanofibre scaffolds will be attached to surrounding tissues as a temporary replacement and sustain physiological loading, and therefore more accurate information on fibre degradation is required for scaffold design.

With material choice being a determinant factor in overall scaffold properties, it is possible to fine tune scaffold properties through post-electrospinning process optimization. For example, electrospun fibres can be annealed to induce crystallization, which modifies scaffold strength and extensibility. Gandhi et al have presented several examples of post-spinning treatment and their effects on the properties of electrospun silk nanofibres (Gandhi, Yang et al. 2009). In addition to annealing, crosslinking is a common method for modifying scaffold structural properties. Previous work on alginate has shown that crosslinking with divalent ions such as calcium could enhance alginate nanofibre integrity in aqueous environments, although extensibility of the fibres reduced significantly (Leung, Yang et al. 2010). Indeed, crosslinking has also been suggested in electrospinning proteins such as collagen and gelatin as well as other polysaccharides like chitosan in order for the resultants scaffolds to improve their integrity under physiological loads (Luo, Kirker et al. 2000, Newton, Mahajan et al. 2009).

1.1.8 Nanofibres for Drug Delivery in Wound Dressings Applications

In addition to serving as a protective barrier and a platform for skin regeneration, wound dressings may contain therapeutic agents or active ingredients for enhancing the quality of healing. By using polymers as drug carriers, it is possible to reduce drug dosage or dosing frequency required to achieve therapeutic levels, reducing local or systemic side effects (Langer 1998). Examples of polymer drug carriers include micro- or nano-particles (Ravi Kumar, Bakowsky et al. 2004), hydrogels and soft implants (Sershen and West 2002), implant coatings (Gollwitzer, Ibrahim et al. 2003), films (Jackson, Smith et al. 2004), and fibres (Ranganath and Wang 2008, Kenawy, Abdel-Hay et al. 2009). Fibres again attract attention as previously discussed, with an increasing number of publications focusing on nanofibre carriers (Meinel,

Germershaus et al. 2012). Among different nanofibre fabrication techniques, electrospinning provides many avenues for incorporating functional components into the polymer matrix, either through direct blending, covalent binding, emulsifying, and co-axial electrospinning (Ji, Sun et al. 2011, Meinel, Germershaus et al. 2012). In addition, electrospinning allows for control over the micro/nanostructure of the scaffolds, with great flexibility in terms of materials choice. Electrospun fibres have been shown in previous studies to better support uniform drug release compared to films due to the large surface area available. The large surface area also allows drug to be more uniformly distributed in the scaffolds. In the work by Taepaiboon et al (Taepaiboon, Rungsardthong et al. 2006) comparing PVA nanofibres and films, it was determined that anti-inflammatory drugs loaded into nanofibres achieved cumulated release that are closer to the loaded amount compared to cast films, as the higher surface area to volume ratio in electrospun fibres can facilitate more efficient release and less drugs entrapment. In a later study by Wang et al (Wang, Cao et al. 2012), it was found that tetracycline hydrochloride (TCH), an antibacterial agent, had higher tendency to form aggregates in cast films compared to nanofibres of poly(3-hydroxybutyrate-co-3-hydroxyvalerate) (PBHV). The aggregate formation of TCH in PHBV cast films led to a higher extent of burst release observed after 20 hours, at 58% release compared to 24% for nanofibres. However, at the end of the 120 hour study by Wang et al, the overall release observed from the nanofibres was higher than from the cast films, at 94.0% for nanofibres compared to 68.2% for cast films, which confirmed the observation by Taepaiboon et al on nanofibres being more efficient drug delivery matrices. Similar comparisons between electrospun fibres and cast films were also made using the painkillers aspirin (Del Gaudio, Ercolani et al. 2013) and paracetamol (Cui, Li et al. 2006), with identical conclusions that electrospun fibres can facilitate higher degree of drug release. In addition to cast films, other comparisons have been made with microspheres and microfibres. Using the same argument of larger surface area being beneficial for more complete release, Ranganath et al showed that PLGA submicro-fibres better facilitated release of paclitaxel compared to PLGA

microfibres (Ranganath and Wang 2008). In addition, Ionescu et al showed that the osteoarthritis drug chondroitin sulfate was released more gradually with lower burst from PCL nanofibres compared to microspheres (Ionescu, Lee et al. 2010).

In terms of wound healing, antibiotics are thus far the most common class of therapeutics incorporated in nanofibre dressings due to the importance of preventing infections early in the wound healing process in ensuring immediate survival. Release rate control methods for antibiotics generally focus on the short term, from hours to one or two days, which is related to length of the inflammation period. Antibiotics are one of the most common types of drugs studied in nanofibre-based carriers, with common examples such as cefazolin (Katti, Robinson et al. 2004), rifampin (Zong, Kim et al. 2002), and fusidic acid (Said, Aloufy et al. 2011) in PLA or PLGA based nanofibres. While targeting the inflammation stages early in the regeneration process, antibiotic-loaded scaffolds tend to be quick releasing. Incorporation of anti-inflammatory drugs that can also act as pain killers have also been widely demonstrated, such as the work on ibuprofen and aspirin release from various matrices including poly(vinyl pyrrolidone) (PVP) (Yu, Shen et al. 2009), PLA (Immich, Arias et al. 2013), zein (Huang, Zou et al. 2013), and PCL (Del Gaudio, Ercolani et al. 2013). In addition to preventing prolonged inflammation and infection, Bölgen et al also proposed an antibiotic-loaded scaffold that can prevent abdominal adhesion (Bölgen, Vargel et al. 2007). In their scaffold design, Bölgen et al showed that a layer of electrospun PCL could act as a physical barrier against postsurgical tissue adhesion, and when the layer is loaded with the antibiotic Biteral, the scaffold further reduced adhesion in animal model, likely through reducing the bacteria that could change the balance between fibre deposition and resorption.

After the immediate survival of patients is ensured, promoting timelier skin regeneration and wound closure is the next step of interest. In the past two decades, many research groups have

examined incorporation of cell signaling molecules such as growth factor into wound healing, either via direct topical application (Brown, Nanney et al. 1989), or through wound dressings (Ji, Sun et al. 2011). The use of several growth factors, including transforming growth factor β 1 (TGF- β 1) (Puolakkainen, Twardzik et al. 1995, Lee, Li et al. 2003), platelet derived growth factor (PDGF) (Bourke, Al-Khalili et al. 2003, Murray, Rice et al. 2003), epithelial growth factor (EGF) (Brown, Nanney et al. 1989, Ulubayram, Cakar et al. 2001), and fibroblast growth factor (FGF) (Liu, Cai et al. 2007), on tissue cell activities and regeneration have been extensively documented in previous work on tissue repair scaffolds. For example, Schneider et al reported a timelier wound closure upon application of an electrospun silk scaffold containing EGF, which regulates cell attachment, proliferation, and differentiation (Schneider, Wang et al. 2009). The scaffold was tested on a 3D human skin wound model, produced by culturing fibroblast cells in collagen layers, then inflicting a wound via punching and removing a 1.5 cm section from the culture. The silk/EGF scaffold showed feasibility in increasing the rate of wound closure, which outperformed an as-electrospun blank silk scaffold by a factor of four in terms of percentage of wound closure after 48 hours. Yang et al demonstrated the incorporation of basic fibroblast growth factor (bFGF) in the core of a nanofibre with a PEG-PLLA copolymer shell via emulsion electrospinning (Yang, Xia et al. 2011). The controlled release of bFGF from the core-shell nanofibre scaffold enabled significant reduction of wound area of diabetic ulcers on rats, compared to the copolymer scaffold without bFGF. On the other hand, studies on PDGF-incorporated polyurethane scaffolds showed that rate of granulation tissue formation is enhanced in rat skin excisional wounds (Li, Davidson et al. 2009). While large variations were observed between existing studies on the extents of therapeutic effect of growth factors loaded scaffolds on animal models and human trials, ranging from minimal effect to significantly positive depending on the animal species, these studies nonetheless showed potential in successfully encouraging expedited healing, which can be useful in large or chronic wounds.

Enhancing the growth of granulation tissue only addresses one stage in the intricate wound healing process. After the formation of granulation tissue, wound closure would occur, while the granulation tissue would undergo angiogenesis such that oxygen and nutrient transport can be restored for epithelialization to take place. While incorporation of growth factors has been shown to expedite this process, it may also cause undesirable effects in subsequent stages of wound healing. A major concern is that granulation tissue production is enhanced to an extent that it does not cease at an appropriate time, leading to excessive collagen deposition and thus hypertrophic scarring, or even keloids in extreme cases. The potential side effects of growth factor incorporation was also suggested by Hromadka et al in their review (Hromadka, Collins et al. 2008), with evidence from the study by Liu et al showing that expression of TGF- β is significantly higher in adult wounds compared to scarless fetal wounds (Liu, Wang et al. 2004), confirming earlier studies that showed correlation between TGF- β expression and formation of hypertrophic scarring and keloids.

1.1.9 Fibroproliferative Disorders and Current Treatment

Fibroproliferative disorders (FPDs) are those that involve abnormal, often excessive tissue accumulation and contraction that ultimately causes progressive damage to normal tissue structure and functions. An analogy for skin regeneration and the onset of FPD is shown in Figure 5, using fence building as an example (Tredget, Nedelec et al. 1997).

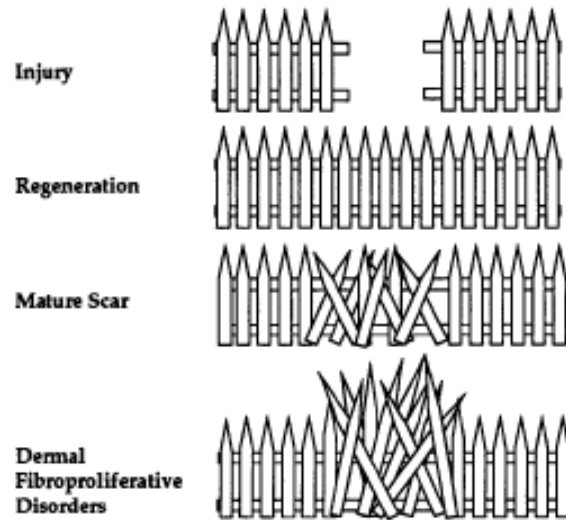


Figure 5: Representation of skin regeneration and fibroproliferative disorders using an analogy of building fences. Image obtained with permission from (Tredget, Nedelec et al. 1997).

The process from injury to scar maturation represented in Figure 5 is consistent with that described in section 1.1.3, in that the injury site is repopulated by new collagen produced, which would undergo contracture as the scar matures. However, at the onset of FPD, collagen production outpaces degeneration and proliferation becomes uncontrollable (Tredget, Nedelec et al. 1997). Hypertrophic scarring and keloids are two examples of FPDs, but are different in that hypertrophic scars are fibrous lesions that are thicker than normal skin and are confined within the wound, whereas keloids can extend beyond the wound boundaries. Unlike normal skin which contains distinctive collagen fibre bundles, hypertrophic scars contain nodular collagen structure with possible crosslinks (Tuan and Nichter 1998). On the outside, hypertrophic scars are thicker than normal skin with reduced epithelial ridges, and often have a redder colouration. Keloids, on the other hand, contain thick, large collagen fibres and significantly less α -smooth muscle actin-positive fibroblasts than hypertrophic scars (Tredget, Nedelec et al. 1997). While the property mismatch between hypertrophic scars and normal tissues reduces gradually to a certain extent during the wound remodeling that can last up to two years, keloids rarely regress due to the lack of cellularity in keloids. Both hypertrophic

scarring and keloids are detrimental to patient recovery from burn and other trauma due to the difference in tissue properties. Both reduce patient mobility around the wound area due to the thicker collagen layers and possibly excessive tissue contractions, which can diminish patient mobility and delay their return to productivity. The differences in thickness and colouration also pose cosmetic inconveniences. In addition, the increased concentration of mast cells in hypertrophic scars and the resultant increase in histamine release have been linked to itchiness (Tredget, Nedelec et al. 1997), which, combined with reduced tissue mobility, can lead to significant discomfort. Nerves in the scar tissues may also be entrapped in the nodular collagen network, causing sensation issues such as numbness which can be dangerous to patients.

Devising methods to treat FPDs requires a thorough understanding on how they are formed. As mentioned previously, these FPDs are formed by an excessive deposition of collagen by fibroblast cells. There are several conditions in which the over-proliferation or over-deposition can occur. Patients suffering from prolonged inflammation are susceptible to hypertrophic scarring, with the effects outlined by Deitch et al (Deitch, Wheelahan et al. 1983) in their clinical work showing the correlation between severe inflammation in wounds and hypertrophic scar formation. During the inflammation process, cytokines such as growth factors are released and activated via platelet degranulation. These cytokines are responsible for granulation tissue formation, angiogenesis and re-epithelialization. Despite the importance of cytokines to the initial healing response in the proliferation stage, their prolonged or exaggerated presence may ultimately lead to FPDs. In a study by Kovacs and DiPietro (Kovacs and DiPietro 1994), several growth factors have been identified to be involved in the development of hypertrophic scarring, including TGF- β , PDGF, and insulin-like growth factor – I (IGF-I). TGF- β is solely responsible for attracting a range of cells including fibroblasts, and enhances production of ECM proteins. PDGF and IGF-I, on the other hand, contributes collaboratively towards increased ECM synthesis. Studies by Lynch et al (Lynch, Colvin et al. 1989) showed that cells induced with

PDGF and then IGF-I led to significantly enhanced ECM deposition compared to cells induced with either one of the factors. In addition to prolonged inflammation, the use of growth factor incorporated wound dressings may also increase the risk of hypertrophic scar formation, unless their concentration can be carefully controlled towards the end of the proliferation stage.

Another drawback from the increased cellular activity as a result of prolonged inflammation and growth factor-aided wound healing is the extent of wound contraction. If the contraction proceeds beyond the sufficient level for re-epithelialization, in a condition called scar contracture, extensive deformation may result on the skin leading to reduced mobility and poor aesthetics. The exact mechanism for contracture is still debatable, whether by myofibroblast activity or other factors in the extracellular environment (Tredget, Nedelec et al. 1997). However, excessive contracture may be prevented by maintaining ECM component and cytokine signals at similar levels to normal tissues, rather than at their enhanced levels in an unmanaged wound.

Some patient groups are also more susceptible to FPDs. It is well known that hypertrophic scarring and keloids are more common in ethnicities with darker pigmented skins, such as patients of African and Hispanic descent. For example, earlier ethnicity studies on keloid patients reported high incidence (4.5% - 16%) of keloid formations among Hispanic and African American population, whereas incidence of hypertrophic scarring was estimated to be higher (RS English 1999). Another report also suggested that keloids are 5 – 15 times more prevalent in African American population compared to Caucasian American (IC LeFlore 1980). In addition to ethnicity, increased susceptibility to FPD can also be due to familial heritability, as suggested in studies by Shih et al (B Shih 2010). Patients who are more susceptible may also experience onsets of FPDs much sooner than others, thereby creating more challenges in obtaining balanced wound healing with appropriate levels of ECM production.

Several methods currently exist for reducing FPD symptoms such as hypertrophic scar formations, with some being invasive and others more preventative. One of the common treatment methods is to inject corticosteroids into the lesion, which acts as an anti-inflammatory agent (Tredget, Nedelec et al. 1997). By applying a minimal effective dosage at 3 to 4 week intervals, studies have shown that corticosteroid therapy can improve scarring, through reducing expression of cytokines such as TGF- β and others that can inhibit collagenase activity. Kiil et al (Kiil 1977) reported that a 50% response rate was achieved when the treatment was used on keloids over 5 years, while another study on showed a roughly 10% recurrence rate after 4 years. Common side effects of corticosteroid injection include pain at the injection site and possible local tissue atrophy. A more invasive method for removing lesions is surgical excision in which scar tissues are physically removed. Since surgical excision involves reopening the wound site, minimizing tissue trauma is important, while also ensuring that potential for residual inflammation is removed. Surgical sites can also be chosen strategically to reduce wound tension. By itself, surgical treatment is known for its high recurrence rate, with some studies reporting rates above 50% (Darzi, Chowdri et al. 1992), although the treatment can be more successful if the affected area is small. Another example of an invasive technique is by laser treatment. Using a non-ablative laser, such as 585 nm pulsed-dye laser (Alster and Williams 1995), this method has been reported to improve skin surface textures via selective photothermolysis of skin cells. An example of a more preventative method for wounds is pressotherapy, in which pressure is applied on the wound, either via a pressure garment or silicone gel sheet, to produce a hypoxic environment that reduces fibroblast proliferation and subsequent collagen deposition. Pressotherapy can also be used as a complimentary treatment after surgical excision of the lesion. Treatment usually begins at the onset of re-epithelialization, and the pressure is applied 24 hours a day until scar maturation. However, results from studies on pressotherapy have been mixed, with some suggesting that the benefits are not significant.

While each of the existing methods for treating hypertrophic scarring and keloids have individually shown potential in reducing symptoms, there is seemingly a lack of consistency in the reported effectiveness among studies, with some showing high recurrence rates. It is therefore desirable to identify a non-invasive method that can effectively reduce scarring by utilizing the current knowledge on scar formation mechanisms described in this section.

1.1.10 Antifibrogenic Drugs and its Use in Scaffolds

Existing treatments for FPDs such as hypertrophic scarring and keloids mostly rely on physically removing lesions or depriving cells of a suitable environment for collagen synthesis, with the exception of corticosteroid injection. In addition to corticosteroids, other therapeutic agents have been suggested to have a potential in scar reduction, although they have not been used widely in a clinical setting. In fact, there is currently no approved drug in the market that specifically treats fibrosis. In several studies, the potential anti-scarring effects of the antiemetic drug Tropisetron (A Stegemann 2013) and the antiallergic drug Transilast (S Shigeki 1997) have been discussed, but current results have only showed their ability to relieve the irritation and other symptoms on patients who have already developed scars and keloids, while their ability to prevent FPDs is not confirmed.

In their review, Hromadka et al suggested fibromodulin maybe a potential therapeutic agent as it is a modulator of TGF- β , supported by a separate study showing that early neutralization of TGF- β by an antibody was able to reduce scarring (Hromadka, Collins et al. 2008). This method, similar to the corticosteroid treatment, involves eliminating cytokines that may increase fibroblast proliferation and collagen synthesis. However, another possible method to reduce

scarring is the increase of collagenase, such that the balance between tissue synthesis and digestion can be achieved, leading to scar maturation without excess collagen.

Earlier studies showed that relaxin may have a positive impact on scar reduction, by increasing expression of a matrix metalloproteinase (MMP), a proteinase that cleaves ECM molecules and growth factors (Li, Kilani et al. 2013). Experiment in porcine models showed that relaxin was able to improve healing only when applied systemically, but not when applied topically due to its short residence time and difficult penetration into the skin (Unemori and Amento 1990). Despite the limitations in the relaxin treatment, the existing work nonetheless showed feasibility in enhancing MMP expression to facilitate ECM degradation in the remodeling stage. Thus far, over 20 types of MMP have been found, and the type that is stimulated in the work on relaxin is known as MMP-1.

In search of an effective therapeutic agent for scar prevention, Ghahary et al co-cultured fibroblast cells with keratinocytes, and reported a 10-fold increase in collagenase expression over a control fibroblast culture (Ghahary, Karimi-Busheri et al. 2004). The collagenase that was stimulated in this case includes MMP-1, MMP-3, MMP-8, and MMP-24, all of which can degrade ECM components. The increase indicated that there must be a keratinocyte releasable factor that is responsible for stimulating collagenase expression, referred to as keratinocyte-derived antifibrogenic factor (KDAF). Through a series of chromatographic characterization and peptide mapping, the KDAF was found to be a stratifin. As a confirmation, Ghahary et al was able to show that stratifin treated fibroblast showed a marked increase in collagenase expression. With potential in reducing hypertrophic scarring via upregulating MMP, Ghahary et al proceeded to testing stratifin on animal models in which stratifin was delivered to a fibrotic rabbit ear model via a carboxymethyl cellulose (CMC) gel topical agent (Rahmani-Neishaboor, Yau et al. 2010). The stratifin treatment showed a 2.8-fold increase in MMP-1 expression and a corresponding

48% reduction in collagen density compared to the untreated controls. Reduction in hypertrophic scarring on the rabbit ears was also visually evident after stratifin treatment.

In a follow-up study, stratifin was incorporated into PLGA microspheres with chitosan core, and were delivered to wound sites on the backs of ten Sprague-Dawley rats via a poly(vinyl alcohol) film (Rahmani-Neishaboor, Hartwell et al. 2012). Similar to the rabbit ear models, the results from the rat models showed a similar reduction in collagen deposition as well as tissue cellularity, further showing potential for stratifin use as an antifibrogenic agent.

While proteins such as fibromodulin, relaxin and stratifin may be effective in preventing FPDs, their stability in solutions may pose risks in manufacturing due to protein denaturation. Despite previous studies on electrospinning showing that nanofibres containing proteins could be successfully electrospun, subsequent treatment on these nanofibres has not been considered. In order to optimize release properties, it is beneficial to be able to modify nanofibre carrier properties via techniques such as crosslinking and heat treatment, which may be damaging to proteins loaded. As a result, a non-protein based drug that has anti-scarring effect is beneficial. In addition to stratifin, the Ghahary group also identified another antifibrogenic agent in kynurenine, a metabolite of tryptophan with molecular structure shown in Figure 6 (Li, Kilani et al. 2013).

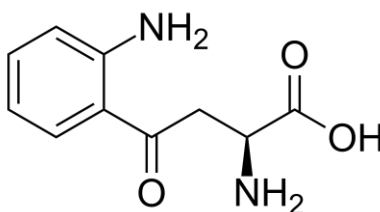


Figure 6: Molecular structure of kynurenine

The discovery originates from the use of an allogeneic skin substitute that expresses an immunomodulating enzyme, Indoleamine 2, 3-dioxygenase (IDO), to prevent rejection. While earlier studies showed that IDO expression prevented immune rejection of foreign xenogeneic cells, later studies also indicated that when applying skin substitutes populated by IDO-transduced fibroblasts onto rabbit ear wound models, the resultant scar was flatter than an untreated control, with significantly lower cellularity in the scar tissue. It was also found that MMP-1 expression in the treated wounds were higher than in the control. In their recent study, Li et al reported that kynurenine, which is releasable from the IDO expressing skin substitute when tryptophan is converted into kynurenine, is the contributor of the ECM modulation effect in the IDO expressing skin substitute (Li, Kilani et al. 2013). In fact, Li et al showed that kynurenine treatment by means of a kynurenine-incorporated carboxymethyl cellulose (CMC) gel can lead to increased MMP-1 and MMP-3 expression, and contributed to significantly reduced scarring when applied onto rabbit ear wounds, as shown in Figure 7.

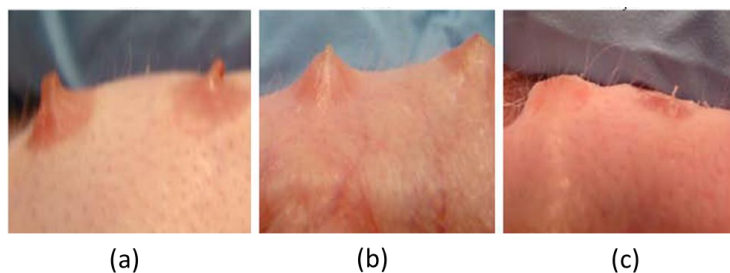


Figure 7: Clinical appearance of rabbit ear scars that was (a) untreated, (b) treated with CMC carrier only and (c) treated with CMC loaded with kynurenine. Image obtained with permission from (Li, Kilani et al. 2013)

Two potential antifibrogenic agents have been identified in this section, stratifin and kynurenine, with the first being a protein and the latter being a metabolite. From a drug carrier design point of view, kynurenine may be more desirable over stratifin as the choice of drug to be electrospun into nanofibre-based structures, based on consideration on several processing aspects. First, as

a protein, stratifin is significantly more difficult and costly to produce, compared to kynurenine. The stratifin used in the studies by Ghahary et al have been recombinant proteins produced by protein cloning using stratifin from human keratinocytes, as described previously. While both recombinant stratifin and kynurenine can be readily purchased as commercial products from vendors such as Sigma-Aldrich, the cost of recombinant stratifin can be up to 20,000-folds higher. In addition, as a protein, stratifin can be denatured upon handling and nanofibre processing, posing challenges in storage as well as solvent and polymer selection for electrospinning.

1.1.11 Nanofibre for Controlled Drug Delivery

With the intricate nature of the tissue regeneration process, precise control of therapeutic release rates is important, as specific therapeutic effects may be beneficial for one stage but detrimental in the next. For example, antibiotics may be useful at the inflammation stage but may interfere with fibroblast growth in the proliferation stage, whereas growth factors may help proliferation and ECM deposition but may cause scarring due to excessive collagen production. In applications other than skin regeneration, specific needs on the duration in which scaffolds must support drug release also exist. For example, bone and neural tissue repair may require longer release of growth factors to support regeneration of otherwise non-healing tissues in a harsh environment. The need for specific release duration is especially important for treating FPD because sub-optimal timing may negatively affect initial healing and wound closure. Figure 8 provides a schematic representation of different ideal release behaviors for various applications.

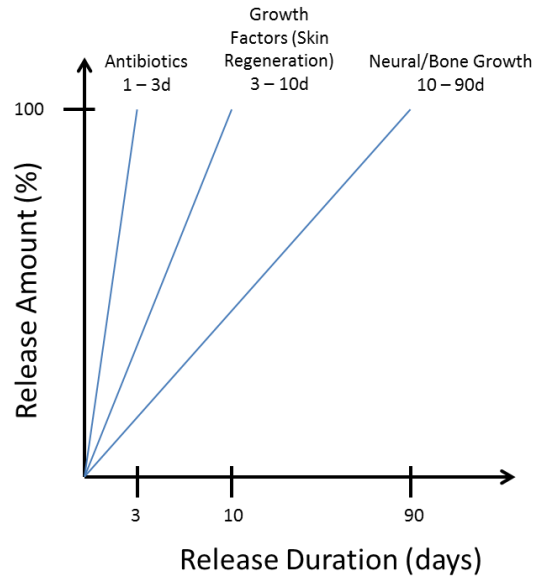


Figure 8: Examples of ideal release behaviors for different applications

Ideally, drug release from carrier matrices should be stable at a uniform rate such that the drug-loaded scaffold can remain effective throughout the duration that it is applied. On a release vs. time graph such as that shown in Figure 8, the ideal release would resemble an upward trending straight line. However, such uniform release profiles are very difficult to achieve in reality, due to different physical phenomenon affecting the scaffold, such as surface effect, diffusion, and matrix degradation (Siepmann and Siepmann 2008, Son, Kim et al. 2014). As a result, strategies have been formulated in the recent decade to control release rate of therapeutics from nanofibres to optimize tissue regeneration by taking advantage of the knowledge on the drug release mechanisms.

Drugs incorporated in nanofibre matrices can be released from the surrounding environment via a combination of different mechanisms. Drugs on the nanofibre surface can be dissolved and diffused out of the nanofibre membrane as it is penetrated by body fluids. Removal of drugs on fibre surface often corresponds to the burst phase of drug release. The extent of burst release may increase with the surface area on the nanofibre, therefore fibres with smaller fibre diameter

or higher ratio of pores can have quicker burst release. In some cases, such as oral formulations and some antibiotic applications, burst release is acceptable whereas in others such as anticancer drugs and growth factor moderators, burst release is to be avoided (Bourke, Al-Khalili et al. 2003, Liu, Xiao et al. 2004, Chew, Wen et al. 2005, Cui, Li et al. 2006, Yu, Shen et al. 2009, Immich, Arias et al. 2013). Detailed analysis of this method of drug release is thus far limited, especially in nanofibre matrices. Srikar et al have recently derived a semi-empirical release model that describes drug desorption from nanofibre surface, as shown in equation 1 below:

$$\frac{M_t}{M_{d0}} = \alpha \left[1 - \exp\left(\frac{-\pi^2 t}{8\tau_r}\right) \right] \quad \text{Equation 1}$$

The model relates fractional release M_t / M_{d0} (in which M_t is the mass of drugs released at time t and M_{d0} is the initial mass of drugs) to a porosity factor α that is a ratio of the drug concentration on the surface to that in bulk, and characteristic time τ_r which depends on porosity size and effective diffusion coefficient (Srikar, Yarin et al. 2008, Gandhi, Srikar et al. 2009). The model was based on Fick's second law of diffusion, as shown in equation 2 below in which C is the drug concentration, D is the diffusion coefficient of the drug in body fluid, and x is the drug position.

$$\frac{dC}{dt} = D \frac{d^2C}{dx^2} \quad \text{Equation 2}$$

The model was formulated with the assumption that drug concentration on fibre surface changes with time because diffusion of surface drugs out of the nanofibre membrane via body fluid was considered much faster than solid-state diffusion of drugs within the fibre.

In the Srikar model, instead of treating each nanofibre as a monolithic cylinder, a series of small, interconnected cylindrical pores was assumed to exist on the surface as well as throughout the

interior. Another assumption was also made in that the pore surface area accessible by body fluid is much higher than the surface area of a monolithic fibre of the same dimension, such that most of the release is contributed by drug desorption from the pore surface. In electrospinning, porosity in nanofibres can be created during solvent evaporation as the solution jet travels from the voltage source to the grounded collector (Ramakrishna, Fujihara et al. 2005). With this assumption, Srikar et al expected that increasing polymer concentration or molecular weight in the matrix electrospinning solution would increase solution viscosity, which will then reduce the porosity within fibres and therefore the release rate. The hypothesis that increasing solution viscosity can reduce the release rate may help explain the phenomenon observed in other studies that showed drug release decreasing with increasing fibre diameter, such as the work by Xie et al on tetracycline hydrochloride loaded PLA nanofibres (Xie and Wang 2006) and that by Chen et al on an antitumor drug 5-fluorouracil loaded PLA nanofibres (Chen, Huang et al. 2012). Experimentally, Srikar et al (Srikar, Yarin et al. 2008) has also proven their expectation using PMMA and PCL nanofibres incorporated with Rhodamine 610 dye, reporting a steady decrease in cumulative release with the increase of PCL concentration in the electrospinning solution from 11 wt% to 15 wt%. Similar trends in decreasing cumulative Rhodamine 610 release were also observed when molecular weight of PMMA increased from 120 – 996 kDa. While Srikar et al has successfully demonstrated their desorption-controlled release model using a dye, Gandhi et al later presented the first study that analyzed desorption-controlled release of therapeutics using the Srikar model, which involves PCL nanofibres loaded with an anti-integrin antibody as well as bovine serum albumin (BSA) (Gandhi, Srikar et al. 2009). In the study, Gandhi et al confirmed the prior observation by Srikar et al that increasing polymer concentration can lead to reduction in cumulative release. In addition, Gandhi et al also pointed out that addition of additives, such as BSA, may increase the nanoporosity in fibres leading to increased release rate.

Drugs that are not on the fibre surface release via different mechanisms. After removing any surface drug from the fibres, the resultant concentration gradient between the fibre bulk and surface drives drug diffusion towards the surface, as described by Fick's second law shown in equation 2, with D denoting the diffusion coefficient of drug in the fibre matrix in this case. Solving the Fick's second law, while assuming that drug transport through the nanofibre membrane is the rate-limiting step, can help formulate models for quantifying drug release. Using the boundary conditions for thin films suggested by Crank (Crank 1979), the one-dimensional solution to Fick's second law becomes a release versus time relation as shown in equation 3, in which M_∞ is the amount of drugs released at infinite time, D is the diffusion coefficient of drugs in the film, and L is the film thickness.

$$\frac{M_t}{M_\infty} = 4 \left(\frac{Dt}{\pi L^2} \right)^{0.5} \quad \text{Equation 3}$$

Equation 3 is one form of the famously known “square root of time” release kinetics and is often used to describe drug release controlled by Fickian diffusion. It is also important to note that the use of one-dimensional solutions to the Fick's law requires the assumption that the surface of the nanofibre membrane in the length and width directions is much greater than its thickness, such that edge effect can be disregarded (Siepmann and Peppas 2011). The use of such release models also requires the drugs to be uniformly distributed among the matrix and that no drugs are accumulated in the liquid around the membrane.

Another commonly used model for describing diffusion-controlled release is the Higuchi equation, which has been one of the first relationships for quantifying drug release from films and perhaps the most popular one in relevant literature since its publication in the 1960s (Siepmann and Siepmann 2008). Like Crank's solution to Fick's second law, Higuchi also assumed one-dimensional release from a thin film and that the media surrounding the film is a

perfect sink with no drug accumulation. In addition, Higuchi assumed that the drug concentration in the film is much greater than its solubility in the surrounding fluid, such that long time is required for drug molecules far from the film surface to dissolve, thereby creating a pseudo-steady-state (Siepmann and Siepmann 2008). A schematic representation of drug concentration-distance profile under Higuchi's assumptions is shown in Figure 9 below, in which the film contains drug at concentration C_{ini} , with its surface in contact with a perfect sink at concentration zero.

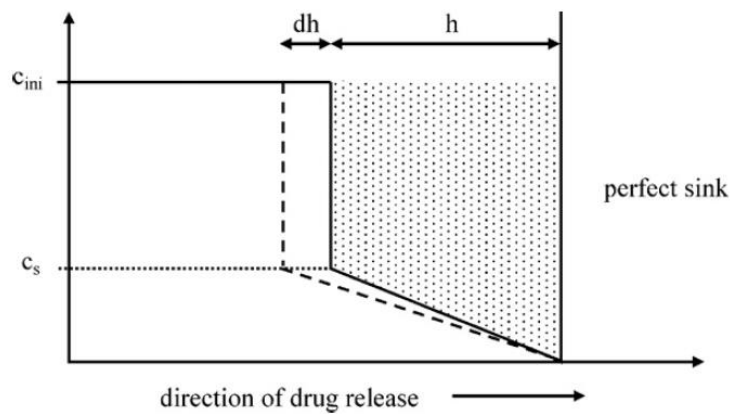


Figure 9: Schematic representation of the drug concentration vs. distance profile at pseudo-steady-state. Image obtained with permission from (Siepmann and Peppas 2011)

At a distance h from the surface of the film, the drug concentration will be reduced to the maximum concentration soluble in the matrix, C_s , while the rest is leached into the fluid. As more drug molecules are leached out, h will expand until only drug molecules that are soluble in the matrix remain. Using the trapezoidal geometry of the concentration profile, the amount of drugs released at a given time can be interpreted as:

$$\frac{M_t}{A} = h \left(C_{ini} - \frac{C_s}{2} \right) \quad \text{Equation 4}$$

In which A is the surface area of the film. During a given time interval dt , the distance h will expand by dh , which can be determined by isolating from the derivative of equation 4. Since this

system is under pseudo-steady-state, Fick's first law of diffusion can be employed to help find the time-dependence of h , which ultimately leads to the Higuchi equation:

$$\frac{M_t}{A} = \sqrt{2C_{ini}C_S D t} \quad \text{Equation 5}$$

$$M_t = K_H \sqrt{t} \quad \text{Equation 6}$$

Since C_S and D are not always immediately known, equation 5 is often represented in a more general form in the literature, as shown in equation 6. The simplification on the Higuchi equation serves as a simple empirical tool for fitting experimental release data to theoretical models. However, as pointed out by Siepmann and Peppas in their recent work, misconceptions may occur as a result of oversimplification of theoretical models (Siepmann and Peppas 2011). For example, both the Higuchi model and the Crank's solution follow the square root of time (denoted SRT in this thesis) release kinetics, which means data that fit equation 6 can apply to both interpretations of diffusion-controlled release. In fact, many drug release systems that follow the behavior represented in equation 6 has been described as obeying the Higuchi model in literature, even though the underlying assumptions may be closer to Crank's solution instead. Siepmann and Peppas therefore warned that oversimplification can undermine the theoretical basis on which release models are built.

One of the important assumptions made in SRT release models is that the porous matrix remains constant throughout the diffusion process with no swelling. Several studies have shown that the use of several hydrophobic matrix polymers, including PCL and PCLEEP, can lead to agreement with SRT kinetics (Chew, Wen et al. 2005). However, many polymers for biomedical applications undergo swelling in water or body fluid, during which drugs can be released through relaxation of the polymer chains, and release kinetics such as the Crank and Higuchi solutions will no longer apply. Siepmann and Peppas suggested that the water uptake during

swelling is linearly related to time (Siepmann and Peppas 2011), and also the drug transport from a swelling polymer carrier is the sum of the drugs transported through diffusion and those through carrier relaxation, leading to equation 7 below, in which K_1 is the diffusional rate constant and K_2 is the relaxation rate constant. In subsequent studies, the equation has since been written in the more general form shown in equation 8 below.

$$M_t = K_1\sqrt{t} + K_2t \quad \text{Equation 7}$$

$$\frac{M_t}{M_\infty} = K_M t^n \quad \text{Equation 8}$$

Equation 9 is known as the power law, in which n is the rate exponent, which indicates the relative contribution from the diffusional component versus the relaxation component (Korsmeyer, Gurny et al. 1983). For a film-like geometry, a value below 0.5 for n indicates that the system follows Fickian diffusional release behavior, whereas a value of 1 indicates release purely due to matrix relaxation, and any values in between indicate a combination of both effects. For cylindrical geometries, the threshold n values for purely diffusional and relaxation release become 0.45 and 0.89, respectively, whereas those for spheres are 0.43 and 0.85 (Korsmeyer, Gurny et al. 1983). By rewriting the equation in the more general form as in equation 8, parameterization using drug release data can be done much more easily by taking the logarithm of both sides of the equation, thereby providing a simpler tool for empirically estimating the drug release mechanism. For many nanofibre drug delivery systems, the value of n would depend on the swelling properties of the scaffold, which relates to the hydrophilicity of the polymer matrix.

Drugs may not always be released through surface desorption or diffusion, as they may be entrapped within the fibres, especially for those that have large molecular sizes or those that have high solubility in the matrix but low solubility in water. In this case, drug release may occur

via the eventual erosion of the matrix when drug molecules are released into the surrounding fluid. Erosion of the matrix occurs through either enzymatic or hydrolytic degradation which have been described in section 1.1.7. As chains in the polymer matrix cleave, those that reduce to sufficiently small lengths may be able to diffuse out of the matrix, leading to bulk matrix loss. Several quantitative models have been suggested to describe drug release via matrix erosion. For example, the Hopfenberg model, shown in equation 9, is one of the popular ones due to its simplicity (Hopfenberg 1976).

$$\frac{M_t}{M_\infty} = 1 - \left(1 - \frac{k_0 t}{C_0 a} \right)^m \quad \text{Equation 9}$$

In formulating the model, Hopfenberg assumed that drug release is proportional to the matrix surface area that changes with time, and that the erosion process follow zero-order kinetics on a slab-like matrix. The resultant Hopfenberg model is shown in the equation below, in which k_0 is the erosion rate constant, C_0 is the initial drug concentration, and a is a geometric constant. The exponent m depends on the geometry, where $m = 1$ for slab-like matrices, $m = 2$ for cylinders and $m = 3$ for spheres. However, the use of the Hopfenberg model requires the assumption that surface area of the matrix changes immediately and uniformly after immersion, which is often not the case especially for less water-soluble polymers. In a later study involving marginally water-soluble matrices, Heller and Baker suggested that drug diffusion plays a significant role in the overall release behavior, especially in the early stage before the onset of bulk degradation (Heller and Baker 1980). Using PLA and PLGA matrices as examples, the authors showed release behaviors that follow an SRT release kinetics initially, followed by a rate decrease as the diffusion distance increase, and finally increases again as the matrix becomes more permeable following bulk erosion. In another study, Lee formulated another model based on movements of a diffusion front and an erosion front (Lee 1980). In verifying his model, Lee showed that release behavior depends greatly on the drug solubility in the matrix. When the

drug concentration in the matrix is much higher than its solubility, the release behavior approaches zero-order kinetics shown by Hopfenberg. However, as the ratio of initial drug concentration versus drug solubility decreases, the release profile began to resemble diffusional release.

Figure 10 below summarizes the models described thus far in a simple graphical representation, assuming 5-day release for all mechanisms.

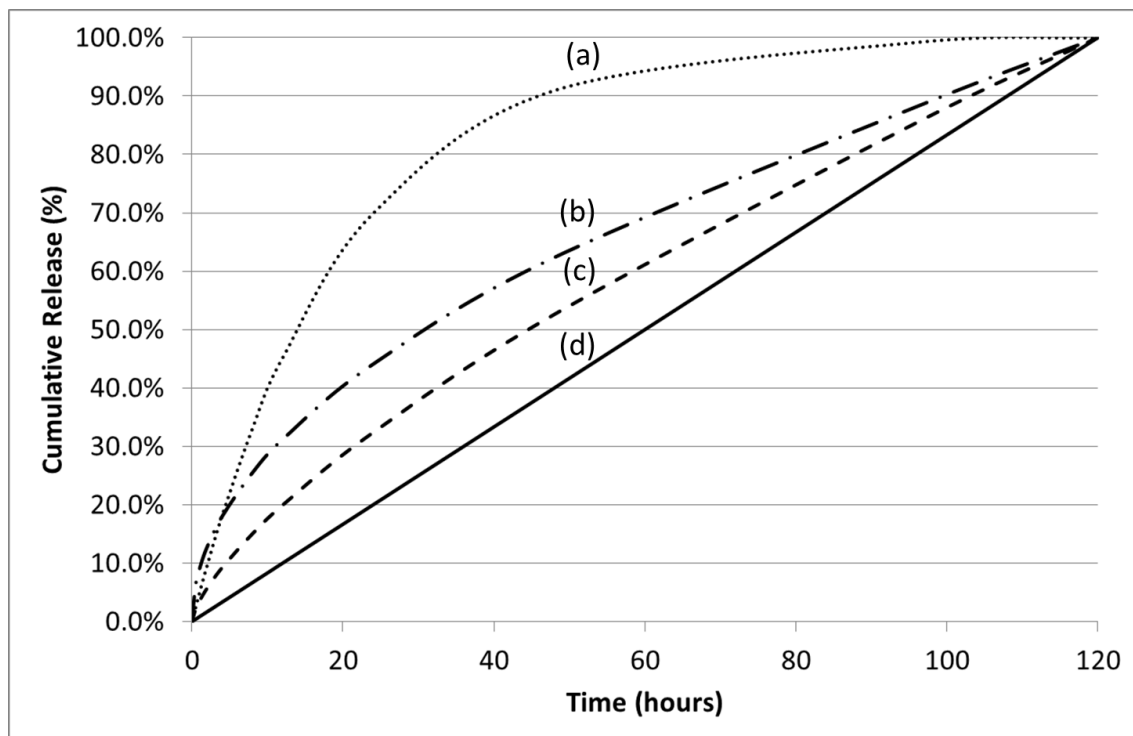


Figure 10: Graphical representation of theoretical release profiles for (a) surface desorption controlled release with $n = 0.7$, (b) square root of time diffusion release, (c) mixed diffusion-swelling release with $n = 0.7$, and (d) swelling or erosion controlled zero order release.

While many models have been proposed to describe drug release kinetics via different release mechanisms, it is important to note that in many practical systems, a combination of release from surface desorption, diffusion, and erosion is at play, and the use of the models described in this section are only a first step in approximating the release behavior from systems in which

one of the release mechanisms is rate-limiting. Any attempt to elucidate the dominant release mechanisms using these models must also be supported by other physical evidence. In addition, the empirical nature of these models renders them unsuitable as predicative tools for drug release from a new system. However, these models can be useful tools in quantitatively analyzing experimental drug release data, while allowing comparison between similar systems to observe the effect of material and process parameters on release.

1.1.12 Factors Controlling Drug Release

Matrix material choice plays a significant role in determining the mechanism and kinetics of drug release, with deciding factors including their hydrophilicity, molecular structure, degradation and drug compatibility. Among these factors, matrix compatibility with drugs is one of the most important one that could dictate material choice. Compatibility between the matrix polymer and drugs is required for a homogeneous mixture for facilitating diffusion or degradation-controlled release. If the drug has high solubility in the matrix, a solid solution may be formed in which drug molecules are dispersed within the matrix at the molecular level. On the other hand, if the drug has low solubility in the matrix, a solid suspension may be formed in which drugs solidify throughout the matrix, leading to two distinct phases (Gilchrist, Rickard et al. 2012). Also, if the amount of drug loading into a matrix is higher than its solubility in the particular matrix, the excess may also be crystallized throughout the matrix, as observed by Cui et al when an increasing amount of paracetamol was loaded into PLA. Differentiation between solid solution and suspension can often be made through thermal analysis such as differential scanning calorimetry (DSC) and X-ray diffraction (XRD) (Cui, Li et al. 2006), since drug molecules in solid solutions can lead to change in glass transition temperature (T_g) as well as crystallinity in the matrix, whereas solid suspensions can exhibit two distinct phases. In solid solutions, there is

stronger interaction between the drug and matrix which favors more sustainable release. Nanofibre formation via the electrospinning technique may also be effective in avoiding drug crystallization, due to the rapid solvent evaporation during electrospinning as a result of the whipping motion generated by the decreasing bending stability as the fibre jet travels towards the collector. The potential in reducing drug crystallinity in electrospun nanofibres over other forms such as films may help explain the reduction in burst release when comparing between films and nanofibres of the same formulations. In a study on ibuprofen release from zein nanofibres, Huang et al showed that ibuprofen was dispersed in the matrix as solid solution, with the resultant release profile exhibiting combined diffusion-swelling kinetics with no major burst release (Huang, Zou et al. 2013). In a similar study, Zeng et al compared the release of anticancer drugs doxorubicin hydrochloride and paclitaxel from PLA (Zeng, Yang et al. 2005). The doxorubicin hydrochloride, which formed a solid suspension in PLA, showed significant burst release whereas the paclitaxel, which formed a solid solution in PLA, showed a stable, near zero-order release. In many other studies where the nature of drug dispersion is not characterized, a general trend can be seen in which burst release tend to occur when hydrophilic drugs are dispersed in hydrophobic matrices. In a study on the antibiotic cefoxitin sodium release from PLGA/PLA nanofibres, Kim et al showed that burst release can be reduced by adding a poly(lactic acid) – poly(ethylene glycol) (PLA-b-PEG) copolymer which contains a hydrophilic phase, highlighting the need for hydrophilic polymers to support hydrophilic drug release (Kim, Luu et al. 2004). In a later study, Gandhi et al demonstrated the release of a mixture containing the hydrophilic BSA and an anti-integrin antibody from hydrophobic PCL, and characterized the resultant rapid release as surface-desorption controlled (Gandhi, Srikar et al. 2009).

In addition to the matrix-drug compatibility, the hydrophilicity of the nanofibre matrix itself also contribute significantly to the release rate especially the extent of burst release, as it affects the

rate at which fibres are swollen with body fluid, thereby dictating the rate at which drugs on the fibre surface are transported away. As a result, polymer hydrophilicity is another important consideration in selecting nanofibre matrix, after drug-polymer compatibility is confirmed. Usually, matrices that swell more easily tend to facilitate faster release due to quick desorption of drugs from fibre surface, through quicker polymer chain relaxation. In several studies on the highly hydrophilic poly(vinyl pyrrolidone) (PVP), anti-inflammatory drugs such as ibuprofen and ketoprofen were released completely within minutes, even though the authors observed that the drugs were not crystallized on the PVP nanofibre surface (Yu, Shen et al. 2009, Yu, Branford-White et al. 2010). In particular, Huang et al showed that the release of ketoprofen from PVP nanofibres followed zero-order release kinetics (Huang, Branford-White et al. 2012), suggesting that the quick release is a result of either quick swelling or quick erosion of the matrix. Another example of a highly hydrophilic nanofibre matrix is PVA, with which studies have shown can lead to release of vitamins and ketoprofen ranging from minutes to hours (Kenawy, Abdel-Hay et al. 2007, Li, Kanjwal et al. 2013). Other polymers that are commonly used for biomedical applications, such as PLGA, PLA, and PCL, are less hydrophilic than PVA and PVP. Accordingly, these hydrophobic polymers tend to support longer release durations in the range of days to several weeks. In addition, when the degree of crystallinity of these matrices were increased, via heat treatment or methanol soaking, release rate decreases due to the reduction in chain relaxation (Kenawy, Abdel-Hay et al. 2009). However, the overall drug release also reduces as a result of increased crystallinity, leading to entrapment in the nanofibres. PCL can be rendered more hydrophobic by forming a copolymer with ethyl ethylene phosphate (PCLEEP). In a study by Chew et al, PCLEEP nanofibres facilitated release of neural growth factor for over 90 days, and the resultant release profile followed power law kinetics with a coefficient that weighs towards diffusive release (Chew, Wen et al. 2005).

As drug release rate is dependent on the ability of molecules to diffuse through or desorb from matrices, or the erosion rate of the matrices themselves, molecular weight of drugs and matrices also affect the design of a drug release system. Intuitively, greater molecular weight can often reduce the drug release rate. For nanofibre matrices, larger molecular weight adds impedance against drug diffusion. In terms of drug molecules, Taepaiboon et al conducted a comprehensive study on the effect of drug molecular size by comparing the release of four anti-inflammatory drugs with different molecular weights and water solubility, as shown in Table 1, from PVA nanofibres (Taepaiboon, Rungsardthong et al. 2006).

Table 1: Release comparison between four anti-inflammatory drugs from PVA nanofibres

Drug	Molecular Weight	Water Solubility	Total Drug Release
Sodium Salicylate	160.1 g/mol	Highest	97%
Diclofenac Sodium	318.1 g/mol		76%
Naproxen	230.3 g/mol		98%
Indomethacin	357.8 g/mol	Lowest	42%



While drug water solubility has affected the release behavior, Taepaiboon et al suggested that the drug molecular weight played a more significant role in both the release rate and the amount of cumulative release, especially considering that naproxen, with its lower water solubility, achieved a faster release and higher total release than diclofenac sodium. In subsequent studies involving growth factors, with molecular weights tens to hundreds-folds larger than those studied by Taepaiboon et al, researchers were able to show stable release over weeks to months, such as the study by Nie et al on BMP-2 release from PLGA nanofibres, in which stable release over 60 days was achieved (Nie, He et al. 2009).

Drug-matrix interaction can also be aided by bond formations. One of the most common drug-matrix interactions is hydrogen bonding formed between hydroxyl groups of the matrix and the amino groups of drug molecules (Taepaiboon, Rungsardthong et al. 2006). However, the study by Taepaiboon et al showed that formation of hydrogen bonding between sodium salicylate and PVA had minimal effect in controlling the release rate, as it experienced rapid burst release compared to naproxen and indomethacin which do not form hydrogen bonds with PVA. In addition to hydrogen bonding, drug molecules or matrices can also be modified to facilitate covalent bonding, although this has only been demonstrated with larger molecules such as peptides and growth factors (Casper, Yang et al. 2007, Yoo, Kim et al. 2009). However, due to the permanent nature of the bonds, covalently bonded molecules on nanofibres may not release, as shown in the study Casper et al on fibroblast growth factor (FGF-2) loaded collagen nanofibres. Moreover, covalent bonding formation from the drug molecule may also deactivate functional groups required for therapeutic effects (Biondi, Ungaro et al. 2008). A recent study by Nitanan et al also attempted to control drug release via ion-exchange processes (Nitanan, Akkaramongkolporn et al. 2013). By binding cationic drugs on sulfonated polystyrene nanofibres via electrostatic effect, Nitanan et al showed stable drug release via ion exchange in saline solutions, which followed diffusion kinetics. However, the system suggested by Nitanan et al required specific charge properties on both drug molecules and fibres, thereby limiting the applicability on other drugs. In addition, since ion exchange is an equilibrium-driven process, drug release may not be complete if equilibrium in the ion displacement reaction is reached. Indeed, in Nitanan's study, total release of the five model drugs ranged from 53% to 77% as a result of the reaction reaching equilibrium while drug molecules remained on the fibres.

In addition to matrix and drug choices, processing parameters such as fibre diameter has also been experimentally shown to affect tortuosity for solvent penetration and therefore the drug

release rate (Katti, Robinsin et al. 2005). In general, thinner fibres contain more surface area such that a higher portion of loaded drugs can be reached by penetrating fluid, leading to higher release rates either via diffusion or surface desorption. The inverse relationship between decreasing fibre diameter and increasing drug release rate has been shown in various studies in the past, such as Song et al's study on rifampicin-loaded PLGA (Song, Gao et al. 2012), Xie et al's study on tetracycline hydrochloride-loaded PLA (Xie and Wang 2006), and Ranganath et al's study on paclitaxel-loaded PLGA (Ranganath and Wang 2008). However, these studies also showed that while drug release was faster, the total release from thinner fibres was higher than their thicker counterparts. Similar to the comparison between nanofibres and cast films, thicker fibres are less penetrable by fluids and therefore may retain drugs that are essentially entrapped inside the matrix. While entrapped drugs may be able to diffuse out of the matrix, the process is much slower and less uniform than the liquid state diffusion of drugs away from the fibre surface. While there are methods to enhance inter-fibre and intra-fibre porosity, current studies do indicate that thin fibres are more efficient drug carriers than thicker ones. However, with current studies showing that the slower burst release of drugs loaded in thicker fibres are also met with lower overall release, it is apparent that the real effect of fibre diameter on drug release remain an open question.

1.2 Knowledge Gap and Research Scope

The current study aims to formulate a nanofibre-based wound dressing design approach to facilitate incorporation and optimal release of a new generation of therapeutic agents. Using kynurenine as an example to demonstrate the development process, a new product can be created that addresses the challenges in wound healing control. In traditional treatments for acute wound healing, the main objective was to prevent infections that would render the wound

chronic, whereas for chronic wound treatment, the main objective was to stimulate healing via growth factors. The kynurenine-loaded dressing proposed in the current study will instead focus on controlled healing, which is important at the later stages of the healing process. The proposed dressing would be effective for open wounds that can be acute or chronic. For acute wounds, kynurenine release would allow timely cessation of ECM production, whereas for chronic wounds, kynurenine would help alleviate the potential overproduction of ECM due to growth factor addition that might be required for ensuring healing at the early stage. The socio-economic impact of an advanced dressing that addresses controlled healing for both acute and chronic wounds is significant. Earlier literature outlined estimates that the worldwide market for acute wound care would reach US \$15.3 billion per year by 2010 (Sen, Gordillo et al. 2009). Among acute wound patients, there are reported 500,000 burn patients per year in the US requiring medical attention (American Burn Association 2009), whereas the worldwide estimates were in the 7 – 10 million patients range (Bradley, Cullum et al. 1999). The number of patients undergoing surgery also reached 40 – 50 million per year worldwide (Bradley, Cullum et al. 1999). In addition to primary care, post-treatment care and loss of productivity also present a major cost. For example, in the US, the number of chronic wound patients was estimated to be 6.5 million, which translated to an annual cost of US \$25 billion per year. With a significant market and a clear unmet need in wound healing control, new dressing designs that can optimize a new generation of therapeutics such as kynurenine will be tremendously beneficial to the public.

To design an effective kynurenine delivering dressing, it is necessary to determine how the drug can be encapsulated in the fibre matrix. Compared to other forms of application, including topical agents such as microsphere and CMC gel, application through a nanofibre scaffold is highly beneficial for scarring control. Most topical methods require reapplication after a short amount of time, and while it is possible for smaller wounds, this method can become disruptive

for larger wounds that require removal of the wound cover, and more so if the patient is under pressotherapy. The cost of medical care associated with frequent dressing change is also significant, due to the extra workload on caregivers. Kynurenine in nanofibre scaffolds, on the other hand, require less frequent reapplication if given the correct composition to support a sustained release, which can remain effective under a pressure garment for days. With its potential use for longer duration than most topical applications, release control becomes very important. The timing for stimulating MMP expression is of utmost importance due to the need to maintain an intricate balance between ECM synthesis and degradation to ensure wound closure without any FPD symptoms. If all the loaded kynurenine is released shortly after application, ECM deposition can be reduced prematurely, leading to incomplete healing. However, if kynurenine does not release within a suitable time frame, MMP expression for digesting excessive ECM components may be compromised, diminishing the scaffolds antifibrogenic ability. In the previous study by Li et al, kynurenine-loaded CMC gel were applied daily for three weeks, starting one week after wound infliction which corresponded to the onset of re-epithelialization (Li, Kilani et al. 2013). In the Li et al study, the kynurenine dosage received by the subject was $50 \mu\text{g}/\text{cm}^2$ of wound area per day. Similarly, a kynurenine-loaded nanofibre scaffold can be applied one week after injury, but by allowing for sustained release, the scaffold will not need to be changed daily, which is desirable because daily scaffold change may disrupt wound healing, and post a more significant labour cost as more caretaker attention is required for more frequent dressing change. Release duration of 3 – 5 days is therefore desired to allow for wound inspection and dressing change, while minimizing disruption to the healing process.

The major challenge in this project is the facilitation of kynurenine release over an extended period of time, as with any hydrophilic, small molecule drugs. For kynurenine, there is an added challenge that it is only soluble in aqueous solutions containing sodium hydroxide, and the choices of polymer matrix are limited to those that are compatible with aqueous phases, such as

PVA and PVP, which has been shown thus far to favour quick release ranging from minutes to hours. In addition, with a low molecular weight of 208.2 g/mol, kynurenine does not have a sufficiently large size to impede diffusion or desorption like peptides. In current literature, studies on delivery of water-soluble drugs via nanofibres remain scarce, with limited examples. Figure 11 summarizes different therapeutics that are not peptides or growth factors that have their release behaviors from nanofibres studied in existing literature.

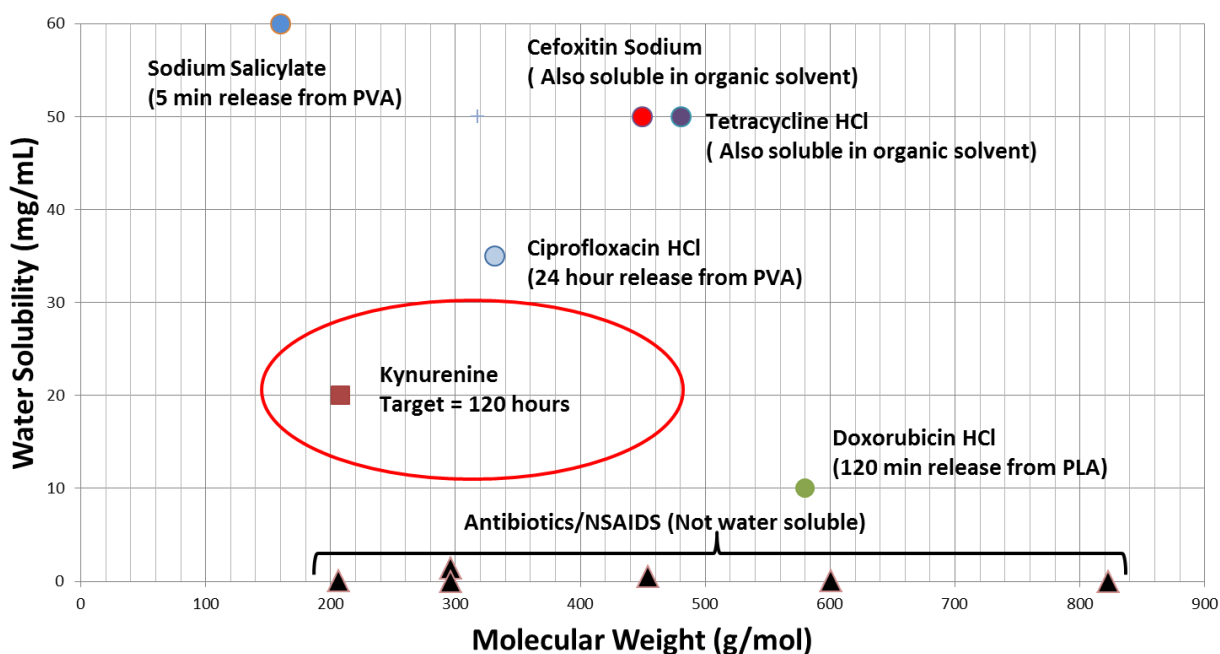


Figure 11: Summary of drugs studied as part of nanofibre controlled drug delivery systems

There are several examples in which water-soluble drug have been incorporated, but most of the existing studies have been focused on the release of water-insoluble antimicrobial agents and other non-steroidal anti-inflammatory drugs (NSAIDs) from nanofibres. Among the water-soluble drug release studies, none has been able to facilitate stable release past one day. Sodium salicylate, with the smallest molecular size, was released from its PVA carrier in less than 5 minutes (Taepaiboon, Rungsardthong et al. 2006). Antimicrobial agents such as ciprofloxacin sodium, and the cancer drug doxorubicin sodium have also been studied, but both

showed quick release within several hours. Other hydrophilic drugs, such as tetracycline hydrochloride, are compatible with organic solvents and water insoluble matrices such as PLA (Xie and Wang 2006) and PLGA (Kenawy, Abdel-Hay et al. 2009), and therefore cannot help address the challenges posed by kynurenine. Among the existing studies on water-soluble drugs, Jannesari et al was able to demonstrate a more stable release of ciprofloxacin hydrochloride by controlling the amount of drug loading, with 75-80% of the loaded drugs released in 1 day (Jannesari, Varshosaz et al. 2011), although it is still far from the duration targeted in this study. Accordingly, using current knowledge and techniques, a kynurenine-loaded nanofibre wound dressing will likely yield a rapid burst release with all drugs dispensed in a matter of hours. The development of a drug delivery system that can facilitate a controllable, stable release of such water-soluble small molecules will therefore be a significant contribution to nanofibre drug delivery technology.

From a broader perspective, successful fabrication of a nanofibre release system for kynurenine can be used as an example showing the establishment of a need-based approach in controlling drug release behavior from nanofibres. In particular, the proposed design approach will enable tailoring drug release profiles from 1 to 5 days to suit the dynamic needs for different situations and patients, such as those who are more susceptible to FPD as mentioned in section 1.1.9. In studies published thus far, achievement of specific durations of drug release has been demonstrated via altering matrix choices with different hydrophobicity or degradation rate in most cases. These methods, though suitable for antibiotics and anticancer drugs that are compatible with a wide range of polymers and organic solvents, are not applicable on hydrophilic drugs with limited material compatibility. In addition, these methods rely mainly on proper material selection and do not involve any control over material properties, limiting their flexibility in application. For example, if an antibiotic is loaded at a specific concentration in PLA, a stable release may be achieved over duration of approximately 2 weeks. However, if a

specific situation requires the release of the same antibiotic in different durations, such as 1 week, then using existing knowledge, the material must be changed, such as using the more hydrophilic PLGA as a carrier, leading to a completely different product.

When a specific drug and matrix material is considered, variations in release behaviors have also been demonstrated through changing drug concentration or fibre diameter. Drug concentration has seemingly the most significant effect on the release rate, because increasing concentration also increases the chance of drug crystallization on fibre surface which leads to burst release. However, in many clinical applications the drug dosage is not a free design variable, and it may not be possible to alter the dosage purely for achieving a specific release profile. For example, the proposed dosage for a kynurenine release system is approximately $200 \mu\text{g}/\text{cm}^2$ of wound area (Li, Kilani et al. 2013). On the other hand, while changing matrix fibre diameter has also been shown to alter release behavior especially in the burst stage, it can also lead to reduction in overall release due to drug entrapment in larger diameter fibres. As a result, the effectiveness of controlling drug release through the fibre diameter remains questionable.

Existing studies on nanofibre-based drug release systems thus far have been able to provide important fundamental knowledge on possible factors that affect drug release. However, most of them have been of proof-of-concept nature and shed limited light on how the knowledge can be applied in different systems. Specifically, questions remain on how the current knowledge can be applied in designing a system when there are specific requirements on release duration, drug dosage, and drug-matrix compatibility. As a result, the target outcome of the current study on kynurenine releasing scaffold is a set of guidelines in designing future nanofibre drug carriers that are fully compatible with the drug and can be tailored to suit specific needs for different skin and eventually other tissue applications. Such an outcome will be tremendously useful for

development of drug carriers for the emerging area of small molecule therapeutics which require much more specific release properties than the antibiotics used currently.

This dissertation will discuss in detail the development of a nanofibre carrier for kynurenine that is capable of supporting stable release ranging from one to five days. The study will rely mainly on single-nozzle electrospinning techniques, as it remains the most scalable electrospinning technique yet. Moreover, there is no strong evidence suggesting that other techniques such as coaxial core-shell electrospinning can significantly delay the release of small molecules such as kynurenine, since most existing work on core-shell nanofibre carriers has focused on protein delivery. The study will also attempt to incorporate drugs only by direct blending with the matrix, again for scalability because a homogenous solution can readily be utilized in emerging mass-electrospinning techniques such as multiple nozzles (Gangwal and Wright 2013), upward needleless electrospinning (Yarin and Zussman 2004), and bubble electrospinning (Liu and He 2007), which are all aimed at increasing the number of fibre jets that can be drawn from a given polymer solution.

1.3 Project Objectives

The investigations that will be conducted in this study were designed to examine several hypotheses generated upon reviewing existing literature. The hypotheses are as follows:

- 1) Proper material selection will help identify polymer matrices that are compatible with the drug of interest. The suitability can be verified by examining drug encapsulation, drug-polymer interaction, and drug release.

- 2) Without changing the drug carrier matrix material, it is possible to control both the release duration and extent of burst release by modifying the material via processing or addition of supporting materials.
- 3) The use of continuous nanofibres is beneficial for forming a wider variety of planar and non-planar structures. Such flexibility in structure allows drug-loaded nanofibres to help close a variety of open wounds, which is especially beneficial to patients who are more susceptible to complications such as FPDs.

The first step of the study will be to select a suitable matrix for kynurenine, which would begin with a theoretical approach using solubility parameters that will identify a material candidate, followed by fabrication via electrospinning and validation of the candidate material use with kynurenine through release behavior analysis and detailed characterization of drug-polymer interaction. Here, the release models discussed in section 1.1.11 would be relied on as indicators of possible release mechanisms and extent of burst release. It is important to note that due to the empirical nature of the release models used, they cannot be used as a theoretical explanation or as a precise predicative tool for release behavior. The results from this part of the study will support the coupled use of empirical release models and drug-polymer characterization as a tool for describing release mechanism and behavior. Subsequently, the discussion would focus on the release control aspect of the development, and the effect of different material and processing parameters on the release behavior would be observed. The discussion on release rate control would also expand into investigating the effect of matrix modification such as crystallization and crosslinking, as well as incorporation of barrier layers in a composite matrix design, which have never been comprehensively explored in literature thus far. It will be shown, in the release rate control discussion, that stable release over the desired duration can be achieved with the selected material system, and the fabrication and modification parameters can be controlled to tailor release within the one to five day range. The result of

these investigations is the realization for methods for controlling drug release via controlling material and processing parameters, and knowledge on the relative effects of each parameter that impacts release behavior. Finally, the applicability of the carriers developed using the design process outlined in this dissertation would be discussed, with two candidate forms proposed, including planar dressings and braided sutures. The mechanical properties of these forms would be compared to commercially available products as a validation step to ensure they can be applied and handled like existing wound dressing products. A detailed development flowchart is shown in Figure 12.

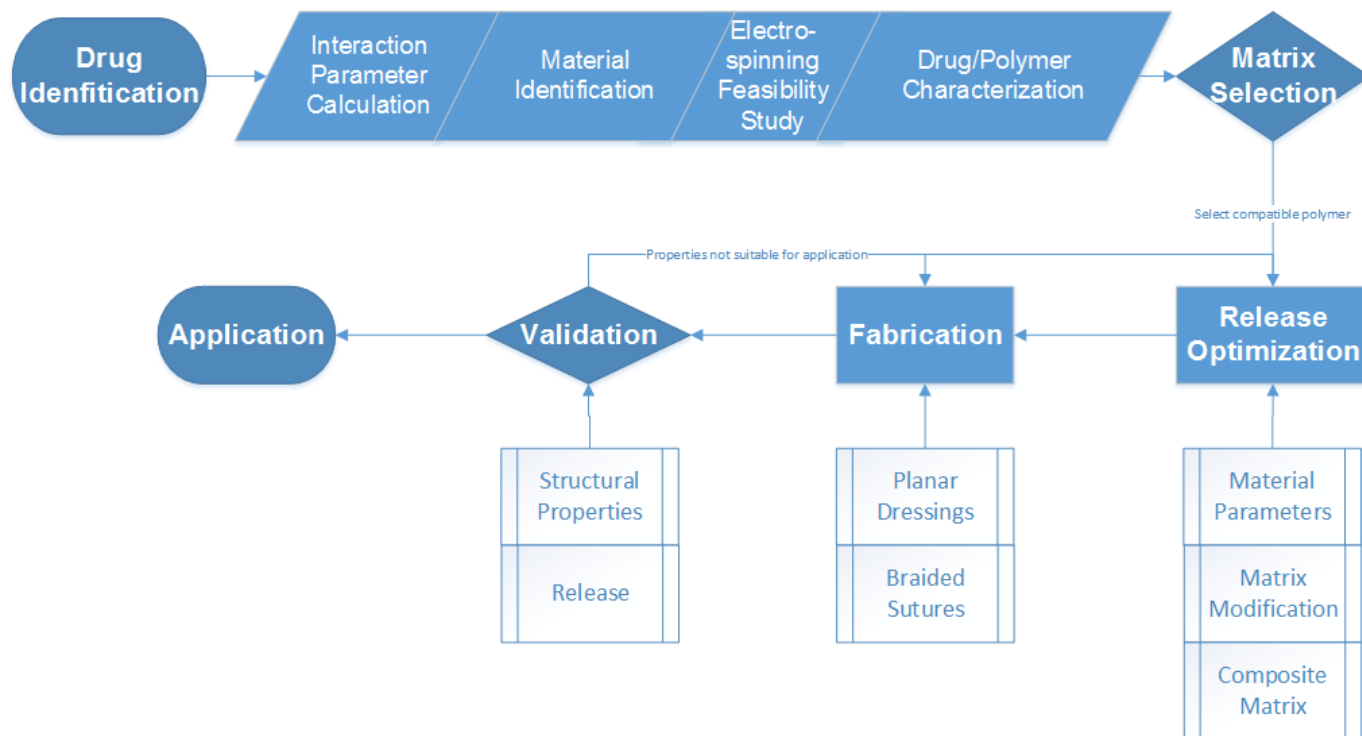


Figure 12: Nanofibre wound dressing development flowchart

2 Matrix Selection for Kynurenine-Loaded Nanofibre Scaffold

2.1 Introduction

Success in the development of kynurenine-loaded nanofibres would rely heavily on the ability to facilitate sustained release of hydrophilic small-molecule drugs over durations of more than one day. This is an area in drug delivery that remained largely unexplored. Before any release control methods are formulated, it is important to first identify the material platform for supporting kynurenine loading. The two pressing questions that need to be addressed are which material and in which form should be used to carry kynurenine. As stated in the previous section, electrospun fibres are examined in this study due to its manufacturability, connectivity, scalability, and drug-loading efficiency. The only question that remains is the material choice. Compatibility between kynurenine and the polymer carrier is of utmost importance. Previous studies on fibrous drug scaffolds have shown that when the drug is not compatible with its carrier, it tends to crystallize on fibre surface, resulting in immediate release of all loaded drugs. The search for a compatible carrier for kynurenine can be conducted via a combination of theoretical and experimental approaches. As a starting point, theoretical calculations were conducted to determine the solubility of kynurenine in a range of polymers, as drug solubility is a good indication of its compatibility with the carrier. High solubility of kynurenine in the candidate polymer could indicate formation of an amorphous solution or dispersion, which may suppress burst release as opposed to a solid dispersion. Next, to verify theoretical calculations, drug – polymer mixtures can be electrospun into fibres for drug release tests. Comparisons can be made using polymers with low drug solubility as a negative control to confirm the effect of using compatible polymers on reducing burst release. Theoretical calculations such as solubility parameters have been used in literature to characterize drug delivery systems and identify the

nature of drug encapsulation. Liu et al relied on solubility parameters to select polymers to be used as films and micelles for Ellipticine delivery (Liu, Xiao et al. 2004). However, theoretical calculations have not been routinely used in drug delivery material selection since, especially in nanofibre-based formulations. The goal of the current work, in addition to finding a suitable carrier for kynurenine, is to establish solubility parameter calculation as a useful tool in the material selection process for nanofibre drug carriers.

Identifying a suitable carrier for kynurenine is only the first step. Methods for extending and controlling release rates must also be considered. While previous studies have determined a range of material and processing parameters that can affect drug release rates, such as carrier hydrophilicity, fibre diameter, and carrier degradation, the current work seeks to facilitate controlled drug release through first determining and then manipulating the drug release mechanisms. In literature involving drug release from electrospun fibres, there has not been a consistent method for determining release mechanisms, while most studies relied on fitting release data with empirical release models, such as the square-root-of-time and desorption models, to determine the dominant release mechanism. However, as Siepmann and Peppas (Siepmann and Peppas 2011) pointed out, many assumptions have been made in deriving empirical models and determining release mechanisms purely based on correlation with these models without taking the assumptions into consideration may lead to misrepresentation of the carriers' behaviors in real life. While empirical models will still be employed in the current study, physical, chemical and thermal characterizations will be used alongside as supporting tools for rationalizing the determination of release mechanism. For example, comparison between release rate and carrier degradation rate can help determine the role of erosion on the release behavior. In addition, fourier-transform infrared (FTIR) spectroscopy can be used to identify chemical bonds formed between the carrier and any functional additives. X-Ray Diffraction (XRD) and differential scanning calorimetry (DSC) have also been used in drug delivery studies

to determine whether the drug is dispersed as an amorphous or crystalline phase and if it is miscible with the carrier. This study will also explore the feasibility in using time of flight secondary ion mass spectroscopy (ToF-SIMS) as a tool to determine drug distribution in the carrier, thereby providing important hints for elucidating drug release mechanisms from observed data.

The battery of chemical and thermal characterization can help determine the nature of drug encapsulation in fibres as well as drug-polymer interaction, which can provide more concrete insights on the drug release behavior, as opposed to speculations provided by fitting release models. Using the methods proposed in this study, arguments on whether release is controlled by desorption, diffusion, or matrix erosion can be made with experimental evidence. A more rigorous determination of kynurenine release mechanism from electrospun fibres will set a strong foundation for subsequent phases of the current work when this knowledge is used to manipulate the carrier material in order to tailor specific release profiles.

The study will begin with solubility calculations to identify candidate polymers to be used as carriers. The top candidate will be electrospun with kynurenine into fibrous dressings, which will then be subjected to physical, chemical and thermal characterization. The kynurenine release behavior will also be assessed via release assays. Characterization and release assay results will help elucidate the extent of drug encapsulation, whether kynurenine is well dispersed in the matrix or crystallized on the surface. In addition, when combined with the use of empirical models established in previous studies, analysis on the dominant drug release mechanism will be conducted.

2.2 Methods

2.2.1 Solubility Calculation

Compatibility between kynurenine and the polymer carrier was approximated by calculating the Flory-Huggins interaction parameter (χ_{sp}) between the two phases using equation 11 below, in which V_s is the molar volume of kynurenine, R is the ideal gas constant, and T is the temperature.

$$\chi_{sp} = (\delta_{drug} - \delta_{polymer})^2 \frac{V_s}{RT} \quad \text{Equation 10}$$

The Flory-Huggins parameter is proportional to the enthalpy of mixing between two phases (Huggins 1942, Brown, Nanney et al. 1989, Fried 2003, Flory 2004). Therefore, a lower value would indicate favorable mixing between kynurenine and the carrier whereas a larger value would indicate phase separation. For kynurenine to be considered soluble in the carrier, the Flory-Huggins parameter must be less than 0.5 (Bicerano 2002).

$\bar{\delta}_{drug}$ and $\bar{\delta}_{polymer}$ are the solubility parameters for kynurenine and polymer matrix, respectively, suggested by Hilderbrand and Scatchard for predicting solvency between solute and solvent (Hildebrand and Scott 1964). The Hilderbrand-Scatchard solubility parameters were based on van Krevelen's definition of cohesion energy of molecules (Van Krevelen and Te Nijenhuis 2009), and can be obtained by summing the squares of bond forces resulting from dispersion (δ_d), polar (δ_p), and hydrogen bonding (δ_h), as shown in equation 11.

$$\delta_{total}^2 = \delta_d^2 + \delta_p^2 + \delta_h^2$$

Equation 11

The bond forces are themselves depending on the molar dispersion constant (F_{di}), polar attraction constant (F_{pi}), and hydrogen bonding energy (E_{hi}).

$$\delta_d = \sum \frac{F_{di}}{V}$$

$$\delta_p = \frac{(\sum F_{pi}^2)^{1/2}}{V}$$

$$\delta_h = \left(\sum \frac{E_{hi}}{V} \right)^{1/2}$$

Equation 12

As this study is the first to examine solubility of kynurenine, values for molar dispersion and polar attraction constants, as well as the hydrogen bonding energy are not available in literature. These values were determined through the group contribution method using the data in the work of van Krevelen (Van Krevelen and Te Nijenhuis 2009). Briefly, F_{di} , F_{pi} and E_{hi} values of each chemical component of a kynurenine molecule were found and then their sums were used to determine the Hilderbrand-Scatchard solubility parameters. The calculated kynurenine solubility parameter was then applied on equation 10 to determine the required range of matrix solubility parameter that will satisfy the $\chi_{sp} < 0.5$ requirement. Candidate matrix materials can then be identified through a search for experimentally obtained solubility parameter values for various polymers in existing literature, summarized in Appendix 1.

2.2.2 Electrospinning

After initial screening for candidate materials via solubility calculation, suitable carrier polymers and corresponding solvents were purchased through Sigma Aldrich. Kynurenine, also purchased from Sigma-Aldrich, was dissolved in 1 M sodium hydroxide at a range of concentration from 0 to 75 mg/mL. After ensuring full dissolution of kynurenine in sodium

hydroxide, the solution was neutralized to pH 7 using 13 M hydrochloric acid. The neutralized drug solution was then added to a compatible solution containing the carrier polymer at an appropriate concentration. In all samples, 1 mL of kynurenine solution was added to 9 mL of polymer solution to create a 10 mL electrospinning solution. The resultant drug-polymer mixture was then loaded into a Katotech electrospinning unit in a glass syringe fitted with an 18 gauge needle. The electrospinning solution was charged by a high-voltage power supply inside the electrospinning unit to 15 – 25 kV through the syringe needle, while the solution was being pumped at a rate of 0.3 – 1.5 mL/hr. Electrospun fibres were collected onto a 10 cm x 10 cm area of an aluminum plate collector to keep fibre membrane thickness and drug concentration consistent.

2.2.3 Drug Release Assay

Kynurenine release from electrospun fibrous membranes can be assessed spectrophotometrically through light absorption. The goals of the drug release assay are to determine if kynurenine is inside the membrane, to loosely observe if kynurenine is evenly distributed throughout the 10cm x 10cm membrane, and to obtain the drug release rate and amount at different time. To perform the assay, fibre membranes were cut into 1cm x 1cm sections, and then soaked in 1X phosphate buffered saline (PBS) solution in well-plates and incubated at 37°C. The PBS solution was removed from each well at pre-determined times and replaced with fresh PBS. The solution removed, known hereafter as the releasate, was then mixed with a solution containing p-dimethylaminobenzaldehyde (DMAB) dissolved in acetic acid. The DMAB can react with the amino group in kynurenine to form a coloured compound that can be detected by light absorption at a wavelength of 490 nm. The absorption test was performed

using a Biotek FLx800 fluorescence microplate reader. The amounts of drug released from the fibre samples was determined from an average of six measurements.

Data on cumulative kynurenine release at different time points can be fitted with each of the empirical release models discussed in section 1.1.11 to estimate the dominant drug release mechanism. Instead of visually comparing the drug release curves to the model curves, the drug release data can be plotted in different ways to assess the closeness to each of the models, as shown in Table 2 below. Each model equation was rewritten to form a straight-line equation so that release data can be plotted specifically to determine the fit to each model. In each case the variables M_t/M_∞ and t were known, but would need to be plotted in the form shown in Table 2. Example plots for demonstrating how the simplified straight-line equations are used to determine the degree of correlation to individual empirical models are shown in Appendix 2.

Table 2: Plotting method for kynurenine release data for determining fit with empirical release models

Model	Model Equation	Simplified Straight-line Equation
Surface Desorption	$\frac{M_t}{M_{d0}} = \alpha \left[1 - \exp\left(\frac{-\pi^2 t}{8\tau_r}\right) \right]$	$\ln\left(1 - \frac{1}{\alpha} \frac{M_t}{M_\infty}\right) = -\frac{\pi}{8\tau_r}$
Diffusion	$\frac{M_t}{M_\infty} = K_H \sqrt{t}$	$\frac{M_t}{M_\infty} = K_H t^{0.5}$
Mixed Diffusion and Swelling	$\frac{M_t}{M_\infty} = K_M t^n$	$\log\left(\frac{1}{K_M} \frac{M_t}{M_\infty}\right) = n \log(t)$
Matrix Erosion	$\frac{M_t}{M_\infty} = 1 - \left(1 - \frac{k_0 t}{c_0 a}\right)^n$	$\frac{M_t}{M_\infty} = \frac{k_0}{c_0 a} t$

Further simplification was made by assuming the constant α in the surface desorption model, as well as the constant K_M in the mixed diffusion and swelling model to be unity. For the matrix erosion model, the exponent m represents a geometric factor, and for slab-like geometries the factor could be assumed to be unity as well. Once the release data is plotted according to the straight-line equations shown in Table 2, its closeness to each model can be compared via the R^2 value.

In addition to the release behavior, the uniformity of drug distribution among the nanofibre membrane was measured by comparing the drug concentration in different 1 cm x 1 cm sections among the 10 cm x 10 cm membrane. The shelf life of the kynurenine and kynurenine-incorporated materials was also measured via the spectrophotometric technique, as kynurenine that has degraded could not react with DMAB. To measure shelf life, 1 cm x 1 cm sections of electrospun kynurenine-loaded PVA fibres and kynurenine-PVA cast films were kept in scintillation vials at room temperature for up to three months, and removed after different durations to measure the amount of kynurenine that remains in each sample. The electrospun fibres and film samples were also compared with a solution sample to observe the differences between kynurenine shelf life in fibres and in solution or gel.

2.2.4 Characterization

Fibre morphologies of the electrospun membranes were observed using a Hitachi S-3000N scanning electron microscope (SEM) at 5 kV accelerating voltage and 15mm working distance. Observations were made after fibre removal from the aluminum collector. Fibre diameters were measured using image analysis software ImageJ, and an average of 50 measurements was

reported for each fibre sample. In addition to fibre morphology after electrospinning, that of fibre samples removed at different time points during the drug release test were also examined via SEM. Information on the fibre morphology after soaking in PBS can be used alongside with the drug release amount observed at the same time point as a tool to help determine the release mechanism.

The presence and distribution of kynurenine in the fibres were observed using ToF-SIMS. A PHI TRIFT V nanoTOF instrument was utilized with Au¹⁺ gun operated at 30 keV with an aperture size of 200 μm . Positive spectra were acquired from a 400 μm x 400 μm area with the total ion dose less than 1012 ions/ cm^2 . Mass spectra were collected in the mass-to-charge (m/z) range of 0-1850 amu; spectra were calibrated with the known masses associated with peaks for the species H^+ , CH_3^+ , C_3H_5^+ . In the series of ToF-SIMS investigations in this study, kynurenine powder was first analyzed to identify its signature peaks, which would include one at 208.21 atomic mass units (amu), which corresponds to the kynurenine molecular weight. Moreover, it is also possible to identify peaks below 208.21 amu corresponding to different parts of the kynurenine molecule, which will be useful if parts of the kynurenine molecule is bonded to PVA, which would reduce the signal strength at 208.21 amu. Subsequently, blank PVA nanofibres and those loaded with varying concentrations of kynurenine were analyzed to identify presence of kynurenine. Since only secondary ions from the top layer of the sample surface could be analyzed by ToF-SIMS, the depth resolution is limited to approximately 2 nm. As a result, identification of kynurenine in the nanofibre samples would indicate that kynurenine resides on the fibre surface, whereas its absence would imply that kynurenine is encapsulated within the fibre. To ensure that the absence of kynurenine on fibre surface is in fact due to its encapsulation instead of its depletion from the sample, the kynurenine-loaded nanofibres were dissolved in water and a cast film of the water was analyzed. Furthermore, to gain insight on the

encapsulation effectiveness of nanofibres, a comparison was made by analyzing a cast film of PVA-kynurenine.

Formation of chemical bonds between kynurenine and the carrier polymer were determined using Fourier-Transform Infrared (FTIR) spectroscopy. For each fibre sample, 50 scans between wavenumbers 4000 cm^{-1} and 400 cm^{-1} were conducted in a Shimadzu IRPrestige-21 FTIR Spectrometer to obtain a representative spectrum. FTIR spectra for blank polymer fibre without kynurenine as well as that for pure kynurenine powder were also obtained as a comparison to the spectra for loaded fibres so that shifts in peaks corresponding to different bond formation can be observed. The objective in performing FTIR analysis is to determine if kynurenine and PVA interact via bond formation, which, according to their chemical structure, would likely be hydrogen bonding. The focus in comparing between samples would be on specific bonds that could be affected by hydrogen bond formation. First, the O-H stretching peak found at $3000 - 3500\text{ cm}^{-1}$ would indicate whether kynurenine would bond with the OH groups of the carrier polymer, which was selected as a suitable kynurenine carrier as will be discussed in subsequent sections, or whether addition of kynurenine would disrupt the hydrogen bonding between the OH groups within or between PVA chains. Moreover, hydrogen bond formation could also happen between kynurenine and the C-O groups in PVA and C=O groups in the PVAc residuals, which could be observed by changes in the peaks found in the $1040 - 1130\text{ cm}^{-1}$ and $1620 - 1670\text{ cm}^{-1}$ ranges, respectively. The changes in bond interaction would be in the form of variations in peak intensity and shifting of the peak location. As hydrogen bond formation is of interest in this investigation, it is desirable to eliminate the effect of moisture in the samples as much as possible. The nanofibre samples were stored in a vacuum oven at 50°C overnight to remove water while preventing PVA annealing which would change the bonding.

X-ray diffraction was performed on kynurenine powder and fibre samples to identify the presence of crystalline phases. A Rigaku MultiFlex XRD unit was used and samples were scanned from 2θ of 5° to 45° at a rate of $1^\circ / \text{min}$. The analysis began with kynurenine powder, which is a crystalline solid, in order to obtain its signature peaks. Analysis of blank nanofibres and those containing an increasing kynurenine concentration were then performed. The objective in comparing the XRD results between samples is to first determine whether kynurenine crystallizes in the PVA matrix, and then to identify whether it would eventually crystallize with increasing kynurenine concentration. Formation of kynurenine crystallites in the PVA matrix would be indicated by observation of sharp peaks at the same location as the ones found in the kynurenine powder spectra. However, observation of crystalline peaks is also dependent on the crystallite size, as governed by the Scherrer equation shown below, in which Φ is the crystallite size, S is a dimensionless shape factor, λ is the x-ray wavelength, β is the full width at half maximum intensity of the XRD peak, and θ is the Bragg angle. The crystallite size must be greater than Φ to be resolved by the XRD.

$$\phi = \frac{S\lambda}{\beta \cos \theta}$$

2.2.5 Thermal Analysis

The thermal properties of kynurenine-loaded fibres would be useful in determining the state of drug encapsulation by the carrier. Fibre samples were analyzed for their decomposition temperature via thermal gravimetric analysis (TGA) using a TA Instrument Q1000 Thermal Gravimetric Analyzer. Approximately 5 mg of each sample was placed on a platinum pan and then heated from 40°C to 600°C at a rate of $10^\circ\text{C}/\text{min}$ under nitrogen gas purge flowing at

40mL/min. The decomposition temperatures of the samples obtained from TGA were used as a limit for differential scanning calorimetry (DSC) analysis. DSC analysis was performed using a TA Instrument Q800 Differential Calorimeter. Approximately 2 mg of each sample was placed in an aluminum hermetically sealed pan. The samples were first heated to a maximum allowed temperature at a rate of 10°C/min, followed by cooling to 25°C. After equilibrating at 25°C, the samples were subjected to a second heating cycle to the maximum temperature at 10°C/min. The exothermic heat flow behavior at the second heating cycle was reported for each sample. The objective in the DSC analysis is to determine if the thermal response of kynurenine-loaded PVA would change with increasing kynurenine concentration, thereby indicating that kynurenine forms a solution with the matrix polymer. If the kynurenine is not mixed in with the matrix material, increasing its concentration would not cause any change in the matrix thermal behavior. In addition, glass transition temperature of the matrix polymer could also be used as an indicator of thermal behavior change, and could be determined by the middle point in the transition between the two heat capacity values.

2.3 Results

2.3.1 Solubility Calculations

The first step for determining kynurenine compatibility with polymer carriers is to calculate the dispersion, polar, and hydrogen bond forces for kynurenine molecules, which could then be used to calculate the Hilderbrand-Scatchard solubility parameter. Using the group contribution method suggested by van Krevelen, F_{di} , F_{pi}^2 , and E_{hi} were calculated to be $3160 \frac{\sqrt{MJ/m^3}}{mol}$, $781400 \frac{MJ/m^3}{mol^2}$, and 28800 J/mol , respectively. The calculation is described in further details in Appendix 1. The molar volume of kynurenine was determined to be $155.38 \text{ cm}^3/\text{mol}$. With these

parameters, equations 11-13 yielded a kynurenine solubility parameter ($\delta_{\text{kynurenine}}$) of 25.13 $\sqrt{\text{MJ}/\text{m}^3}$.

Compatible pairing between kynurenine and polymer requires a Flory-Huggins interaction parameter below 0.5. At standard application temperature of 37°C, equation 10 would suggest that the compatible polymer carrier would have a Hilderbrand-Scatchard solubility parameter close to 25.13 $\sqrt{\text{MJ}/\text{m}^3}$ or between 22.05 $\sqrt{\text{MJ}/\text{m}^3}$ and 28.01 $\sqrt{\text{MJ}/\text{m}^3}$. Polymers with solubility parameter outside of this range may phase separate upon mixing with kynurenine, leading to kynurenine crystallizing on fibre surface and subsequent burst release. Using experimentally obtained polymer solubility parameters presented in the work by van Krevelen (Van Krevelen and Te Nijenhuis 2009) and Liu et al (Liu, Xiao et al. 2004), as well as solution property requirements for electrospinning, a material screening criteria is formulated. Detailed explanation of the criteria and its application for the current study is presented Appendix 1. Using the criteria, the most suitable polymer carriers identified are poly(vinyl alcohol) (PVA) ($\delta_{\text{PVA}} = 25.8 - 29.1\sqrt{\text{MJ}/\text{m}^3}$) and poly(lactic-co-glycolic acid) (PLGA) ($\delta_{\text{PLGA}} = 23.1\sqrt{\text{MJ}/\text{m}^3}$). As a negative control, poly(vinyl acetate) (PVAc) ($\delta_{\text{PVAc}} = 20\sqrt{\text{MJ}/\text{m}^3}$) was also chosen to verify the reliability of solubility calculations.

2.3.2 Electrospinning

Having determined PVA and PLGA as suitable carriers for kynurenine, the next step is to fabricate kynurenine-loaded fibres via electrospinning. Three grades of PVA were selected for this study, all in the Mowiol series from Sigma Aldrich, including a low molecular weight ($M_w = 63,000$) low hydrolysis (88%), medium molecular weight ($M_w = 130,000$) low hydrolysis (88%),

high molecular weight ($M_w = 205,000$) low hydrolysis (88%), and medium molecular weight ($M_w = 125,000$) high hydrolysis (98%). Table 3 below summarizes the four types of PVA used in this study.

Table 3: Summary of the three types of PVA used in electrospinning

PVA Name	Average Molecular Weight (M_w)	Degree of Hydrolysis	Concentration for Electrospinning
PVA 8-88	67,000	88%	8 – 10 wt%
PVA 18-88	130,000	88%	8 – 10 wt%
PVA 40-88	205,000	88%	8 – 10 wt%
PVA 20-98	125,000	98%	10 wt%

The degree of hydrolysis in each grade of PVA is a measure of the extent of its formation reaction from poly(vinyl acetate) (PVAc) and ethanol. For example, a 88% hydrolyzed PVA would contain 88 mol% PVA in its polymer chain and 12 mol% PVAc. Figure 13 below shows the molecular structure of the partially hydrolyzed PVA polymer used in this study.

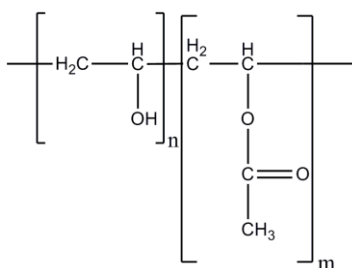


Figure 13: Chemical structure of partially hydrolyzed PVA, in which n is the fraction of PVA hydrolyzed and m is the residual ($m = 1 - n$)

For PLGA, a product grade with a lactic acid to glycolic acid molar ratio of 85:15 was selected, and its molecular structure is shown in the figure below.

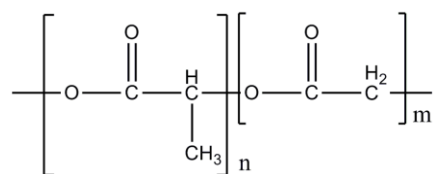


Figure 14: Structure of PLGA, containing n mol% of lactic acid and m mol% of glycolic acid.

Polymers and kynurenine were dissolved separately, with kynurenine solution prepared as described in section 2.2.2. PVA was dissolved in distilled water at a concentration of 8 – 12 wt%. PLGA, a water insoluble polymer, was dissolved in trifluoroethanol instead due to its compatibility with a low content of water. In preparation for kynurenine-loaded PVA fibres, the kynurenine solution was blended with the PVA in water solutions at a ratio of 1:9 and thoroughly mixed in a vortex mixer. For kynurenine-loaded PLGA fibres, the kynurenine solution was added to the PLGA in trifluoroethanol solution at a ratio of 1:10, and mixed in sonication bath and vortex mixer.

Electrospinning of blank PVA with low degree of hydrolysis, including the 8-88, 18-88, and 40-88, was successful for the entire range of concentrations from 8 – 12 wt% as well as a wide range of voltages (15 – 25 kV). However, PVA with high degree of hydrolysis, the 20-98, was more difficult to electrospin as the Taylor cone was only stable over a narrow range of voltages (20 – 22 kV). It has been suggested in the past that with a higher degree of hydrolysis, PVA molecules have a higher tendency to form hydrogen bonds between the alcohol groups of one another, leading to an increase in surface tension. The increase in surface tension was more pronounced when kynurenine solutions were added to the PVA 20-98 solution, when a Taylor cone could not be formed regardless of PVA concentration or electrospinning voltage. With the addition of surfactant Triton X-100, kynurenine-loaded PVA 20-98 solution could be electrospun although fibre jet formation was only stable when the solution was removed from the electrospinning chamber and mixed every three hours. When kynurenine was added to the PVA

18-88 and PVA 40-88 solutions, on the other hand, electrospinning was not impeded as both solution formed fibre successfully without requiring any surfactants. While both solutions were electrospun at a range of polymer concentrations from 8 – 12 wt%, it was found that concentrations ranging from 8 - 10 wt% yielded the most consistent fibre morphology, and 10 wt% was ultimately selected because higher polymer concentration can help improve kynurenine solubility. Table 4 below summarizes the fibre diameters and standard deviations observed on electrospun fibres from the different PVA grades at various concentrations.

Table 4: Fibre Diameters and standard deviations observed on PVA electrospun at different concentrations, average of 50 observations were presented

Polymer	Fibre Diameters		
	8 wt%	10 wt%	12 wt%
PVA 8-88	121 ± 70 nm	180 ± 54 nm	197 ± 103 nm
PVA 18-88	198 ± 49 nm	252 ± 46 nm	317 ± 74 nm
PVA 40-88	301 ± 83 nm	426 ± 78 nm	507 ± 112 nm
PVA 20-98	--	277 ± 174 nm	--

The difference in fibre diameters observed from the same polymer electrospun at different concentrations was due mainly to the difference in solution viscosity. At higher polymer concentrations, the viscosity of the solution is correspondingly higher, and if the electrospinning voltage remained unchanged, deformation of the solution droplet and fibre jet would be more difficult due to larger resistance against flow, leading to larger fibre diameters. Figure 15 below shows the morphology of PVA fibres electrospun from the four solutions.

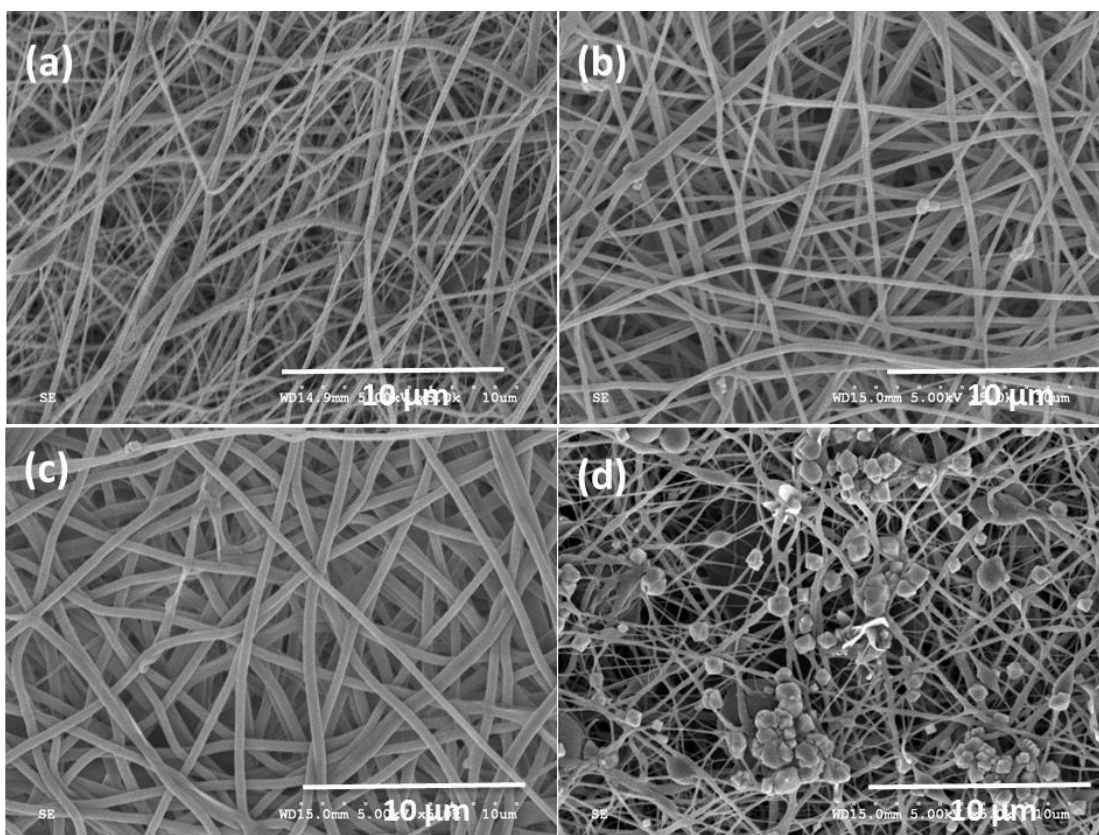


Figure 15: PVA concentration and degree of hydrolysis effect on kynurenine-loaded electrospun fibre morphology for a) PVA 8-88, b) PVA 18-88, c) PVA 40-88 and d) 20-98. SEM images were taken at 5000X magnification

In Figure 15d, the bead-like morphology resulting from the PVA 20-98 solution was the result of increased surface tension, causing imbalance between solution viscosity and surface tension during electrospinning, and the subsequent instability in Taylor cone and fibre jet formation. Correspondingly, the fibre diameter distribution of the sample spun from the PVA 20-98 was also significantly higher than those spun from other grades at the same concentration. Figure 16 also shows the kynurenine solution concentration effect on fibre morphology, with solutions containing 5 – 75 mg/mL kynurenine added to the PVA 18-88 solution at a 1:9 ratio for electrospinning, corresponding to kynurenine concentrations of 0.5 wt% to 7.5 wt% in the overall electrospinning solution.

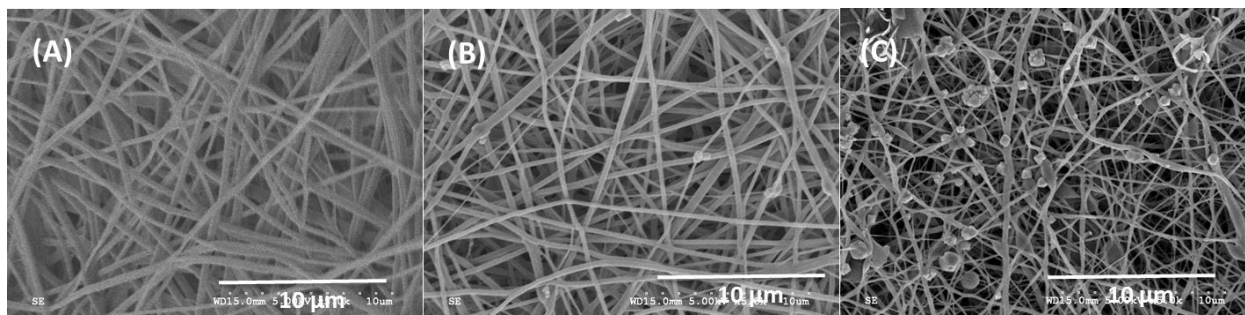


Figure 16: Effect of drug concentration at a) 0.5 wt%, b) 2.0 wt%, and c) 7.5 wt% (to overall electrospinning solution) on fibre morphology. SEM images were taken at 5000X magnification

By electrospinning a 10 mL solution of kynurenine-loaded PVA onto a collector with an area of 10 cm x 10 cm, a kynurenine loading of 0.5 wt% corresponded to 50 $\mu\text{g}/\text{cm}^2$ of fibres, whereas the 200 $\mu\text{g}/\text{cm}^2$ optimal dosage could be achieved when kynurenine loading is at 2.0 wt%. As shown in Figure 16, there are no significant changes in fibre morphology, with fibre diameters remaining mostly similar.

Electrospinning of the kynurenine-loaded PLGA solution was more difficult due to the polymer hydrophobicity. Although the trifluoroethanol solvent was miscible with water, PLGA is mildly hydrophobic, which caused the solution to phase separate. With a combination of vortex mixing and sonication, the drug-loaded solution was stable for electrospinning for a period of three hours, and the solution was removed and mixed again. Figure 17 below shows the morphology of kynurenine-loaded PLGA.

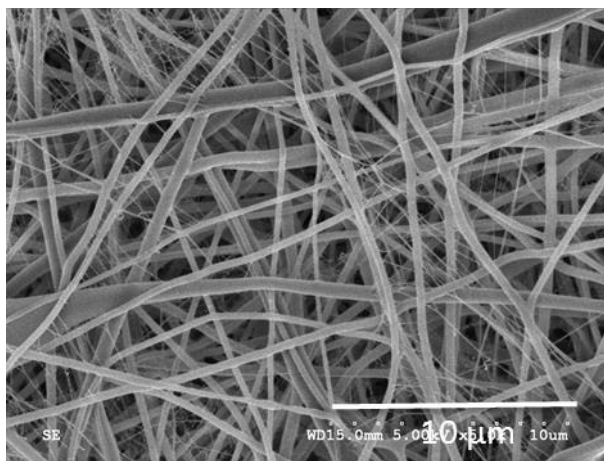


Figure 17: SEM Image (5000X) of kynurenine-loaded PLGA fibres

While the fibres are mostly uniform, several areas along the membrane showed a thin, web-like structure, which is likely a result of solution instability leading to portions with lower viscosity.

In the preparation of a kynurenine-loaded PVAc negative control, PVAc was dissolved in a mixture of water and acetic acid. However, when the kynurenine solution was added to the PVAc solution, the drug precipitated immediately, rendering the solution unable to be electrospun.

2.3.3 Kynurenine Release

The drug release assay conducted in this study was designed to observe and quantify kynurenine release from electrospun PVA and PLGA fibres, such that a release versus time curve can be illustrated. From this part of the study, it is expected that kynurenine release rate, dominant release mechanism, shelf life and uniformity of drug loading can be determined. Also, by comparing the release profiles of nanofibre samples and cast film samples, the effect of material form on the drug release behavior can be observed.

Figure 18 below shows the kynurenine release behavior from PVA fibres over five hours, with a comparison with cast film using PVA 18-88.

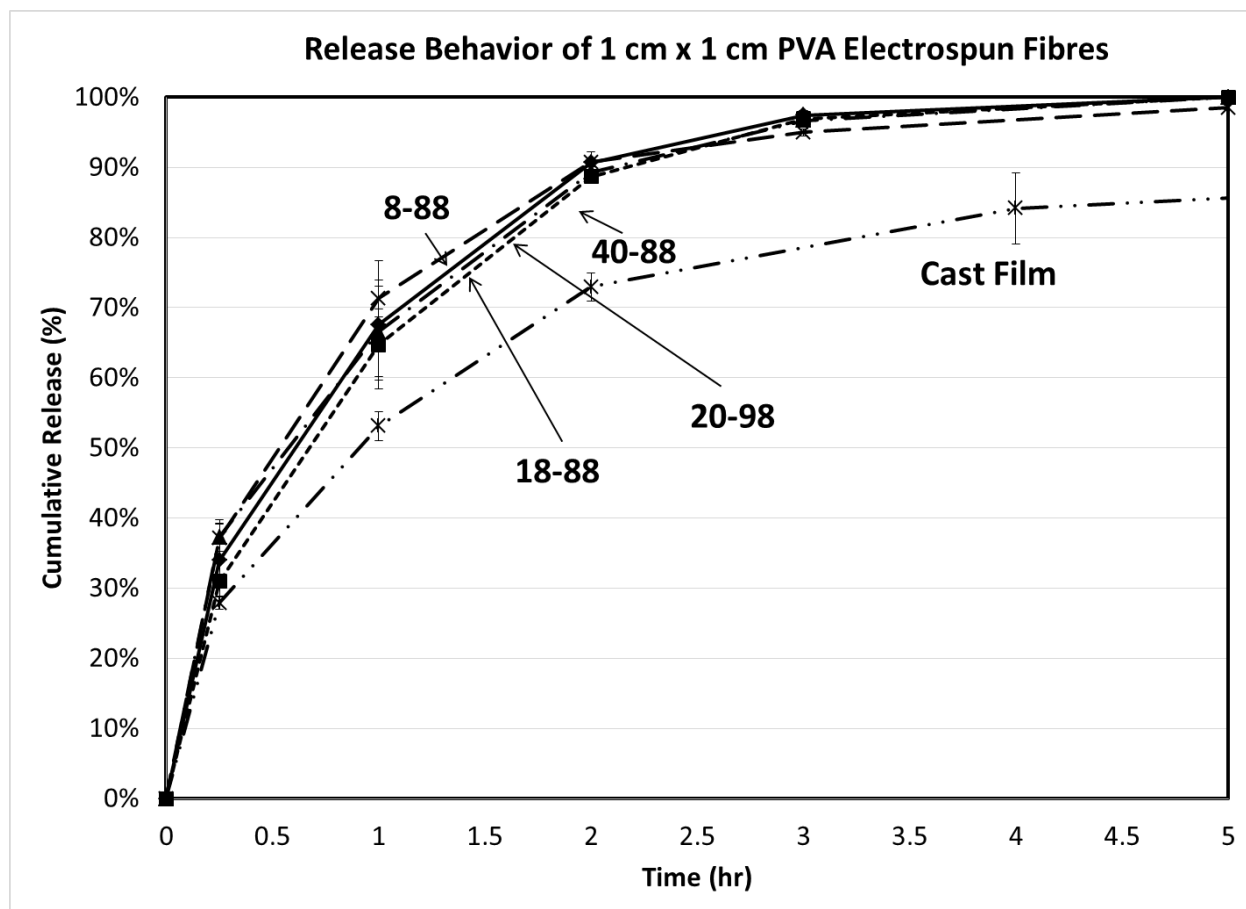


Figure 18: Kynurenine release from PVA electrospun fibres from different polymer grades

All PVA nanofibre samples were electrospun from 10wt% concentration to keep kynurenine to PVA ratio constant. As seen in Figure 18, release from all four PVA grades were seemingly identical, with most of the release occurring within two hours. The four release profiles were fitted into different release models as described in Table 2, and their closeness of fit to each model was compared using the R^2 value as shown in Table 5.

Table 5: Comparing release data fitness to empirical models, based on different PVA grades

Sample	Closeness of Fit (R^2)			
	Diffusion	Mixed Diffusion and Erosion	Surface Desorption	Matrix Erosion
8-88 PVA	0.9919	0.9758	0.9823	0.8023
18-88 PVA	0.9983	0.9276	0.9956	0.8467
40-88 PVA	0.9993	0.9887	0.9960	0.8648
20-98 PVA	0.9948	0.9932	0.9963	0.8379
18-88 Cast Film	0.9989	0.9823	0.9460	0.9487

For PVA with low hydrolysis ratio, the release behavior followed the SRT mechanism most closely, whereas for PVA with high hydrolysis ratio, release followed surface desorption more closely. However, it is apparent that the data for the low hydrolysis PVA also fit very closely with surface desorption, and that for highly hydrolyzed PVA also fit closely with diffusion and mixed diffusion and swelling mechanisms. Considering the standard deviation of the data is up to 9%, analyzing the R^2 value alone will not be able to conclusively identify the dominant release mechanism, and further examination of physical evidence is required. However, the data was sufficient to show that matrix erosion was not the dominant mechanism, despite PVA being soluble in aqueous solutions such as PBS. To quantitatively compare between the three samples, diffusion release was assumed and the diffusion coefficients (K_H) were compared. Although the data in Table 5 could not provide conclusive evidence that diffusion is the dominant release mechanism, examining K_H values of different samples could nonetheless provide meaningful quantitative comparison between the release kinetics of the samples due to their closeness to the diffusion release model. As the diffusion coefficient describes the slope of

the M_t/M_{d0} vs. $t^{0.5}$ curve, a higher value would indicate faster diffusion. Results showed that the PVA 8-88 has the fastest diffusion ($K_H = 0.6475$), followed by PVA 18-88 ($K_H = 0.6455$) and PVA 40-88 ($K_H = 0.6325$), with PVA 20-98 showing the slowest diffusion ($K_H = 0.6282$), although the differences were small and statistically insignificant. There is also a slightly downward trend in the diffusion constant as PVA molecular weight increases, following equation 13 below, although this trend was not perfectly linear, with a correlation of $R^2 = 0.911$. Note that equation below is only valid when all other parameters were kept constant.

$$K_H = 0.6566 - 1 \times 10^{-7} [PVA \text{ molecular weight}] \quad \text{Equation 13}$$

Like the electrospun nanofibres, the PVA cast film also showed burst release within the first two hours, followed by a plateau afterwards. However, the cast film was not able to reach 100% kynurenine release, unlike the electrospun samples. In addition, kynurenine release from the cast film sample showed higher correlation to the diffusion-controlled release model, with a more pronounced difference from the correlation to the desorption-controlled release model compared to the electrospun samples.

In addition to comparing between PVA grades and between nanofibres and cast films, the effect of PVA concentration, and kynurenine content was also examined by varying PVA concentration in the electrospinning solution. Table 6 presents the closeness of fit for nanofibres with varying level of drug loading and different diameters, to the four empirical models described above.

Table 6: Effect of nanofibre diameter and drug loading on kynurenine release from PVA 18-88 nanofibres

Electrospinning		Closeness of Fit (R^2)				K_H
PVA Concentration	Drug Loading	Diffusion	Mixed Diffusion and Erosion	Surface Desorption	Matrix Erosion	
8 wt%	2.0 wt%	0.9670	0.9293	0.9496	0.6177	0.6786
10 wt%	2.0 wt%	0.9983	0.9276	0.9956	0.8467	0.6455
12 wt%	2.0 wt%	0.9989	0.9676	0.9937	0.9028	0.6221
10 wt%	0.5 wt%	0.9986	0.998	0.9774	0.9278	0.6258
10 wt%	7.5 wt%	0.9855	0.9851	0.9872	0.8453	0.7056

Again by assuming diffusion-controlled release and comparing the K_H values, trends were observed in which increasing fibre diameter and decreasing drug loading on PVA 18-88 nanofibres led to reduction in the release rate, following the behavior described in equations 14 ($R^2 = 0.990$) and 15 ($R^2 = 0.999$), respectively.

$$K_H = 0.7900 - 0.0141[\text{PVA Concentration}] \quad \text{Equation 14}$$

$$K_H = 0.6214 + 0.0113[\text{Kynurenine Concentration}] \quad \text{Equation 15}$$

An attempt was also made to determine the correlation between nanofibre diameters and K_H , by examining PVA nanofibres spun at 10 wt% concentration but at different voltages. PVA nanofibres obtained from 10 wt% 8-88, 18-88, and 40-88 were also added to the observation as it was established in equation 13 that molecular weight had small effect on the release kinetics. The resultant comparison, presented in Figure 19, showed no clear trend between nanofibre diameter and release kinetics as the K_H fluctuated about a value of 0.6400.

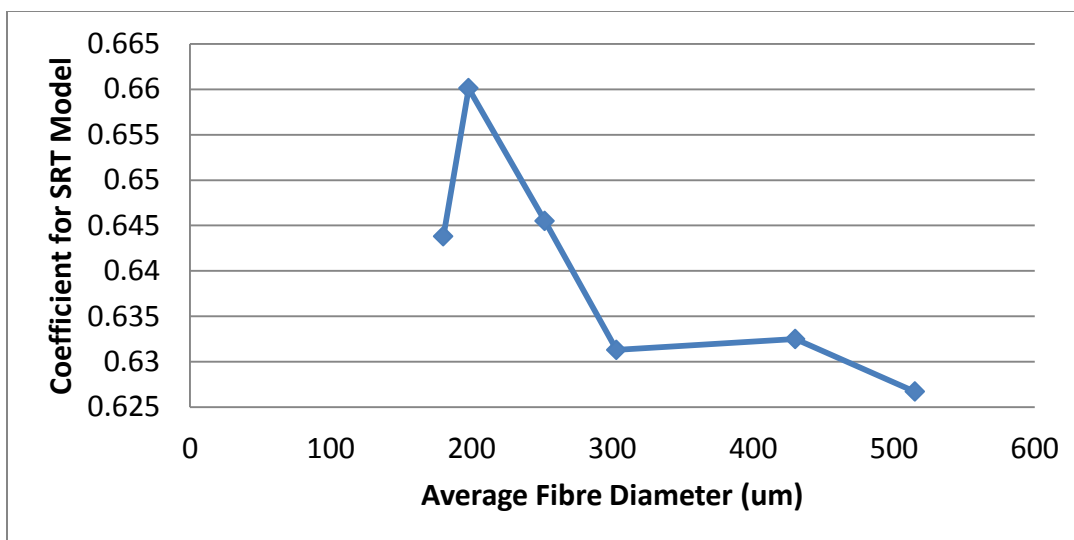


Figure 19: Effect of fibre diameter on K_{tr} . All samples are based on 10 wt% polymer loading

To assess the uniformity in kynurenine distribution among the electrospun PVA fibre membrane on an assembly scale, the drug content in ten 1 cm x 1 cm piece samples, cut from a 10 cm x 10 cm membrane were examined. The total kynurenine content loaded into the PVA was calculated to be 20.0 $\mu\text{g}/\text{mg}$ of fibre. The average measured kynurenine content in the ten samples was $20.141 \pm 0.480 \mu\text{g}/\text{mg}$, which translates to a 2.38% standard deviation, indicating uniform kynurenine loading on the macro scale, such that each section cut from the electrospun nanofibre membrane contained a the same amount of kynurenine.

In addition to PVA, the kynurenine release from PLGA was also examined, and was compared to the 18-88 PVA as shown in Figure 20.

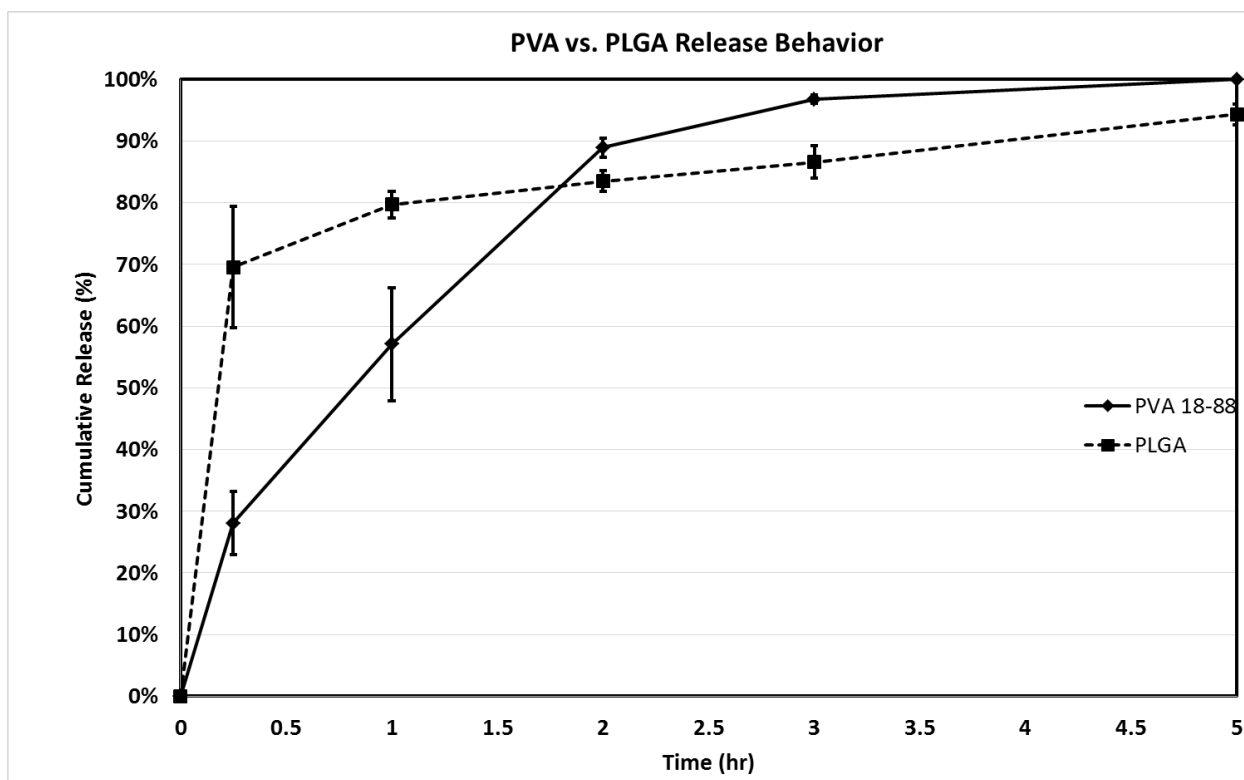


Figure 20: Release behavior from PLGA in comparison with PVA 18-88

Compared to PVA, PLGA facilitated a more profound burst release within the first 15 minutes, followed by a steady release throughout the remainder of the examination time. While the release data from PVA samples correlated relatively close to one or more empirical models, it was noticed that the release from PLGA did not. When examined closely, it is apparent that the PLGA sample indeed showed a two-stage release behavior. Samples taken at 5, 15 and 20 minutes showed that the release within first 15 minutes exhibited a linear behavior versus time, indicating a pure swelling or erosion controlled release. The release after 15 minutes, however, showed a different release profile, which corresponds to the diffusion, mixed diffusion and swelling, and surface desorption models with R^2 values of 0.9997, 0.9991, and 0.9984, respectively. Considering that the kynurenine in the PLGA samples were first dissolved in water and then mixed into the PLGA/TFE solution, the two-stage release behavior could suggest imperfect mixing between the two phases, thereby creating water-rich regions containing most

of the kynurenine, approximately 70% according to Figure 20, with the rest dispersed within the PLGA carrier. When the PLGA samples come into contact with the PBS solution, the water-rich regions dissolve within a short time, creating a swelling-like release behavior due to the quick penetration of PBS. After the kynurenine in water-rich regions is depleted, the remainder of the kynurenine would release from within the PLGA carrier. The comparison between PLGA and PVA samples showed the importance of using a water-soluble polymer for carrying kynurenine to prevent such immediate burst release.

The shelf-life of kynurenine in PVA electrospun fibres was compared to that in a PVA cast film and solution as shown in Figure 21. It can be seen that while kynurenine underwent quick degradation in solution, it remained relatively stable in fibres. In addition, kynurenine also experienced degradation in cast films, although to a lesser extent compared to solution. The likely reason for the difference in shelf-life between the three material forms is the water content in the carrier, as kynurenine could degrade into alanine and anthranilate via hydrolysis. As a result, kynurenine would be expected to degrade quickest in water-rich carriers such as solution or gel.

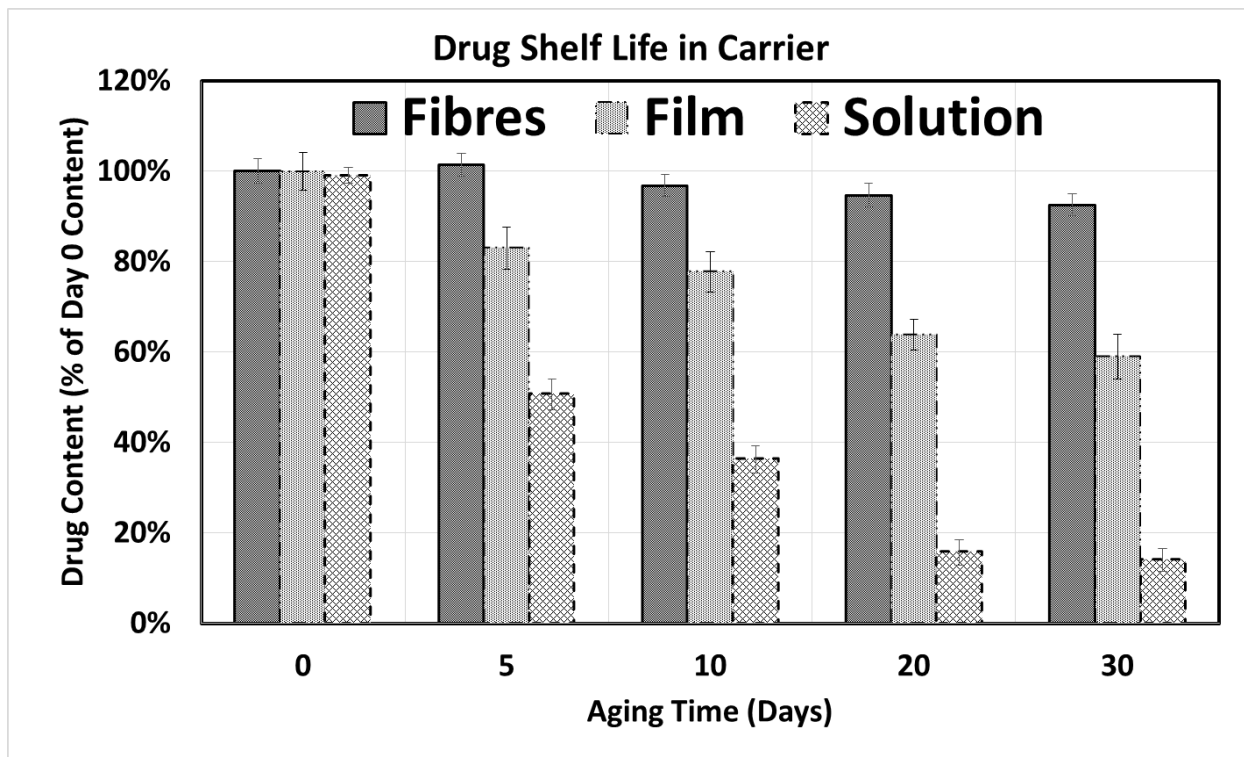


Figure 21: Shelf life comparison between kynurenine in PVA fibre, film and solution

To relate release behavior to fibre morphology, SEM images of the samples were taken at different times during the release test. The SEM images would show how fibres react to PBS soaking and how fibre surface will change. The surfaces of the samples taken from the three grades of PVA and the PLGA after 15 minutes of soaking in PBS are shown in the Figure 22.

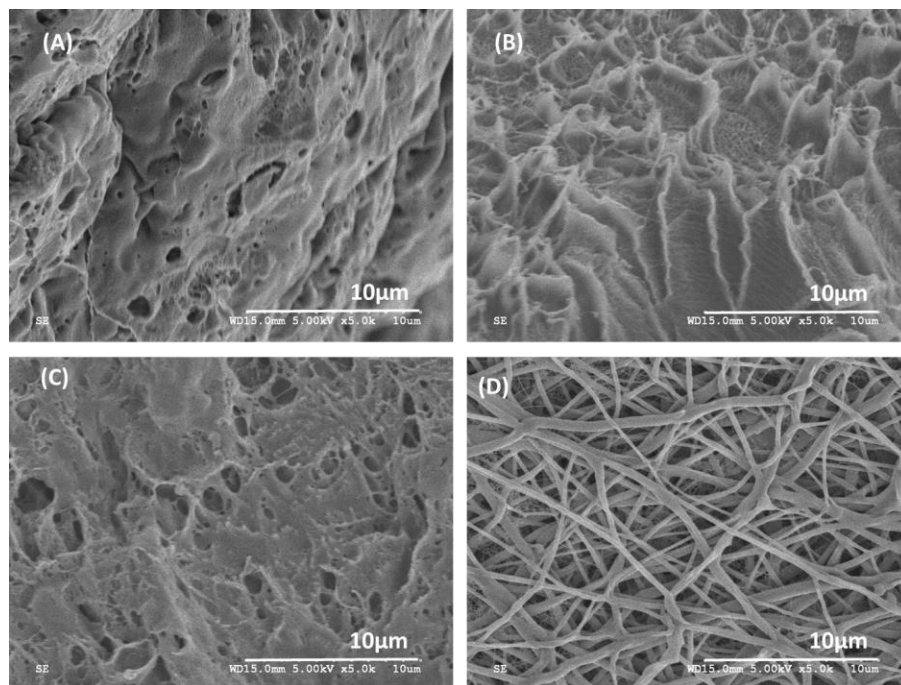


Figure 22: SEM images (5000X) of fibres after soaking in PBS for 15 minutes for (a) 18-88 PVA, (b) 40-88 PVA, (c) 20-98 PVA, and (d) PLGA

As shown in Figure 22, PVA loses the fibrous morphology after soaking in PBS, due to its hydrophilicity and quick water uptake. The PVA essentially forms a porous film, especially the grades with low degree of hydrolysis, while the 20-98 PVA retained some fibrous structure. The PLGA sample was mostly unchanged after soaking for 15 minutes, which is expected due to its lower water solubility compared to PVA. The effect of water uptake was more pronounced after 1 hour, when all of the PVA samples, regardless of grade, had transformed into non-porous films, as shown in Figure 23.

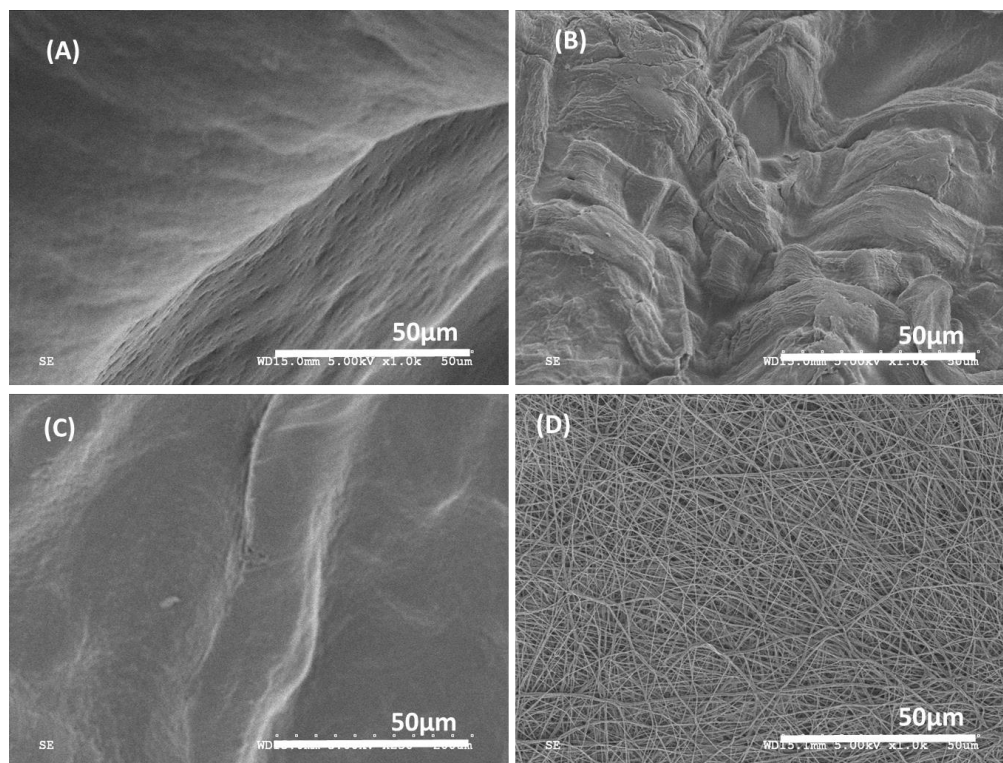


Figure 23: SEM images (1000X) of fibres after soaking in PBS for 1 hour for (a) 18-88 PVA, (b) 40-88 PVA, (c) 20-98 PVA, and (d) PLGA

2.3.4 Nanofibre Characterization

The kynurenine-loaded electrospun nanofibres were subjected to a battery of chemical characterization. The objective of the chemical characterization is to determine how kynurenine interacts with the carrier polymer. More specifically, it is of interest to determine whether kynurenine is amorphously dispersed in the carrier matrix or crystallized on the fibre surface, and whether kynurenine forms chemical bonding to the carrier polymer.

ToF-SIMS was performed to identify kynurenine from the fibre surface. Through analyzing the secondary ions desorbed from the sample by an ion beam, ToF-SIMS can help determine the

mass of the ionized species from the sample. A ToF-SIMS spectra for kynurenine is shown in Figure 24 below.

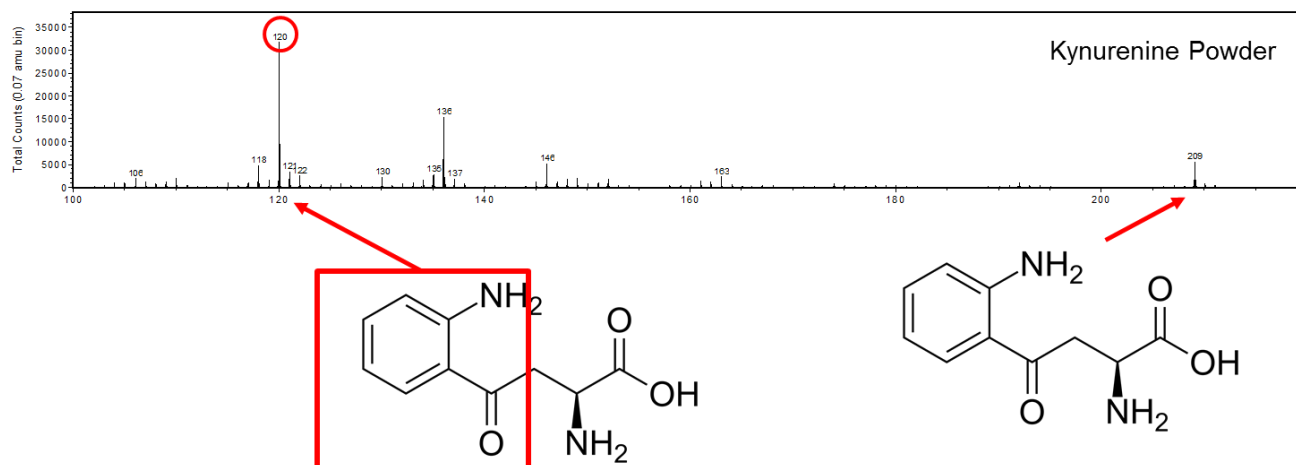


Figure 24: ToF-SIMS spectra of kynurenine

The X axis in the diagram represents the mass of the ion in atomic mass unit (amu), whereas the Y axis represents the signal strength. The peak observed at 209 amu corresponds to kynurenine based on the similarity to its molecular weight. However, it was noticed that the peak at 120 amu, which corresponds to the end of a kynurenine molecule containing benzene, amino, and C=O groups, is much stronger, which can serve as a more powerful indicator of kynurenine detection. Having been able to identify kynurenine from ToF-SIMS, electrospun samples were also tested to determine the presence of kynurenine. Figure 25 presents the results of the ToF-SIMS analysis.

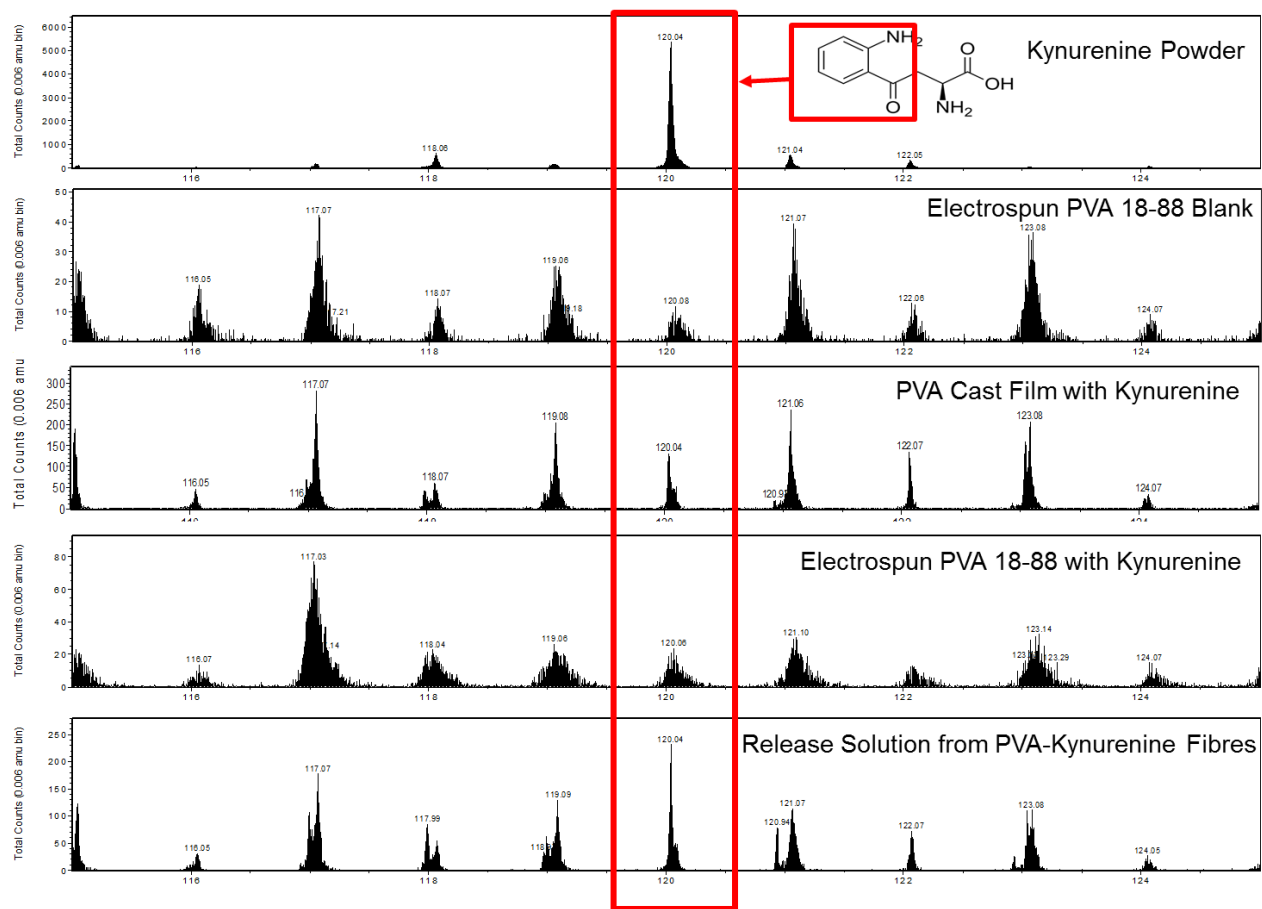


Figure 25: ToF-SIMS spectra (zoomed into the 115 – 125 amu range) for electrospun PVA with kynurenine, and control samples including kynurenine powder, blank PVA fibres, PVA cast film with kynurenine, and dried solution obtained during the release assay.

In addition to kynurenine powder and the kynurenine-loaded PVA fibres that are of interest, several samples were also included as control. A sample of electrospun PVA fibres without kynurenine was added to establish a baseline, whereas a dried sample of the PBS solution obtained at the end of the release test, which contains dissolved PVA and released kynurenine, was added to confirm presence of kynurenine in the fibre and determine the maximum signal strength of kynurenine expected from the fibre samples. Another sample of PVA cast film containing kynurenine was also included to compare the effect of material form on drug encapsulation. From Figure 25, a peak was seen at around 120 amu for each sample; however, upon closer examination, it was noted that for the PVA fibre sample without kynurenine, the

peak at 120 amu was broader and has much lower signal strength (less than 20 counts) compared to the other samples such as the released solution (count in the hundreds). Also, the peak location was slightly different from the kynurenine control, at 120.08 amu versus 120.04 amu. The comparison between signal strength and peak position allow determination of whether kynurenine is present. For the electrospun PVA fibres with kynurenine, the peak was identified at 120.08 amu, with a broad peak with low signal strength, with a count of approximately 20, much like the one observed in the blank electrospun PVA, indicating that kynurenine could not be detected from the loaded PVA fibre sample. However, when the loaded PVA fibres were dissolved in PBS, the analysis on the dried solution reveal kynurenine presence at 120.04 amu with strong signal strength having counts in the hundreds, indicating that the fibres must contain kynurenine. These observations suggest that kynurenine was not present on the fibre membrane surface but within the fibres, such that kynurenine secondary ions were not detected due to the ion beam only being able to ionize up to a depth of approximate 2 nm. In addition to the blank control, comparison between the kynurenine-loaded fibres and cast film also showed that while kynurenine could not be detected from the fibre membrane surface, it was detected from the cast film surface, as noted by the narrow and strong signal at 120.04 amu. In this comparison, it can be seen that electrospun fibres may be a more effective method for encapsulating kynurenine than cast films.

FTIR spectra of the electrospun PVA with and without kynurenine were also obtained to further investigate drug-matrix interaction, as shown in Figure 26 with the spectrum of kynurenine powder as reference.

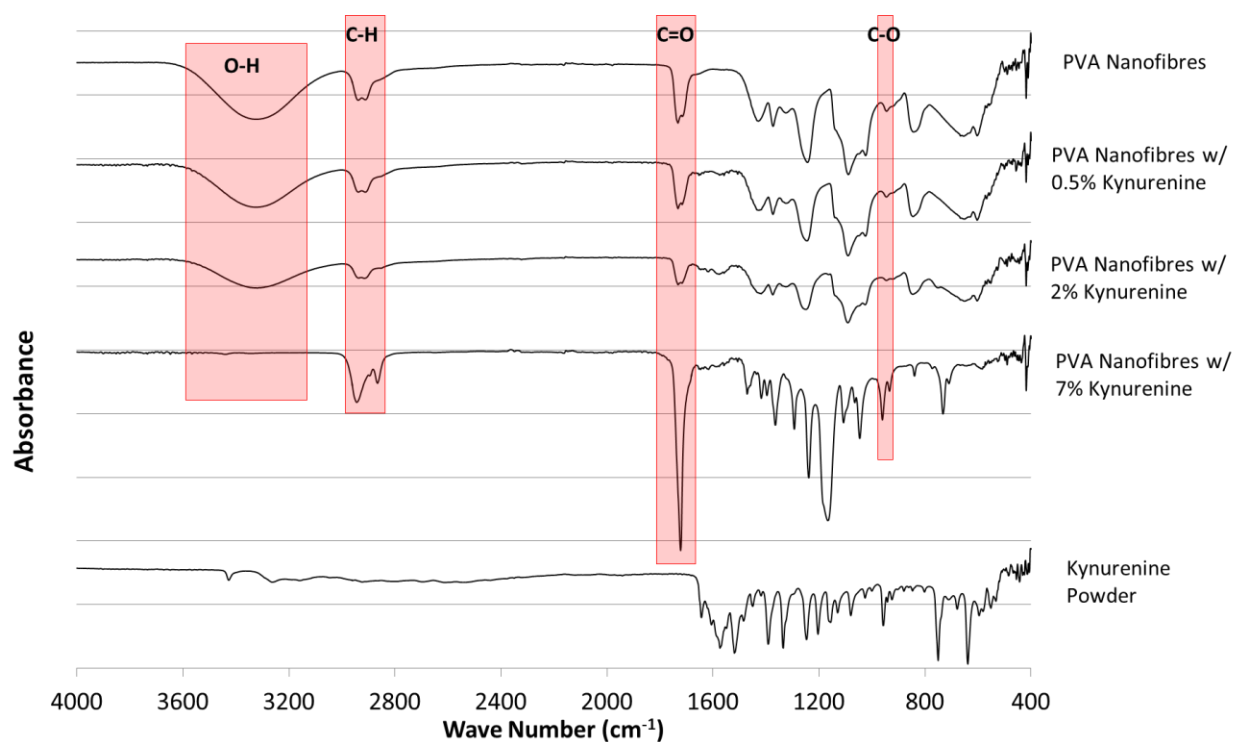


Figure 26: FTIR Spectra of as-electrospun PVA and PVA nanofibres with various kynurenine loading. Spectrum of kynurenine powder was also shown as a reference

From Figure 26, changes in the bonding within the PVA-kynurenine could be identified with increasing kynurenine concentration. As kynurenine concentration increased, the most obvious change is the weakening of the peak around 3300 cm^{-1} , which corresponds to the O-H stretch. As PVA is known to form intermolecular and intramolecular hydrogen bonding with neighbouring chains or itself, the weakening of the O-H peak in this case indicated a loss of inter or intramolecular PVA hydrogen bonding as a result of kynurenine addition, further suggesting the presence of interaction between kynurenine and PVA. To examine the nature of this interaction, the peaks corresponding to the C-O bonds in PVA, at the $1040 - 1130\text{ cm}^{-1}$ range, and the C=O bonds in PVAc residuals, at the $1700 - 1750\text{ cm}^{-1}$ range, were examined. At the $1700 - 1750\text{ cm}^{-1}$ range, two peaks were identified, with the one closer to 1750 cm^{-1} corresponding to free C=O bonds whereas that closer to 1700 cm^{-1} corresponding to hydrogen bonded C=O (Buslov,

Sushko et al. 2011). As the kynurenine concentration increased, the relative intensities of the two peaks changed from being roughly equal to having a significantly stronger peak towards the 1700 cm^{-1} end, indicating hydrogen bond formation at the C=O groups in the partially hydrolyzed PVA. Furthermore, the C-O peak at the $1040 - 1130\text{ cm}^{-1}$ range gradually shifted towards lower wavenumbers as kynurenine concentration increased, suggesting hydrogen bond formation at the C-O groups in the PVA molecular as a result of kynurenine addition. The changes observed at the O-H, C=O, and C-O bonds indicate that the inter and intramolecular PVA hydrogen bonding at the O-H groups was lost as a result of new hydrogen bond formation between the N-H, C-O, and O-H groups in kynurenine and the C=O and C-O groups in PVA. This hypothesis is also supported by the change observed in C-H bonding at the 2850 cm^{-1} range, which is likely a result of the change in C-H bond stretch in the PVA or PVAc due to the shift in hydrogen bonding location from the O-H to the C=O or C-O bonds. The other questions that must be answered is whether the change in hydrogen bonding between samples with different kynurenine concentration was due to difference in water content in the fibre samples. However, examining the FTIR data, the signature peaks of entrapped water, which would be detected at 1630 cm^{-1} and 1660 cm^{-1} (Buslov, Sushko et al. 2011), were not present, indicating that storing the fibre samples inside vacuum oven prior to FTIR analysis was sufficient in eliminating potential analysis errors due to water presence.

In addition to characterizing the bonding between PVA and kynurenine, it is also of interest to examine the state of kynurenine in the PVA matrix – whether it blends in the PVA as an amorphous mixture or if it crystallizes as a solid. XRD was therefore performed with the results shown in Figure 27 below.

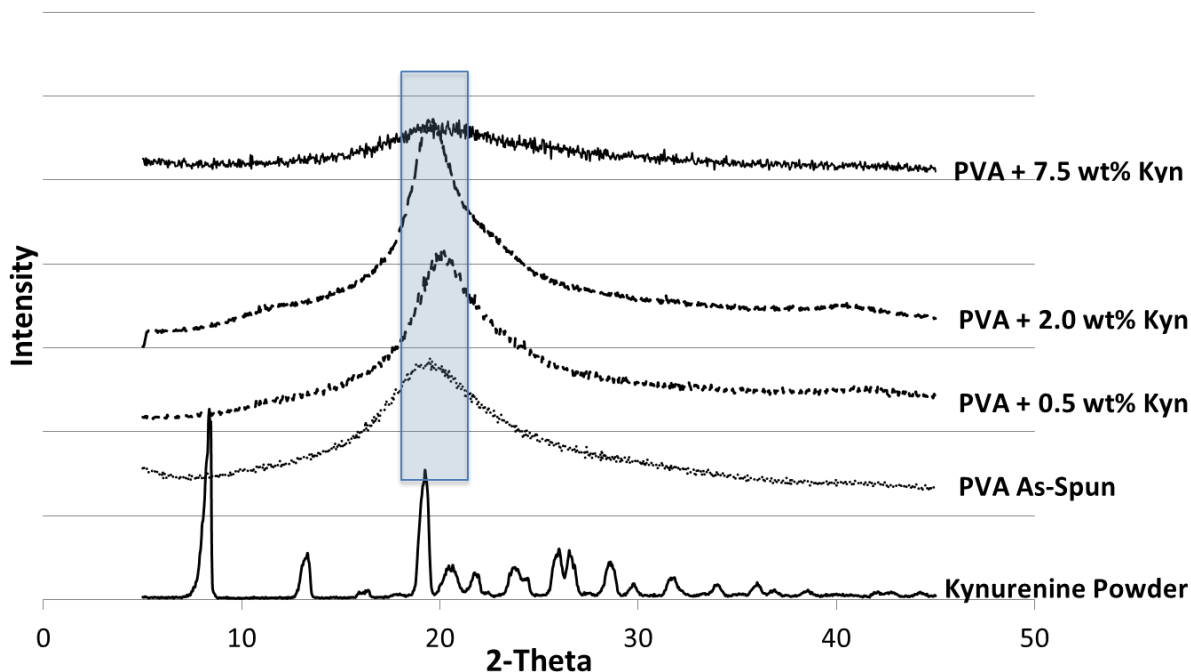


Figure 27: XRD spectra of PVA nanofibres with and without kynurenine loaded, with spectrum of kynurenine powder included as reference

The XRD spectra for all PVA samples, regardless of the amount of kynurenine loading, showed a broad peak, typical of an amorphous material, centered at a 2θ of 19.5° , which has been indexed in literature as the $10\bar{1}$ plane, a signature of PVA (Assender and Windle 1998). The peak appeared diffuse as a result of scarring of the X-ray in various directions, likely indicating a low degree of crystallinity in the polymer. In addition, the major peaks observed from kynurenine powder, at 2-Theta of 8.4° , 13.1° , and from $25^\circ - 30^\circ$, were not observed in the kynurenine-loaded PVA. The results in Figure 27 therefore suggest that at the current resolution, no kynurenine crystallites were detected.

2.3.5 Thermal Analysis

XRD results did not show indications of crystallized kynurenine; however, it is still unclear whether the drug is dispersed in the matrix as a distinct phase or if it formed a solution with the polymer. DSC analysis was conducted as a result to further determine the nature of drug-polymer interaction. Figure 28 compares the DSC thermograms of the nanofibre samples with and without kynurenine.

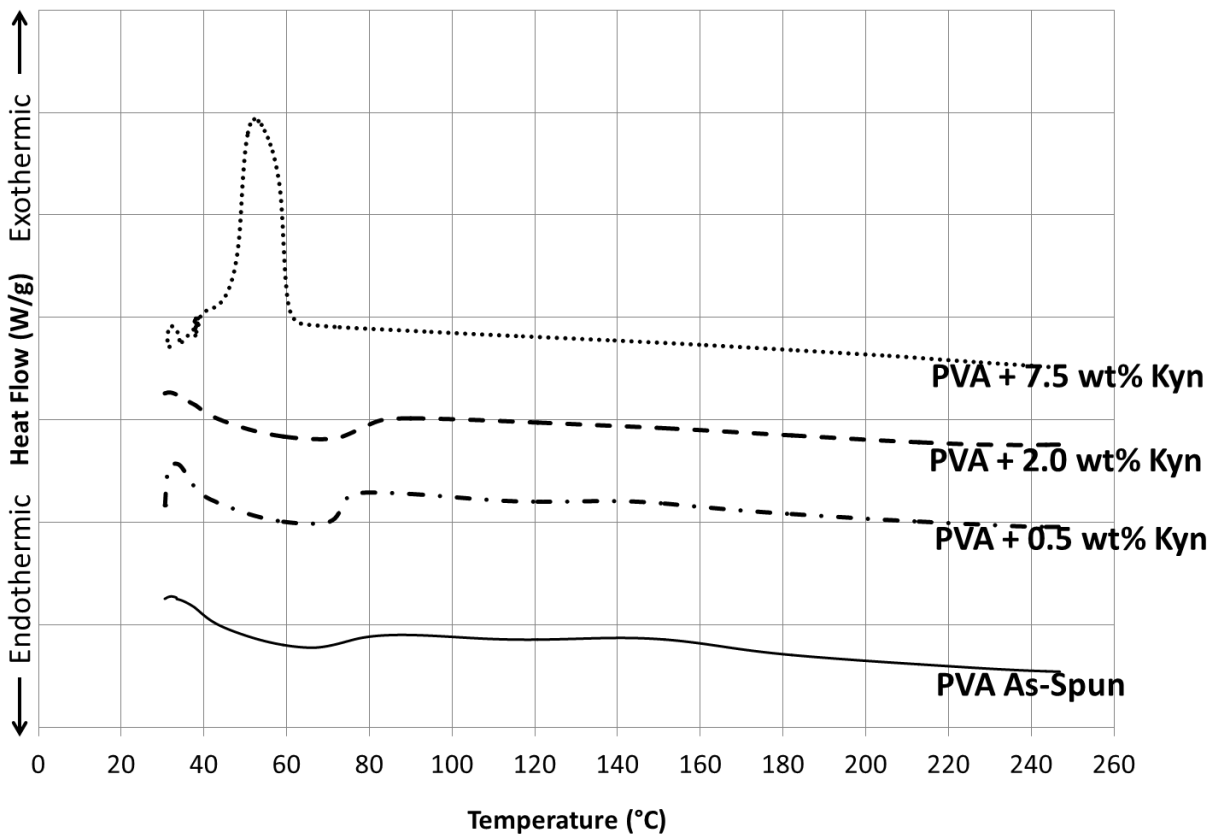


Figure 28: DSC Thermograms comparing as-electrospun PVA nanofibres and PVA nanofibres with different kynurenine loading

With the exception of the PVA sample containing 7.5 wt% kynurenine, all the other PVA samples showed an endothermic change starting at 40°C through to 70°C. Although the glass

transition of pure PVA is approximately 80°C, the grade of the PVA used in this study was partially hydrolyzed, with the remainder being poly(vinyl acetate) with a glass transition temperature of approximately 30°C. The transitions observed in the current DSC study therefore corresponded to the glass transition of the PVA matrix used. PVA nanofibres with a high kynurenine loading of 7.5 wt% showed an exothermic transition starting at 45°C. The mechanism behind the exothermic reaction observed for PVA could be a result of kynurenine crystallization or reaction between kynurenine and PVA, but determining the exact mechanism behind the exothermic transition is beyond the scope of the current study. To determine if kynurenine forms an amorphous solution or dispersion in the PVA matrix, the glass transition temperatures of the PVA blank can be compared to those of the PVA samples containing 0.5 wt% and 2 wt% of kynurenine loading. If kynurenine forms an amorphous solution with PVA, the glass transition of PVA would change with the addition of kynurenine, and if kynurenine is dispersed within the PVA matrix, no change would be expected in PVA glass transition. From an average of five measurements, the glass transition temperatures for the PVA blank, PVA with 0.5 wt% and 2.0 wt% kynurenine loading were 51.98°C ± 0.77°C, 53.18°C ± 0.95°C, and 54.51°C ± 1.23°C, respectively. With a kynurenine loading of 0.5 wt%, the average glass transition temperature increased by 2.3%, although the difference was not statistically significant with a P-value of 0.0597. As kynurenine loading increased to 2.0 wt%, the average glass transition temperature increased by an additional 2.5%, but the difference was less significant, with a P-value of 0.1239. Although the stepwise comparisons yielded statistically insignificant results, if the glass transition temperatures of the blank PVA fibres and the PVA fibres with 2 wt% kynurenine were compared, the 4.9% increase in glass transition temperature was statistically significant with a P-value of 0.0098. Therefore, examining the overall effect of kynurenine addition on PVA glass transition temperature, it can be concluded that kynurenine likely formed an amorphous solution in the PVA matrix.

2.4 Discussion

The results from this portion of the study showed that kynurenine can be successfully incorporated into a polymer carrier and electrospun into fibres. The solubility calculation in section 2.3.1 helped identify PVA and PLGA as two polymers with which kynurenine are compatible with. The reliability of the solubility calculations was confirmed by the successful kynurenine loading into solutions with the two polymers initially, unlike the PVAc solution due to its high Flory-Huggins interaction parameter with kynurenine. However, the solubility test could only suggest polymers that in theory are compatible with kynurenine, but could not shed practical insights on whether solutions of two the two species can remain stable when different solvents are involved. In solution mixing, both the PVA and kynurenine solutions are aqueous and therefore their processing is the most straightforward. PLGA was dissolved in tetrafluoroethanol, which is compatible with water but requires prolonged mixing. PVAc was dissolved in an acetic acid/water mixture, which should be compatible with water. However, upon addition of kynurenine, precipitate was formed, further highlighting the difficulty of mixing kynurenine in solvents other than water. Through electron microscopy and drug release assay, it can be seen that the kynurenine-loaded PLGA fibres were not homogeneous. In terms of the fibre morphology, the thin, web-like structures along the regular fibrous network indicates that the viscosity of the solution may not have been consistent, possibly due to segregation between the polymer rich and water-rich phases, as PLGA and water are not compatible with one another. The drug assay also showed burst release of 70% of the loaded drug content from PLGA within the first 15 minutes, further suggesting that there were water-rich regions on the fibres. These results showed that despite a low Flory-Huggins interaction parameter between PLGA and kynurenine, solvent properties must also be considered for successful processing.

To this front, PVA serves as an ideal carrier due to a combination of low interaction parameter and solvent compatibility.

In terms of fabricating kynurenine-loaded PVA fibres, several grades were used to examine the effect of PVA molecular weight and degree of hydrolysis. It was immediately apparent that incorporating kynurenine into the less water soluble highly hydrolyzed PVA was difficult, as it increases surface tension past the spinnable range, unless a surfactant was added. Even with surfactant, the 20-98 PVA solution becomes unstable after several hours and the electrospun fibre morphology was not uniform. It has been suggested in the past that more highly hydrolyzed PVA molecules have higher tendency to form hydrogen bonds between themselves (Park, Ito et al. 2010). However, without kynurenine, the 20-98 PVA could be electrospun into uniform fibres without surfactants. The change brought upon by kynurenine addition leads to the hypothesis that the drug formed hydrogen bonds with PVA molecules leading to increase in surface tension. In fact, FTIR characterization results supported the claim that kynurenine formed hydrogen bonds with PVA. The less hydrolyzed PVA proved to be significantly easier to process in fibre fabrication. Release profiles of the different PVA grades also showed that increasing molecular weight has a minor downward effect on the release rate although the difference is minimal.

When compared to PLGA, kynurenine release from PVA was more gradual with significantly lower burst release. In the case of PLGA, 70% of the loaded kynurenine was released within the first 15 minutes, whereas for PVA, the 70% release was achieved between one to two hours. However, the 100% release within five hours observed from PVA is significantly lower than the five-day target. The goal of this part of the study is to first identify compatible carrier and determine the kynurenine release mechanisms. As a first estimation, drug release mechanism was determined by comparing the drug release data with empirical release models used in

existing literature. In the case of PVA, although the kynurenine release profiles suggested that release is predominately controlled by SRT diffusive release, its correlation was very close to that for surface desorption controlled release, thereby putting the validity of such a claim in question. As a result, the predominant release mechanism cannot be accurately identified without studying further physical evidence, much like the concern raised by Siepmann and Peppas on the misinterpretations caused by the reliance of such empirical models (Siepmann and Peppas 2011). However, as a means to compare the release kinetics between different samples, diffusion-controlled release was assumed such that the coefficient in the SRT model equation could be used as a comparison metric. The diffusion model equation was chosen over the desorption model equation and power law because the coefficient K_H provided the simplest relationship between release and time. While the zero-order erosion based release model provided a purely linear relationship between release and time, it did not correlate well with the release data. Comparison between the K_H values between PVA samples with different molecular weight, diameter, and drug loading, several trends could be identified, as summarized in Table 7.

Table 7: Release kinetics dependence on material parameters

Factor	K_H Dependence	R^2
PVA Molecular Weight	$K_H = 0.6566 - 1 \times 10^{-7} [\text{Molecular Weight}]$	0.911
Polymer Loading	$K_H = 0.7691 - 0.005 [\text{PVA Concentration}]$	0.977
Drug Loading	$K_H = 0.6214 + 0.0113 [\text{Kyn Concentration}]$	0.999

Examining the K_H dependence on these parameters, it is immediately apparent that the molecular weight of PVA had an insignificant impact on the release kinetics. Considering the 88% hydrolyzed PVA is commercially available at molecular weights ranging from 31,000 to 205,000, the resultant K_H would vary by approximately 1.3% at a specific polymer and kynurenine concentration. Although PVA molecular weight has small effect on kynurenine

release kinetics, it is an important parameter for electrospinning uniform fibres that would determine the electrospinning concentration required, as highlighted in the work by Koski et al (Koski, A, Yim, K, Shivkumar, S, 2004). PVA concentration in the electrospinning solution, on the other hand, played a slightly more significant role in controlling release kinetics. At the electrospinnable range of 5 – 15 wt% for PVA 18-88, the K_H of the resultant fibres varied by approximately 7.8%. The impact of PVA concentration on release kinetics is likely due to the increase in fibre density as a result of higher polymer loading, which could enhance difficulty for water penetration and kynurenine diffusion. Similarly, the kynurenine loading also has an impact on the release kinetics, as the K_H varied by approximately 12.3% between 0.5 – 7.5 wt% of kynurenine loading, although at low kynurenine dosages, the effect of further reducing drug concentration would diminish. The relationship between drug loading and release kinetics is likely the concentration gradient: as concentration gradient increase due to higher drug dosage may increase the potential for kynurenine diffusion to the surrounding fluid. Among the three factors, none were able to appreciably change the release duration, as all samples showed complete kynurenine release within five hours. As a result, changing feed material parameters would only be able to facilitate fine adjustment of the extent of burst release but not the overall release trend.

As mentioned in section 1.1.11, kynurenine interaction with the polymer is an important factor in determining release properties. If the drug is crystallized on the fibre surface, it will likely undergo burst release controlled by surface desorption mechanism. If the drug is dispersed within the carrier matrix amorphously, then its release would likely be controlled by fibre swelling or drug diffusion, or a combination of both. To determine the kynurenine-PVA interaction several tests were performed. The ToF-SIMS results showed that no kynurenine was detected from the fibre surface. However, kynurenine was detected from the dried sample of PBS solution with dissolved drug-loaded PVA fibres, indicating that kynurenine was encapsulated within the fibre

at a depth of over 2 nm. The observation of kynurenine-free fibre surface provided evidence that the release was more likely controlled by diffusion instead of surface desorption. One possible explanation for the release data correlation to both the diffusion and surface desorption models is that although the release is predominantly controlled by diffusion, the high wettability of the hydrophilic PVA allowed quick access of the PBS solution to the kynurenine molecules that are closer to the surface, thereby creating an initial release profile that also resembles surface desorption release.

Knowledge that kynurenine was encapsulated within the nanofibres via ToF-SIMS studies was able to partially address the question on the nature of drug-polymer interaction set out in this study. However, simply being encapsulated inside the PVA matrix is not sufficient for understanding the nature of drug release. Although ToF-SIMS result showed that kynurenine was not crystallized on fibre surface, if the drug was dispersed within the PVA fibres as a crystalline solid, release could still resemble a desorption-controlled profile, whereas if kynurenine forms a solid solution with PVA, the release mechanism might more likely be diffusion-controlled. XRD results showed that regardless of the amount of kynurenine loaded into PVA, the XRD spectra showed a broad peak resembling that of an amorphous polymer. More importantly, the XRD spectra of the kynurenine-loaded PVA showed none of the crystalline peaks of kynurenine visible. Based on the Scherrer equation, which relates crystallite size to XRD peak location and full width at half maximum, the smallest kynurenine crystallites that can be detected would be roughly 14 nm. The evidence from XRD studies suggested kynurenine exists in the PVA matrix either as amorphous form or in crystallites smaller than 14 nm. If kynurenine exists in the matrix amorphously, it dispersed in the PVA matrix or can form a solution. DSC results showed a trend in which the PVA glass transition temperature increased with kynurenine addition, suggesting that kynurenine is in solution with PVA, which further supported the hypothesis that kynurenine is amorphously mixed into the PA matrix. The

observations that kynurenine exists in the PVA matrix in amorphous form and as a solution support the hypothesis that kynurenine release was controlled mainly by diffusion instead of desorption. Unlike many existing studies that determine the dominant drug release mechanism simply by comparing release data to empirical models, the detailed characterization approach described in this study could provide physical evidence to support the hypotheses made when comparing with empirical models.

From Figure 21 it was evident that kynurenine has a significantly more stable shelf life in electrospun fibres as opposed to cast films or solution. The observation that 10% of the loaded kynurenine remained active in solution after 30 days is a strong indication of the importance of a dry kynurenine carrier, and that hydrated formulations such as hydrogel may not be suitable. Even if a hydrated kynurenine carrier is applied immediately after fabrication, loss of drugs would occur during the five-day release period, according to Figure 21 that showed approximately half of the loaded drug remained in the solution after five days. The comparison between the drug loss in electrospun fibres and cast films also showed that a dried carrier may not be sufficient to maintain kynurenine integrity on its own, as drug loss was still observed in the cast films. Although the longer time required for cast films to dry compared to the quick water evaporation that takes place during the electrospinning process may have played a role in the shortened kynurenine shelf life in cast films, it could not explain the continued, albeit minor drug loss throughout the 30-day period. Drug loss from cast films may also be due to kynurenine exposure to the environment. As shown in the ToF-SIMS results, kynurenine was detected on the film surface whereas it was shown to be encapsulated in nanofibres. The surface-residing kynurenine could have been lost due to hydrolytic degradation. The results showed nonetheless that it is important for kynurenine to be well-encapsulated in a dry matrix, and electrospun fibres fulfill both of these requirements.

It is clear from the SEM micrographs in Figure 22 that electrospun PVA could not maintain its fibre morphology after soaking in PBS solutions due to its hydrophilicity. Even the least water soluble grade, the 20-98 PVA, completely lost its fibrous morphology after 1 hour. The transition from a fibrous structure to a porous gel-like structure and ultimately to a non-porous structure may help delay drug release by reducing surface area. However, the benefits of the electrospinning technique remains regardless of the morphology change in PBS, such as prevention of drug aggregation, availability of material choice, and flexibility for fabricating hierarchical structures. Furthermore, release assay results after 30 days showed that electrospun fibres are the most capable in preserving kynurenine shelf-life, compared to liquid and cast film forms. The electrospun PLGA was able to maintain fibrous morphology in PBS solution.

While encapsulation of kynurenine in the PVA matrix and its subsequent complete release were demonstrated, another important aspect is whether the released kynurenine remained active after the fabrication process. While the biological properties of the dressing is outside the scope of this thesis, results from a separate study nonetheless showed the enhanced ability of fibroblast cells treated with kynurenine-loaded nanofibres to express MMP. In Figure 29, the control sample represented MMP expression on fibroblast cells that were not treated. By treating the cells with kynurenine in the culture media, the level of MMP expression increased significantly. It was also observed that treating fibroblast cells with blank nanofibres did not have appreciable effects on MMP expression, whereas those treated with kynurenine-loaded nanofibres had significantly higher MMP expression at a similar level to that from cells treated with kynurenine.

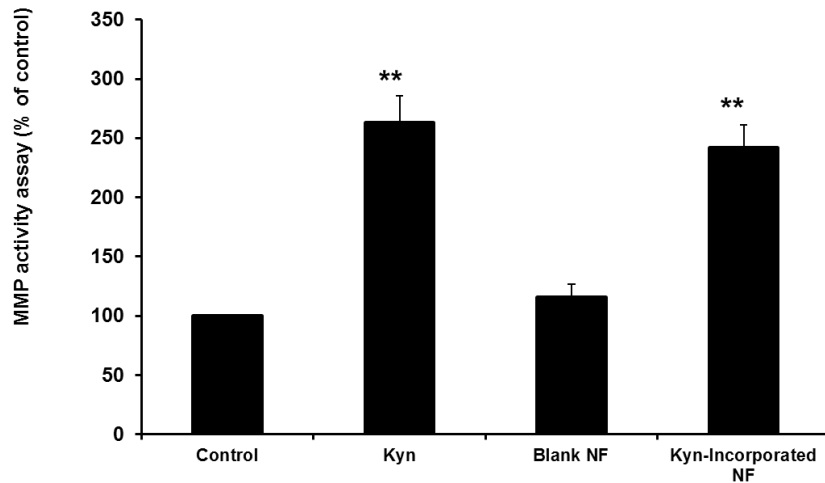


Figure 29: MMP expression comparison between untreated fibroblast cells (Control) and those treated with blank nanofibres (Blank NF), kynurenine (kyn), and kynurenine-loaded nanofibres (Kyn-Incorporated NF)

2.5 Conclusion

This chapter presented the first investigation on kynurenine loading into nanofibres for releasing into wounds. The challenge in this study is that kynurenine is only soluble in aqueous solutions, which eliminated possibility in using many other materials that have been shown to promote stable release in existing literature. In addition, among previous work, the material choice for carrier has not been well rationalized. In this study, a systematic method for carrier material selection was introduced. First, a theoretical approach was utilized based on solubility parameter calculations as a screening tool for potential carrier materials. The calculations were able to determine the polymers that are compatible with kynurenine in theory including PVA and PLGA. However, from a practical point of view, the calculations did not take into consideration how the two phases are mixed. Indeed, kynurenine-loaded PLGA performed poorly in terms of solution stability during electrospinning, fibre morphology, and burst release at the beginning of

the release study. PVA, on the other hand, formed a stable electrospinning solution with kynurenine and the resultant fibres had a more gradual release behavior compared to PLGA. The difficulty in mixing kynurenine in PVA with higher molecular weight and degree of hydrolysis suggested that the drug could form hydrogen bond with PVA.

Kynurenine release data from the electrospun nanofibres were also compared to empirical release models presented in previous work to help determine the dominant release mechanism. Release from PVA correlated closely to both the SRT diffusion release as well as the surface desorption release models. The difficulty in determining the most plausible mechanism showed that comparison with empirical models could only be used as a reference tool but not evidence for accurately identifying the dominant release mechanism. However, most studies in existing literature that examines drug release from nanofibres relied solely on empirical model correlation to justify their assertion on the most plausible mechanism. Expanding from existing work, this study utilized a systematic methodology to help interpret drug release behavior that could compliment the observations from empirical model comparison. ToF-SIMS showed whether kynurenine was present on fibre surface and therefore helped determine if surface desorption was involved, whereas XRD and DSC revealed the physical state of the drug inside the carrier, which can affect the initial release behavior. FTIR provided insights to whether bonds were formed between the drug and the carrier. SEM could also be used to observe morphological changes on the scaffold during release to correlate these changes to the observed release behavior.

In-depth studies on the release kinetics also helped identify factors that would impact kynurenine release kinetics. While the molecular weight of PVA was found to have minimal impact on the release profile, the PVA concentration in the electrospinning solution and

kynurenine dosage loaded into the solution played much more significant roles in determining the release behavior, and therefore should be considered in customizing release profiles.

Unlike the electrospun drug-loaded fibre scaffolds published in existing literature, the kynurenine-loaded PVA explored in this study may not be utilized for its surface properties such as cell adhesion. Indeed, SEM images showed that PVA swelled quickly and fibrous morphology is lost within a short time. However, the results of this study did show that electrospinning was an effective way to fabricate a carrier that can facilitate uniform drug distribution and stable release, while prolonging kynurenine shelf life when compared to other forms of application.

While this chapter presented systematic approaches for drug carrier material selection and release mechanism analysis, much improvement can be made in terms of the rate of kynurenine release observed from electrospun PVA. The release assays showed complete release within five hours, with 90% of the kynurenine released within the first two hours, a result that is comparable with previous studies on antibiotics and painkillers release using electrospun PVA as carriers. However, as MMP production is only helpful in the later stages of wound healing and may be harmful if released prematurely, the current methods and results are clearly insufficient. To further extend the release period of kynurenine and to accomplish the five-day target for release, simply mixing the two phases and electrospinning would not be sufficient, and methods for carrier modification must be considered.

3 Matrix Modification for Controlling Kynurenine Release

3.1 Introduction

In the previous chapter, PVA was identified as a suitable fibre matrix material for kynurenine loading, and extensive studies were conducted to characterize the drug-polymer system, leading to the determination that the dominant release mechanism is drug diffusion through the PVA fibre, followed by dissolution into the surrounding liquid. However, although PVA was proven compatible with kynurenine, it is a highly hydrophilic polymer that swells and degrades quickly in aqueous environment, which is contradictory to the primary goal of this research of producing a dressing that supports stable kynurenine release over five days. Indeed, it was shown in the previous chapter that regardless of the PVA grade used in electrospinning, all loaded kynurenine was released within five hours, with most of the release taking place in the first two hours. Unfortunately, the carrier choice could not be substituted at will, unlike in other studies involving drug release from electrospun fibres, due to the stringent kynurenine compatibility and processing requirements. Therefore, to reach the release target set out in this research, the PVA kynurenine carrier system must be modified accordingly.

As shown in the SEM images taken during the release studies, PVA fibres became swollen very quickly, with the distinctive fibrous morphology lost within 15 minutes, which led to very fast kynurenine diffusion out of the carrier. Accordingly, modifications aimed at reducing burst release should focus on either slowing the wetting of the PVA fibres or decreasing their extent of swelling. This chapter will outline the investigations on approaches to modify the electrospun PVA-kynurenine nanofibres. The investigations carry two main objectives. First, as previously

mentioned, it is desirable to extend the kynurenine release period from five hours to 120 hours in order to show the feasibility of the carrier use in scar reduction. Second, the knowledge on the effects of different modification technique on release properties may be useful in developing methods to produce carriers with specific release periods between one to five days for more versatile use on different situations and patients.

PVA, although selected primarily for its compatibility with kynurenine, is a polymer with properties in aqueous environments that are customizable through chemical and physical modifications. Several previous studies have examined PVA chemical crosslinking and crystallization via heat treatment. For example, Lee et al showed marked reduction in the solubility of electrospun PVA after heat treating at temperatures ranging from 150°C - 210°C (Lee, Yoo et al. 2007). However, fibre mechanical properties suffered significant degradation at temperatures over 190°C due to partial decomposition of the PVA. Ding et al also showed significant decrease in PVA fibre water uptake when treated at temperatures ranging from 120°C - 180°C, while significant bulk degradation resistance was observed when the fibres were treated at temperatures above 150°C (Ding, Kim et al. 2002). The decreases in swelling observed in heat treated fibres were attributed by authors such as Park et al (Park, Ito et al. 2010) to increased crystallinity, indicated by a downward trend in water uptake with increase in PVA crystallinity, as determined via DSC analysis. In terms of chemically crosslinking PVA, reagents such as sodium tetraborate (Bassil, Ibrahim et al. 2009), maleic acid, glyoxal (Ding, Kim et al. 2002), and glutaraldehyde (Yoon, Hsiao et al. 2009) have been used in the past with successful results. Chemical crosslinking have also been shown to require significantly less treatment time compared to heat treatment, often in the order of minutes (Ding, Kim et al. 2002). In their 2002 work, Ding et al showed that while heat treatment times of at least 75 – 100 minutes were required to markedly reduce water uptake in PVA electrospun membranes, the same could be accomplished with five minutes of curing time for chemical crosslinking (Ding,

Kim et al. 2002). Several chemical crosslinking have been known to cause irritation or health hazards, especially glutaraldehyde, which is toxic and strongly irritating. However, it has been shown in a previous study that with sufficient washing with distilled water followed by lyophilization, electrospun fibres crosslinked with glutaraldehyde could be made safe for fibroblast cell adhesion and proliferation in in vitro studies (Leung, Hartwell et al. 2013).

In addition to modifying the PVA carrier, a multi-layered design can also be considered. Several previous studies have also proposed multi-layered fibrous structures for controlled release of single or multiple drugs (Ionescu, Lee et al. 2010, Okuda, Tominaga et al. 2010, Immich, Arias et al. 2013). In the case of single drugs, multiple-layered structures containing polymers with different morphologies or hydrophobicity have been used to produce bi-phasic drug release profiles. For example, Yohe et al modified the surface of a PCL fibre membrane to render it more hydrophobic, leading to a bi-phasic drug release profile (Yohe, Colson et al. 2012). Huang et al sequentially electrospun multiple layers of ketoprofen loaded poly(vinyl pyrrolidone) (PVP) and ethyl cellulose, which have different hydrophobicity, to create a release system with both early and sustained release (Huang, Branford-White et al. 2012). In the example by Huang et al, the burst release of ketoprofen was observed from PVP within 300 minutes whereas gradual release was observed from ethyl cellulose over 3000 minutes. By producing a layered structure of PVP and ethyl cellulose, a steadier release profile was obtained with a higher amount of initial release while the long-term release was also retained. In delivering multiple drugs, multi-layered structures allow drugs that do not share common compatible carriers to be combined into one system. With different surface properties, the different layers can release the drugs at different times, such as having one drug released completely, and then having the second drug release.

Due to the exclusivity of kynurenine with water-soluble polymers, adopting a multi-layered, kynurenine-loaded structure will have limited effect on reducing matrix swelling in aqueous

environments. This study will therefore adopt a different approach, while building on the existing knowledge of multi-layered structures. Instead of having multiple layers of drug-loaded fibres, layers of more hydrophobic fibre without kynurenine will be used to surround the kynurenine-loaded PVA layer. The hydrophobic shell will effectively form an envelope around a PVA core. The addition of a shell is expected to delay water penetration into the PVA core, which in turn will reduce the rate of swelling. To further restrict water penetration, the effect of replacing the fibrous shell with a non-porous film will also be assessed. In this study, PLGA will be examined as the polymer of choice for both the fibrous and non-porous film shell layers, mainly due to its hydrophobicity that is tunable by controlling the lactic acid to glycolic acid ratio. Moreover, the compatibility between kynurenine and PLGA, as hypothesized in the calculations from section 2.3.1, may be advantageous especially when PLGA is applied as a non-porous shell. The multilayer concepts proposed in this study are shown in Figure 30.



Figure 30: Graphical representation of the multilayer concept proposed in this thesis. The schematic on the left shows PVA/kynurenine nanofibres covered by PLGA nanofibre layers, whereas the schematic on the right shows PVA/kynurenine nanofibres dip-coated with PLGA

3.2 Materials and Methods

3.2.1 Materials

PVA 18-88 was the grade of choice in this study, because of its ease of electrospinning and drug release performance that was almost identical to the other PVA grades. Chemical

crosslinking of the PVA was performed using sodium tetraborate and maleic acid purchased from Sigma Aldrich, and glutaraldehyde purchased from Fisher Scientific. Four grades of PLGA with lactic acid contents of 50 mol%, 65 mol%, 75 mol% and 85 mol% were purchased from Lactel Absorbable Polymers as the shell layers. Tetrahydrofuran (THF) and dimethylformamide (DMF), both purchased from Fisher Scientific, were used as the solvent for PLGA.

3.2.2 Electrospinning Procedure

The electrospinning procedure for kynurenine-loaded PVA was introduced in section 2.2.2. Briefly, 20 mg kynurenine was dissolved in 1 mL sodium hydroxide, followed by neutralization with a 14M hydrochloric acid. The solution was then added to 9 mL of a 10 wt% PVA 18-88 solution and vortex mixed until homogenous for electrospinning, to yield a solution containing 2 wt% kynurenine. Electrospinning was carried out at a voltage of 20 kV, pump rate of 0.4 mL/hr and a needle to collector distance of 20 cm. Electrospun fibres were collected onto a 10cm x 10cm area of an aluminum plate collector to keep fibre membrane thickness and drug concentration consistent.

3.2.3 PVA-Kynurenine Fibre Modification

Both chemical crosslinking and heat treatment of the PVA were attempted in this study. For heat treatment, the kynurenine-loaded PVA fibre membranes were placed in a convection oven at temperatures of 75°C, 100°C, 125°C, 150°C and 175°C for two hours, followed by cooling in air.

For chemical crosslinking, PVA fibres were treated with one of maleic acid, sodium tetraborate, or glutaraldehyde. In using sodium tetraborate, which reacts with PVA within minutes, a 4 wt%

aqueous solution was prepared and sprayed onto the PVA fibre membrane, after which the membrane was allowed to react for five minutes followed by washing in distilled water. The crosslinking solution was sprayed onto the membrane instead of being used as a bath to prevent excessive water on the membrane surface, which may cause premature kynurenine release.

Maleic acid, which requires longer reaction time with PVA, in the order of two hours, were prepared as a 10 wt% aqueous solution and added to the PVA electrospinning solution, such that crosslinking can take place as the PVA is electrospun, thereby eliminating the need for an additional treatment step.

Glutaraldehyde treatment was performed by soaking the kynurenine-loaded PVA fibres into a bath containing 25% glutaraldehyde dissolved in a 1:1 mixture of water and ethanol. The soak time was five minutes followed by washing in distilled water and lyophilization for 48 hours.

3.2.4 PLGA Protective Shell Incorporation

PLGA was applied as the protective shell portion of the multi-layered kynurenine carriers, either in the form of electrospun fibres or non-porous films. While in its saturated form, the PLGA shell is not expected to interact with kynurenine molecules diffused out of the PVA matrix, there are nonetheless several purposes in coating the kynurenine-loaded PVA fibres with either a fibrous or non-fibrous PLGA shell. First, as it was determined in section 2 that kynurenine diffusion is the dominant drug release mechanism, the PLGA shell around the drug-loaded layer would enhance the tortuosity of the diffusion path, delaying kynurenine release. Moreover, in the case of a non-fibrous coating, the available surface area of the dressing could also be significantly

changed, in addition to further enhancement in diffusion tortuosity. By reducing the available surface area, PVA-kynurenine coated with PLGA would experience slower swelling, which would translate to lower chain and kynurenine mobility in the matrix, thereby extending the drug release duration.

For fibrous PLGA shells, each grade of PLGA was dissolved at a concentration of 15 wt% in a mixture of THF and DMF at a volume ratio of 85:15. The solutions were then electrospun at a voltage of 17 kV, pump rate of 1.0 mL/hr and a distance of 20 cm, onto a 10 cm x 10 cm collector, until half of the prepared solution was deposited. Once the targeted deposition thickness was reached, kynurenine-loaded PVA fibres, cut into 1cm x 1cm pieces, are placed 1 cm apart on the PLGA fibre surface, as shown in Figure 31.



Figure 31: Kynurenine-loaded PVA on PLGA fibres in the fabrication of PLGA/PVA multi-layered fibrous structure

The remaining half of the PLGA solution was then electrospun onto the collector, such that the PVA pieces were completely covered in PLGA. In this portion of the study, the total volume of the PLGA solution electrospun was varied from 10 mL to 20 mL to identify the effect of shell

thickness. After electrospinning, the resultant membrane was cut into small pieces each containing a PVA piece at the centre, surrounded by a PLGA fibre envelope. The pieces were subsequently clamped between two steel plates to ensure bonding between layers, especially the PLGA shells. By doing so, all dimensions of the kynurenine-loaded PVA would be covered by the PLGA shell, preventing premature release along the edges.

For the multilayer kynurenine structure with PLGA non-porous surface layer, the kynurenine-loaded PVA pieces were dip-coated into a 20 – 30 wt% PLGA solution. While dip-coating was a relatively simple process, the post-coating treatment method was more closely examined as it can have a significant impact on coating effectiveness. To develop the optimal fabrication method, several factors were examined.

- 1) Drying the coat at room temperature versus at above the glass transition temperature of PLGA.
- 2) Applying pressure on the sample during the drying process.
- 3) Applying a single dip-coating step on the kynurenine-loaded PVA versus double coat.

To examine the first factor, single coated fibres were placed between two steel plates with pressure applied by clamping the two plates together using a C-clamp to prevent the fibre membranes from deforming. Then, the fibres were dried at either room temperature or at 75°C for two hours to determine the effect of drying below or above the PLGA glass transition temperature of 60°C. In examining the effect of pressure application during the drying process, double-coated fibres were dried at 75°C for two hours either as unrestricted pieces or between two steel plates clamped together. The third factor was examined by preparing double coated samples that were coated, dried at 75°C for two hours under pressure, followed by application of a second coat which was dried at 75°C for two additional hours. Figure 32 shows a general

representation of the dip-coating process described, with PVA nanofibres being dipped into PLGA solution, followed by drying in a convection oven between two steel plates clamped together. The application of a second coat was also represented in Figure 32.

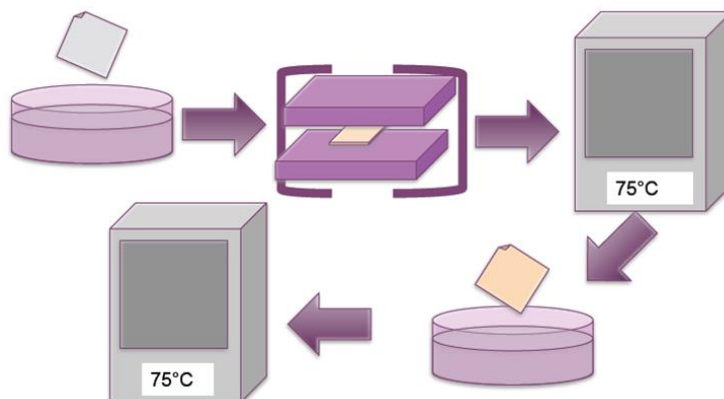


Figure 32: General representation of the dip-coating process

3.2.5 Fibre Characterization

After each modification to the PVA fibre membrane, its morphology was monitored using a Hitachi S-3000N scanning electron microscope (SEM) at 5 kV accelerating voltage and 15 mm working distance. Morphological parameters such as fibre diameter and uniformity, found using the same method as mentioned in section 2.2.4, were compared to identify any effects resulting from each treatment. For the crosslinked and heat treated fibre samples, fibre morphology after soaking in PBS was also observed at different time points to determine the effect of treatment on fibre morphology retention. For multilayer samples, cross-sectional SEM images were taken to observe layer boundaries and to measure layer thickness, with samples prepared by the cold fracture technique, which involves first freezing the sample in liquid nitrogen until brittle, followed by fracturing the samples at the centre by bending.

In this study, the main performance metric that indicates the effectiveness of the modification steps is the drug release behavior, as the primary goals in modifying the PVA matrix were to lengthen the kynurenine release period and reduce burst release. Kynurenine release from electrospun fibrous membranes was spectrophotometrically as described in section 2.2.3. Crosslinked fibre membranes were cut into 1 cm x 1 cm sections before soaking into the 1X phosphate buffered saline (PBS) solution in well-plates. The multilayered samples with PLGA fibrous shells, already containing 1 cm x 1 cm sections of the kynurenine-loaded PVA fibres, have larger dimensions at 1.5 cm x 1.5 cm due to the sealing between the top and bottom shell layers outside the edges of the PVA fibres. On the other hand, the multilayered samples with non-porous shell were 1cm x 1cm dimensions because the PLGA coat did not significantly add to the membrane dimensions. After incubation at 37°C for predetermined lengths of time, the releasate was mixed with a solution containing p-dimethylaminobenzaldehyde (DMAB) dissolved in acetic acid so that any presence of kynurenine could be detected by the Biotek FLx800 fluorescence microplate reader. The amount of drug released from the fibre membrane cutout was again determined from an average of six measurements.

3.3 Results

3.3.1 Modification of PVA-Kynurenine Fibre Membranes

Kynurenine-loaded PVA fibres were processed through heat treatment or chemical treatment as described in section 3.2.3. Upon chemical treatment with sodium tetraborate aqueous solution, it was noticed that the fibre membrane immediately transformed into a clear, gel-like structure, indicating that the fibrous morphology was lost. The transformation is likely due to significant

swelling of the PVA fibres prior to its reaction with the sodium borate crosslinking agent. In addition, it was also noticed that kynurenine was leached out of the PVA membrane upon coming into contact with the sodium borate solution, as the fibre surface became yellow in appearance which is characteristic of dissolved kynurenine. When the PVA fibres were treated with glutaraldehyde in water/ethanol solution, the membrane remained intact and was not transformed into a clear gel, but kynurenine leaching was still evident. In fact, release assays showed that the amounts of kynurenine remaining in the membranes after chemical treatment were highly inconsistent between samples, with subsequent release assay detecting cumulative release ranging from 20% to 65% of the loaded kynurenine, regardless of the crosslinker used. As a result, crosslinking techniques based on solution baths were not recommended for modifying drug release from PVA.

PVA crosslinking with maleic acid was also examined in this study. When a maleic aqueous solution was mixed into a blank PVA electrospinning solution without kynurenine, it was noticed that solution viscosity increases and eventually form a gel after two hours, which would allow time for the solution to be electrospun before the crosslinking reaction completes. However, with a kynurenine-loaded PVA solution, no viscosity change was observed upon addition of maleic acid, and the resultant fibre remained highly soluble in water similar to untreated PVA fibres. Based on this observation, it is apparent that hydrogen bonding between kynurenine and PVA, as indicated in the FTIR results presented in Chapter 2, has an impeding effect on PVA crosslinking with maleic acid. This phenomenon will be discussed in more details in section 3.4.

Among the treatments attempted, only heat treatment was able to effectively change PVA water resistance while preventing kynurenine leaching. Figure 33 below shows PVA fibre morphology after heat treatment at different temperatures.

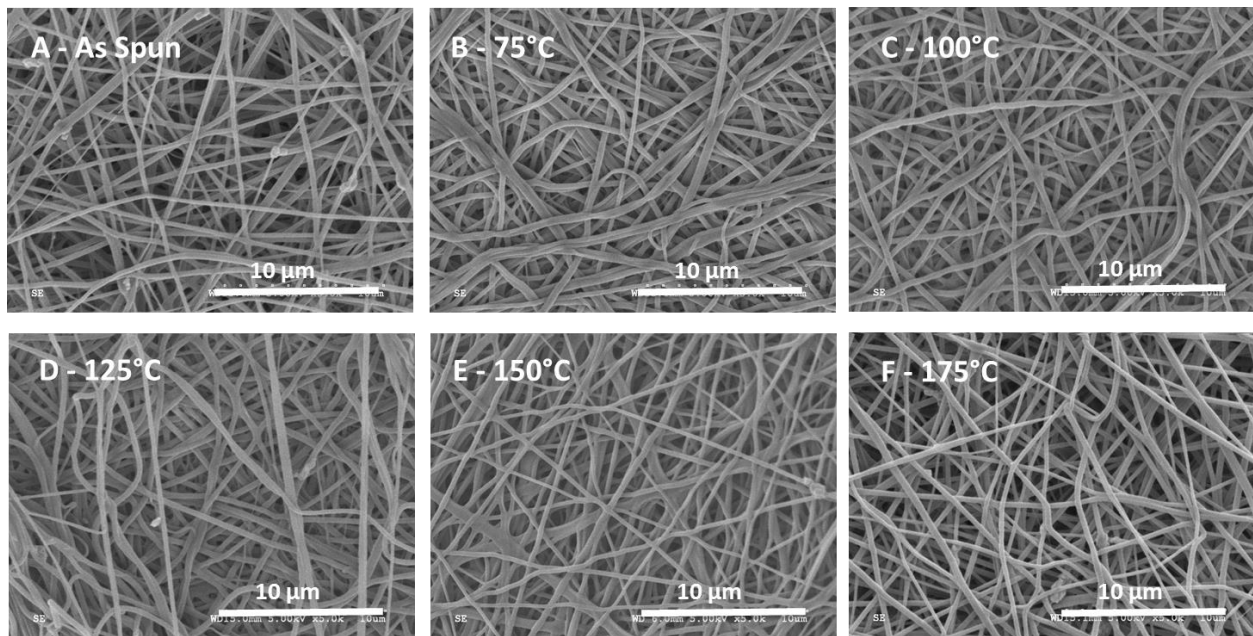


Figure 33: PVA fibre morphology comparison between fibres as-spun and after heat treatment at temperatures ranging from 75 - 175°C for two hours

From the SEM images, the heat treatment did not have significant effect on fibre morphology and diameter, other than the formation of welds between fibres as the treatment temperature increased. On the other hand, the effect of heat treatment on PVA fibre swelling and water uptake was significant. SEM images of samples soaked in PBS solution for 15 minutes, as presented in Figure 34, showed that PVA treated at 125°C or below have lost the fibrous morphology, while the structure remained somewhat porous.

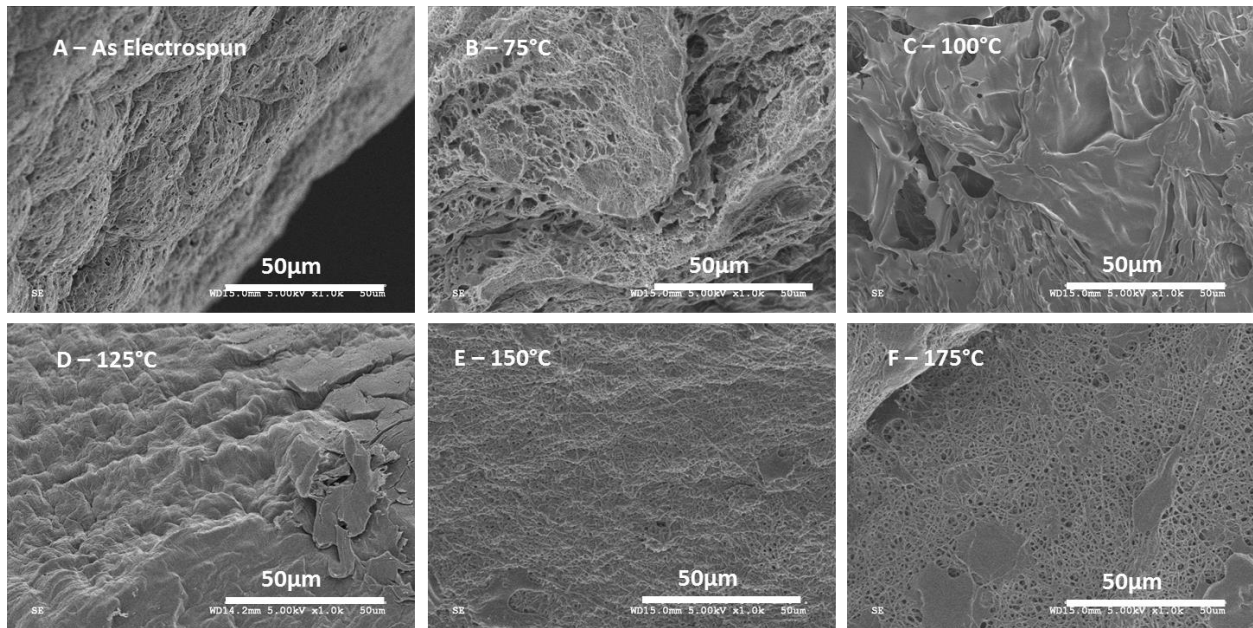


Figure 34: Nanofibre morphology of heat treated PVA after soaking in PBS solutions for 15 minutes

Improvements on morphology maintenance were possible when heat treatment temperature was above 150°C. The change was more pronounced when observing SEM images taken after soaking for 1 hour, as shown in Figure 35, in which the porous structures in most samples have been lost, and even the 150°C heat treated sample showed a fused morphology.

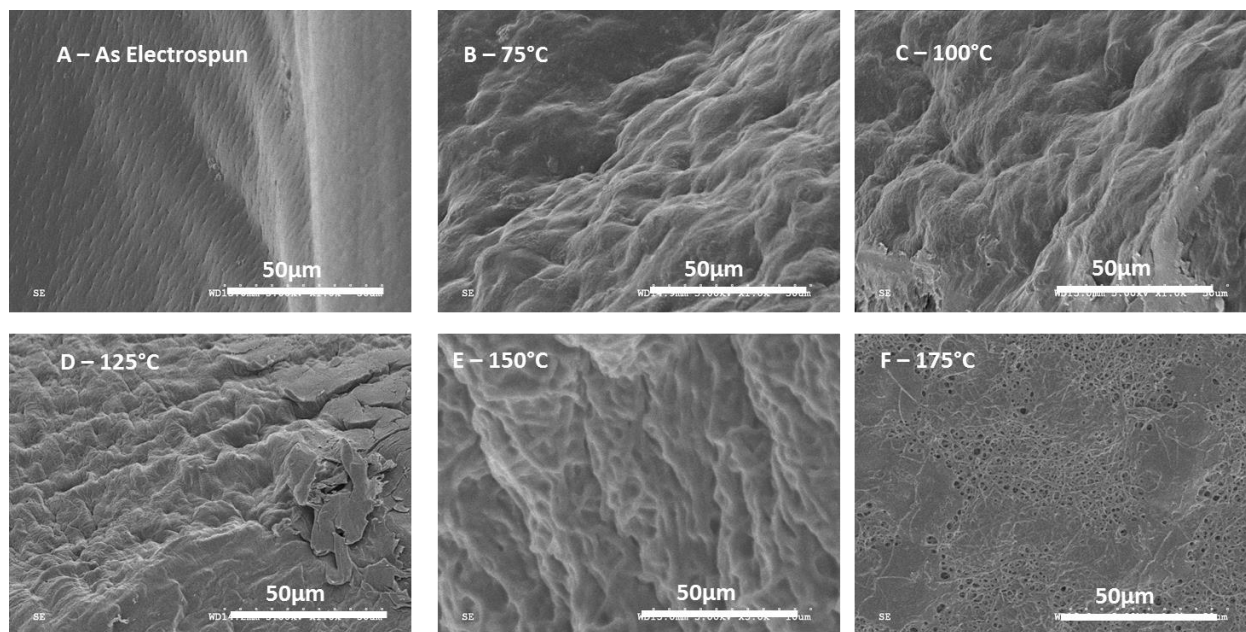


Figure 35: Nanofibre morphology of heat treated PVA after soaking in PBS solutions for 1 hour

The PVA treated at 175°C shown a high degree of stability in PBS solution, maintaining its fibre morphology until 4 hours of soaking, as shown in Figure 36.

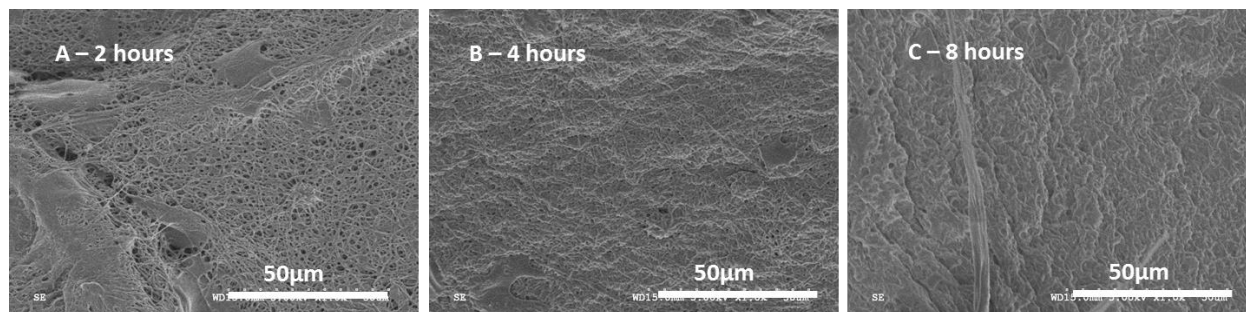


Figure 36: Nanofibre morphology change on PVA heat treated at 175°C up to 8 hours

Drug release behavior of the heat treated samples remains the most critical performance metric because reduction in PVA solubility does not translate to more gradual release, as observed from the comparison between the 88% hydrolyzed and 99% hydrolyzed PVA in Chapter 2. The effect of PVA heat treatment on kynurenine release properties is shown in Figure 37.

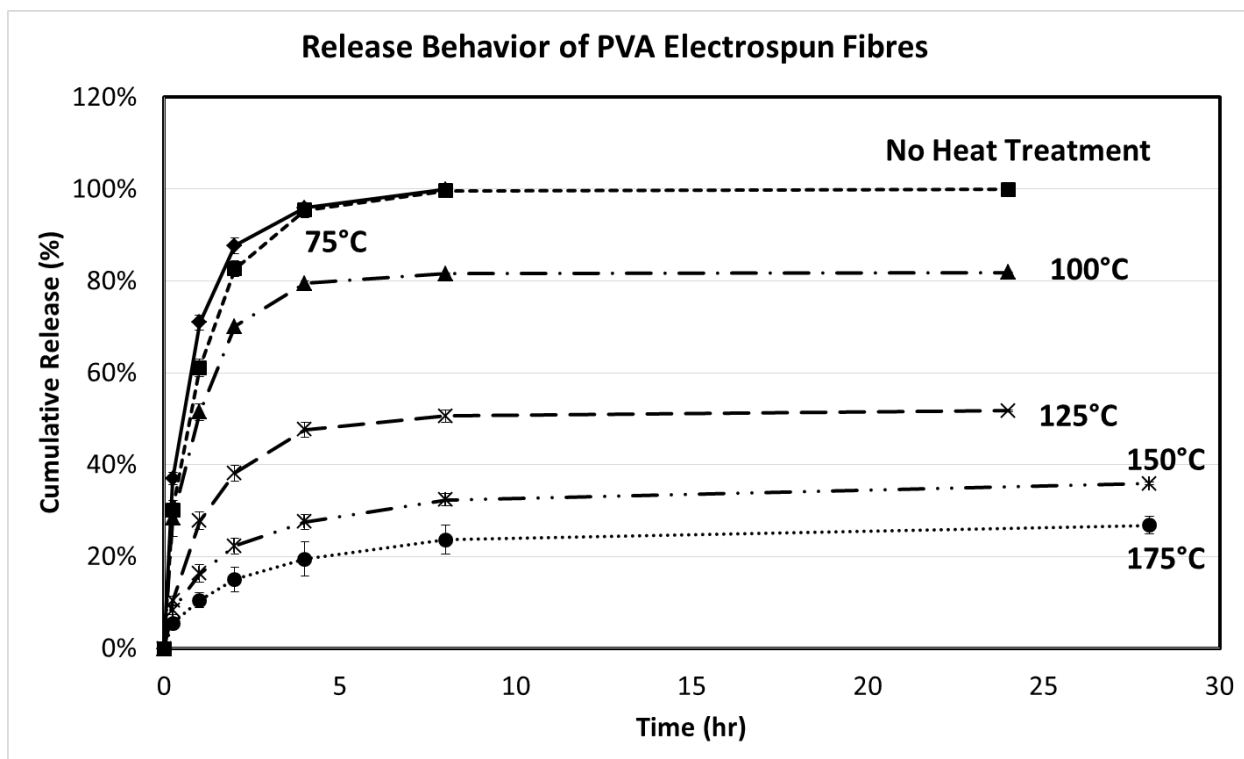


Figure 37: Effect of PVA heat treatment temperature on kynurenine release

Even with heat treatment at 75°C, reduction in burst release was evident. While the untreated PVA reached 90% kynurenine release in two hours, the 75°C treated PVA reached the same extent of release in three hours, although 100% release was still within eight hours which was well short of the five day target. It was also noticed that as heat treatment temperature increased, the total amount of drugs release was reduced. For samples heat treated at above 100°C, kynurenine release would reach a plateau after four to eight hours, followed by a prolonged period of slow release in which less than 0.5% of the loaded kynurenine would release every 24 hours. The minuscule release would continue past five days, but the cumulative release remained similar to the level observed at eight hours. To investigate whether the reduction was due to kynurenine degradation or entrapment as a result of increased PVA crystallinity, the stability of kynurenine over a range of temperatures was also measured by subjecting 5 µg of kynurenine under heat at different temperatures. The results, shown in Figure

38, suggested that drug loss may occur under heat treatment at higher temperatures, as kynurenine assays showed lower concentration detected.

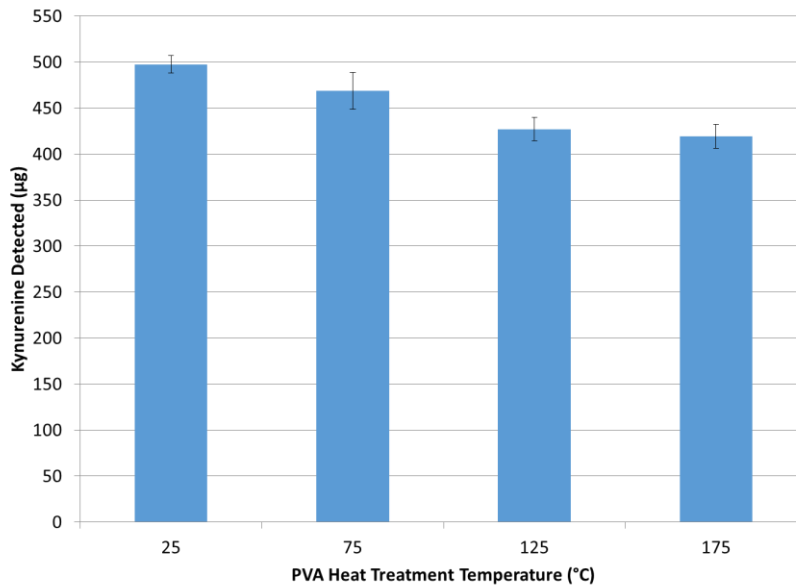


Figure 38: Kynurenine stability over the range of heat treatment temperatures

However, the maximum drug loss of approximately 15% at 175°C could not support the significant loss observed from the release assay with nanofibres, indicating that the loss is likely due to kynurenine entrapment in the crystalline PVA network.

By fitting the release data to the models described in chapter 2, it was noticed that all crosslinked PVA samples corresponded closest to the SRT model, suggesting that kynurenine diffusion is the dominant release mechanism. Table 8 summarizes the degree of correlation as well as the diffusion coefficient for each of the crosslinked samples, using release data for each sample normalized by the total release of the particular sample.

Table 8: Release mechanisms and corresponding coefficients for each crosslinked sample

Heat Treatment	Release Model	Coefficient	Correlation
As-Electrospun	Square Root of Time (Diffusion) Model	0.6455	0.9983
75°C		0.6110	0.9999
100°C		0.6021	0.9965
125°C		0.5351	0.9906
150°C		0.4099	0.9991
175°C		0.3424	0.9995

For example, the diffusion coefficient for the 175°C sample was calculated by taking the cumulative release as 100%. Release data normalization can more precisely depict the release kinetics because with a low cumulative release for samples treated at higher temperature, the coefficients will be misleadingly low. As seen in Table 8, the diffusion-controlled release indeed proceeded more gradually under heat treatment. It was also observed that while K_H underwent minimal changes at treatment temperature below 100°C, it decreased significantly with temperature when the fibres were treated at above 100°C, following equation 17 below with a correlation of $R^2 = 0.934$.

$$K_H = 0.8648 - 0.0029[\text{Treatment Temperature in } ^\circ\text{C}] \quad \text{Equation 16}$$

3.3.2 Multilayered Structure with Fibrous Shell

Protecting the kynurenine-loaded PVA fibres with an electrospun PLGA fibrous shell was proposed to impede water penetration through the drug carrier and reduce the rate of kynurenine release at the initial stages. Figure 39 shows the cross section of a multilayered structure fabricated via the method described in section 3.2.4.

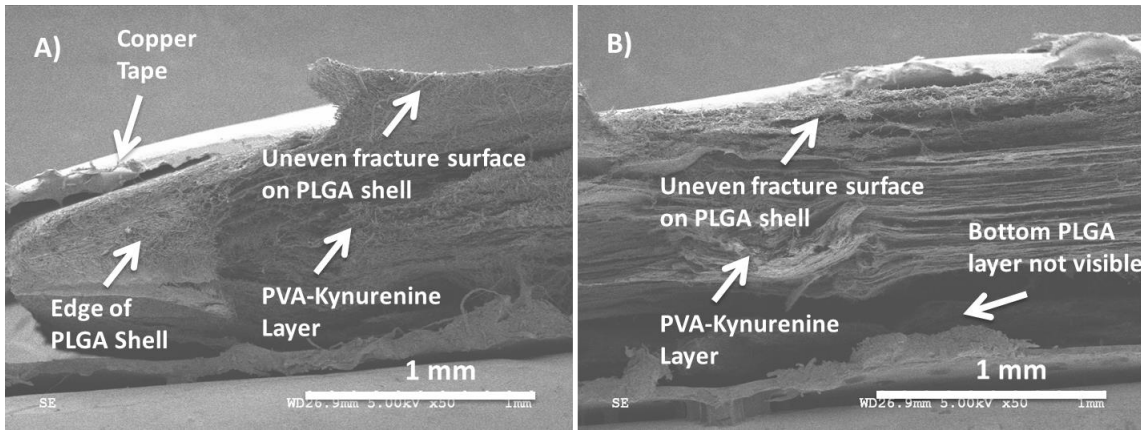


Figure 39: SEM image of the multilayered nanofibre after cold fracture, with (a) showing the separation between the PVA-kynurenine centre and the PLGA envelope from the edge, and (b) showing the two layers farther from the edge

From the SEM images, the edge of the shell, the PLGA top layer and the PVA layer can be seen. The bottom layer was not visible due to an uneven fracture surface formed during the cold fracture step. Also, when the SEM image is taken further away from the edge of the layered structure, as in Figure 39b, differentiation between PLGA and PVA layers became difficult due to the similarity in fibre morphology at the fracture surface. SEM images taken at high magnifications, as presented in Figure 40, also showed the difficulties in identifying the boundary between the layers due to uneven fracture surface.

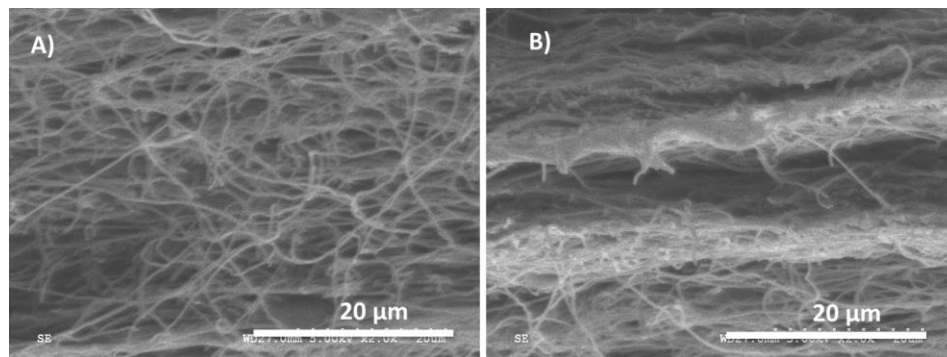


Figure 40: SEM Images (2000X) on the multilayered nanofibres, with (a) focusing on the middle layer and (b) focusing on the top layer

The difficulty in differentiating between layers prevented accurate measurements of layer thickness. As a result, thickness values reported were approximates based on measurements made on a low-magnification image using ImageJ. In addition to examining the cross section, the integrity of the seal between the PLGA layers was also tested through immersing in PBS at 37°C. Figure 41 showed the cross sections of the multilayered structure that was cut open after four and 24 hour immersion in PBS solution.

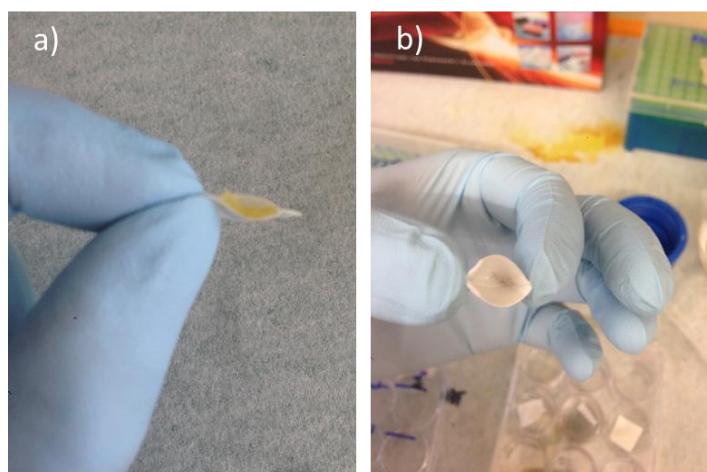


Figure 41: Cross-sections of PVA-kynurenine with PLGA nanofibrous shell after soaking in PBS for (a) 4 hours and (b) 24 hours

From the figure, it can be seen that the seal on the sides remained intact, whereas the PVA layer at the centre has become swollen after four hours, and mostly dissolved after 24 hours, indicating that the nanofibrous shell still allowed water permeation. This observation suggests that while the PLGA shell is able to delay the water penetration into the kynurenine-loaded PVA, the effect on kynurenine release rate reduction might be limited due to the amount of water that could penetrate the porous shell still being significant, as indicated by the PVA dissolution after 24 hours.

Indeed, the kynurenine release behavior, as displayed in Figure 42, showed that the kynurenine release duration was improved, but the burst release was still significant.

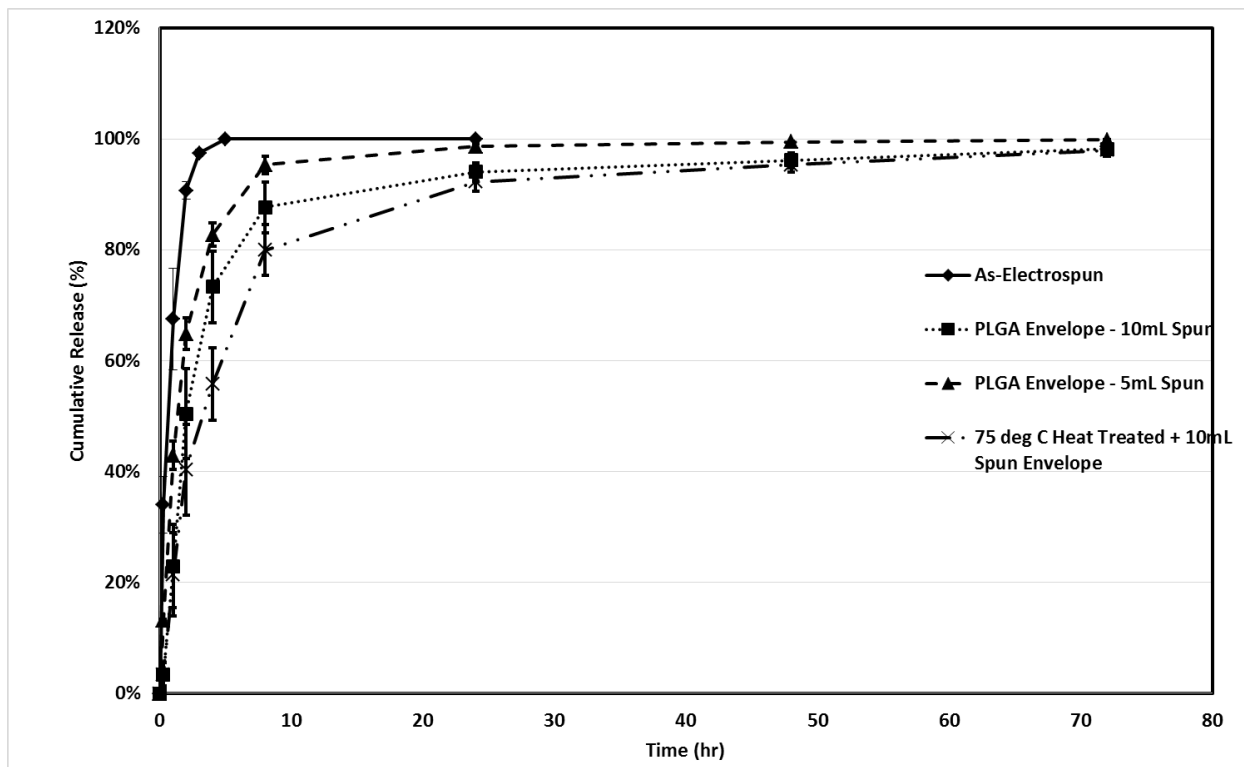


Figure 42: Kynurenine release from PVA nanofibres with electrospun layers of PLGA as envelopes. The effect of the amount of PLGA electrospun on each side was also shown

For the PVA/kynurenine reference sample without shell, 90% of the loaded drug released within two hours, whereas for the fibres with a PLGA shell, the same amount of drug released in 10 hours. Interestingly, the final 10% of the kynurenine released very gradually for an additional 60 hours. All samples shown in Figure 42 had the first 60% of release fitting most closely to the SRT release model, suggesting that diffusion of kynurenine out of the PVA matrix, through the PLGA layer may be the dominant release mechanism for the majority of the loaded kynurenine.

As observed when comparing between samples with different amount of polymers in the shell, increasing the thickness of the PLGA nanofibre layer had limited effect on reducing the release rate. With 5 mL of PLGA solution electrospun, the approximate thickness of the PLGA shell was $243 \pm 47 \mu\text{m}$, and the release profile, when fitted to the SRT release model, had a K_H of 0.4399. When the volume of PLGA solution electrospun was doubled to 10 mL, the corresponding PLGA shell thickness was approximately $455 \pm 71 \mu\text{m}$, and the release data was fitted with a K_H coefficient of 0.3798. From Figure 42, it was observed that even when shells were electrospun with more PLGA solution, the release behavior at the burst phase remained similar, with the main difference being the onset of the release plateau.

Attempts to further delay the diffusion of drugs out of the PVA inner layer were made by replacing the PVA centre with a heat treated PVA centre, with the effect also shown in Figure 42. Compared to the PLGA shell addition alone, the combined effects of heat treating the fibres and adding the PLGA shell were more pronounced ($K_H = 0.3011$). The delay in burst release on heat treated samples at the initial stages of the release study shown in Figure 37, when combined with the burst reduction effect of a PLGA shell, translated to a lower burst release, although the overall effect on release duration was not significant.

3.3.3 Dip-Coated Structure with Non-Porous PLGA Shell

As shown in the previous section, surrounding the kynurenine-loaded PVA fibres with a PLGA fibrous shell was effective in reducing the initial burst release and lengthening the overall release duration. While the release delaying effect was only found to be mildly affected by shell thickness, this part of the study aims to further reduce burst release by forming a PLGA non-porous shell around the PVA fibre via dip-coating.

In forming the non-porous shell, a dip-coating method was developed, as described in 3.2.4, which involved first dipping PVA fibres into PLGA solution and drying under pressure at a temperature above the PLGA melting point, followed by coating the fibres a second time and drying without pressure at the same temperature. The method was designed to ensure that the PLGA solution flow through the porous PVA fibre network effectively to form a uniform coat with a higher packing factor and reduced porosity. To confirm the validity of this assumption, several release assays were performed to determine the effect of the three factors in fabricated that was listed in section 3.2.4.

The release properties of the resultant PLGA coated PVA fibres that have undergone different treatment are shown below. In terms of drying temperature after dip-coating, it was seen from Figure 43 that significant burst reduction effect was achieved by drying at a higher temperature above the PLGA glass transition at approximately 55°C.

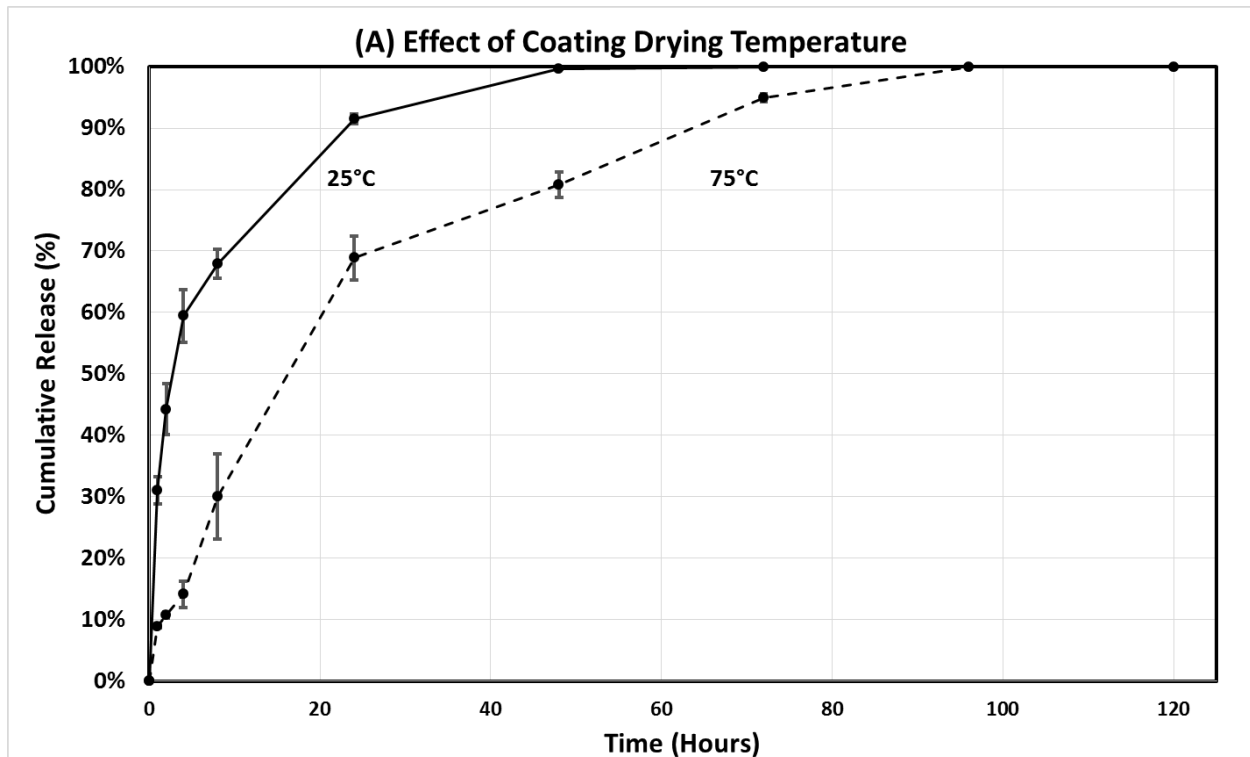


Figure 43: Effect of coat drying temperature on kynurenine release

While a 90% kynurenine release required 22 hours on the dip-coated sample dried at room temperature, the same level of release required 63 hours on the sample dried at 75°C. In addition, the time required for complete kynurenine release extended from 48 hours to 96 hours. The slowing of kynurenine release may be due to the PLGA coating, in fluid form, penetrating the PVA fibrous network at a temperature above its glass transition, allowing more complete and uniform coating of PVA fibres by PLGA. To further ensure that the PLGA solution could penetrate the PVA fibre network and coat the inside of the PVA membrane, pressure was applied during the drying process by clamping the coated sample between two metal plates while drying at 75°C. The effect of pressure application during the drying process can be seen in Figure 44, which showed further burst suppressing effect, especially after eight hours.

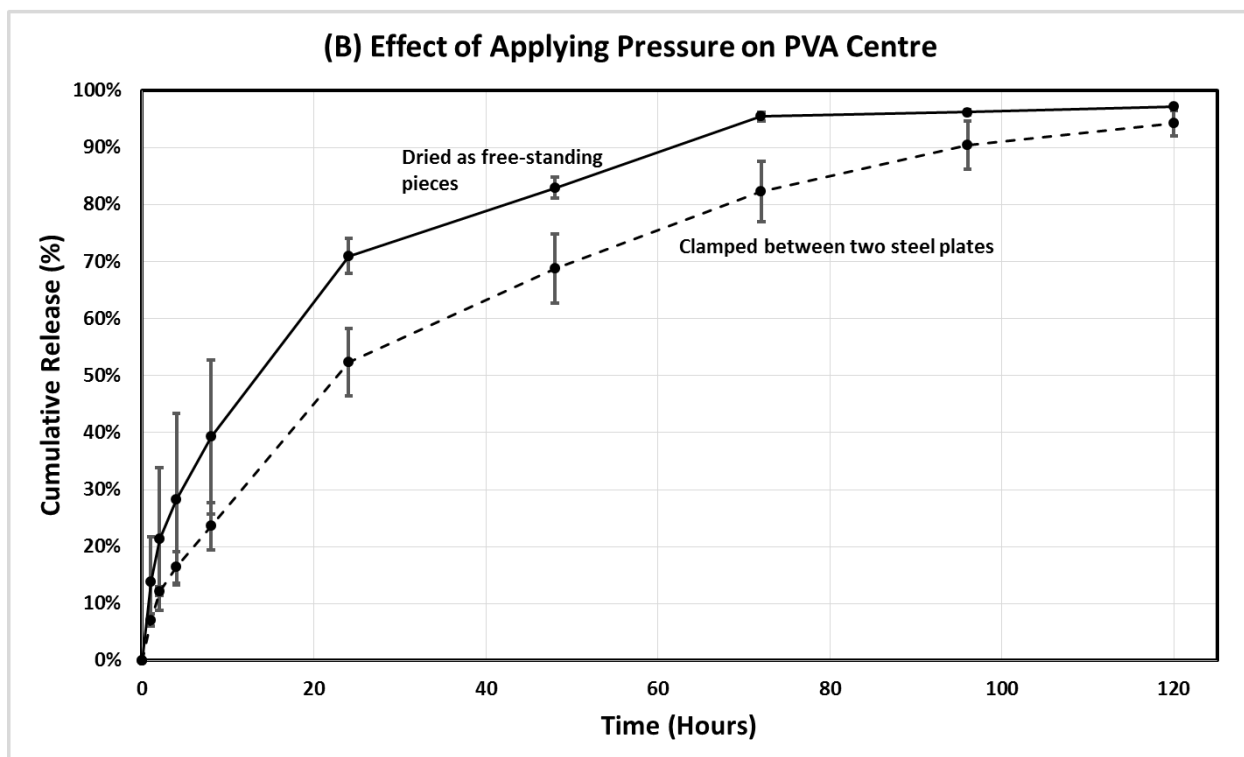


Figure 44: Effect of clamping dip-coated PVA while drying on kynurenine release

Compared to the sample dried without applied pressure, which achieved a 90% kynurenine release in approximately 63 hours, the sample dried under pressure achieved the same release in 96 hours, while the overall release duration extended to 120 hours. In addition to adding pressure during the drying process, addition of a second PLGA coat after allowing PLGA solution to penetrate the PVA fibre network was also performed to introduce further reduce drug diffusion. A comparison between single and double dip-coating is presented in Figure 45, which showed that double dip-coating was able to facilitate more sustained release behavior.

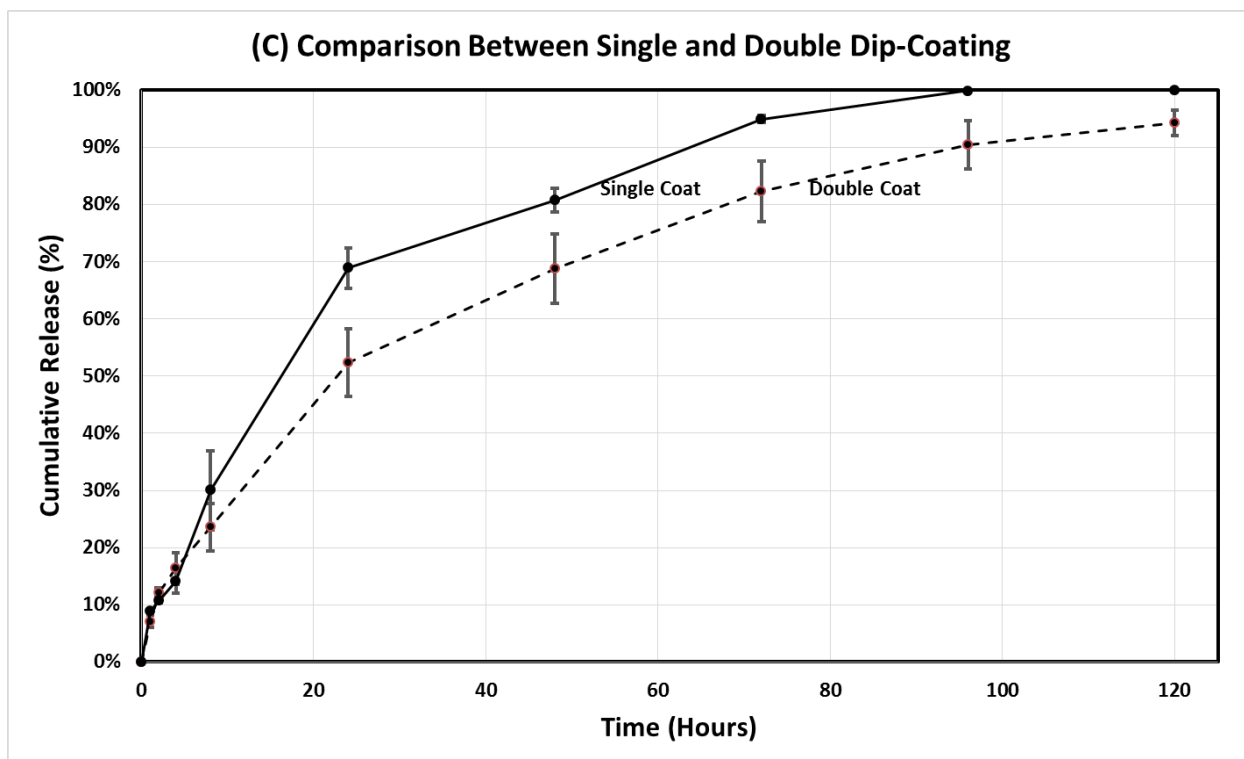


Figure 45: Single and double PLGA dip-coating and effect on kynurenine release

Interestingly, addition of a second coat did not significantly increase the thickness of the layer, yielding a thickness of $577 \pm 87 \mu\text{m}$ compared to $513 \pm 115 \mu\text{m}$ with one coat. In addition, the effect of double-coating on kynurenine release was only pronounced after eight hours, whereas the initial release behavior was very similar to the single-coated samples. The similarity in initial release behavior between the single and double coated samples indicates that while the surfaces of both samples are equal in hydrophilicity and therefore the kynurenine molecules closest to the surface of the PVA core would release in similar manners, the more densely coated samples would ultimately delay subsequent kynurenine release due to increased tortuosity against kynurenine diffusion.

Having optimized the dip-coating process, the effect of coating solution concentration was also examined. By varying the PLGA concentration from 10 wt% to 30 wt%, solution viscosity varied significantly, as summarized in Table 9 below.

Table 9: PLGA dip-coating solution properties, resultant sample thickness, and effect on release kinetics

Solution Concentration	Solution Viscosity	Coated Sample Thickness	K_H of Release
10 wt%	49 mPa-s	$275 \pm 20 \mu\text{m}$	0.1358
20 wt%	462 mPa-s	$577 \pm 87 \mu\text{m}$	0.1042
30 wt%	2538 mPa-s	$883 \pm 257 \mu\text{m}$	0.1188

The increase in viscosity with increasing concentration also caused coated samples to become thicker. However, the high viscosity also led to difficulties in maintaining consistency in coating thickness. The effect of the varying dip-coating concentration on kynurenine release is shown in Figure 46, with all three samples correlating closely to the SRT model.

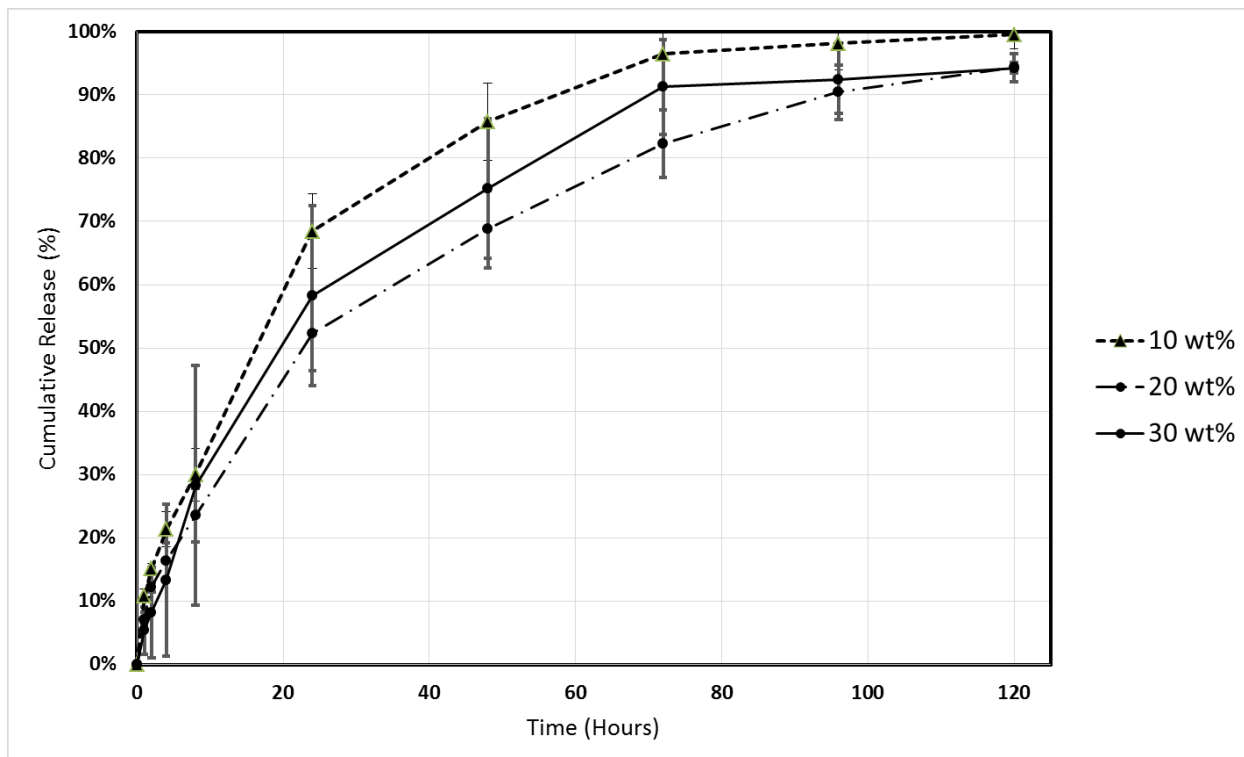


Figure 46: Effect of coating concentration on kynurenine release

As seen from Figure 46, the average sample thickness has a minor contribution to delaying kynurenine release. However, the highly inconsistent thickness of the sample coated with the 30 wt% PLGA solution seemingly had a negative effect on the long term release sustainability, with quicker kynurenine release after eight hours, although the large standard deviation in release measurement render the difference between the 20 wt% and 30 wt% coated samples statistically insignificant. In fact, it was found that the diffusion-controlled release kinetics did not correlate either dip-coating solution concentration, viscosity, or coated sample thickness. The results nonetheless showed the importance of coating uniformity on the carrier's ability to consistently sustain long term kynurenine release.

In addition to optimization of the dip-coating process and solution, methods for controlling the release duration and burst release rate were also explored via using different grades of PLGA in the dip-coating solution. By varying the ratio of the more hydrophobic lactic acid (LA) and the more hydrophilic glycolic acid (GA), hydrophilicity of the PLGA coat can be controlled, which may impact the rate of water penetration and drug diffusion from the fibres. The effect of the four grades of PLGA on the hydrophilicity of the dip-coated samples was determined by wettability measurement results, which are shown in Figure 47. As seen from the figure, the average wetting angle increased with LA content in the PLGA from 50% to 75%, while further increase to 85% showed no effect on the wettability.

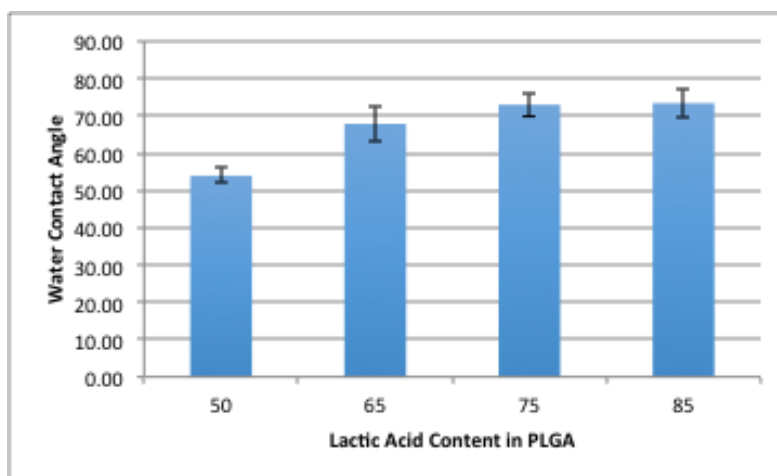


Figure 47: Effect of lactic acid content in PLGA on wetting angle on coated nanofibres

Figure 48 compares the kynurenine release behaviors between four grades of PLGA that was coated on the drug carrier.

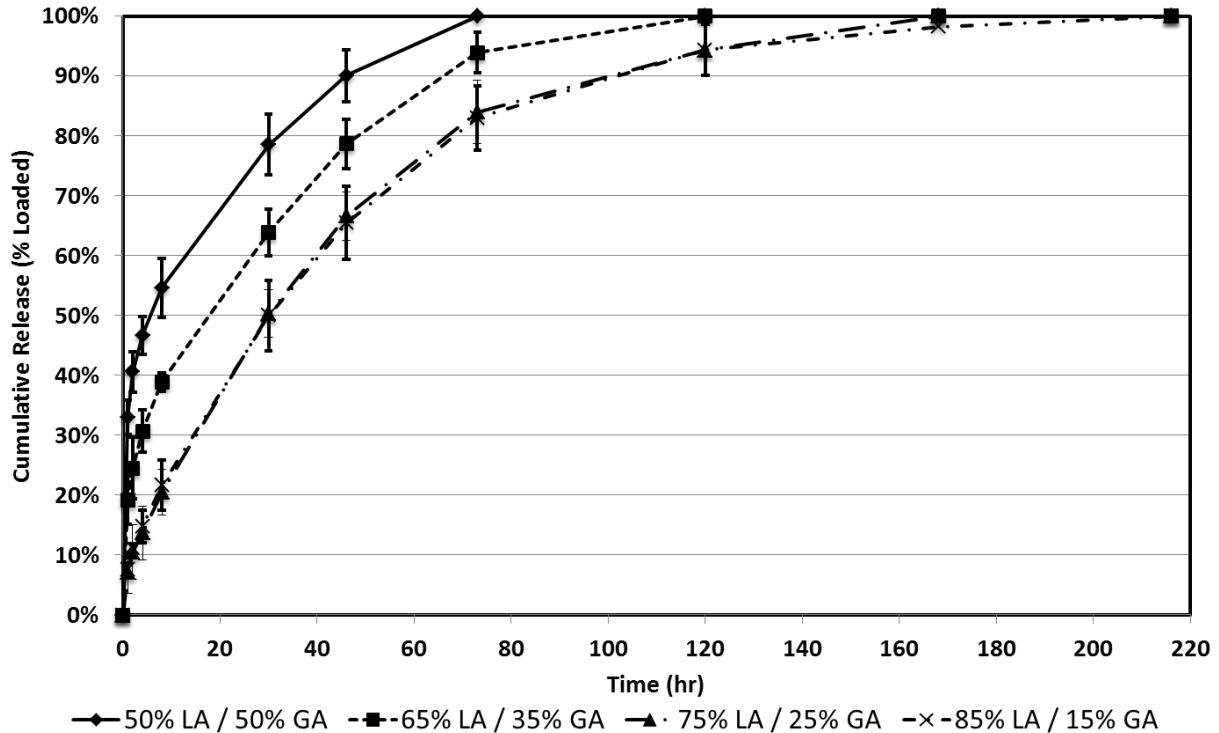


Figure 48: Kynurenine release from PLGA coated samples with different lactic acid content in the coatings

At a LA:GA ratio of 50:50, the coating is the most hydrophilic and the resultant coated carrier has the shortest release duration of 72 hours. The release duration extended to 120 hours as the LA:GA ratio increased to 65:35, while the shape of the release curve remained similar, indicating similar release mechanisms. Further increase of the LA:GA ratio to 75:25 and 85:15 showed minor effect on extending the release duration. Although the time required to release 100% of the loaded kynurenine was extended to 168 hours, most of the kynurenine has already been released by the 120 hour mark. The similarity between samples with LA content of 75% and those with 85% corresponded well to their nearly identical wettability.

It was also found that the release data for each of the four grades of PLGA coating followed both the SRT and the power law model with high levels of correlation. The fit between the data

and the two diffusion-based models were nearly identical. However, the diffusion constants for the fitted power law models were below 0.56, which is suffice to safely assume that the dominant release mechanism for the coated samples was diffusion as opposed to swelling. To quantitatively compare kynurenine diffusion rates between the four grades of PLGA coating, the SRT model coefficient K_H was used. As the LA:GA content in the coating increased, the coefficient decreased steadily from 0.1885 at 50% LA ($R^2 = 0.9968$), to 0.1107 at 65% LA ($R^2 = 0.9713$), to 0.0994 and 0.0975 for 75% ($R^2 = 0.9878$) and 85% LA ($R^2 = 0.9924$), respectively, thereby indicating a more gradual diffusional release with increasing LA content. In the attempt to correlate K_H to lactic acid content, it was observed that K_H did not correlate linearly with K_H ($R^2 = 0.805$), but instead, it was linearly proportional to the wetting angle, following equation 18 with correlation of $R^2 = 0.979$.

$$K_H = 0.4408 - 0.0047[\text{water contact angle}] \quad \text{Equation 17}$$

3.4 Discussion

The studies presented in the previous chapter showed that kynurenine releases from a PVA fibrous carrier predominantly by diffusion. In addition, by using hydrophilic carriers such as PVA, all of the loaded kynurenine released in less than five hours, with a major portion release in a burst fashion within the first two hours. The quick release was attributed to the fast swelling of the hydrophilic carrier and subsequent diffusion of kynurenine through the swollen fibres, as indicated by the SEM images taken during the drug release assay. The main focus of the work presented in this chapter is therefore to utilize the knowledge gained from the previous chapter to delay water penetration and kynurenine diffusion. The work presented in this chapter demonstrated three methods for modifying the matrix to control kynurenine diffusion.

The first method was to create a fibrous matrix containing a tighter network of polymer chains by either chemically crosslinking PVA or promoting PVA crystallinity via heat treatment. Chemical crosslinking of PVA fibres and gels have been widely demonstrated in existing literature, using aqueous solutions of glutaraldehyde and sodium borate. However, the use of aqueous crosslinking solutions on kynurenine-loaded PVA caused premature drug release as kynurenine was leached into the crosslinking solution. The use of maleic acid in PVA solution, which has been shown to react slowly with PVA thereby facilitating in-situ crosslinking during electrospinning, showed no effect on kynurenine-loaded PVA. The lack of effectiveness of maleic acid was due to the hydrogen bonds formed between kynurenine and the hydroxyl groups in the PVA molecule, which is also the same groups that maleic acid are expected to form crosslinks with. The lack of feasibility of crosslinking kynurenine-loaded PVA meant that heat treatment was the only matrix modification option for delaying drug release.

Heat treatment provides energy to PVA chains enabling them to rearrange and form crystalline regions. Detailed crystallinity studies were not conducted in this research as they have been extensively explored in numerous previous studies. Indeed, heat treatment at 75°C was sufficient to see a slight suppression in the burst release behavior, although the overall release duration remained unchanged. As the heat treatment temperature increased to 175°C, kynurenine release rate also decreased as observed from the calculated coefficient to the SRT model. It was observed that release kinetics decreased in a linear fashion when the heat treatment temperature was above 100°C. In addition, the release duration was extended with increasing heat treatment temperature. However, the reduction in release was also met with a corresponding decrease in cumulative release, ultimately resulting in a loss of 70% of the loaded kynurenine in the sample heat treated at 175°C. Release assay tests on kynurenine treated at different temperatures showed that although drug degradation occurred at high temperatures to a small extent, it could not be the main reason for the low overall release

observed from the heat treated nanofibres. Moreover, fibre morphology observation showed a lower level of water uptake through reduced fibre swelling at high temperature, which, as demonstrated in previous studies, is a result of the increased crystallinity in the PVA limiting water penetration (Byron and Dalby 1987, Wan and Lim 1992). The reduced water penetration into the PVA network, especially the crystalline region, is a likely reason for the observed kynurenine entrapment. Nonetheless, the drug entrapment in the PVA membrane greatly limited the practicality of the heat treatment technique for antifibrogenic applications, as it could only be performed up to a modest 75°C to ensure complete release of the loaded drug within the time frame of interest, which, as mentioned previously, had minimal effect on release kinetics. However, by looking at the heat treatment from a broader perspective to examine the transferability to future drug carrier development, the technique was able to control release kinetics to a more significant extent compared to adjusting feed electrospinning solution parameters. Not only was heat treatment able to change the extent of burst release, it was also able to lengthen the drug release period.

Although PVA heat treatment at low temperatures had limited effect on the PVA-kynurenine system, which was not nearly sufficient to facilitate sustained kynurenine release over five days, its effect could be greatly amplified by combining with other modification techniques, which, in this study, was the addition of a PLGA diffusion barrier. Similar to the heat treatment, the addition of a PLGA fibrous shell was effective in reducing kynurenine burst release, but with limited effect. However, unlike heat treatment, the fibrous shell was able to extend the overall release duration, as the final 10% of the loaded kynurenine remained in the carrier after the burst release and required an extended length of time to be released. The nonlinear trend near the end of the release profile is likely caused by buildup of fluids containing dissolved kynurenine at the pocket inside the PLGA fibrous envelope, created after the dissolution of the PVA fibre, which required longer time to diffuse through the PLGA barrier.

The diffusion barrier effect was further enhanced by dip-coating the kynurenine-loaded PVA into PLGA solutions, instead of electrospinning layers of PLGA fibres around the carrier. By simply applying one coat of PLGA with 85% lactic acid content, the release duration extended to 60 hours with the burst phase significantly suppressed. The optimization study on the PLGA coating process was carried out with a hypothesis generated from initial dip-coating study that although the PVA fibre surface was covered by a PLGA film, the inter-fibre spaces might not be coated which would still allow fast drug diffusion. This hypothesis was confirmed by the positive results obtained from improving PLGA flow into the fibre network. By increasing coating treatment temperature past the PLGA glass transition, PLGA was more able to penetrate the PVA fibre network due to softening, although the increase in PLGA crystallinity also played a significant role in water penetration. Adding pressure on the coated PVA fibres during heat treatment also helped ensure uniform internal coating by the PLGA, which led to further reduction of burst release. It was also found that adding a second coat of PLGA contributed to noticeable reduction in the release rate after 8 hours, due to the increased tortuosity against kynurenine diffusion. The effect of coating optimization on kynurenine release also showed the importance of available surface area of the drug-loaded carrier and its packing density on the release behavior. As processing measures were taken to help the coating solution penetrate into the fibre network, such as increasing processing temperature and adding pressure, the available surface area of the kynurenine-loaded was reduced. In this case, the available surface area can be considered the interface between PVA fibres and the surrounding air, which is replaced by water once the layer is wetted, due to its high hydrophilicity. Coating the PVA with PLGA replaces the PVA/water interface with a PVA/PLGA interface, and the proportion would change by increasing the PLGA coating solution penetration into the PVA fibre network, or in other words, the packing density. While the PVA/water interface was replaced by a PVA/PLGA interface, PLGA/water and PLGA/air interfaces would also be created simultaneously. However,

since it is known that PLGA is less hydrophilic than PVA, the PLGA/water interface would be correspondingly smaller, reducing the availability of pathways for kynurenine diffusion, as the drug must be carried out of the carrier by water.

In addition to coating process optimization, the investigation on the effect of the LA:GA ratio in PLGA demonstrated the ability to tailor kynurenine release ranging from 72 to 120 hours, which is a significant improvement from the 2 to 5 hour burst release from the as-electrospun kynurenine-PVA. However as the release behavior is non-linear, it is important to determine the duration in which the amount of kynurenine released is above the 50 $\mu\text{g}/\text{cm}^2$ per day. The release results in terms of absolute kynurenine release are shown in Figure 49.

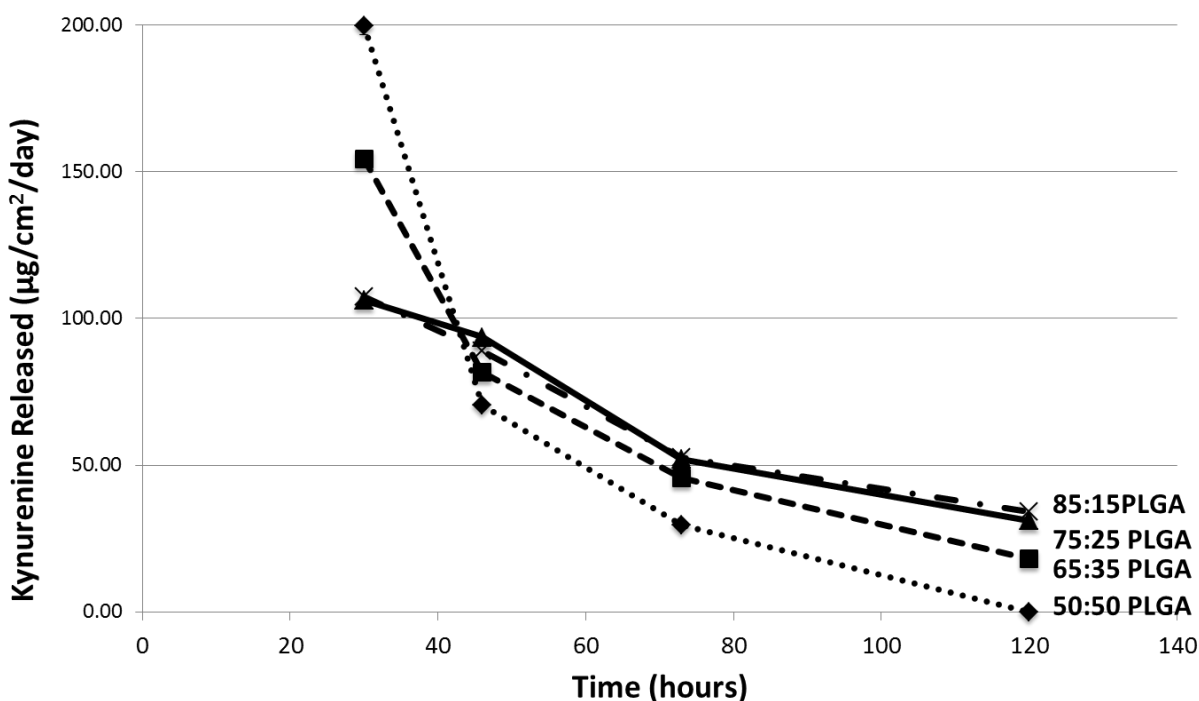


Figure 49: Kynurenine release dosage vs. time for PLGA dip-coated kynurenine-PVA

It was observed that with the more hydrophobic PLGA coating, the kynurenine release is more stable, and remained above the 50 $\mu\text{g}/\text{cm}^2$ per day dosage for 80 hours, which satisfies the release target of 3 – 5 days. Moreover, to ensure a longer period of time during which the

release remains above the dosage requirement, the initial kynurenine concentration in the electrospinning could be increased. As determined in section 2, increasing kynurenine loading in the electrospinning solution had a relatively minor effect on the burst release behavior, as represented by the small change in K_H .

Ultimately, the results from the matrix modification showed that it is possible to extend the release duration to the 3 – 5 day target. The most significant release delaying effect was observed when kynurenine-loaded PVA fibres were dip-coated with PLGA, forming a film-like shell, and more so when the inter-fibre spaces were also coated. While in the previous chapter, it was shown that PVA fibrous structure was quickly lost and therefore could not maintain itself as a fibrous dressing, the dip-coating study shown in this chapter focused on intentionally rendering the drug carrier non-fibrous to reduce kynurenine diffusion. This is unlike existing studies on electrospun fibrous drug carrier, which focused on electrospun fibres mainly due to the large surface area for cell attachment and for minimizing drug retention in the matrix. Although this investigation arrived at the conclusion that the optimal kynurenine release system is non-fibrous, the electrospinning process remained an important step in fabricating the kynurenine carrier for several reasons. First, the use of electrospun fibres enables even distribution of kynurenine throughout the core, allowing uniform release. In addition, it was shown in the previous chapter that electrospinning can help embedding drugs in fibre interior, whereas casting produced films with kynurenine exposed on the surface. This distinction is important and can affect the release rate and duration after dip-coating. When water penetrates the PLGA coating, if kynurenine molecules were aggregated near the interface between the PVA core and the PLGA shell, they would be able to readily diffuse out of the system, whereas for a well-coated fibrous core, kynurenine must follow a more tortuous diffusion path. The comparison is analogous to the cast film versus electrospun fibre comparison in the previous chapter that showed a higher portion of the loaded kynurenine residing on the film surface. In

the dip-coated form presented in this chapter, the PVA fibres could be used more as a drug-releasing device due to the lack of surface features that sets electrospun fibres apart from other material class, but they can be incorporated into a wound as part of a system such as underneath a pressure garment, or inside a hydrogel scaffold held together by a wound dressing, similar to the composite scaffold proposed by Han et al consisting of PCL nanofibres embedded within a PEG hydrogel matrix (Han, Johnson et al. 2012). Moreover, if there is desire to adopt the dip-coated fibres as a standalone kynurenine-releasing wound dressing, the knowledge gained in fibrous shell fabrication presented in section 3.3.2 can be applied, by electrospinning a fibrous envelope around the dip-coated core, while the fibrous shell can be composed of a variety of fibres suitable for the specific environment. In this application, the shell could provide fibrous surface for cell attachment and tissue regeneration, whereas the edges could be utilized for suturing onto the affected tissue.

3.5 Conclusion

The investigations conducted in this chapter focused on demonstrating matrix modification techniques that could allow drug release tailoring. Most notably, the duration of kynurenine release was extended from five hours for the as-electrospun PVA carriers to 120 hours for the dip-coated carriers. For a PVA-based formulation, release periods in the range of days such as the ones demonstrated in this chapter are a first, especially considering the drug is a highly water-soluble small molecule. As it was established in the previous chapter that the choices for kynurenine carrier were limited to PVA by its solvent incompatibility and pH sensitivity, the rest of the investigations that involved kynurenine release control focused on modifying a very restricted material system to lengthen release, where there is no flexibility in altering material choices. The work in this study is therefore one of the first in this area, which is unlike existing

studies in which demonstrations on release rate control mainly relied on changing or blending matrix materials and, to a lesser extent, adjusting polymer concentration and molecular weight.

It was also established in the previous chapter that the formation of hydrogen bonds between PVA and kynurenine restricted the use of PVA with high hydrolysis, such that only PVA grades with 88% hydrolysis were feasible grade for electrospinning. In this chapter, it was also shown that as matrix modification work progressed, additional challenges were posed by kynurenine. Due to its hydrophilicity, kynurenine had a tendency to release prematurely in crosslinking solutions, thereby rendering all solution-based crosslinking ineffective. However, these crosslinking techniques may become useful in future drug carrier development studies involving less water-soluble therapeutics.

Despite the limitations posed by the use of kynurenine, suppression of kynurenine burst release and extension of its release duration were observed from applying different modification techniques. Under heat treatment, burst release was noticeably reduced starting at a treatment temperature of 75°C, although the overall percentage of drug release began to decrease starting at a treatment temperature of 100°C. By adding an electrospun PLGA shell, improvements were observed on both burst release reduction as well as release duration lengthening, while limited contribution was also noticed from adjusting the PLGA shell thickness. In addition, a drug retention effect was also observed from the layered samples in which the final portion of the drug required a longer time to release. The most significant effect was observed from PVA carriers that were dip-coated in PLGA solutions, which showed immediate improvements over as-electrospun PVA in the initial study by extending the release duration to 60 hours. Via several dip-coating process optimizations to allow the PLGA to better penetrate the PVA fibre network, the release duration of the dip-coated samples was further extended to 120 hours.

For the kynurenine system, by dip-coating the PVA with PLGA solution, drug release was slowed by rendering the carrier non-porous. Unlike existing studies on electrospun drug carriers, the kynurenine carrier presented in this study, in its as-fabricated form, cannot be used doubly as a scaffold that releases drug and provides large surface area for cell activities. On the other hand, this study focused entirely on release control, as the stringent compatibility of kynurenine with polymer carriers presented a more pressing need for a material system that can facilitate sustained release. Also considering that the kynurenine carrier is to be applied post-epithelialization, the need for release control far outweighs the desirable surface effect that previous work focused on. Indeed, by utilizing a hybrid kynurenine carrier containing dip-coated electrospun fibre, common challenges associated with both cast-film carriers and electrospun fibrous carriers were overcome. The electrospun fibrous core provided a platform for uniform drug distribution and prevented kynurenine from aggregating on the carrier surface, which are common for gel and film carriers as observed from the results from Chapter 2. Furthermore, the electrospun core was able to prolong kynurenine shelf life as shown in the initial drug release assay results. However, electrospun fibres were often associated with quicker burst release due to the large surface area in contact with surrounding fluids. As a result, the current hybrid design was able to overcome the burst release issue while maintaining the desirable drug carrying capabilities of electrospun fibre carriers.

Another important outcome of the study presented in this chapter is gaining the ability to not only lengthen but also to tailor the drug release. By using a combination of heat treatment and fibrous shell, release ranging from two hours in the as-electrospun form to 48 hours could be achieved. Further modification by dip-coating the carrier with PLGA with varying LA:GA ratios yielded tunable release durations from 60 hours to 200 hours. The ability to tailor release duration between these ranges allows for flexible adjustment for dressing change intervals as

well as customizable application on a wider variety of wound conditions, such as different skin properties and the level of exudation. The processes presented in this chapter could also be applied to other hydrophilic drug and carrier systems, potentially opening opportunities for other possible small-molecule hydrophilic drug such as amino acids and its metabolites, which may be beneficial for regenerating other types of tissues as well.

These investigations therefore demonstrated two methods for drug release control, in addition to adjusting feed material parameters presented in Chapter 2. With matrix modification, it is possible to further tailor the extent of burst release as well as the duration of release. With encasing the drug carrier in a separate phase, an even broader control over release duration can be accomplished.

4 Carrier Design Fabrication into Practical Dressing Materials

4.1 Introduction

The advancement in the field of incorporating therapeutics into the electrospinning process allows resultant fibre membranes to become more useful than the traditional passive scaffolds aimed at protecting and supporting wound sites. Instead, the new generation of electrospun scaffolds can be engineered to engage in the surrounding biological environments and stimulate specific responses, including anti-inflammatory, healing promotion, and anti-scarring that was the expected effect of kynurenine. In the previous chapters, detailed investigations on kynurenine and carrier compatibility and methods for lengthening drug release duration were presented. The studies resulted in an electrospun PVA-based fibrous carrier that could effectively encapsulate kynurenine, as well as a series of modification methods that led to customizable release from two hours to 200 hours. The control over kynurenine release from the fibrous scaffolds helps ensure that appropriate cellular responses are stimulated at the correct timing. While the release properties of the current kynurenine carrier design have been able to reach the target set out prior to the study, it is also necessary to ensure that the modifications made to the carrier does not significantly compromise its mechanical properties. Traditionally, electrospun fibres can be applied topically with relative ease after sterilization. In applications where dressings are replaced regularly, requirements on mechanical property maintenance are lower than in implanted scaffold applications, further lowering the stringency on scaffold properties. For external wound applications, the scaffolds must have sufficient strengths to be handled during the manufacturing process as well as by medical professionals during placement on wounds, when the scaffolds are mostly subjected to tensile loads. Although it has been shown in the past that electrospun fibres have superior tensile strengths compared

to short fibre scaffolds and hydrogel scaffolds, it is desirable to assess the effect of matrix modification on the tensile properties. The challenge in assessing mechanical properties of electrospun scaffolds is the lack of standards in terms of the strength requirements for wound dressings. However, for electrospun dressings, it is useful to compare mechanical properties with existing porous or microfibrinous wound dressings, because the existing products are known to be sufficient for the same applications. For fibrous dressings, tensile strengths in the order of 10 MPa have been reported (Rho, Jeong et al. 2006), which is also similar to the upper ranges of reported values for the tensile strength of native skin at approximately 20 MPa (Shevchenko, James et al. 2010). In terms of stiffness, values up to 130 MPa for Young's modulus of existing dressings have been reported in literature (Elsner, Berdicevsky et al. 2011). In general, it is desirable for wound dressings to not be overly stiff compared to native skin as dressing stiffness may limit patient motion and cause discomfort. Reported values for Young's modulus for native skin vary greatly depending on the test method, subject age and location of the skin, with a wide range from 0.008 MPa (Pailler-Mattei, Bec et al. 2008) up to 70 MPa (Shevchenko, James et al. 2010).

In Chapter 3 it was also established that in its as-fabricated form, the optimal kynurenine carrier is a PVA fibrous membrane coated with PLGA, which may not be an ideal surface for wound dressing on its own. While there are many possibilities in which the carrier can be applied as part of a wound dressing system, such as in a topical gel or in a wound pad under pressure garments, it is nonetheless attractive to examine another system with an electrospun nanofibrous morphology on the carrier surface to avoid the need for applying multiple layers and to maximize surface for cell attachment.

Prior to the investigations presented in this thesis, recent work on electrospinning has already shown that it is an effective, flexible method to create planar devices for applications requiring

large surface area, including drug carriers. While being relatively simple to utilize, electrospinning is also scalable, thereby allowing fibre production in pilot and industrial scales. In addition, the early results of the current study also showed that electrospinning was able to help encapsulate kynurenine in a suitable carrier and prevent aggregation on the surface, while allowing the drug to be uniformly distributed throughout the fibre membrane. However, like most existing literature on electrospun fibres for medical applications, the focus of this study has been thus far on nonwoven, planar fibrous membranes, while another major benefit of electrospun fibres has been mostly neglected. Due to their continuous nature, electrospun fibres can be much more versatile in applications than planar structures as they can be fabricated into various three-dimensional textile structures, which is also a major benefit compared to short, discrete fibers that are used in some wound dressings such as Kaltostat[®]. In addition to materials choice and nozzle configurations, electrospinning collectors can also be easily modified to yield specific fibre configurations such as nonwoven, aligned bundles, and crisscross. These continuous configurations can also serve as the basis of fabricating higher order nanofibre-based structures when combined with tradition textile fabrication techniques (Ko 1997). Among different forms of textile structures, sutures are of particular interest because of their usefulness in wound closure. The ability to incorporate the desirable surface properties of nanofibres into sutures will open up new opportunities for medical applications because in addition to topical applications, sutures can also be used widely in other surgical and reparative procedures involving internal organs. The well-documented effectiveness of nanofibres as drug carriers adds another incentive to fabricate them into sutures.

Functionally, sutures fabricated from nanofibres containing kynurenine could also be tremendously beneficial to patients with sharp trauma or surgical incision wounds. Under normal circumstances, applying a kynurenine-loaded suture to an acute wound immediately after injury may not be ideal because the stimulation of MMP production may interfere with tissue

production at the proliferation stage. However, as mentioned earlier, patient groups with darker pigmented skin are more susceptible to FPDs, and may develop scars and keloids shortly after surgery or injury. As such, ability to form kynurenine-loaded PVA into sutures will be desirable for ensuring wound closure while maintaining balance between ECM production and digestion.

Feasibility for fabricating nanofibre-based sutures has been demonstrated in several previous studies (He, Huang et al. 2009, Hu, Huang et al. 2010, Weldon, Tsui et al. 2012). The first challenge in suture development is to fabricate nanofibres into thread-like structures. Ko et al presented one of the first studies on electrospinning nanofibre threads by incorporating rollers at the ground collector that attenuate the nanofibres. In subsequent studies, aligned nanofibres were electrospun onto a rotating disc collector and then used as a drug-loaded thread. Using this technique, Weldon et al fabricated anesthetic-loaded threads using PLGA, and showed that local anesthesia was achieved in rat models with wounds healing normally after one week. In another study, Hu et al used P thread collected on a disc to produce a braided suture using a circular braider (Hu, Huang et al. 2010). The resultant suture, which was coated with a chitosan solution, showed biocompatibility in rats with no adverse effects. Subsequent studies by Hu et al on PLA sutures loaded with cefotaxime sodium also showed antibacterial effects. Despite the feasibility of nanofibre threads and braids in wound healing and in biocompatibility, mechanical properties for these structures remained below commercial sutures in terms of tensile strength, which are often in the range of several hundred MPa. Vicryl sutures, composed mainly of poly(glycolic acid) (PGA), have a tensile strength in the range of 460 MPa (Stamboulis, Hench et al. 2002). Other examples of commercial sutures include Maxon[®] sutures in the range of 600 MPa, and PDS sutures in the range of 470 MPa (Mäkelä, Pohjonen et al. 2002). In comparison, the braided PLA suture reported by Hu et al has tensile strength in the range of 90 MPa. In terms of breaking force, the sutures fabricated by Hu et al, which corresponded to size 2-0 sutures, were in the range of 8 N, which is close but less than the 10.2 N required in the US

Pharmacopeial Convention Standards (Hu and Huang 2010). While individual nanofibres are known for their superior tensile strength along its longitudinal direction, the strength of nanofibres assemblies such as mats and yarns are often lower and insufficient for suture applications. Unlike nanofibre applications as nonwoven dressings, sutures must bear tensile loads and they must ensure wound closure. In addition to the shortcoming in tensile properties, the current fabrication method for nanofibre yarns could also be improved, as the disc collection method yields one yarn per electrospinning run, and requires yarn unloading after each run, which may limit scalability of the process.

This chapter presents investigation on incorporating the design of the kynurenine-loaded PVA fibre carrier into two applicable forms, including dressing and sutures, which are the two most common forms applied on cutaneous and burn wounds. It is important to ensure that kynurenine carriers fabricated into either forms can be handled and utilized. In the dressing part of the study, samples can be created by surrounding the dip-coated PVA with a fibrous envelope. In this case, the tensile properties of the assembly as well as suturing strength must be assessed. For sutures, the study objective is twofold. Since it has been shown in the previous studies that yarns and sutures created by electrospinning have lower strength compared to other textile materials, the primary objective is therefore to develop modifications to the electrospinning and braiding techniques that can improve the mechanical properties of nanofibre-based sutures, by combining electrospun fibre yarns with commercial microfibre reinforcement yarns to produce a hybrid suture. In this study, yarns composed of kynurenine-loaded PVA were the main constituent of the sutures, with silk yarns from silkworm silk chosen for the reinforcement phase in the hybrid suture due to their known tensile properties and common use in sutures. Building on the successful work by Hu et al in braided nanofibre sutures (Hu, Huang et al. 2010), 3D hexagonal braiding was employed to fabricate hybrid sutures. In addition, to improve the scalability of the yarn production process, nanofibre electrospinning was performed onto a

modified drug collector containing multiple aluminum strips, instead of electrospinning onto a rotating disc. In doing so, multiple yarns could be produced simultaneously, compared to one at a time on a rotating disc, thereby significantly enhancing the productivity of nanofibre yarns and ultimately the hybrid sutures.

4.2 Materials and Methods

4.2.1 Materials

PVA with 88% average hydrolysis and a weight average molecular weight of 130,000 and kynurenine purchased from Sigma Aldrich were used as described in section 2.2.1, using distilled water and 1M sodium hydroxide as solvents, respectively. For manufacturing dressings, an electrospun envelope was created using PLGA with a LA:GA molar ratio of 85:15, purchased from Lactel Absorbable Polymers, with THF and DMF purchased from Fisher Scientific as solvents. For manufacturing sutures, kynurenine-loaded PVA was used as the matrix phase, and reinforced during the braiding process with commercial silk microfibre yarns (#100 by YLI Corporation, USA), which was selected due to its similar mechanical properties to many commercial silk sutures. Commercial wound dressing products including Kaltostat® and Tegaderm were purchased from local pharmacies. The skin substitute sample used as comparison benchmarks were a gift from the BC Professional Firefighters Burn and Wound Healing Laboratory.

4.2.2 Dressing Fabrication

As dressings are planar designs, its fabrication will be similar to previous electrospun samples. The drug carrier was prepared by first dissolving 20 mg kynurenine in 1mL sodium hydroxide,

followed by neutralization with a 14M hydrochloric acid. The neutralized solution was then added to 9 mL of a 10 wt% PVA 18-88 solution and vortex mixed until homogenous for electrospinning. Electrospinning was carried out at a voltage of 20 kV, pump rate of 0.4 mL/hr and a needle to collector distance of 20cm. Electrospun fibres were collected onto a 10 cm x 10 cm area of an aluminum plate collector to keep fibre membrane thickness and drug concentration consistent. Following electrospinning, the PVA fibres, cut into 1 cm x 1 cm pieces, were first dip-coated in a 20 wt% PLGA 85:15 solution and then heat treated at 75°C for two hours while being placed between two steel plates clamped together. After the first heat treatment, the coated fibres were dip-coated again in the same PLGA solution followed by a second heat treatment at 75°C for two hours. To prepare shells for holding the dip-coated kynurenine carrier, PLGA was first dissolved at a 15 wt% concentration in a solvent system containing a 3:1 mix of THF and DMF by weight, and then electrospun at a voltage of 17 kV, pump rate of 0.6 mL/hr and a needle to collector distance of 20cm. After 6 mL of the PLGA solution was electrospun, the process was paused and the coated kynurenine-PVA fibres were placed on the PLGA fibre surface, followed by electrospinning of an additional 6 mL of PLGA solution. The resultant membrane therefore resembles a 10 cm x 10 cm PLGA fibre containing 1 cm x 1 cm pieces of coated kynurenine-loaded PVA inside. The membrane was then cut into individual pieces with the coated PVA being at the centre of each piece, with a 0.5 cm edge on each side that contained only PLGA fibres.

4.2.3 Suture Fabrication

The dissolved PVA was loaded into a 10 mL disposable syringe with an 18-gauge needle, both from BD (USA), and subsequently electrospun at a voltage of 20 kV and a distance of 10cm using a NANON-01A Nanofibre Electrospinning Unit (MECC Co., Japan). Nanofibres were

collected on a parallel series of six aluminum foil strips affixed on a grounded rotating belt collector. After electrospinning, PVA nanofibres were removed from the aluminum strips and twisted into yarns by hand, following the method outlined in the work by Uddin et al (Uddin, Ko et al. 2009) on fabricating nanocomposite fibre yarns. Briefly, the thin strip of nanofibres removed from the aluminum collector was held down on one end and twisted on the other. Yarn diameter was controlled by adjusting the width of the aluminum collector strips as well as the deposition thickness. The two factors were controlled by varying the aluminum collector strip width and volume of solution electrospun at three levels each. The three levels to the two factors were 0.2 mL, 0.4 mL, and 0.6 mL for volume of electrospinning solution and 0.5 cm, 0.75 cm, and 1.0 cm for width of the collector strip. The deposition volume of PVA was then calculated as the product of electrospun layer thickness and strip width. To stabilize the PVA yarns and ensure integrity in aqueous environments, the yarns were heat treated at 100°C in a convection oven by ThermoFisher Scientific (USA) for two hours. For suture fabrication from yarns, six stabilized yarns were loaded onto a three-dimensional hexagonal braider designed in collaboration between the Advanced Fibrous Materials Laboratory at the University of British Columbia and the Institut für Textiltechnik at the RWTH Aachen University. The braiding setup is shown in Figure 50a, in which each nanofibre yarns was loaded onto one of six yarn carriers at the base of the apparatus and are joined together at the top. The base of the apparatus, which holds the yarn carriers as shown in Figure 50b, contains hexagonal gears that can rotate, leading to coordinated movements of the yarn carriers, which in turns allow the yarns to intertwine and ultimately form braids.

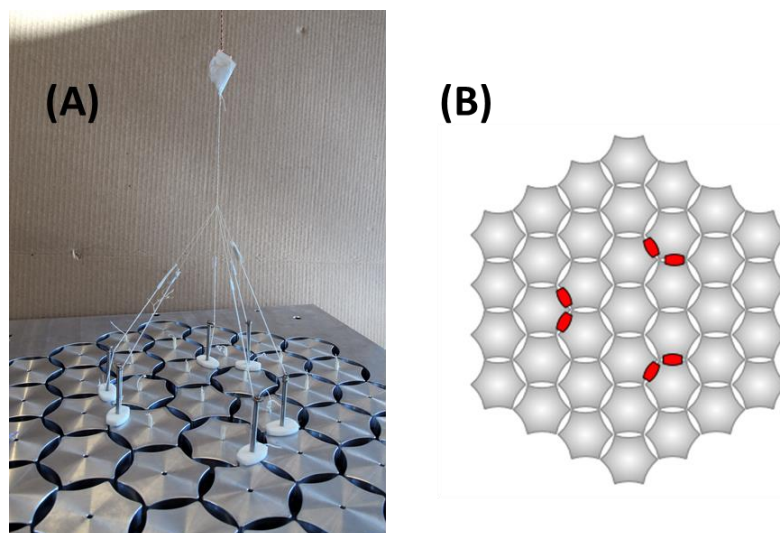


Figure 50: (A) 3D Hexagonal Braider used in the fabrication of nanofibre-based hybrid sutures, with a schematic of the rotating yarn carrier shown in (B)

To investigate the effect of reinforcement with commercial silk yarn, two approaches were examined. The first was a surface reinforcement approach in which the six nanofibre yarns used for braiding were partially replaced by the reinforcing yarns. The second was a core reinforcement approach in which six nanofibre yarns were braided around a varying number of reinforcing yarns that act as the core. After the optimal reinforcement was determined, the braided suture was dip-coated in a 10 wt% PLGA solution for controlling kynurenine release.

4.2.4 Characterization

In suture manufacturing, two important performance metrics were the maintenance of fibrous structure during yarn fabrication and the structural uniformity of the braid. To ensure the uniformity of the electrospun yarn and braided suture, optical characterization was performed using a Nikon (Japan) Eclipse LV100 Optical Microscope. Yarn and suture diameters and braiding angles were measured using the image analysis software ImageJ. The surface of the suture was evaluated using a Hitachi (Japan) S-3000N Scanning Electron Microscope to ensure

that the large surface area on the nanofibres is maintained after yarn twisting and braiding. The surface morphology of the braided suture was also compared to that of the commercially available Lukens® Silk Size 0 Black Braided Suture.

As the primary goal of this study is to fabricate the kynurenine carrier into robust structures for application, tensile testing was another main focus of the characterization stage. For both dressings and sutures, the tensile were examined using a Katotech (Japan) KES-G1 micro-tensile tester. For dressings, specimens with 3 cm length and 0.5 cm width were prepared, whereas for sutures, braids and their component yarns were cut into sections 3 cm in length. The prepared specimens were then mounted on a paper frame and loaded into the upper and lower jaws of the tensile tester. Each sample was tested at a strain rate of 0.02 cm/s, and the average tensile strength, and maximum elongation were obtained from an average of 10 repeats for each type of dressing, yarn, and braid samples. However, unlike monolithic materials, textile products fibrous dressings and sutures do not have uniform cross sections, which contain a varying ratio of fibre and air, and as such, stress calculations using force and cross-sectional area are no longer valid. As a result, tensile properties of nanofibres and their resultant structures were determined using the method outlined in the work of JWS Hearle (Hearle and Morton 2008). In the case of textiles, since the cross sectional area is not a reliable measure of the amount of materials per unit length, the concept of linear density becomes important. Calculated using equation 18 below, the linear density represents the amount of materials present in a given length of the textile. Note that the width and thickness of the textile do not play a role in the calculation as these dimensions are assumed to be small compared to the length. Once the linear density is determined, load data from tensile testing was then used to calculate the specific strength for textiles, which depends on the linear density as shown in equation 19, instead of force divided by area. Specific stress has the unit grams per tex, with tex being a textile unit for describing linear density and defined as grams per 1000 metres of

material. However, to be able to compare with conventional materials reported in literature, it would be useful to convert specific stress to engineering stress, expressed in MPa. As the specific stress is expressed in force per unit linear density, the engineering stress could be obtained simply from converting the linear density to an area using the polymer density. By multiplying the inverse of the linear density by the polymer density, as shown in equation 20, the real area of the textile could be determined because the linear density term contained mass per unit length whereas the polymer density contained mass per unit volume.

$$\text{Linear Density } \left(\frac{g}{m}\right) = \frac{\text{Sample Mass (g)}}{\text{Length (m)}} \quad \text{Equation 18}$$

$$\sigma_{\text{specific}} \left(\frac{N}{\text{tex}}\right) = \frac{\text{load (g)}}{\text{linear density } \left(\frac{g}{m}\right) \times \frac{1000m}{1 \text{ tex/g}}} \times 0.00981 \frac{N}{g} \quad \text{Equation 19}$$

$$\sigma_{\text{Eng}}(\text{Pa}) = \sigma_{\text{specific}} \left(\frac{N}{\text{tex}}\right) \times 10^3 \frac{m}{1000m} \times \rho_{\text{polymer}} \left(\frac{g}{\text{cm}^3}\right) \times 10^6 \frac{\text{cm}^3}{\text{m}^3} \quad \text{Equation 20}$$

The major challenge in interpreting the mechanical properties of nanofibre-based wound dressing is the lack of standardized requirements on strength, stiffness, and extensibility of the materials. As a result, comparisons are made with commercial wound dressing products to define what levels of properties are considered sufficiently robust. For dressings, a freeze-dried skin substitute (INTEGRA™) composed of a collagen matrix with a silicone top coat, an alginate-based short microfibre wound dressing (Kaltostat®), and a polyurethane film based protective dressing (Tegaderm®) were used as a benchmark. Short fibre dressings such as Kaltostat® have lower strength, stiffness and extensibility due to the lack of connectivity between fibres, whereas film dressings such as Tegaderm® have higher strength, stiffness and extensibility. The nanofibre dressings can therefore be considered sufficiently robust if their mechanical properties fall between the lower end (short fibre dressings) and higher end (film

dressings) of the commercial products. If nanofibre mechanical properties fall outside of the range for commercial products, then it may not be suitable for application. For all dressing samples, tensile testing was performed on both the dry and wet form. To wet the tensile specimens, samples were soaked in a PBS solution at 37°C for 1 hour. In addition to the tensile properties of the dressings, the ability of the dressings to be sutured onto wounds may also become important for feasible application as a burn dressing. Feasibility for suturing was investigated by comparing the suture retention strength of the dressing samples of comparable thickness, following the standard method outlined in section 5.8 of the American National Standards Institute (ANSI)/Association for the Advancement of Medical Instrumentation (AAMI) document ANSI/AAMI VP20:1994 entitled 'Cardiovascular Implants–Vascular Graft Prostheses' (Instrumentation 1994). Briefly, a size 5-0 polyglactin 910 suture (Vicryl[®], Ethicon) was inserted through the edge of the samples, 2 mm from the end of the sample, while the loose ends of the suture was secured on the top grip of the KES-G1 tensile tester, and the lower end of the sample was secured on the lower grip, as shown in Figure 51. During the test, the lower group would extend until the suture is completely pulled through the sample, and the load at which it occurs was recorded as the suture retention.

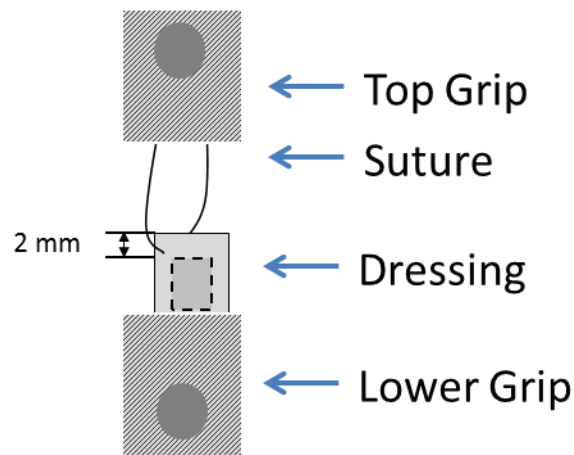


Figure 51: Suture retention test setup

In addition to suture tensile properties, kynurenine release from the fabricated sutures were also examined, in order to confirm that the desirable release properties observed from planar structures could be transferred to a tubular one. Kynurenine release assays were performed as described in previous sections. Instead of a 1 cm x 1 cm piece of a planar structure, a 5 cm section of the braided suture was cut and soaked in PBS solution for initiating kynurenine release.

4.3 Results

4.3.1 Dressings

The cross section of the dressing, prepared by the cold fracture technique and observed using an Olympus LEXT laser confocal microscope, is shown in the Figure 52 below.

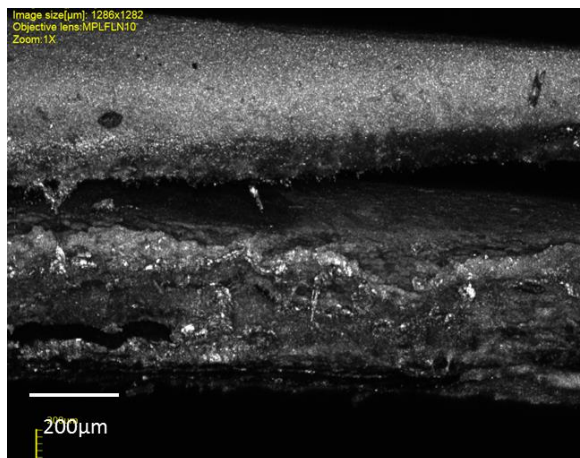


Figure 52: Laser confocal microscopy of the cross-section of the dressing design consisting of a PLGA nanofibrous shell around a PLGA dipcoated PVA core.

Using ImageJ, the thickness of the overall dressing is 300 μm at the edges, and 577 μm at the centre including the dip-coated PVA core. Table 10 below compares the tensile strength, elastic modulus, maximum elongation and suture retention of the PLGA dressing shell, drug-loaded

PVA layers before and after dip-coating, as well as skin substitute, Tegaderm® and Kaltostat® as benchmarks.

Table 10: Tensile properties comparison between PLGA dressing shell, kynurenine-loaded fibres as-electrospun and after dip coating, and commercially available wound products.

		UTS (MPa)	Young's Modulus (MPa)	Strain (cm/cm)	Suture Retention (N)
PLGA Shell	D	4.386 ± 1.082	47.789 ± 0.776	1.035 ± 0.148	3.37 ± 0.43
	H	4.934 ± 0.300	50.396 ± 4.790	0.980 ± 0.007	3.46 ± 0.70
Kyn-PVA Fibres	D	21.311 ± 2.438	1155.64 ± 173.719	0.312 ± 0.066	N/A
	H	N/A	N/A	N/A	N/A
Dip-coated Kyn-PVA Fibres	D	10.333 ± 0.863	182.142 ± 12.029	0.639 ± 0.073	N/A
	H	9.673 ± 0.417	178.361 ± 11.733	0.587 ± 0.063	N/A
Skin Substitute	D	10.348 ± 1.569	39.448 ± 0.035	0.035 ± 0.002	1.14 ± 0.05
	H	0.775 ± 0.068	5.371 ± 0.155	0.285 ± 0.011	0.37 ± 0.23
Tegaderm®	D	285.313 ± 20.022	73.945 ± 5.038	6.465 ± 0.167	6.80 ± 0.65
	H	279.644 ± 14.827	71.912 ± 1.768	6.283 ± 0.155	6.93 ± 0.41
Kaltostat	D	0.571 ± 0.085	1.017 ± 0.461	0.235 ± 0.024	N/A
	H	0.182 ± 0.133	0.461 ± 0.184	0.313 ± 0.026	N/A

Table 10 also shows the tensile properties of the samples before and after hydration, denoted D for dry and H for hydrated. The as-electrospun kynurenine-PVA fibres were not tested in hydrated form due to its quick degradation in wet environments. Tensile test results showed that the as-electrospun PVA fibres were significantly stronger but also stiffer than other constructs tested. While dip-coating reduced the tensile strength and Young's modulus of the drug carrier, the stiffness was still higher than the benchmark textile products, while the tensile strength became comparable to dried skin substitutes. The use of PLGA shell further reduced the stiffness to a similar level as native skin, despite a moderate decrease in tensile strength. The maximum elongation of the PLGA shell is also superior to PVA fibres as well as the benchmark products. Suture retention loads of the PLGA shell and the skin substitute are also compared in Table 10.

4.3.2 Sutures

4.3.2.1 Kynurenine-Loaded PVA Yarns

PVA fibres were successfully electrospun onto aluminum strips, with an average nanofibre diameter of 309 ± 19 nm. The electrospun fibres were also successfully twisted into yarns. By electrospinning 0.2 mL polymer solution onto collector strips with widths of 0.5 cm, the resultant yarn diameter was 133.10 ± 12.13 μ m. When the twisted PVA fibre yarns were heat treated to improve stability in aqueous environments, the nanofibre diameter increased to 366 ± 57 nm. On the other hand, yarn diameter reduced by approximately 15% to 113.02 ± 23.61 μ m. The heat treatment caused the fibre diameter as well as the diameter distribution to increase as a result of fibres forming welds between one another, into a somewhat fused morphology. Yarn diameter decreased slightly likely due to densification as a result of fibres fusing with one another and the removal of water trapped in the voids inside the fibrous structure. Figure 53a and b compare the fibre morphology before and after being twisted to yarns, indicating that the fibrous morphology was maintained throughout the yarn fabrication process.

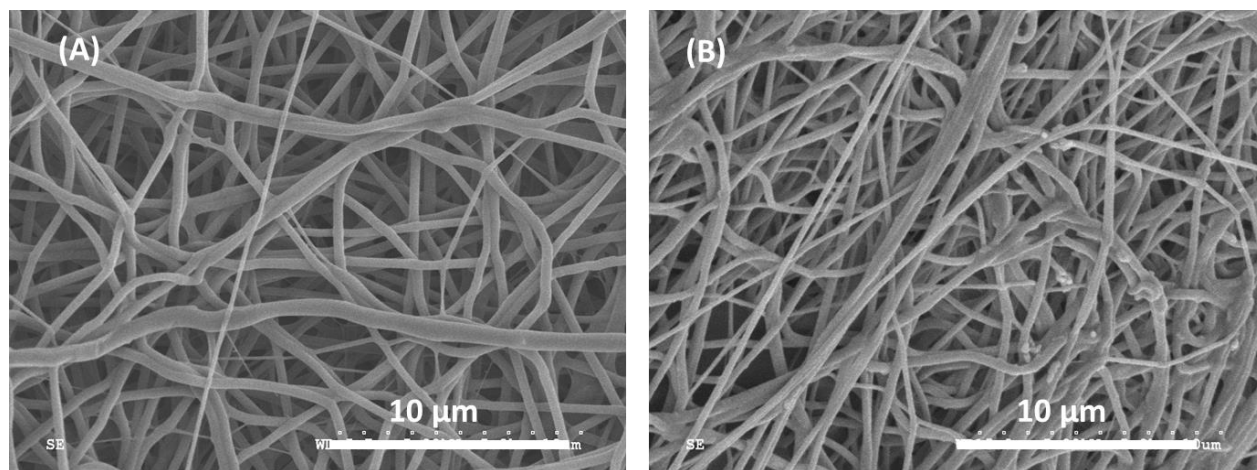


Figure 53: SEM micrograph (5000X magnification) of nanofibres (A) as-electrospun and (B) twisted into yarns

To optimize the diameter of the yarns, deposition volume was controlled via three levels each of strip width and deposition thickness. The effect of deposition volume on yarn diameter is shown in Figure 54.

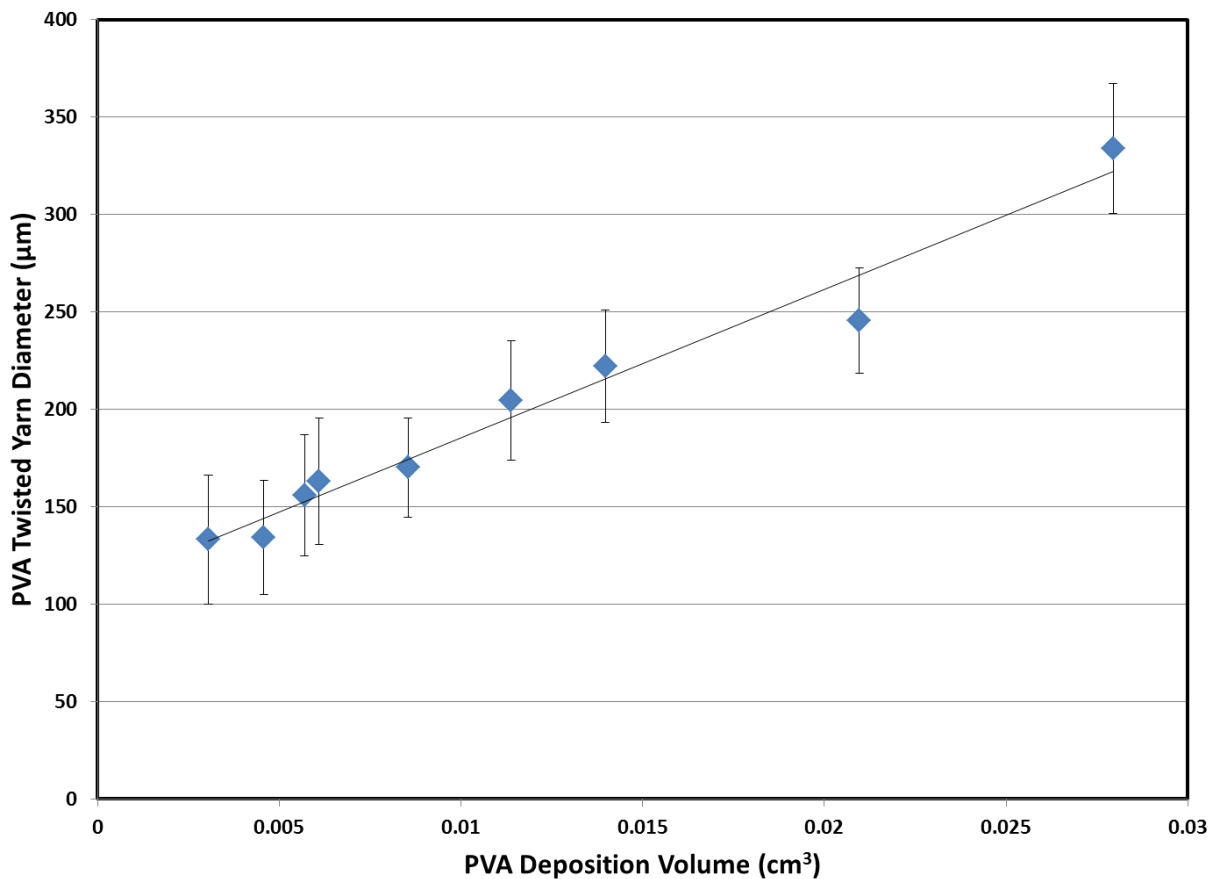


Figure 54: Yarn diameter controlled by PVA deposition volume

The yarn diameter varied linearly with the PVA deposition volume, as indicated by the fitting linear equation shown in equation 18, with a coefficient of determination of 0.971 over the deposition volume range between 3.05×10^{-3} to $2.79 \times 10^{-2} \text{ cm}^3$.

$$\text{Yarn Diameter} = 7619.9(\text{Deposition Volume}) + 109.21$$

Equation 21

While further attempts were made to reduce yarn diameter by decreasing collector strip width or reducing thickness through volume electrospun, it was found that strips narrower than 0.5 cm were not feasible as such thin strips were prone to nanofibre membrane breakage upon removal from the aluminum collector. In addition, when the volume of PVA solution electrospun was below 0.2 mL, which corresponds to a deposition thickness of $3.05 \times 10^{-3} \text{ cm}^3$, removal of the thin layer of deposited fibres from the collector strip was also exceedingly difficult, often causing tear along the length of the strip. The lowest yarn diameter that was achieved thus far with reproducibility is therefore approximately 130 μm .

4.3.2.2 Suture Fabrication

Upon subjecting six twisted PVA yarns to 3D hexagonal braiding, it was apparent that the main challenge to obtaining uniform braids is the varying tension that the yarns were subjected to as the yarn carriers move, leading to individual yarns being pulled more tightly than others. As the carriers move from the inner to the outer positions, the excess tension also caused yarn breakage. To eliminate the non-uniformity in tension subjected to the six yarns, an elastic thread was added to connect the yarn carrier to the bottom end of the PVA yarns, such that all extension and contractions would be transferred to the elastic thread. The modification was useful as uniform braids were produced. Using six PVA yarns with an average diameter of approximate 130 μm , sutures with an average diameter of $310.11 \pm 10.40 \mu\text{m}$ were braided, which corresponds to sutures with sizes between 2-0 and 0. An optical microscope image of the nanofibre suture is shown in Figure 55b. As comparison, optical microscope image of a Lukens® Silk Size 0 Black Braided Suture is also shown Figure 55a.

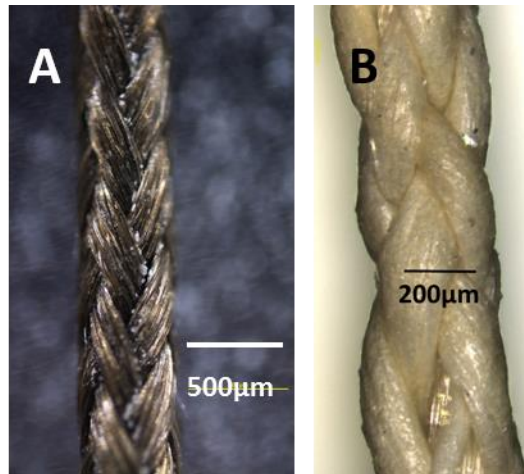


Figure 55: Comparison between (a) Lukens® Silk 0 Commercial Suture and (b) the braided electrospun PVA suture

It was noted that the nanofibre-based braided sutures have a slightly lower average braiding angle at 17.7° compared to the Lukens® suture at 23.2° , which may have implications on their tensile strength comparison as a larger portion of the yarns are aligned in the longitudinal direction in the nanofibre-based suture.

One of the main focuses of this study is to optimize suture mechanical properties by reinforcing nanofibre yarns with commercial microfibre yarns during braiding. Two reinforcement approaches were examined, including surface reinforcement and core reinforcement. For surface reinforcement, the six PVA nanofibre yarns in the braided structure were partially replaced with YLI silk microfibre yarns, forming sutures with nanofibre to microfibre yarn ratios of 2-4, 3-3, and 4-2. As control samples, sutures composed entirely of PVA nanofibre yarns and silk microfibre yarns were also included. Suture diameters varied depending on the number of reinforcement yarn added, with sutures containing two silk reinforcement yarns being $292.09 \pm 1.53 \mu\text{m}$, a 3-3 mix hybrid suture being $295.49 \pm 6.91 \mu\text{m}$, sutures with four silk reinforcement yarns being $265.02 \pm 6.21 \mu\text{m}$, and a full silk yarn suture being $253.19 \pm 5.84 \mu\text{m}$. The braided structures corresponded sutures with sizes ranging from 4-0 to 3-0. Figure 56 is a SEM

micrograph of a surface-reinforced suture containing three PVA nanofibre and three YLI silk yarns, showing two distinctive phases, with one being more fibrous than the other.

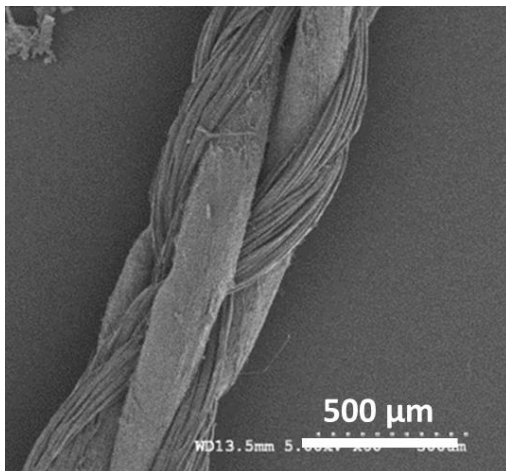


Figure 56: SEM micrograph of a surface-reinforced braid containing three PVA nanofibre yarns and three YLI silk yarns

The phase that appears more fibrous in Figure 56 is the YLI silk yarns, with each yarn containing multiple smaller threads. The PVA nanofibre yarns, on the other hand, had a denser appearance due to them being viewed at a low magnification, which was required to view the entire braid.

Another type of suture reinforcement is through addition of core composed of silk microfibre yarns. Sutures were fabricated by vertically securing silk yarns at the center of the hexagonal braider, with six PVA nanofibre yarns braided around the silk. Figure 57a shows a SEM micrograph of a suture containing six PVA nanofibre yarns braided around one YLI silk yarn. To identify the presence of the core reinforcement, the braid was intentionally loosened and another SEM micrograph was taken, as shown in Figure 57b.

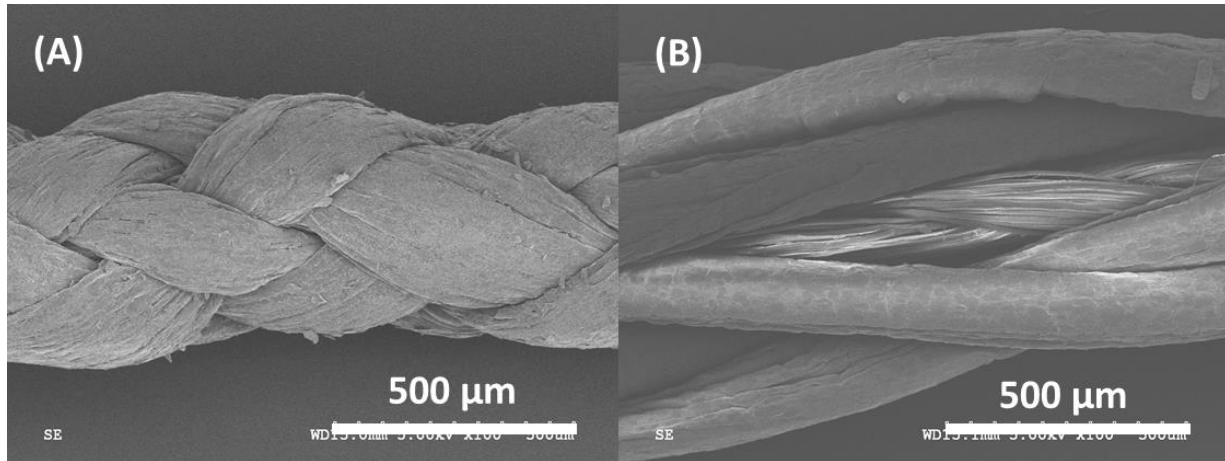


Figure 57: SEM image of the core-reinforced braid, with (A) showing the braid as-fabricated, while the braid shown in (B) was intentionally loosened to show the YLI silk core reinforcement

To further examine the reinforcement effect, different cores containing one to three silk yarns were produced. With different numbers of silk reinforcement yarns the suture diameter varied. Braiding the six PVA yarns around a commercial silk yarn increased the braid diameter to $381.98 \pm 18.46 \mu\text{m}$. Further increase was noticed when two silk yarns were used, to $482.95 \pm 23.83 \mu\text{m}$. With three silk yarns as core, the diameter increased to $515.60 \pm 21.89 \mu\text{m}$. During the braiding process of the core-reinforced nanofibre sutures, it was noticed that the silk yarn at the core can bend, which created protrusions when PVA yarns were braided around it. The protrusion phenomenon, known as core popping, is likely due to the movement of the nanofibre yarns around the core during braiding as well as the difference in tension applied to the core and shell yarns. To eliminate core popping, the tension experienced by the core must be monitored and released when necessary, which can be accomplished by simply pulling on the core yarns to ensure they remain straight throughout the braiding process.

4.3.2.3 Tensile Properties

As the goal of the study is to develop electrospinning and braiding modification techniques for ultra-fine fibre sutures, tensile testing results become an important metric in measuring the feasibility of our approach. Figure 58 below compares the tensile behavior of the surface-reinforced sutures containing different numbers of silk yarns. For full comparison, the tensile behavior of a suture composed solely of the YLI silk yarn is also shown. Sutures composed solely of the silk yarns showed a tensile strength in the range of 101.65 ± 5.56 MPa, significantly higher than those composed of PVA nanofibres which had a tensile strength of 13.73 ± 1.77 MPa. The results also showed a linear increase in tensile strength with increasing number of YLI silk yarns on the surface, thereby following a simple rule of mixture. The maximum elongation, on the other hand, decreased significantly with the presence of silk yarns, from 77% to 29% with two silk yarns. Replacement of additional silk yarns on the surface further decreased the maximum elongation until reaching that of the silk yarn at 24%.

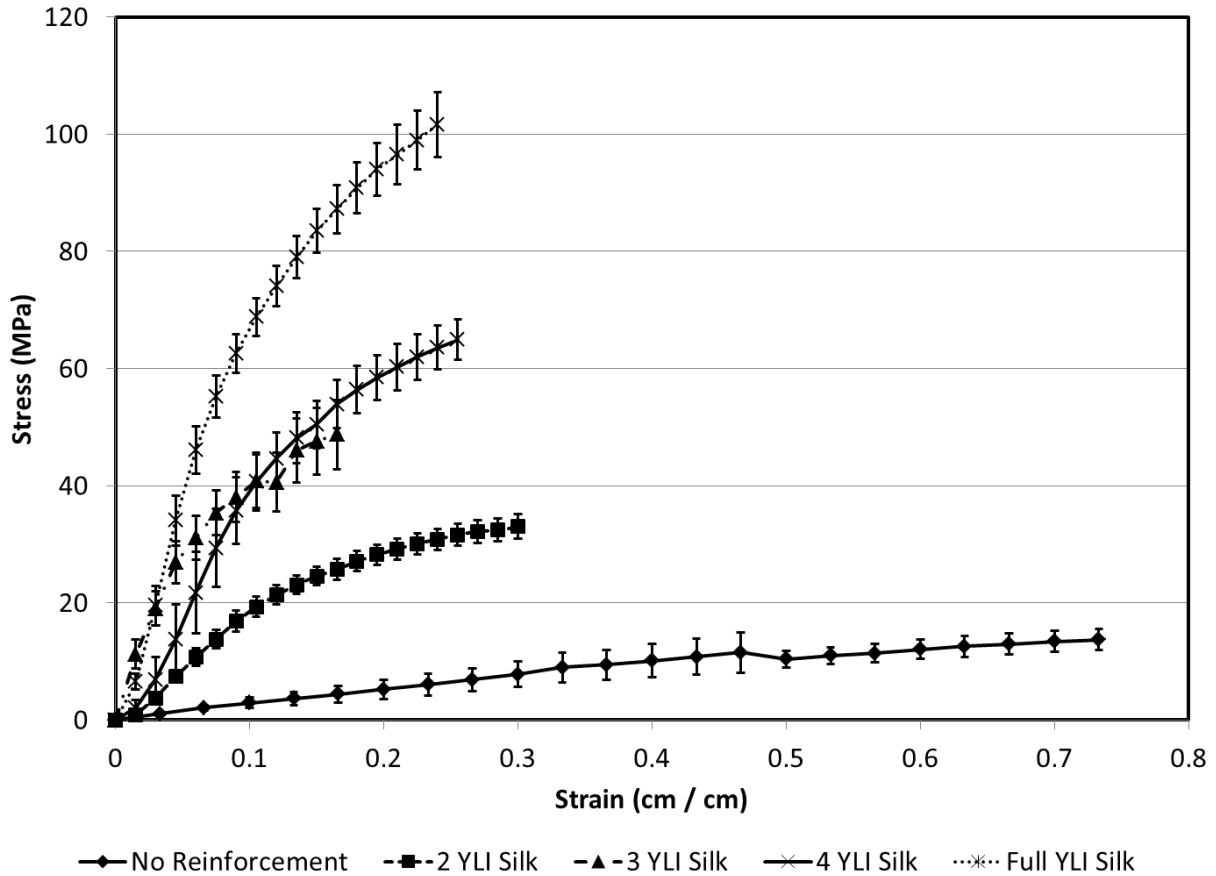


Figure 58: Tensile behavior comparison between sutures surface-reinforced with silk microfibres

A comparison between core-reinforced nanofibre sutures is shown in Figure 60. Unlike the surface-reinforced sutures, the tensile strength increase was not linearly proportional to the number of silk yarns added as the core. By braiding the PVA yarns around one silk yarn, the tensile strength increased by 154% to 34.91 ± 4.81 MPa. The tensile strength increase eventually plateaus with further addition of yarns at the core. Further reinforcement with a second silk yarn yielded an additional 84% increase, while a third silk yarn led to a further 15% increase. Overall, the tensile strength of the suture reinforced with three YLI silk yarns is a 436% increase over the suture without reinforcement. In terms of elongation, the trend observed was similar to the surface-reinforced sutures as the presence of a silk yarn at the core decreased

maximum elongation significantly. However, unlike the surface-reinforced sutures, the maximum elongation of the core-reinforced sutures did not change with further incorporation of silk yarns.

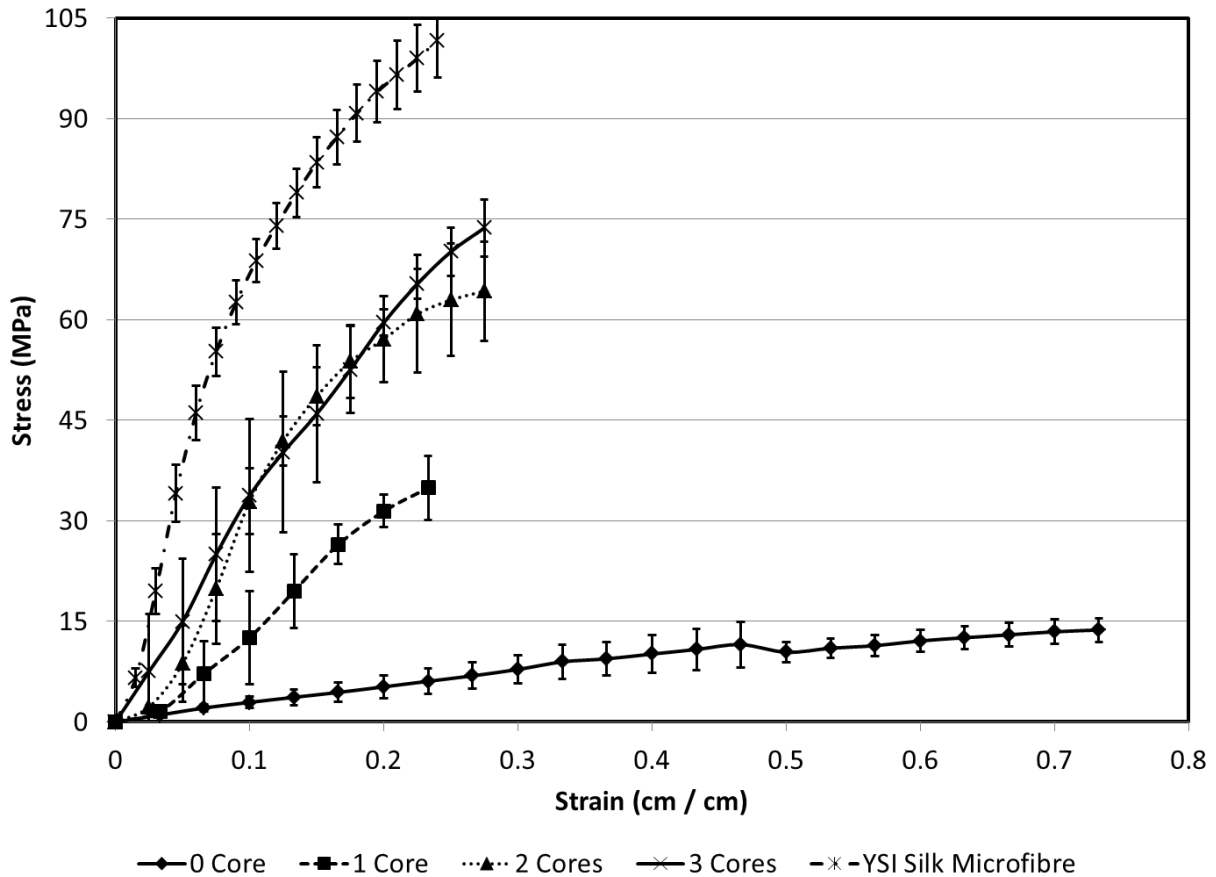


Figure 59: Tensile behavior comparison between sutures core-reinforced with silk microfibres

To examine further suture strengthening, a one-core reinforced braid composed of PVA yarns electrospun with a drum collector rotating at 2000 rpm was also tested. As seen in Table 11, enhancing fibre alignment was able to increase tensile strength by roughly 30% and maximum elongation by 20%.

4.3.2.4 Dip-Coated PVA Suture

The dip-coating step was added to the suture manufacturing process as it was established that coating electrospun fibres with PLGA was an effective method for controlling kynurenine release. Figure 60 below compares the surface of the suture before and after dip-coating.

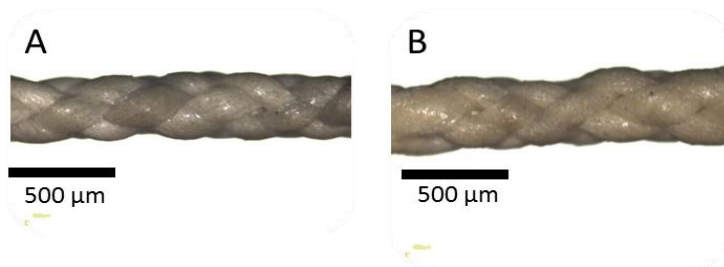


Figure 60: PVA-kynurenine braids (a) before and (b) after dip-coating with PLGA solution

The effect of dip-coating on the tensile properties of the PVA suture is shown in Table 11. Similar to the comparison between planar PVA-kynurenine nanofibres before and after dip-coating, the PVA suture coated with PLGA exhibited a lower tensile strength compared to the uncoated PVA, while the Young's modulus was decreased, with a similar maximum strain.

Table 11: Summary of tensile properties of aligned and dip-coated sutures

Sample Type Reinforcement	Diameter (μm)	Tensile Strength (MPa)	Young's Modulus (MPa)	Maximum Strain (cm/cm)
All PVA Braid (No Reinforcement)	310.11 ± 10.40	13.73 ± 1.77	25.11 ± 7.21	77.10 ± 5.00
Vicryl 5-0 Suture (Commercial Product)	117 ± 5.85	319.08 ± 16.50	9134.92 ± 1688.19	43.08 ± 10.10
PVA Braid with 1 YLI Silk Core – PVA electrospun at 20 rpm	381.98 ± 18.46	34.91 ± 4.81	164.15 ± 16.58	24.50 ± 5.50
PVA Braid with 1 YLI Silk Core – PVA electrospun at 2000 rpm	388.87 ± 22.42	42.66 ± 7.33	100.04 ± 12.64	29.74 ± 4.54
Dip-coated PVA Braid with 1 YLI Silk Core – PVA electrospun at 20 rpm	433.79 ± 60.79	19.07 ± 4.98	114.57 ± 21.33	24.48 ± 5.78

The kynurenine release from coated sutures was compared against a planar carrier also coated with 10 wt% PLGA. The comparison, presented in Figure 61, showed nearly identical release characteristics in the first four hours. However, with longer release period, it was observed that kynurenine release from the coated suture became quicker than from the planar dressing. The release profile of the coated suture has a $R^2 = 0.990$ correlation to the SRT model, with the resultant $K_H = 0.1618$, 20% higher than that observed from the planar dressing.

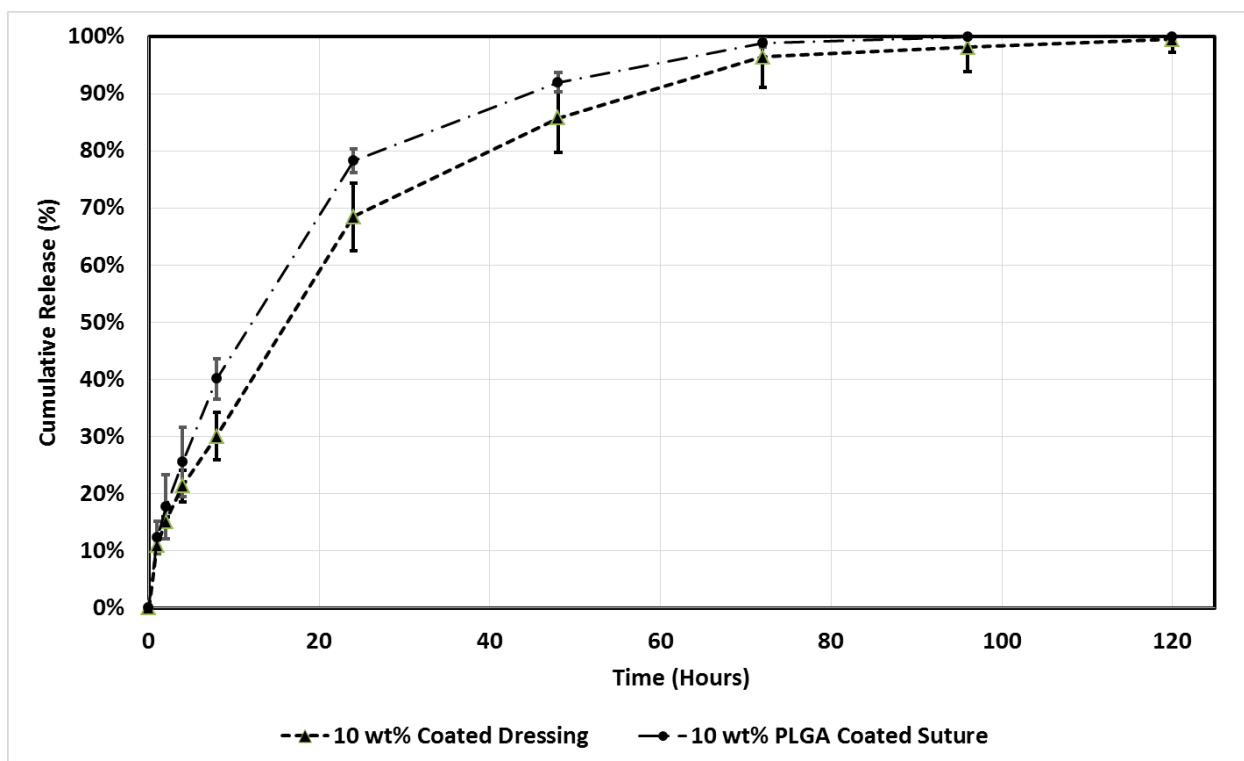


Figure 61: Kynurenine release from sutures vs. planar dressing, both coated with 10 wt% PLGA

4.4 Discussion

Having optimized drug release characteristics of the PVA kynurenine carrier, it is necessary to develop methods for fabricating the desirable design into robust, applicable products. In this

chapter, two product forms were explored, including dressing and suture. In the case of dressings, the proposed incorporation of the dip-coated, kynurenine-loaded PVA carriers into an electrospun PLGA fibre shell was aimed at providing a fibrous backing for the drug carriers and a high surface area interface with the underlying wound. The PLGA shell was not expected to significantly affect drug release duration, as it was shown in the previous chapter that the PLGA shell could delay fluid penetration in the first 12 – 24 hours, which is short compared to the five to seven day release observed in the dip-coated samples. For suture fabrication, the objective was to show that the same material system for the kynurenine carrier is versatile and can be used for fabricating sutures, thereby translating the ability of the electrospinning technique to produce continuous fibres into useful, higher order structures.

The main challenge against fabrication and characterization for applicability is the lack of universal standards for assessing whether a dressing is fit for handling and application. While several standard testing methods exist, such as tensile testing, and suture retention test, the actual requirements for parameters such as ultimate tensile strength, Young's modulus, and suture retention load, are not clear. Another approach, used often in existing literature, is to compare the properties of manufactured products to those of the native skin. However, even for skin the reported values for mechanical properties vary greatly between different studies, as mentioned in section 4.1. In this study, therefore, commercially available products were also used as a benchmark in addition to native skin properties.

In the case of dressings, by comparing tensile properties in the dry form between commercially available products and the fibre carrier and dressings and sutures created in this study, it is possible to determine if the proposed kynurenine-carrying dressings are sufficiently robust for handling. On the other hand, comparisons made in the hydrated state of the products as well as literature values for native skin could help determine if the dressings are suitable for topical

application. Two commercially available dressings were chosen for comparison in this study. Kaltostat[®], a short fibre alginate dressing, is a highly absorbent dressing designed for exuding wounds such as burns and ulcers. Kaltostat[®] has relatively low tensile properties, as it is usually applied with a backing or secondary dressing that provides adhesive properties, and therefore provides lower limits for properties requirement. A skin substitute, comprised of bovine collagen gel topped by a polyurethane layer much like Integra[®], was also used in this study to provide reference on a scaffold that is applied deeper in the wound site and often sutured to surrounding wound edges. In addition to suture retention properties, the dry and hydrated tensile properties of skin substitutes are useful comparison guidelines because the scaffolds would be handled in the dry form but applied in a highly moist environment. Lastly, Tegaderm[®], a polyurethane dressing applied on wounds for protection and moisture retention, provides upper limits on the tensile properties. While Tegaderm[®] is usually applied by adhesive bonding, the suture retention properties are not as important to this study as the skin substitute.

In general, the tensile strength of electrospun fibres were shown in this study to be in the same order of magnitude compared to a dried skin substitute composed of collagen fibres, which also agreed with the strength values of fibre dressings such as Resolut LT reported in literature (Elsner, Berdicevsky et al. 2011). In addition, the electrospun dressing strength was an order of magnitude higher than that of Kaltostat[®], indicating that the dressings are sufficiently strong in tension to be handled during fabrication and clinical application. In a moist environment, however, the use of a PLGA shell backing becomes much more important, as PVA fibres suffer degradation upon contact with water such that their tensile properties could not be consistently measured. Unlike products such as the skin substitute and Kaltostat[®], the PLGA dressing shell did not show degradation in tensile properties after hydration, and while the tensile strength was higher than the commercial products, it falls within the same order of magnitude as the reported tensile strength values for native skin, depending on the location and patient age. When

comparing the Young's modulus however, the as-electrospun PVA was found to be 30 – 100 folds stiffer than commercial products. While the PLGA dip-coating process reduced the Young's modulus by roughly 80%, the drug carrier remained much stiffer which may pose challenges in handling. On the other hand, the PLGA shell has a significantly lower Young's modulus, which makes it similar to the dried skin substitute in terms of handling. Although the dip-coated PVA inside the PLGA shell would remain stiff, the PLGA shell nonetheless provides a more flexible edge to the dressing for integration with surrounding skin. The Young's modulus of the PLGA shell does not change upon hydration, and became an order of magnitude stiffer than the hydrated commercial products, while still falling between the reported range for native skin. In addition to providing a more flexible interface with surrounding skin, the PLGA shell also has an added benefit of being extensible, with breaking strains roughly three folds higher than commercial products in both dry and hydrated forms.

Being a planar structure, the conversion of the PVA kynurenine carrier into a dressing was an apparent course of action. However, converting the same material system into non-planar structures such as sutures can pose challenges, yet will be tremendously useful as kynurenine-loaded sutures may help reduce scarring on small area or surgical wounds. In this study, a new method for producing nanofibre yarns by electrospinning onto aluminum strips was introduced, enabling greater scalability by allowing multiple yarns to be fabricated simultaneously, as opposed to existing methods that rely on a spinning disc collector. In addition, the yarns produced had consistent diameters, indicating repeatability for the fabrication method. The yarn diameters were shown to be dependent deposition thickness, which is directly related to the strip diameter as well as the volume of polymer solution electrospun, and their impacts were quantified through a factorial experiment. Since both input factors rely heavily on the solution concentration, electrospinning and collector setup instead of the material choice, the fabrication method should be applicable to different polymers. However, a major challenge associated with

this fabrication method is that due to the need to remove electrospun nanofibre from the collector strips, a minimum deposition must be achieved to ensure clean removal. As observed in the samples with low strip width or low electrospun volume, the deposition of the nanofibres might not be sufficient, leading to breakage or incomplete removal, which can be detrimental to both the dimensional consistency and structural integrity of the resultant yarns. In this study, the minimum yarn diameter achievable was approximately 110 μm , although future studies on collector modification, such as altering collector material, may allow further reduction in the yarn diameter.

In terms of suture fabrication, it was shown in previous reports by authors such as Hu et al as well as the current study that sutures composed solely of electrospun nanofibres were lacking in tensile strength, which could be a bottleneck in putting nanofibre sutures into practical use. In this study, two reinforcement techniques were examined to determine an effective method for strengthening fibre sutures. Rather than reaching a specific strength, this study aimed to develop methods for optimizing the tensile strength of electrospun fibre sutures via introducing reinforcement phases, with commercial silk yarn for clothing applications selected for simplicity. Through surface reinforcing the suture by replacing PVA nanofibre yarns with the YLI silk yarns, the tensile strength increased linearly with the number of silk yarns incorporated. However, surface reinforcement also reduced the content of PVA and kynurenine and therefore defeats the purpose of an electrospun suture. To maintain the functional properties of the braided kynurenine - PVA suture, strengthening through core reinforcement may be a more desirable option. By simply adding one YLI silk yarn as the suture core, the tensile strength increased by almost three-folds. Addition of yarns at the core further increased the tensile strength, although to a lesser extent. With three yarns added at the core, the tensile strength increased to approximately six times the original value. The strengthening effect of a core-reinforced suture with three core yarns was almost identical to the surface-reinforced suture with four of the six

nanofibre yarns replaced with the YLI silk yarns, at six times the original strength. However, the core-reinforced suture was able to maintain the electrospun fibre features whereas the surface-reinforced suture contained mostly commercial silk yarns on the surface.

To preserve the sustained kynurenine release behavior observed in the planar carriers, the braided PVA sutures were also coated with PLGA. As it was identified in Chapter 3 that the concentration of the PLGA coating solution has overall insignificant effect on release kinetics, a 10 wt% concentration was selected due to its lower viscosity for easy handling and uniform coating. Comparing with a 10 wt% PLGA coated planar nanofibre membrane, the kynurenine release rate was nearly identical within the first four hours, likely due to a similar coating thickness and therefore the diffusion behavior of kynurenine molecules near fibre surface was similar. However, after four hours, quicker kynurenine release was observed from the coated suture sample. The probable reason for such an observation is that unlike a planar kynurenine-loaded membrane that has a uniform distribution of drug, the core-reinforced suture did not contain kynurenine at the centre. In addition, the thickness of the planar PVA carrier is also higher than the diameter of the PVA suture. As a result, the reduced thickness of the coated suture would reduce the diffusion path of kynurenine whereas the lack of a drug-loaded core for coated suture would ensure quicker depletion in the carrier. The demonstration of sustainable kynurenine release from the nanofibre sutures is significant nonetheless because it is an important aspect in addressing the hypothesis that the electrospinning technology can facilitate fabrication of wound dressing material into different structures that would help patients who are more susceptible to FPDs.

Commercially, it is common for sutures to be coated with polymers such as chitosan for antibacterial properties. While the PLGA coating explored in this study was aimed at controlling kynurenine release, it is also possible to incorporate antibiotics into the PLGA coat to impart the

same antibacterial functions. In terms of tensile properties, the PLGA, being a weaker polymer under tensile loads compared to PVA, did not contribute to the suture tensile strength.

Compared to commercial products such as the Vicryl[®] suture, the braids fabricated in this study remained significantly weaker. However, it is also worth noting that the reinforcement yarns used in this study, which was selected based on simplicity, was also weaker than commercial silk sutures, with maximum elongation at approximately half of the commercial suture. In fact, the results from this study showed that the core-reinforced braids reached up to 70% of the reinforcement yarn strength, while maximum elongation was roughly equal to the reinforcement phase. Optimization of the braided suture tensile properties would therefore rely on the search for a stronger reinforcement yarn with higher elongation. In addition, the 38% increase in tensile strength observed when the PVA fibres were collected in a rotating drum collector at 2000 rpm showed further possibilities in strengthening the sutures via aligned fibre morphology in the yarns.

4.5 Conclusion

This chapter presented investigations on converting the optimal kynurenine carrier design into clinically applicable structures, including dressing and suture. Two major aspects in product development were explored, including processing and characterization. While dressings could be fabricated by adding fibre layers around the drug carrier, suture, which deviate from the planar form that most electrospinning studies focused on in the past, required the establishment of new fabrication processes. This study presented a novel technique to simultaneously fabricate multiple electrospun kynurenine-loaded yarns that were ultimately braided into sutures. In demonstrating feasibility in suture fabrication using nanofibres, this investigation also showed

the benefits in using continuous nanofibres as opposed to discrete nanofibres for controlled wound healing applications. While short, discrete fibre dressings, such as Kaltostat, may be desirable for absorption of wound exudate in the earlier stages of wound healing, continuous fibre allows more flexibility in creating applicable forms for a wider range of patients with different needs, such as patients who are more susceptible to FPDs.

In terms of characterizing the fibre products, the goal is to determine if the dressings or sutures are sufficiently robust for handling and for clinical application. However, the major challenge in characterization is that there are no established minimum requirements on the robustness of the fibre dressings and sutures. As a result, the bulk of the characterization part of the investigation was focused on comparing the electrospun products with commercially available ones.

In developing a dressing system with the kynurenine carrier, electrospun layers of PLGA were added around the dip-coated PVA to provide a soft, breathable surface with large surface area for contact with the wound area. Tensile test results also showed that the PLGA fibres were similar to native skin in stiffness, thereby enhancing its suitability to act as the interface between the wound and the drug carrier which is significantly stiffer. In addition, the ultimate tensile strength of the PLGA dressing shell fell within the range of the native skin tensile strength, while its extensibility was significantly higher. More importantly, when comparing against commercially available products, it was found that the PLGA dressing shell possesses tensile and suture retention properties between functional dressings like Kaltostat® and protective dressings like Tegaderm®. Furthermore, both tensile and suture retention properties of the PLGA dressing do not deteriorate in hydrated environments, unlike the more hydrophilic dressings. The results from these comparisons therefore suggest that the PLGA dressings fabricated in this study are sufficiently robust to be handled like other commercially available wound dressings, and to be

sutured or otherwise adhered onto a moist wound while providing protection against physiological loads exerted by patients.

For suture development, several modifications have been made to the electrospinning and braiding processes to produce a nano/microfibre hybrid suture that combines the desirable properties of electrospun drug carrier and the superior mechanical properties of commercial microfibre yarns. In electrospinning, PVA fibres were electrospun onto a collector composed of parallel aluminum strips and then twisted into yarns upon removal from the collector. By electrospinning into parallel strips, multiple yarns can be produced simultaneously as opposed to electrospinning on rotating discs that could obtain one yarn at a time. In fabricating sutures from PVA yarns, this study sought to address the lack of tensile strength observed in previous studies, and explored two approaches for suture reinforcement. Commercial silk microfibre yarns were added in the braiding stage as a reinforcement phase, either on the surface or at the suture core, which enabled significant increase in tensile strength. Sutures were successfully prepared with different number of reinforcement yarns, yielding suture sizes ranging from 2-0 to 2. Release assays also showed that once dip-coated with PLGA, a similar level of control kynurenine release to that in coated planar dressings could also be demonstrated in the suture form.

Among the two reinforcement methods examined, core-reinforcement seemed more feasible considering it is able to enhance tensile strength with less material, as well as to maintain the nanofibrous suture surface. However, a major challenge with the manufacturing process was also identified in this study. The issue of core-popping was addressed quickly in this study, but the solution required close monitoring of the braiding process and applying tension regularly, both of which are highly manual processes and more scalable solutions may be required.

While the tensile strength of the nanofibre sutures remained below that of sutures such as Maxon®, Vicryl, and PDS, the improvements observed in the current study are a significant indication that further modifications can be made to reduce the gap in properties between nanofibre and commercial sutures. Indeed, the fabrication method used in this study could be flexible with material choice, allowing biocompatible polymers with different mechanical properties or those containing therapeutic agents to be fabricated into sutures. For example, in applications where a higher maximum elongation is required, the PVA nanofibres can be replaced by poly(caprolactone) (PCL) or poly(glycolic acid) (PGA) nanofibres, which have been shown in our previous work to have higher maximum tensile strain compared to heat-treated PVA. In addition, while this study showed the effectiveness of reinforcing nanofibre sutures with commercial silk yarns for strengthening purposes, it is important to note that the reinforcement phase is not limited to a specific material. The flexibility in material choice for the reinforcement phases adds an additional layer of control, allowing fabrication of nanofibre sutures with highly customized properties, thereby opening opportunities for use in a wider range of tissue applications.

5 Summarizing Discussion, Conclusion and Recommendations

5.1 Summarizing Discussion

The research depicted in this dissertation aimed to fill the knowledge gap in nanofibrous carriers for hydrophilic, small molecule drugs. The majority of existing studies focused on either hydrophobic or protein-based drugs, which have been effective in addressing many medical needs because many common drugs, including antibiotics, anti-inflammatory, and cancer treatment drugs are hydrophobic. On the other hand, some of the more novel therapeutic agents considered for wound healing, such as growth factors and other proteins, have much larger molecular size and therefore have their unique release properties. However, as more novel, small molecule therapeutics are discovered, such as kynurenine that was identified by Ghahary et al, there is a clear need for better understanding on release control of these agents to optimize therapeutic effect. Kynurenine was used extensively in this research as a representative example because it fits the profile a hydrophilic drug with a small molecular size. From the viewpoint of kynurenine carrier development, the objective was to control its release over five days to obtain optimal scar-reduction effect without having to interrupt the wound area by replacing the drug carrier. However, on a broader scope, the major milestone to be accomplished in this research was to demonstrate that the release of a hydrophilic, small molecule drug can be tailored and extended over an extended period of time instead of the immediate burst release that is expected based on current technology.

In addition to investigating drug release, this research also sought to develop a systematic process for drug carrier development, while clearly verifying each step in the process including material selection, characterization and optimization, which have rarely been examined thus far.

Most current studies on electrospun drug carriers involve loading particular drugs of interest into common FDA-approved polymers without justification on the material choice, followed by determination of the drug release profile and superficial approximation of the drug release mechanism by comparing release data to empirical release models. For many cases in which existing therapeutics such as antibiotics and growth factors are of interest, the common method of drug carrier development can lead to useful products with satisfactory performance, due to the high compatibility of these therapeutics with a large range of polymers, and the relative ease of burst release prevention either due to drug hydrophobicity or large molecular size. However, in the case of amino acid-derived drugs like kynurenine, low solvent compatibility could greatly limit the material choice and therefore more careful material selection is required to prevent unintentional burst release. In addition, unlike traditional therapeutics, the high water affinity and small molecular size of these drugs necessitate optimization of the drug carrier for tailoring the release rate, which requires a clear understanding of the release mechanism. In this case, the common method of comparing release data to empirical equations is no longer sufficient for gaining a meaningful understanding of the nature of drug release, as the knowledge obtained in this phase would be significantly important for devising methods for carrier optimization.

Electrospun fibres were chosen as the material form of choice in this research, due to the large surface area on the resultant fibres with nano-scale diameters, which has been shown in previous studies to allow more complete drug release compared to microfibres and films. In addition, the connective nature of electrospun fibres would allow a variety of structures to be fabricated, unlike gel- and film-based carriers, which would be useful when forming into applicable products.

Chapter 2 of this dissertation depicted the investigations into material selection, fabrication and characterization of a kynurenine carrier. Material selection began with a theoretical approach in

which Flory-Huggins interaction parameter and Hilderbrandt-Scatchard solubility parameter of the drug were calculated and compared with several candidate polymers. The theoretical calculations identified PVA and PLGA as suitable carriers. When verifying the calculation results through solubility tests, an additional challenge was identified because kynurenine is only soluble in sodium hydroxide aqueous solutions, thereby eliminating all polymers that require organic solvents, including PLGA. An attempt was made to incorporate water-solubilized kynurenine into PLGA via trifluoroethanol, but the resulting emulsion-like mixture was unstable during electrospinning due to the incompatibility between PLGA and water. Kynurenine release tests also showed significant burst release from the PLGA fibres, as a result of the phase separation between water and PLGA in the mixture. PVA was therefore the only candidate carrier for kynurenine, which was advantageous from the process optimization viewpoint because hydrophilicity of PVA can be modified via heat treatment or chemical crosslinking, and the polymer is also commercially available in various molecular weights and degrees of hydrolysis.

Initial release assay results showed complete release of kynurenine within five hours, which fell much short of the five-day release target set, due to PVA hydrophilicity. Moreover, comparison between the release data and the common empirical release models did not yield insightful results, as the release data fit both diffusion-controlled and desorption-controlled models. The rest of the chapter focused on characterization of the drug-polymer interaction which could more precisely determine the release mechanism. Firstly, XRD was used to determine whether kynurenine is present as crystalline or amorphous phase, which would indicate drug-polymer compatibility. Secondly, kynurenine-loaded fibres were analyzed via DSC to identify whether kynurenine is dispersed or solubilized within the PVA matrix. The determination that kynurenine forms an amorphous solution in PVA confirms the solubility calculation in the earlier phase of the study. Moreover, solubilized kynurenine is also less likely to be released via surface

desorption. To further help eliminate surface desorption as the dominant release mechanism, ToF-SIMS was used to observe kynurenine from the PVA samples. By comparing the MS profiles of the as electrospun and dissolved PVA fibres containing kynurenine, it was determined that kynurenine is encapsulated inside the PVA fibres rather than deposited on the fibre surface. Based on the evidence shown by XRD, DSC, and ToF-SIMS, kynurenine release via diffusion through fluid penetration into the carrier is the most plausible dominant release mechanism.

The electrospun PVA fibres were compared against kynurenine-loaded PVA solutions and cast films in order to determine the merit of electrospinning. While all three states of the carrier were found to be able to uniformly distribute kynurenine in a planar structure, ToF-SIMS results showed that electrospun fibres were able to encapsulate kynurenine within whereas in the case of cast films, drugs were detected on the surface. Electrospun fibres were also shown to provide superior drug stability. Kynurenine was found to degrade in solution which limits its use in gel- and solution-based formulations. In addition, kynurenine degradation was also noticed on cast PVA films despite at a lesser extent compared to solution, which could be related to the drug residing on surface. This finding further justified the use of electrospun fibres in this research as opposed to non-fibrous forms.

Having identified diffusion as the dominant release mechanism, approaches to optimizing kynurenine release were established such that release could be extended from a burst release lasting several hours to a stable release lasting five days. The most direct approach to reducing kynurenine diffusion rate was to make use of PVA's ability to be modified. However, due to the hydrophilicity of both kynurenine and PVA, solution-based crosslinking methods could not be used as they caused premature drug release in the crosslinking bath. In addition, in-situ crosslinking via maleic acid was also ineffective due to hydrogen bond formation between

kynurenine and PVA blocking possible crosslinking sites at the alcohol groups in PVA, as confirmed by FTIR results. On the other hand, heat treatment of the PVA fibres was effective in delaying release to a moderate extent, but was also counteracted by the decrease in the overall portion of kynurenine released, likely due to drug entrapment in the crystalline phases. Further reduction in burst release was achieved by adapting to a composite design in which the PVA kynurenine carrier was enveloped by electrospun or dip-coated PLGA. With an electrospun PLGA envelope, a two-phase release profile was observed in which most of the loaded kynurenine burst released within several hours, much like the as-electrospun PVA, while the remaining kynurenine experienced gradual release over 60 hours. The two-phase release profile was likely a result of fluid build-up in the centre void created through the dissolution of the PVA core. The electrospun envelope design nonetheless showed that the use of a highly porous fibrous layer was not able to significantly delay fluid penetration into the drug carrier. As a result, PLGA dip-coating of the kynurenine carrier was attempted which yielded significant delaying effects on drug release. After a series of investigations on different aspects of the dip-coating process, kynurenine release lasting over 200 hours was achieved, meeting the five day target set initially.

Throughout the release control optimization studies, several factors related to feed material and modification were found to have impact on kynurenine release kinetics, which was represented by the coefficient of the SRT model, K_{Ht} , throughout the thesis due to its correlation to the release data obtained for all samples examined in this study. The impacting parameters were summarized in Table 12. For the PVA – kynurenine system, it was found that adjusting feed material factors such as polymer molecular weight, concentration and drug dosage changed the release kinetics, measured by K_{Ht} , by up to approximately 10%. Heat treatment at different temperatures, while effective in reducing K_{Ht} by 6% to 48% and extending the release duration compared to the as-electrospun PVA fibres, led to drug entrapment. The method that most

effectively extended the release duration was to dip-coat the electrospun fibres with a less hydrophilic polymer such as PLGA. By dip-coating the PVA-kynurenine, reduction in K_H of up to 85%, and extension of release duration of up to 40-folds, compared to the as-electrospun samples, was accomplished.

Table 12: Summary of factors impacting kynurenine release kinetics

Factor	K_H Dependence	Closeness of Fit (R^2)
PVA Molecular Weight	$K_H = 0.6566 - 1 \times 10^{-7} [\text{Molecular Weight}]$	0.911
Polymer Loading	$K_H = 0.7691 - 0.005 [\text{Concentration}]$	0.977
Drug Loading	$K_H = 0.6214 + 0.0113 [\text{Kyn Concentration}]$	0.999
Heat Treatment Temperature	$K_H = 0.8648 - 0.0029 [\text{Temperature in } ^\circ\text{C}]$	0.934
Coating Contact Angle	$K_H = 0.4408 - 0.0047 [\text{contact angle}]$	0.973

For the kynurenine carrier, it could be explained that with a non-porous coat of PLGA, fluid penetration into the drug-loaded PVA layer was made extremely difficult, thereby slowing the transport of kynurenine out of the layer. However, it is important to note that dip-coating the electrospun PVA did not alter the inherent diffusion properties of kynurenine in the polymer matrix. Instead, drug release control was accomplished by converting the kynurenine-loaded PVA into a secondary diffusion-controlled system in which the PLGA layer acts as the transport medium. In fact, the only attempt in altering the inherent diffusion properties of kynurenine in the matrix was the heat treatment performed earlier in the investigation, which was shown to have limited effectiveness. As the end effect in this study was the conversion of the drug carrier into a diffusion-controlled system, whether kynurenine was released from PVA via diffusion or desorption controlled mechanism would indeed not have made a significant difference for this particular system. This realization brings the necessity of the effort made in studying drug-

polymer interaction into question. However, in this particular study involving kynurenine and PVA as representative examples, the drug release profile obtained from assays resembled the empirical models of both diffusion and desorption controlled release due to the hydrophilicity of both the drug and the matrix. Although the release was determined to be diffusion controlled based on physical evidence from DSC, XRD, and ToF-SIMS, the quick and severe swelling of the PVA matrix upon contact with aqueous environments would allow immediate access to drug molecules by penetrating fluids, whereas the small molecular size and water solubility of kynurenine would also allow quick transport out of the matrix. The end result in this case was then a diffusion-controlled release happening quickly that the kinetics could not be differentiated from released by drug simply desorbing from fibre surface into surrounding fluids. From a broader perspective, not all small molecule drugs will have such stringent matrix compatibility as kynurenine, and therefore the situation that two release mechanisms yielding almost identical results cannot be applied to all systems. For these systems, the methodical approach suggested in this research in determining drug-polymer interaction and dominant release mechanisms should nonetheless be considered an important first step in drug carrier development. For systems that are diffusion-controlled, a combination of composite approach and matrix modification such as adjusting crystallinity and crosslinking can be employed to control the diffusion properties. For desorption controlled systems, tailoring of the drug release profiles can be accomplished by conversion into diffusion controlled composite systems and adjustment of mixing parameters to yield different release profiles.

The optimized kynurenine carrier that satisfied drug release targets was produced in the form of a dip-coated fibre membrane, which could be difficult for direct application onto wounds. Furthermore, tensile testing results showed that even after dip-coating with the more flexible PLGA, stiffness of the carrier remained significantly higher than commercially available wound products. In addition to having suitable drug release characteristics, the carrier must also be

handleable by caregivers and users, and have appropriate mechanical response when applied on a wound. To assess the applicability of the PVA kynurenine carrier, two concept products were identified, including dressings and sutures, both of which can be applied as part of an anti-scarring solution. For dressings, a PLGA envelope was electrospun around the dip-coated carrier to provide an interface with the wound, which has suitable stiffness, tensile strength, and extensibility, when compared to commercially available wound dressings and native skin. With suture retention capability comparable with commercial dressings, the PLGA dressing can also be sutured onto a wound site, which may be preferable to adhesive bonding in situations such as excessive exudation. For sutures, a scalable method for fabricating kynurenine-loaded PVA yarns was examined in this study, allowing increased productivity as opposed to the rotating disc method reported in existing literature. The PVA yarns were braided into sutures using three-dimensional braiding, and were reinforced with commercially available microfibre yarns. The reinforcement examined in this study was aimed at overcoming one of the major hurdles for using electrospun yarns in medical sutures, which the lack of tensile strength. By using a commercially available silk yarn to reinforce the core of an electrospun yarn suture, significant strength increase was observed. Although the strength achieved in this study remained below that of commercial sutures, the results nonetheless showed that the reinforcement technique is flexible with material choice, such that further investigations for a more suitable reinforcement can be feasible. Moreover, the PVA suture could also be dip-coated with PLGA to create the optimal kynurenine-carrying system as reported in previous chapters. Through examination on the feasibility of creating dressings and sutures using electrospun fibre membranes, the assertion on choosing electrospun fibres as the material form of choice over others such as cast film and foam was justified.

5.2 Conclusion

In this study, an electrospun nanofibre-based kynurenine carrier was developed, which was shown to be capable of extending drug release from several hours in the as-electrospun form to over five days in the optimized form. From a wound healing perspective, the ability to gradually release kynurenine is tremendously helpful, as the drug-loaded dressing can remain on the wound for a longer time as opposed to requiring frequent replacement, allowing the wound healing process to proceed more smoothly without interruption. Throughout the development process, kynurenine was found to impose stringent limitations against materials and processing methods, as it has high affinity with water, small molecular size, and is only compatible with polymers with aqueous solubility. Therefore, the first and foremost deliverable accomplished in this research is the ability to tailor kynurenine release over periods ranging from two hours to over five days. Moreover, the investigations conducted in this study demonstrated a need-based approach to drug carrier design. Unlike most existing studies in which drugs were loaded into FDA-approved polymers at various concentrations to yield drug release profiles that may or may not be suitable for specific applications, the kynurenine carrier developed in this study considered factors such as dosage requirement and drug compatibility, while targeting a specific release behavior. The bottom-up development process began with material selection, which involved theoretical compatibility calculation and supported by experimental validation, as the theoretical approach does not take into consideration practical issues such as solvent compatibility. Having selected the matrix material and the most suitable grade for fabrication, a series of characterization was performed to elucidate the most dominant drug release mechanism. Such an experimental approach was proven to be a suitable tool for complementing the comparisons with empirical release models and provide measurable and useful insights into the nature of drug release. The approach to understanding drug release mechanism presented in this study will be useful for carrier developments for other drugs in the

future because this knowledge can be utilized in the formulation of methods for tailoring release properties.

In addition to characterizing drug-polymer interactions, this study also examined methods for optimizing kynurenine release, which involved modification to the matrix material, and incorporation of an additional polymer phase. Matrix modification, which could enable control over drug diffusion via crosslinking and matrix crystallization, showed limited effect on the PVA-kynurenine system due to the high water affinity of the drug and hydrogen bond formation with the matrix. However, the techniques can nonetheless be useful to other drug-polymer systems. Incorporation of a second polymer phase, either with a fibrous or a non-porous envelope, allowed conversion of a carrier into a diffusion-controlled composite system, which would be effective for either a desorption or diffusion-controlled carrier in the as-electrospun stage. With the PLGA dip-coated PVA carrier shown in this study, not only could kynurenine release be extended to over five days, but by adjusting coating parameters, tailorable release ranging from two to five days was also possible, thereby enabling greater flexibility for application in different patient conditions. For example, if conditions with the patient arise requiring the removal of the initial dressing before complete release of kynurenine, it can be replaced with a new dressing that facilitate quicker release to maintain optimal stimulation rate for MMPs. The flexibility in tailoring release between the two extremes of five hours and five days would also be tremendously useful when designing carriers for similar drugs in the future, which may have different release requirements.

Throughout this research, three major methods to control drug release from nanofibre matrices were demonstrated. In the first method, material parameters such as polymer molecular weight, electrospinning concentration, and drug dosage were controlled to adjust the extent of burst release. For a diffusion-controlled system, the coefficient K_H could be varied by approximately

10% through the feed material parameters. However, it was observed that adjusting material parameters was not able to appreciably extend the release duration, and therefore this method should be used mainly for fine adjustment in the release behavior. In the case that more significant change in release behavior is desired, for example, if specific application requires two-fold extension of the release duration, other methods must be applied. The second major method proposed in this research was modification of the matrix via crosslinking or heat treatment. Heat treatment was demonstrated in the PVA-kynurenine system to be able to extend the release duration as well as significantly changing the burst release behavior, allowing a 5% – 48% reduction in K_H , although for this particular material, drug entrapment was observed. Matrix modification should nonetheless be pursued in carrier development for other polymer-drug systems due to difference in interactions and hydrophilicity. The third method proposed in this research was a composite approach in which the drug-polymer system was encased in a second phase which possesses different persistence in aqueous environments. For the PVA-kynurenine system, the composite approach was demonstrated by adding a nanofibrous PLGA shell or dip-coating into a PLGA solution, which led to a 30% – 85% reduction in K_H , as well as extension of the release period from five hours to over 200 hours.

With each control method proposed having different impact on burst release and the release duration, strategies can be formulated in future drug carrier development, based on the observations made from this research. The composite approach, with its large degree of control over the overall release behavior, can be used as a coarse adjustment method when deciding the appropriate release duration for a specific drug-material system. Subsequently, matrix modification to the drug-carrying phase can be performed to adjust the early-stage release behavior, such as reducing burst release. Finally, material parameters can be optimized as fine-tuning mechanism for further controlling the extent of the burst release.

Another area that has often been neglected in existing drug carrier development studies is the fabrication into applicable forms and verifying its robustness for handling and application. The study outlined in Chapter 4 investigated two product designs based on the optimized kynurenine release system, including dressing and sutures. The main challenge in these investigations was the lack of industry standards for design criteria establishment, but was mitigated in this study by using experimentally measured properties of commercial products as well as reported properties of native skin in literature as benchmarks. In terms of the dressing, a composite envelope design was proposed in which a PLGA shell with appropriate stiffness, strength, extensibility, and suture retention served as an interface between the drug carrier and the wound. In suture development, it was observed from the limited existing studies that the major drawbacks preventing the use of nanofibre-based sutures were the inferior tensile properties to commercial products and the low productivity. The lack of integrity under tensile load was addressed via reinforcement with commercially available yarns, which yielded significant increase in ultimate tensile strength. In addition, this study has also examined a new approach to produce electrospun yarns in a scalable manner, by using a collector containing multiple aluminum strips as opposed to a rotating disc collector. More importantly, it was also demonstrated that the fabricated suture was also able to facilitate drug release, much like its planar dressing counterpart.

From the perspective of a kynurenine carrier development project, this research has been successful with its major objectives accomplished. Kynurenine-loaded nanofibre was successfully fabricated with the nature of the drug-polymer interaction carefully characterized. The kynurenine release target that was set to optimize MMP stimulation was also achieved, with the ability for the carrier to be tailored to yield release profiles in between the initial observed duration to the final optimized one. In addition, kynurenine-loaded nanofibres were fabricated into clinically applicable forms including dressing and sutures. However, as highlighted in the

project scope, the motivation behind the current research is to establish a methodical approach to develop nanofibre-based drug carriers for a variety of therapeutics to optimize regeneration of a wider range of tissues. Kynurenine has indeed served as a fine example of how such an approach can be applied, due to the stringent processing requirements as a result of its solubility and compatibility. All of the steps in the development process and their outcome were thoroughly demonstrated using the kynurenine example. While several optimization approaches, such as crosslinking and heat treatment, had limited effects on this particular system, they may nonetheless be useful when considering other diffusion-controlled drug-polymer systems in the future.

Overall, the tangible outcomes of the development approach described in this thesis were the high degree of tailoring that could be achieved with a specific material system, yielding a wide range of release periods that could be beneficial for various applications, as well as the ability to fabricate the optimized carrier into products with sufficient integrity. The value of these outcomes is their transferability to future drug carrier development in a general sense. First, a detailed method for material selection and validation could help identify drug-polymer systems with higher stability. Second, a series of approaches to tailoring drug release behavior proposed in this research could help creating a system with a specific release duration as well as initial burst release behavior. Third, the ability to fabricate a desirable drug carrier design into planar and tubular dressing structures can be beneficial for enhancing the market readiness of a new drug carrier or wound dressing design. Following this approach, a wider variety of therapeutics can be applied onto tissues via nanofibre-based carriers with highly specific release properties, enabling stimulation of specific responses in the intricate tissue regeneration process. By moving away from traditional antibiotic or anti-inflammatory agent delivery, and into the niche area of specific tissue responses, patients may be able to enjoy improved healing experience from injuries enabling them to return to livelihood in a quicker manner.

5.3 Recommendations and Future Work

While this thesis has highlighted the successful demonstration of a methodical approach to drug loaded wound dressing development, using kynurenine as a representative example, several areas that can be improved were also realized during the formulation process of the approach presented. The recommendations include both improvements to further release control, as well as continued study on wound dressing process optimization in characterization and fabrication, which will greatly benefit future development of different drug-polymer systems. As a result, the recommendations presented in this section will be an important aspect to be considered for future studies such that the vision of optimizing tissue regeneration using tailored dressing materials, which motivated the current study, can be realized.

In regards to improving drug release control, kynurenine has thus far been mixed directly with the matrix, forming hydrogen bonds. However, its conjugation with matrix polymer has not been explored yet. Conjugation of kynurenine via covalent bond formation with polymers may broaden the range of suitable matrices by eliminating direct blending. Although it was discussed earlier that covalent bond formation has led to drug entrapment in previous work, those studies have focused mainly on peptide drugs with orders of magnitude larger molecular sizes. In addition, conjugation with biodegradable polymers may help facilitate drug release. Feasibility studies in conjugating kynurenine to polymer matrices will therefore involve examinations on whether drug can be released, as well as whether the drug will maintain its function having covalently bonded.

For process optimization in dressing development, the first recommended step towards continued studies is to apply the development approach on another small-molecule, hydrophilic drug, in order to determine if the release behavior of another drug can be tailored as observed

in the kynurenine system. An apparent candidate for this potential study is kynurenic acid, which is an acidic salt of kynurenine formed in an enzymatic reaction catalyzed by kynurenine-oxoglutarate transaminase. While the therapeutic value of kynurenic acid on scarring reduction is outside the scope of this thesis, it may be a desirable candidate for follow-up studies due to its chemical similarity to kynurenine and its higher flexibility in terms of solvent and polymer compatibility. Being soluble in solvents such as DMF, kynurenic acid can be loaded into non-water soluble polymers, which will help determine the universal applicability of the carrier development method demonstrated. In designing a kynurenic acid-loaded dressing, two major changes can be expected. First, by not being restricted to a water-soluble matrix, the dominant release mechanism may be easier to distinguish in a kynurenic-acid system, as opposed to a kynurenine-system in which there were difficulties distinguishing between desorption and diffusion controlled release mechanisms. Secondly, the effects of physical and chemical treatments such as crosslinking and heat treatment may be more pronounced than on a water-soluble polymer, thereby enabling a larger degree of control over the release behavior. Success in replicating, and even improving, the carrier development approach using a different compound such as kynurenic acid would indicate that the approach can be universally applicable thereby increasing its potential for adaptation when formulating new tailored carriers for different therapeutics.

Validation of the development process on a different drug can also help optimize the matrix selection process. In the initial stages of the current study, PVA and PLGA were identified as candidates as kynurenine carriers through theoretical calculations, with PLGA eliminated due to its incompatibility in water. Although validation tests comparing PVA with poly(ethylene oxide) (PEO) and poly(vinyl acetate) (PVAc) confirmed the validity for using PVA as the matrix, it must be noted with a caution because PEO's quicker dissolution rate and PVAc's acidic aqueous environment may have played a significant role in the outcome. Indeed, among polymers that

can be dissolved in completely aqueous environments, PVA is a logical matrix choice due to its ability to be crosslinked and heat treated. The limited choice of suitable water-soluble polymer matrices therefore presented challenges to independent validations of solubility calculations as a method for material selection. However, if the drug can be dissolved in solvents other than water, matrix choice will no longer be limited, allowing more in-depth validation to calculations. For example, if the design process is to focus on kynurenic acid, which is soluble in organic solvents, then polymer matrices such as poly(methyl methacrylate) (PMMA), poly(acrylonitrile) (PAN), poly(caprolactone) (PCL) and PLGA, each having a different range of Hildebrand-Scatchard solubility parameters, can be compared through x-ray and thermal analyses to determine whether calculation results match with experimental observation.

During the release optimization studies, it was found that release behavior is heavily influenced by the surface area of the carrier. The effect is more pronounced when comparing a PLGA fibrous envelope and a non-porous PLGA envelope around a layer of kynurenine-loaded PVA, in which the dip-coated sample showed much longer release duration. While a qualitative relationship between surface area and release was apparent, it would be of interest to quantify that relationship to obtain parameters for process optimization. While there were concerns that techniques such as mercury porosimetry would deform the fibrous structure of the carrier leading to inaccurate results on pore sizes and distributions, the Brunauer-Emmett-Teller (BET) method was attempted to investigate the surface area of the carriers in this study. The BET method relies on gas penetration into specimen and uses information on gas molecule adsorption to determine its specific surface area. However, when using the BET method to determine the surface area of electrospun PVA, it was determined to be $15 \pm 11 \text{ m}^2$ per gram of fibre. The high standard deviation would prevent conclusive comparisons between different specimen groups. In this research, the lack of precise information on surface area was addressed by examining fabrication parameters such as fibre diameter and effect of

consolidating coating layers, which showed varying positive effects on delaying kynurenine release. However, a more reliable approach to characterize carrier surface area would nonetheless provide useful information in process control and future carrier development.

For the kynurenine dressing, designing layered structures became a major part of the release optimization, due to the high hydrophilicity of PVA. Characterization of shell surface properties and layer thickness could be performed in a satisfactory manner using optical, laser confocal, and electron microscopy. However, the interlayer morphology was much more difficult to characterize. While images of the cross-sections could be taken using optical and laser confocal microscope with relative ease, obtaining an appropriate cross-section for observation was itself a major challenge, especially when the PVA was surrounded by a fibrous layer. Simply cutting the layered structures with surgical scissors or blades produced a fused morphology due to fibre deformation. Cold fracture was also attempted to obtain a brittle fracture of the layered dressing, but the large amount of air in the porous structure and the low stiffness of individual fibres prevented a clean and completely brittle fracture, yielding a more moderately-ductile fracture surface. With a non-uniform fracture surface, observation of the cross-section through electron microscopy became difficult because the roughness of the fracture surface is considerably high compared to the depth of field of electron microscopy. Without the ability to examine the interface between layers in high resolution, detailed knowledge on morphology in the transition zone and also interlayer bonding could not be obtained. Therefore, the search for an alternative approach to obtain the cross-section would be tremendously helpful in learning about material interactions in the layered dressings, which may be used as the basis for further structural optimization.

In addition to characterizing layered structures, it would also be desirable to examine methods for fabricating nanofibres that are multilayered at the fibre level instead of assembly level, which

could be achieved via core-shell electrospinning. By fabricating fibres with a PLGA shell and kynurenine-loaded PVA core, the available surface area would greatly increase while maintaining a PLGA/PVA interface like in the dip-coated fibres. Comparing between dip-coated fibre assemblies and core-shell fibres would likely provide insightful knowledge on the effect of fibre surface area. There are two methods for producing core-shell nanofibres, either by coaxial electrospinning or emulsion electrospinning as mentioned in section 1. In fact, both methods have been attempted on the PLGA and PVA-kynurenine system throughout this study. However, the stringent compatibility of the PVA-kynurenine-water system posed difficulties in obtaining a uniform Taylor cone in coaxial electrospinning, as precipitation would occur when the kynurenine-containing phase came into contact with the PLGA phase. Emulsion electrospinning was also attempted with various surfactant levels, but stable electrospinning could not be achieved as the two phases had a high tendency to phase-separate. However, it may be beneficial to examine similar molecules such as Kynurenic acid and its ability to be fabricated into core-shell fibres through the two aforementioned electrospinning methods. With a broader range of solvent compatibility, Kynurenic acid utilization may be feasible for either the coaxial or emulsion electrospinning setup.

The last step in the kynurenine dressing development process was to convert the dip-coated carrier into clinically applicable products such as dressings and suture. The performance metric that was the main focus of this study was tensile properties including Young's modulus, strength and elongation, as well as suture retention. The performance metrics selected focused mainly on mechanical properties to demonstrate that nanofibre-based dressings can withstand loads associated with handling during the manufacturing and application process, and physiological loads once applied on the patient. Also, mechanical properties are heavily influenced by the dressing design outlined in this thesis, and can be tailored to suit specific needs, which fits into the scope of this research. However, ensuring that the nanofibre-based designs are sufficiently

robust to can only show their feasibility to be used as wound dressing materials, but to be considered fully suitable for application on wounds, other properties must also be characterized. An example of such properties is the dressing breathability, which help the transport of water vapour and oxygen, both of which are important for wound healing as well as wearer comfort. Although these properties are outside of the scope of the current research, as they focus more on user experience, but do not address drug release control and robustness of the design, they are nonetheless important areas for further investigations for transformation into marketable products.

In addition to dressings, fabrication of kynurenine-loaded nanofibres into sutures was also investigated as the material system developed for wound dressings could be translated into other material forms, utilizing the continuous nature of electrospun nanofibres. Furthermore, sutures are a useful application of nanofibres for wound healing that has not been widely explored. The investigations conducted in this research have successfully increased the scalability of yarn production and also the tensile strength of the resultant sutures, which highlighted potential in nanofibre-based suture application using the design approach described in this thesis. However, as with the dressings described above, further work is required to transform the sutures into usable products. In the particular case of suture applications, showing tensile properties in its as-fabricated form may only show its resistance to loads while handling. When sutures are applied clinically, they are tied into knots and operate in wet environments. Therefore, tensile testing on knotted sutures would provide greater insights into whether the suture is sufficiently robust to be used in patients. Also, since most suture remains in the wound for up to one week, extensive testing of the tensile properties in aqueous environments as well as property retention would be helpful. Furthering the nanofibre suture characterization and optimization, while being an intricate study by itself, would be tremendously beneficial to

nanofibre wound dressing technology by opening new opportunities in which different products derived from electrospun material systems can be applied to a wider variety of situations.

Like any new medical device, development of a novel nanofibre-based wound dressing is a lengthy process with many challenges that must be addressed to ensure that a product fulfills requirements in terms of therapeutic value, robustness, and user experience. The studies described in this thesis was conducted to examine a large part of the requirements, by answering the two major questions of how release of hydrophilic, small molecule drugs from electrospun nanofibres can be controlled and how drug-loaded nanofibres can be formulated to be applied on wounds. On the other hand, the recommendations outlined in this section take the wider perspective of ensuring the universal applicability of the carrier development method and optimizing physical properties to enhance user experience. These recommendations can be considered as fine-tuning the knowledge obtained from this thesis with the goal of generating a more complete approach to develop novel wound dressings for current and future therapeutics.

References

Alster, T. S. and Williams, C. M. (1995). "Treatment of keloid sternotomy scars with 585 nm flashlamp-pumped pulsed-dye laser." The Lancet **345**(8959): 1198-1200.

American Burn Association (2009). "Burn Incidence Fact Sheet." Retrieved January 20, 2010, from http://www.ameriburn.org/resources_factsheet.php.

Asran, A. S., Henning, S. and Michler, G. H. (2010). "Polyvinyl alcohol–collagen–hydroxyapatite biocomposite nanofibrous scaffold: Mimicking the key features of natural bone at the nanoscale level." Polymer **51**(4): 868-876.

Assender, H. E. and Windle, A. H. (1998). "Crystallinity in poly (vinyl alcohol). 1. An X-ray diffraction study of atactic PVOH." Polymer **39**(18): 4295-4302.

Ayutsede, J., Gandhi, M., Sukigara, S., Micklus, M., Chen, H.-E. and Ko, F. (2005). "Regeneration of Bombyx mori silk by electrospinning. Part 3: characterization of electrospun nonwoven mat." Polymer **46**(5): 1625-1634.

Bassil, M. J., Ibrahim, M. I., Souaid, E., El Haj Moussa, G., El Tahchi, M. R., Boiteux, G., Davenas, J., Lanceros-Mendez, S. and Farah, J. K. (2009). Development of a Flexible Conductive Polymer Membrane on Electroactive Hydrogel Microfibers. MRS Proceedings, Cambridge Univ Press.

Baumgarten, P. K. (1971). "Electrostatic spinning of acrylic microfibers." Journal of Colloid and Interface Science **36**(1): 71-79.

Bello, Y. M. and Phillips, T. J. (2000). "Recent advances in wound healing." Jama **283**(6): 716-718.

Bicerano, J. (2002). Prediction of polymer properties, CRC Press.

Biondi, M., Ungaro, F., Quaglia, F. and Netti, P. A. (2008). "Controlled drug delivery in tissue engineering." Advanced Drug Delivery Reviews **60**(2): 229-242.

Bölgen, N., Vargel, İ., Korkusuz, P., Menciloğlu, Y. Z. and Pişkin, E. (2007). "In vivo performance of antibiotic embedded electrospun PCL membranes for prevention of abdominal adhesions." Journal of Biomedical Materials Research Part B: Applied Biomaterials **81B**(2): 530-543.

Bourke, S., Al-Khalili, M., Briggs, T., Michniak, B., Kohn, J. and Poole-Warren, L. (2003). "A photo-crosslinked poly(vinyl alcohol) hydrogel growth factor release vehicle for wound healing applications." AAPS PharmSci **5**(4): 101-111.

Boys, C. V. (1887). "LVII. On the production, properties, and some suggested uses of the finest threads." Philosophical Magazine Series 5 **23**(145): 489-499.

Bradley, M., Cullum, N., Nelson, E., Petticrew, M., Sheldon, T. and Torgerson, D. (1999). "Systematic reviews of wound care management:(2) dressings and topical agents used in the healing of chronic wounds." Health technology assessment **3**(17 II).

Brown, G. L., Nanney, L. B., Griffen, J., Cramer, A. B., Yancey, J. M., Curtsinger, L. J., Holtzin, L., Schultz, G. S., Jurkiewicz, M. J. and Lynch, J. B. (1989). "Enhancement of Wound Healing by Topical Treatment with Epidermal Growth Factor." New England Journal of Medicine **321**(2): 76-79.

Bunger, C. (1823). "Gelungener versuch einer nasenbildung aus einem vollig getrennten hautstuck aus dem beine." J Chir Augenheilk **4**: 569.

Burke, J. F., Yannas, I. V., Quinby, W. C., Bondoc, C. C. and Jung, W. K. (1981). "Successful Use of a Physiologically Acceptable Artificial Skin in the Treatment of Extensive Burn Injury." Ann. Surg. **194**(4): 413-428.

Buslov, D., Sushko, N. and Tretinnikov, O. (2011). "IR investigation of hydrogen bonds in weakly hydrated films of poly (vinyl alcohol)." Polymer Science Series A **53**(12): 1121-1127.

Byron, P. R. and Dalby, R. N. (1987). "Effects of heat treatment on the permeability of polyvinyl alcohol films to a hydrophilic solute." Journal of Pharmaceutical Sciences **76**(1): 65-67.

Cao, Y. and Wang, B. (2009). "Biodegradation of silk biomaterials." International journal of molecular sciences **10**(4): 1514-1524.

Casper, C. L., Yang, W., Farach-Carson, M. C. and Rabolt, J. F. (2007). "Coating electrospun collagen and gelatin fibers with perlecan domain I for increased growth factor binding." Biomacromolecules **8**(4): 1116-1123.

Chen, S. C., Huang, X. B., Cai, X. M., Lu, J., Yuan, J. and Shen, J. (2012). "The influence of fiber diameter of electrospun poly(lactic acid) on drug delivery." Fibers and Polymers **13**(9): 1120-1125.

Chew, S. Y., Wen, J., Yim, E. K. and Leong, K. W. (2005). "Sustained release of proteins from electrospun biodegradable fibers." Biomacromolecules **6**(4): 2017-2024.

Chew, S. Y., Wen, J., Yim, E. K. F. and Leong, K. W. (2005). "Sustained Release of Proteins from Electrospun Biodegradable Fibers." Biomacromolecules **6**(4): 2017-2024.

Chu, X. H., Shi, X. L., Feng, Z. Q., Gu, Z. Z. and Ding, Y. T. (2009). "Chitosan Nanofiber Scaffold Enhances Hepatocyte Adhesion and Function." Biotechnology Letters **31**: 347-352.

Chua, K. N., Lim, W., Zhang, P., Lu, H., Wen, J., Ramakrishna, S., Leong, K. W. and Mao, H. (2005). "Stable immobilization of rat hepatocyte spheroids on galactosylated nanofiber scaffold." Biomaterials **26**: 2537-2547.

Ciofani, G., Raffa, V., Pizzorusso, T., Menciassi, A. and Dario, P. "Characterization of an alginate-based drug delivery system for neurological applications." Medical Engineering & Physics **In Press, Corrected Proof**.

Compton, C. C., Butler, C. E., Yannas, I. V., Warland, G. and Orgill, D. P. (1998). "Organized Skin Structure Is Regenerated In Vivo from Collagen-GAG Matrices Seeded with Autologous Keratinocytes." The Journal of Investigative Dermatology **110**(6): 908-916.

Cooley, J. F. (1902). Apparatus for electrically dispersing fluids, U.S. Patents No. 692,631.

Crank, J. (1979). The mathematics of diffusion, Oxford university press.

Cui, W., Li, X., Zhu, X., Yu, G., Zhou, S. and Weng, J. (2006). "Investigation of Drug Release and Matrix Degradation of Electrospun Poly(dl-lactide) Fibers with Paracetamol Inoculation." Biomacromolecules **7**(5): 1623-1629.

D'Amore, A., Stella, J. A., Wagner, W. R. and Sacks, M. S. (2010). "Characterization of the complete fiber network topology of planar fibrous tissues and scaffolds." Biomaterials **31**(20): 5345-5354.

Darzi, M. A., Chowdri, N. A., Kaul, S. K. and Khan, M. (1992). "Evaluation of various methods of treating keloids and hypertrophic scars: a 10-year follow-up study." British Journal of Plastic Surgery **45**(5): 374-379.

Deitch, E. A., Wheelahan, T. M., Rose, M. P., Clothier, J. and Cotter, J. (1983). "Hypertrophic burn scars: analysis of variables." The Journal of Trauma and Acute Care Surgery **23**(10): 895-898.

Del Gaudio, C., Ercolani, E., Galloni, P., Santilli, F., Baiguera, S., Polizzi, L. and Bianco, A. (2013). "Aspirin-loaded electrospun poly(ϵ -caprolactone) tubular scaffolds: potential small-diameter vascular grafts for thrombosis prevention." Journal of Materials Science: Materials in Medicine **24**(2): 523-532.

Desai, K., Kit, K., Li, J. and Zivanovic, S. (2008). "Morphological and Surface Properties of Electrospun Chitosan Nanofibers." Biomacromolecules **9**(3): 1000-1006.

Ding, B., Kim, H. Y., Lee, S. C., Shao, C. L., Lee, D. R., Park, S. J., Kwag, G. B. and Choi, K. J. (2002). "Preparation and characterization of a nanoscale poly (vinyl alcohol) fiber aggregate produced by an electrospinning method." Journal of Polymer Science Part B: Polymer Physics **40**(13): 1261-1268.

Duan, B., Yuan, X., Zhu, T., Zhang, Y., Li, X., Zhang, Y. and Yao, K. (2006). "A nanofibrous composite membrane of PLGA-chitosan/PVA prepared by electrospinning." European Polymer Journal **42**(9): 2013-2022.

Elsner, J. J., Berdichevsky, I., Shefy-Peleg, A. and Zilberman, M. (2011). Novel composite antibiotic-eluting structures for wound healing applications. Active Implants and Scaffolds for Tissue Regeneration, Springer: 3-37.

Epstein, F. H. (1999). "Cutaneous Wound Healing." The New England Journal of Medicine **341**(10).

Falanga, V. (2005). "Wound healing and its impairment in the diabetic foot." The Lancet **366**(9498): 1736-1743.

Flory, P. J. (2004). "Thermodynamics of high polymer solutions." The Journal of chemical physics **10**(1): 51-61.

Formhals, A. (1934). Process and apparatus for preparing artificial threads. United States, Richard, S.G.

Formahs, A. **1975504**.

Fridrikh, S. V., Yu, J. H., Brenner, M. P. and Rutledge, G. C. (2003). "Controlling the Fiber Diameter during Electrospinning." Phys. Rev. Lett. **90**: 144502-144506.

Fried, J. (2003). Polymer science and technology, Pearson Education.

Gandhi, M., Srikar, R., Yarin, A. L., Megaridis, C. M. and Gemainhart, R. A. (2009). "Mechanistic Examination of Protein Release from Polymer Nanofibers." Molecular Pharmaceutics **6**(2): 641-647.

Gandhi, M., Yang, H., Shor, L. and Ko, F. (2007). "Regeneration of bombyx mori silk by electrospinning: A comparative study of the biocompatibility of natural and synthetic polymers for tissue engineering applications." Journal of Biobased Materials and Bioenergy **1**(2): 274-281.

Gandhi, M., Yang, H., Shor, L. and Ko, F. K. (2009). "Post-spinning modification of electrospun nanofiber nanocomposite from Bombyx mori silk and carbon nanotubes." Polymer **50**: 1918-1924.

Gangwal, S. and Wright, M. (2013). "Nanofibres: New scalable technology platform for producing polymeric nanofibres." Filtration+ Separation **50**(2): 30-33.

Ghahary, A., Karimi-Busheri, F., Marcoux, Y., Li, Y., Tredget, E. E., Kilani, R. T., Li, L., Zheng, J., Karami, A. and Keller, B. O. (2004). "Keratinocyte-releasable stratifin functions as a potent collagenase-stimulating factor in fibroblasts." Journal of investigative dermatology **122**(5): 1188-1197.

Gibson, P., Lee, C., Ko, F. and Reneker, D. H. (2006). "Application of nanofiber technology to nonwoven thermal insulation." Journal of Engineered Fibers and Fabrics **2**(2): 32 - 40.

Gilchrist, S. E., Rickard, D. L., Letchford, K., Needham, D. and Burt, H. M. (2012). "Phase separation behavior of fusidic acid and rifampicin in PLGA microspheres." Molecular Pharmaceutics **9**(5): 1489-1501.

Gogotsi, Y. (2006). Nanomaterials Handbook, Taylor & Francis.

Gollwitzer, H., Ibrahim, K., Meyer, H., Mittelmeier, W., Busch, R. and Stemberger, A. (2003). "Antibacterial poly (D, L-lactic acid) coating of medical implants using a biodegradable drug delivery technology." Journal of Antimicrobial Chemotherapy **51**(3): 585-591.

Göpferich, A. (1996). "Mechanisms of polymer degradation and erosion." Biomaterials **17**(2): 103-114.

Guo, S. and DiPietro, L. A. (2010). "Factors affecting wound healing." Journal of dental research **89**(3): 219-229.

Han, N., Johnson, J., Lannutti, J. J. and Winter, J. O. (2012). "Hydrogel–electrospun fiber composite materials for hydrophilic protein release." Journal of Controlled Release **158**(1): 165-170.

He, C. L., Huang, Z. M. and Han, X. J. (2009). "Fabrication of drug-loaded electrospun aligned fibrous threads for suture applications." Journal of Biomedical Materials Research Part A **89A**(1): 80-95.

Hearle, J. W. and Morton, W. E. (2008). Physical properties of textile fibres, Elsevier.

Heller, J. and Baker, R. (1980). "Theory and practice of controlled drug delivery from bioerodible polymers." Controlled Release of Bioactive Materials, Academic Press, New York: 1-18.

Herman, A. R. (2002). "The history of skin grafts." Journal of Drugs in Dermatology **1**(3): 298.

Herndon, D. N., Barrow, R. E., Rutan, R. L., Rutan, T. C., Desai, M. H. and Abston, S. (1989). "A comparison of conservative versus early excision. Therapys in severely burned patients." Ann. Surg. **209**(5): 547-553.

Hildebrand, J. and Scott, R. (1964). "The solubility of nonelectrolytes, 1950." Reinhold, New York: 411.

Hopfenberg, H. (1976). "Controlled release from erodible slabs, cylinders, and spheres." Controlled release polymeric formulations **33**: 26-32.

Hromadka, M., Collins, J. B., Reed, C., Han, L., Kolappa, K. K., Cairns, B. A., Andrady, T. and van Aalst, J. A. (2008). "Nanofiber Applications for Burn Care." Journal of Burn Care & Research **29**(5): 695-703.

Hsu, F.-Y., Hung, Y.-S., Liou, H.-M. and Shen, C.-H. (2010). "Electrospun hyaluronate–collagen nanofibrous matrix and the effects of varying the concentration of hyaluronate on the characteristics of foreskin fibroblast cells." Acta Biomaterialia **6**(6): 2140-2147.

Hu, W. and Huang, Z.-M. (2010). "Biocompatibility of braided poly(L-lactic acid) nanofiber wires applied as tissue sutures." Polymer International **59**(1): 92-99.

Hu, W., Huang, Z. M. and Liu, X. Y. (2010). "Development of braided drug-loaded nanofiber sutures." Nanotechnology **21**(31): 315104.

Huang, L.-Y., Branford-White, C., Shen, X.-X., Yu, D.-G. and Zhu, L.-M. (2012). "Time-engineered biphasic drug release by electrospun nanofiber meshes." International Journal of Pharmaceutics **436**(1): 88-96.

Huang, W., Zou, T., Li, S., Jing, J., Xia, X. and Liu, X. (2013). "Drug-Loaded Zein Nanofibers Prepared Using a Modified Coaxial Electrospinning Process." AAPS PharmSciTech **14**(2): 675-681.

Huggins, M. L. (1942). "Thermodynamic Properties of Solutions of Long-chain Compounds." Annals of the New York Academy of Sciences **43**(1): 1-32.

Immich, A. P. S., Arias, M. L., Carreras, N., Boemo, R. L. and Tornero, J. A. (2013). "Drug delivery systems using sandwich configurations of electrospun poly(lactic acid) nanofiber membranes and ibuprofen." Materials Science and Engineering: C **33**(7): 4002-4008.

Instrumentation, A. f. t. A. o. M. (1994). "Cardiovascular implants-vascular graft prostheses." ANSI/AAMI VP20-94.

Ionescu, L. C., Lee, G. C., Sennett, B. J., Burdick, J. A. and Mauck, R. L. (2010). "An anisotropic nanofiber/microsphere composite with controlled release of biomolecules for fibrous tissue engineering." Biomaterials **31**(14): 4113-4120.

Jackson, J. K., Smith, J., Letchford, K., Babiuk, K. A., Machan, L., Signore, P., Hunter, W. L., Wang, K. and Burt, H. M. (2004). "Characterization of perivascular poly (lactic-co-glycolic acid) films containing paclitaxel." International Journal of Pharmaceutics **283**(1): 97-109.

Jaksic, T. and Burke, J. F. (1987). "The Use of "Artificial Skin" for Burns." Ann. Rev. Med. **38**: 107-117.

Jannesari, M., Varshosaz, J., Morshed, M. and Zamani, M. (2011). "Composite poly(vinyl alcohol)/poly(vinyl acetate) electrospun nanofibrous mats as a novel wound dressing matrix for controlled release of drugs." Int. J. Nanomedicine **6**: 993-1003.

Ji, W., Sun, Y., Yang, F., Beucken, J. J. P., Fan, M., Chen, Z. and Jansen, J. (2011). "Bioactive Electrospun Scaffolds Delivering Growth Factors and Genes for Tissue Engineering Applications." Pharmaceutical Research **28**(6): 1259-1272.

Ji, Y., Ghosh, K., Shu, X. Z., Li, B., Sokolov, J. C., Prestwich, G. D., Clark, R. A. F. and Rafailovich, M. H. (2006). "Electrospun three-dimensional hyaluronic acid nanofibrous scaffolds." Biomaterials **27**(20): 3782-3792.

Katti, D. S., Robinsin, K. W., Ko, F. K. and Laurencin, C. T. (2005). "Bioresorbable Nanofiber-Based Systems for Wound Healing and Drug Delivery: Optimization of Fabrication Parameters." Journal of Biomedical Materials Research Part B: Applied Biomaterials **70B**(2): 286-296.

Kenawy, E.-R., Abdel-Hay, F. I., El-Newehy, M. H. and Wnek, G. E. (2007). "Controlled release of ketoprofen from electrospun poly(vinyl alcohol) nanofibers." Materials Science and Engineering: A **459**(1-2): 390-396.

Kenawy, E.-R., Abdel-Hay, F. I., El-Newehy, M. H. and Wnek, G. E. (2009). "Processing of polymer nanofibers through electrospinning as drug delivery systems." Materials Chemistry and Physics **113**(1): 296-302.

Kiil, J. (1977). "Keloids treated with topical injections of triamcinolone acetonide (kenalog): Immediate and long-term results." Scandinavian Journal of Plastic and Reconstructive Surgery and Hand Surgery **11**(2): 169-172.

Kim, K., Luu, Y. K., Chang, C., Fang, D., Hsiao, B. S., Chu, B. and Hadjiargyrou, M. (2004). "Incorporation and controlled release of a hydrophilic antibiotic using poly (lactide-co-glycolide)-based electrospun nanofibrous scaffolds." Journal of Controlled Release **98**(1): 47-56.

Ko, F. and Gandhi, M. (2007). Producing nanofibre structures by electrospinning for tissue engineering. Nanofibers and nanotechnology in textiles. P. Brown and K. Stevens. Clemson, South Carolina, Woodhead Publishing. **67**.

Ko, F. K. (1997). Medical Applications for Textile Structures. Textile Asia.

Ko, F. K. and Gandhi, M. (2007). Producing nanofiber structures by electrospinning for tissue engineering. Cambridge, UK, Woodhead Publishing.

Ko, F. K., Laurencin, C. T., Borden, M. D. and Reneker, D. (1998). The Dynamics of Cell-Fiber Architecture Interaction. Annual Meeting of the Biomaterials Research Society, San Diego.

Korsmeyer, R. W., Gurny, R., Doelker, E., Buri, P. and Peppas, N. A. (1983). "Mechanisms of solute release from porous hydrophilic polymers." International Journal of Pharmaceutics **15**(1): 25-35.

Kovacs, E. and DiPietro, L. (1994). "Fibrogenic cytokines and connective tissue production." The FASEB journal **8**(11): 854-861.

Kremer, M., Lang, E. and Berger, A. C. (2000). "Evaluation of dermal-epidermal skin equivalents of human keratinocytes in a collagen-glycosaminoglycan matrix (Integra Artificial Skin)." British Journal of Plastic Surgery **53**: 459-465.

Kumbar, S. G., James, R., Nukavarapu, S. P. and Laurencin, C. T. (2008). "Electrospin nanofiber scaffolds: engineering soft tissues." Biomedical Materials **3**(3): 034002.

Kurpinski, K. T., Stephenson, J. T., Janairo, R. R. R., Lee, H. and Li, S. (2010). "The effect of fiber alignment and heparin coating on cell infiltration into nanofibrous PLLA scaffolds." Biomaterials **31**(13): 3536-3542.

Langer, R. (1998). "Drug delivery and targeting." Nature **392**(6679 Suppl): 5-10.

Lee, P.-Y., Li, Z. and Huang, L. (2003). "Thermosensitive Hydrogel as a Tgf- β 1 Gene Delivery Vehicle Enhances Diabetic Wound Healing." Pharmaceutical Research **20**(12): 1995-2000.

Lee, P. I. (1980). "Diffusional release of a solute from a polymeric matrix — approximate analytical solutions." Journal of Membrane Science **7**(3): 255-275.

Lee, S. J., Yoo, J. J., Lim, G. J., Atala, A. and Stitzel, J. (2007). "In vitro evaluation of electrospun nanofiber scaffolds for vascular graft application." Journal of Biomedical Materials Research Part A **83**(4): 999-1008.

Leung, V., Hartwell, R., Elizei, S. S., Yang, H., Ghahary, A. and Ko, F. (2013). "Postelectrospinning modifications for alginate nanofiber-based wound dressings." Journal of Biomedical Materials Research Part B: Applied Biomaterials.

Leung, V., Hartwell, R., Faure, E., Yang, H., Ghahary, A. and Ko, F. K. (2012). Electrospun Nanofibers as Next-Generation Bioactive Tissue Scaffolds. Tissue Engineering and Regenerative Medicine, CRC Press: 229-250.

Leung, V. and Ko, F. (2011). "Biomedical applications of nanofibers." Polymers for Advanced Technologies **22**(3): 350-365.

Leung, V. and Ko, F. K. (2010). "Biomedical Applications of Nanofibers." Polymers Advanced Technologies **22**(3): 350-365.

Leung, V., Yang, H., Gupta, M. and Ko, F. K. (2010). Alginate Nanofibre Based Tissue Engineering Scaffolds by Electrospinning. SAMPE 2010, Seattle, WA.

Leung, V., Yang, H., Gupta, M. and Ko, F. K. (2010). Alginate Nanofibre Based Tissue Engineering Scaffolds by Electrospinning. Society for the Advancement of Materials and Process Engineering 2010 Conference, Seattle, WA.

Li, B., Davidson, J. M. and Guelcher, S. A. (2009). "The effect of the local delivery of platelet-derived growth factor from reactive two-component polyurethane scaffolds on the healing in rat skin excisional wounds." Biomaterials **30**(20): 3486-3494.

Li, D. and Xia, Y. (2004). "Electrospinning of Nanofibers: Reinventing the Wheel?" Advanced Materials **16**(14): 1151-1170.

Li, J., Li, Y., Li, L., Mak, A. F. T., Ko, F. and Qin, L. (2009). "Preparation and biodegradation of electrospun PLLA/keratin nonwoven fibrous membrane." Polymer Degradation and Stability **94**(10): 1800-1807.

Li, M., Mondrinos, M. J., Gandhi, M. R., Ko, F. K., Weiss, A. S. and Lelkes, P. I. (2005). "Electrospun protein fibers as matrices for tissue engineering." Biomaterials **26**(30): 5999-6008.

Li, P., Feng, X., Jia, X. and Fan, Y. (2010). "Influences of tensile load on in vitro degradation of an electrospun poly(l-lactide-co-glycolide) scaffold." Acta Biomaterialia **6**(8): 2991-2996.

Li, W.-J., Cooper Jr, J. A., Mauck, R. L. and Tuan, R. S. (2006). "Fabrication and characterization of six electrospun poly(α -hydroxy ester)-based fibrous scaffolds for tissue engineering applications." Acta Biomaterialia **2**(4): 377-385.

Li, W.-J., Laurencin, C. T., Caterson, E. J., Tuan, R. S. and Ko, F. K. (2002). "Electrospun nanofibrous structure: A novel scaffold for tissue engineering." Journal of Biomedical Materials Research **60**(4): 613-621.

Li, W. J., Mauck, R. L., Cooper Jr, J. A., Yuan, X. and Tuan, R. S. (2007). "Engineering controllable anisotropy in electrospun biodegradable nanofibrous scaffolds for musculoskeletal tissue engineering." Journal of Biomechanics **40**: 1686-1693.

Li, W. J., Tuli, R., Okafor, C., Derfoul, A., Danielson, K. G., Hall, D. J. and Tuan, R. S. (2005). "A three-dimensional nanofibrous scaffold for cartilage tissue engineering using human mesenchymal stem cells." Biomaterials **26**: 599-609.

Li, X., Kanjwal, M. A., Lin, L. and Chronakis, I. S. (2013). "Electrospun polyvinyl-alcohol nanofibers as oral fast-dissolving delivery system of caffeine and riboflavin." Colloids and Surfaces B: Biointerfaces **103**: 182-188.

Li, Y., Kilani, R. T., Rahmani-Neishaboor, E., Jalili, R. B. and Ghahary, A. (2013). "Kynurenine Increases Matrix Metalloproteinase-1 and -3 Expression in Cultured Dermal Fibroblasts and Improves Scarring In Vivo." J Invest Dermatol.

Lim, S. H., Liu, X. Y., Song, H., Yarema, K. J. and Mao, H.-Q. (2010). "The effect of nanofiber-guided cell alignment on the preferential differentiation of neural stem cells." Biomaterials **31**(34): 9031-9039.

Liu, J., Xiao, Y. and Allen, C. (2004). "Polymer–drug compatibility: A guide to the development of delivery systems for the anticancer agent, ellipticine." Journal of Pharmaceutical Sciences **93**(1): 132-143.

Liu, W., Wang, D. R. and Cao, Y. L. (2004). "TGF-Beta: A Fibrotic Factor in Wound Scarring and a Potential Target for Anti- Scarring Gene Therapy." Current Gene Therapy **4**(1): 123-136.

Liu, X. and Ma, P. X. (2010). "The nanofibrous architecture of poly(l-lactic acid)-based functional copolymers." Biomaterials **31**(2): 259-269.

Liu, Y., Cai, S., Shu, X. Z., Shelby, J. and Prestwich, G. D. (2007). "Release of basic fibroblast growth factor from a crosslinked glycosaminoglycan hydrogel promotes wound healing." Wound Repair and Regeneration **15**(2): 245-251.

Liu, Y. and He, J.-H. (2007). "Bubble electrospinning for mass production of nanofibers." International Journal of Nonlinear Sciences and Numerical Simulation **8**(3): 393-396.

Luo, Y., Kirker, K. R. and Prestwich, G. D. (2000). "Cross-linked hyaluronic acid hydrogel films: new biomaterials for drug delivery." Journal of Controlled Release **69**(1): 169-184.

Lynch, S. E., Colvin, R. B. and Antoniades, H. N. (1989). "Growth factors in wound healing. Single and synergistic effects on partial thickness porcine skin wounds." Journal of Clinical Investigation **84**(2): 640.

MacNeil, S. (2007). "Progress and opportunities for tissue-engineered skin." Nature **445**: 874-880.

Madison, K. C. (2003). "Barrier function of the skin: "la raison d'etre" of the epidermis." Journal of investigative dermatology **121**(2): 231-241.

Mäkelä, P., Pohjonen, T., Törmälä, P., Waris, T. and Ashammakhi, N. (2002). "Strength retention properties of self-reinforced poly L-lactide (SR-PLLA) sutures compared with polyglyconate (MaxonR) and polydioxanone (PDS) sutures. An in vitro study." Biomaterials **23**(12): 2587-2592.

Mandal, B. B. and Kundu, S. C. (2010). "Biospinning by silkworms: Silk fiber matrices for tissue engineering applications." Acta Biomaterialia **6**(2): 360-371.

Martin, P. (1997). "Wound Healing - Aiming for Perfect Skin Regeneration." Science **276**: 75-81.

Meinel, A. J., Germershaus, O., Luhmann, T., Merkle, H. P. and Meinel, L. (2012). "Electrospun matrices for localized drug delivery: current technologies and selected biomedical applications." European Journal of Pharmaceutics and Biopharmaceutics **81**(1): 1-13.

Metcalf, A. D. and Ferguson, M. W. J. (2007). "Tissue engineering of replacement skin: the crossroads of biomaterials, wound healing, embryonic development, stem cells and regeneration." Journal of The Royal Society Interface **4**: 413-437.

Mukhatyar, V. J., Salmerón-Sánchez, M., Rudra, S., Mukhopadaya, S., Barker, T. H., García, A. J. and Bellamkonda, R. V. (2011). "Role of fibronectin in topographical guidance of neurite extension on electrospun fibers." Biomaterials **32**(16): 3958-3968.

Murray, M. M., Rice, K., Wright, R. J. and Spector, M. (2003). "The effect of selected growth factors on human anterior cruciate ligament cell interactions with a three-dimensional collagen-GAG scaffold." Journal of Orthopaedic Research **21**(2): 238-244.

Mutsaers, S. E., Bishop, J. E., McGrouther, G. and Laurent, G. J. (1997). "Mechanisms of Tissue Repair: from Wound Healing to Fibrosis." International Journal of Biochemical cell Biology **29**(1): 5-17.

Newton, D., Mahajan, R., Ayres, C., Bowman, J. R., Bowlin, G. L. and Simpson, D. G. (2009). "Regulation of material properties in electrospun scaffolds: Role of cross-linking and fiber tertiary structure." Acta Biomaterialia **5**(1): 518-529.

Nie, H., He, A., Wu, W., Zheng, J., Xu, S., Li, J. and Han, C. C. (2009). "Effect of poly(ethylene oxide) with different molecular weights on the electrospinnability of sodium alginate." Polymer **50**(20): 4926-4934.

Nitanan, T., Akkaramongkolporn, P., Rojanarata, T., Ngawhirunpat, T. and Opanasopit, P. (2013). "Neomycin-loaded poly (styrene sulfonic acid-co-maleic acid)(PSSA-MA)/polyvinyl alcohol (PVA) ion exchange nanofibers for wound dressing materials." International Journal of Pharmaceutics **448**(1): 71-78.

Okuda, T., Tominaga, K. and Kidoaki, S. (2010). "Time-programmed dual release formulation by multilayered drug-loaded nanofiber meshes." Journal of Controlled Release **143**(2): 258-264.

Orlova, Y., Magome, N., Liu, L., Chen, Y. and Agladze, K. (2011). "Electrospun nanofibers as a tool for architecture control in engineered cardiac tissue." Biomaterials **32**(24): 5615-5624.

Pailler-Mattei, C., Bec, S. and Zahouani, H. (2008). "In vivo measurements of the elastic mechanical properties of human skin by indentation tests." Medical engineering & physics **30**(5): 599-606.

Park, J.-C., Ito, T., Kim, K.-O., Kim, K.-W., Kim, B.-S., Khil, M.-S., Kim, H.-Y. and Kim, I.-S. (2010). "Electrospun poly(vinyl alcohol) nanofibers: effects of degree of hydrolysis and enhanced water stability." Polym J **42**(3): 273-276.

Peresin, M. S., Habibi, Y., Zoppe, J. O., Pawlak, J. J. and Rojas, O. J. (2010). "Nanofiber Composites of Polyvinyl Alcohol and Cellulose Nanocrystals: Manufacture and Characterization." Biomacromolecules **11**(3): 674-681.

Pollock, G. D. (1871). "Cases of skin grafting and skin transplantation." Trans. Clin. Soc. Lond. **4**: 37.

Puolakkainen, P. A., Twardzik, D. R., Ranchalis, J. E., Pankey, S. C., Reed, M. J. and Gombotz, W. R. (1995). "The Enhancement in Wound Healing by Transforming Growth Factor- β 1 (TGF- β 1) Depends on the Topical Delivery System." Journal of Surgical Research **58**(3): 321-329.

Rahman-Neishaboor, E., Jackson, J., Burt, H. and Ghahary, A. (2009). "Composite Hydrogel Formulations of Stratifin to Control MMP-1 Expression in Dermal Fibroblasts." Pharmaceutical Research **26**(8): 2002-2014.

Rahmani-Neishaboor, E., Hartwell, R., Jalili, R., Jackson, J., Brown, E. and Ghahary, A. (2012). "Localized controlled release of stratifin reduces implantation-induced dermal fibrosis." Acta Biomaterialia **8**(10): 3660-3668.

Rahmani-Neishaboor, E., Jallili, R., Hartwell, R., Leung, V., Carr, N. and Ghahary, A. (2013). "Topical application of a film-forming emulgel dressing that controls the release of stratifin and acetylsalicylic acid and improves/prevents hypertrophic scarring." Wound Repair and Regeneration **21**(1): 55-65.

Rahmani-Neishaboor, E., Yau, F. M.-k., Jalili, R., Kilani, R. T. and Ghahary, A. (2010). "Improvement of hypertrophic scarring by using topical anti-fibrogenic/anti-inflammatory factors in a rabbit ear model." Wound Repair and Regeneration **18**(4): 401-408.

Ramakrishna, S., Fujihara, K., Teo, W.-E., Lim, T.-C. and Ma, Z. (2005). An Introduction to Electrospinning and Nanofibers, World Scientific Publishing.

Ranganath, S. H. and Wang, C.-H. (2008). "Biodegradable microfiber implants delivering paclitaxel for post-surgical chemotherapy against malignant glioma." Biomaterials **29**(20): 2996-3003.

Ravi Kumar, M., Bakowsky, U. and Lehr, C. (2004). "Preparation and characterization of cationic PLGA nanospheres as DNA carriers." Biomaterials **25**(10): 1771-1777.

Reddy, C. S., Arinstein, A., Avrahami, R. and Zussman, E. (2009). "Fabrication of thermoset polymer nanofibers by co-electrospinning of uniform core-shell structures." Journal of Materials Chemistry **19**(39): 7198-7201.

Reverdin, J. L. (1869). "Grefte epidermique." Bull Soc Imperiale Chir Paris: 493.

Rheinwald, J. and Green, H. (1975). "Serial cultivation of strains of human epidermal keratinocytes: Formation of keratinizing colonies from single cells." Cell **6**: 331-344.

Rho, K. S., Jeong, L., Lee, G., Seo, B.-M., Park, Y. J., Hong, S.-D., Roh, S., Cho, J. J., Park, W. H. and Min, B.-M. (2006). "Electrospinning of collagen nanofibers: effects on the behavior of normal human keratinocytes and early-stage wound healing." Biomaterials **27**(8): 1452-1461.

Rho, K. S., Jeong, L., Lee, G., Seo, B. M., Hong, S. D., Roh, S., Cho, J. J., Park, W. H. and Min, B. M. (2006). "Electrospinning of collagen nanofibers: Effects on the behavior of normal human keratinocytes and early-stage wound healing." Biomaterials **27**: 1452-1461.

Ribeiro, C. C., Barrias, C. C. and Barbosa, M. A. (2004). "Calcium phosphate-alginate microspheres as enzyme delivery matrices." Biomaterials **25**(18): 4363-4373.

Ruzica Jovanovic-Malinovska, S. A. A., Slobodanka Kuzmanova, and Eleonora Winkelhausen, M. C., Christo Tsvetanov (2006). "The use of Poly(ethylene oxide) hydrogels as immobilization matrices for yeast cells." Bulletin of the Chemists and Technologists of Macedonia **25**(2): 113-119.

Said, S. S., Aloufy, A. K., El-Halfawy, O. M., Boraie, N. A. and El-Khordagui, L. K. (2011). "Antimicrobial PLGA ultrafine fibers: Interaction with wound bacteria." European Journal of Pharmaceutics and Biopharmaceutics **79**(1): 108-118.

Schneider, A., Wang, X. Y., Kaplan, D. L., Garlick, J. A. and Egles, C. (2009). "Biofunctionalized electrospun silk mats as a topical bioactive dressing for accelerated wound healing." Acta Biomaterialia **5**(7): 2570-2578.

Schulz, J. T., Tompkins, R. G. and Burke, J. F. (2000). "Artificial Skin." Ann. Rev. Med. **51**: 231-244.

Sen, C. K., Gordillo, G. M., Roy, S., Kirsner, R., Lambert, L., Hunt, T. K., Gottrup, F., Gurtner, G. C. and Longaker, M. T. (2009). "Human Skin Wounds: A Major and Snowballing Threat to Public Health and the Economy." Wound repair and regeneration : official publication of the Wound Healing Society [and] the European Tissue Repair Society **17**(6): 763-771.

Sershen, S. and West, J. (2002). "Implantable, polymeric systems for modulated drug delivery." Advanced Drug Delivery Reviews **54**(9): 1225-1235.

Shevchenko, R. V., James, S. L. and James, S. E. (2010). "A review of tissue-engineered skin bioconstructs available for skin reconstruction." Journal of The Royal Society Interface **7**: 229-258.

Shevchenko, R. V., James, S. L. and James, S. E. (2010). "A review of tissue-engineered skin bioconstructs available for skin reconstruction." Journal of the Royal Society Interface **7**(43): 229-258.

Shin, H. J., Lee, C. H., Cho, I. H., Kim, Y.-J., Lee, Y.-J., Kim, I. A., Park, K.-D., Yui, N. and Shin, J.-W. (2006). "Electrospun PLGA nanofiber scaffolds for articular cartilage reconstruction: mechanical stability, degradation and cellular responses under mechanical stimulation in vitro." Journal of Biomaterials Science, Polymer Edition **17**: 103-119.

Siepmann, J. and Peppas, N. A. (2011). "Higuchi equation: Derivation, applications, use and misuse." International Journal of Pharmaceutics **418**: 6-12.

Siepmann, J. and Siepmann, F. (2008). "Mathematical modeling of drug delivery." International Journal of Pharmaceutics **364**(2): 328-343.

Son, Y. J., Kim, W. J. and Yoo, H. S. (2014). "Therapeutic applications of electrospun nanofibers for drug delivery systems." Archives of pharmacal research **37**(1): 69-78.

Song, X., Gao, Z., Ling, F. and Chen, X. (2012). "Controlled release of drug via tuning electrospun polymer carrier." Journal of Polymer Science Part B: Polymer Physics **50**(3): 221-227.

Srikar, R., Yarin, A. L., Mogaaridis, C. M., Bazilevsky, A. V. and Kelley, E. (2008). "Desorption-Limited Mechanism of Release from Polymer Nanofibers." Langmuir **24**: 965-974.

Stamboulis, A., Hench, L. L. and Boccaccini, A. R. (2002). "Mechanical properties of biodegradable polymer sutures coated with bioactive glass." Journal of Materials Science: Materials in Medicine **13**(9): 843-848.

Sukigara, S., Gandhi, M., Ayutsede, J., Micklus, M. and Ko, F. (2003). "Regeneration of Bombyx mori silk by electrospinning--part 1: processing parameters and geometric properties." Polymer **44**(19): 5721-5727.

Sukigara, S., Gandhi, M., Ayutsede, J., Micklus, M. and Ko, F. (2004). "Regeneration of Bombyx mori silk by electrospinning. Part 2. Process optimization and empirical modeling using response surface methodology." Polymer **45**(11): 3701-3708.

Supp, D. M. and Boyce, S. T. (2005). "Engineered skin substitutes: practices and potentials." Clinics in dermatology **23**(4): 403-412.

Taepaiboon, P., Rungsardthong, U. and Supaphol, P. (2006). "Drug-loaded electrospun mats of poly (vinyl alcohol) fibres and their release characteristics of four model drugs." Nanotechnology **17**(9): 2317.

Tompkins, R. G. and Burke, J. F. (1990). "Progress in Burn Treatment and the Use of Artificial Skin." World J. Surg. **14**: 819-824.

Tredget, E. E., Nedelec, B., Scott, P. G. and Ghahary, A. (1997). "Hypertrophic Scars, Keloids, and Contractures: The Cellular and Molecular Basis for Therapy." Surgical Clinics of North America **77**(3): 701-730.

Tuan, T.-L. and Nichter, L. S. (1998). "The molecular basis of keloid and hypertrophic scar formation." Molecular Medicine Today **4**(1): 19-24.

Uddin, N. M., Ko, F., Xiong, J., Farouk, B. and Capaldi, F. (2009). "Process, Structure, and Properties of Electrospun Carbon Nanotube-Reinforced Nanocomposite Yarns." Advances in Materials Science and Engineering.

Ulubayram, K., Cakar, A. N., Korkusuz, P., Ertan, C. and Hasirci, N. (2001). "EGF containing gelatin-based wound dressings." Biomaterials **22**(11): 1345-1356.

Unemori, E. N. and Amento, E. P. (1990). "Relaxin modulates synthesis and secretion of procollagenase and collagen by human dermal fibroblasts." Journal of Biological Chemistry **265**(18): 10681-10685.

Van Krevelen, D. W. and Te Nijenhuis, K. (2009). Properties of polymers: their correlation with chemical structure; their numerical estimation and prediction from additive group contributions, Elsevier.

Vanstraelen, P. (1992). "Comparison of calcium sodium alginate (KALTOSTAT) and porcine xenograft (E-Z DERM) in the healing of split-thickness skin graft donor sites." Burns **18**(2): 145-148.

Wan, L. S. and Lim, L. (1992). "Drug release from heat-treated polyvinyl alcohol films." Drug development and industrial pharmacy **18**(17): 1895-1906.

Wang, W., Cao, J., Lan, P. and Wu, W. (2012). "Drug release from electrospun fibers of poly(3-hydroxybutyrate-co-3-hydroxyvalerate) grafted with poly(N-vinylpyrrolidone)." Journal of Applied Polymer Science **124**(3): 1919-1928.

Weldon, C. B., Tsui, J. H., Shankarappa, S. A., Nguyen, V. T., Ma, M., Anderson, D. G. and Kohane, D. S. (2012). "Electrospun drug-eluting sutures for local anesthesia." Journal of Controlled Release **161**(3): 903-909.

Xie, J. and Wang, C.-H. (2006). "Electrospun Micro- and Nanofibers for Sustained Delivery of Paclitaxel to Treat C6 Glioma in Vitro." Pharmaceutical Research **23**(8): 1817-1826.

Xie, J., Willerth, S. E., Li, X., Macewan, M. R., Rader, A., Sakiyama-Elbert, S. E. and Xia, Y. (2009). "The differentiation of embryonic stem cells seeded on electrospun nanofibers into neural lineages." Biomaterials **30**: 354-362.

Yamashita, Y., Ko, F., Tanaka, A. and Miyake, H. (2007). "Characteristics of elastomeric nanofiber membranes produced by electrospinning." Journal of Textile Engineering **53**(4): 137-142.

Yang, D.-J., Chen, F., Xiong, Z.-C., Xiong, C.-D. and Wang, Y.-Z. (2009). "Tissue anti-adhesion potential of biodegradable PELA electrospun membranes." Acta Biomaterialia **5**(7): 2467-2474.

Yang, F., Murugan, R., Wang, S. and Ramakrishna, S. (2005). "Electrospinning of nano/micro scale poly (L-lactic acid) aligned fibers and their potential in neural tissue engineering." Biomaterials **26**: 2603-2610.

Yang, Y., Xia, T., Zhi, W., Wei, L., Weng, J., Zhang, C. and Li, X. (2011). "Promotion of skin regeneration in diabetic rats by electrospun core-sheath fibers loaded with basic fibroblast growth factor." Biomaterials **32**(18): 4243-4254.

Yannas, I. V. and Burke, J. F. (1980). "Design of an artificial skin. I. Basic design principles." Journal of Biomedical Materials Research **14**(1): 65-81.

Yarin, A. and Zussman, E. (2004). "Upward needleless electrospinning of multiple nanofibers." Polymer **45**(9): 2977-2980.

Yohe, S. T., Colson, Y. L. and Grinstaff, M. W. (2012). "Superhydrophobic materials for tunable drug release: using displacement of air to control delivery rates." Journal of the American Chemical Society **134**(4): 2016-2019.

Yoo, H. S., Kim, T. G. and Park, T. G. (2009). "Surface-functionalized electrospun nanofibers for tissue engineering and drug delivery." Advanced Drug Delivery Reviews **61**(12): 1033-1042.

Yoon, K., Hsiao, B. S. and Chu, B. (2009). "High flux ultrafiltration nanofibrous membranes based on polyacrylonitrile electrospun scaffolds and crosslinked polyvinyl alcohol coating." Journal of Membrane Science **338**(1): 145-152.

Yu, D.-G., Branford-White, C., Shen, X.-X., Zhang, X.-F. and Zhu, L.-M. (2010). "Solid dispersions of ketoprofen in drug-loaded electrospun nanofibers." Journal of Dispersion Science and Technology **31**(7): 902-908.

Yu, D.-G., Shen, X.-X., Branford-White, C., White, K., Zhu, L.-M. and Bligh, S. A. (2009). "Oral fast-dissolving drug delivery membranes prepared from electrospun polyvinylpyrrolidone ultrafine fibers." Nanotechnology **20**(5): 055104.

Zeng, J., Aigner, A., Czubyko, F., Kissel, T., Wendorff, J. J. and Greiner, A. (2005). "Poly(vinyl alcohol) Nanofibers by Electrospinning as a Protein Delivery System and the Retardation of Enzyme Release by Additional Polymer Coatings." Biomacromolecules **6**: 1484-1488.

Zeng, J., Yang, L., Liang, Q., Zhang, X., Guan, H., Xu, X., Chen, X. and Jing, X. (2005). "Influence of the drug compatibility with polymer solution on the release kinetics of electrospun fiber formulation." Journal of Controlled Release **105**(1–2): 43-51.

Zong, X., Kim, K., Fang, D., Ran, S., Hsiao, B. S. and Chu, B. (2002). "Structure and process relationship of electrospun bioabsorbable nanofiber membranes." Polymer **43**(16): 4403-4412.

Zong, X., Li, S., Chen, E., Garlick, B., Kim, K.-s., Fang, D., Chiu, J., Zimmerman, T., Brathwaite, C., Hsiao, B. S. and Chu, B. (2004). "Prevention of Postsurgery-Induced Abdominal Adhesions by Electrospun Bioabsorbable Nanofibrous Poly(lactide-co-glycolide)-Based Membranes." Annals of Surgery **240**(5): 910-915.

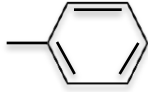
Appendix 1 Matrix Material Selection via Theoretical Approach

Background

Material screening for drug carrier was performed through interaction and solubility parameters as the first step. While the calculation results and candidate material choice were disseminated in Section 2.3.1, this appendix provides a stepwise explanation of the calculation and reaching the conclusion in candidate materials.

Method

The first step for determining kynurenine compatibility with polymer carriers is to calculate the dispersion, polar, and hydrogen bond forces for kynurenine molecules, which could then be used to calculate the Hilderbrand-Scatchard solubility parameter. Using the group contribution method suggested by van Krevelen, as shown in the table below, F_{di} , F_{pi}^2 , and E_{hi} were calculated to be $3160 \frac{\sqrt{MJ/m^3}}{mol}$, $781400 \frac{MJ/m^3}{mol^2}$, and 28800 J/mol, respectively.

Groups	$F_{di} (MJ/m^3)^{0.5}/mol$	$F_{pi}^2 MJ/m^3mol^2$	$E_{hi} (J/mol)$
	1430	12100	0
-COOH	530	176400	10000
-NH ₂ (x2)	560	0	16800
-CH ₂	270	0	0
-CH	80	0	0

-CO	290	592900	2000
Total	3160	781400	28800

The molar volume of kynurenine was determined to be 155.38 cm³/mol, using its density of 1.34 g/cm³ and molar weight of 208.21 g/mol. With these parameters, equations 11-13, shown in Section 2.2.1, yielded dispersion (δ_d), polar (δ_p), and hydrogen (δ_h) bonding forces of 20.34 $\sqrt{MJ/m^3}$, 5.69 $\sqrt{MJ/m^3}$, and 13.61 $\sqrt{MJ/m^3}$, respectively. Calculation for the Hilderbrand-Scatchard parameter using equation 11 thus yielded ($\delta_{kynurenine}$) of 25.13 $\sqrt{MJ/m^3}$.

For a pairing between kynurenine and polymer to be compatible, its Flory-Huggins interaction parameter should be less than 0.5. With a kynurenine molar volume of 155.38 cm³/mol and a wound dressing application at standard body temperature of 37°C, equation 10 would suggest that the compatible polymer carrier would have a Hilderbrand-Scatchard solubility parameter close to 25.13 $\sqrt{MJ/m^3}$ or between 22.05 $\sqrt{MJ/m^3}$ and 28.01 $\sqrt{MJ/m^3}$. Polymers with solubility parameter outside of this range may phase separate upon mixing with kynurenine, leading to kynurenine crystallizing on fibre surface and subsequent burst release. A comprehensive list of experimentally-obtained polymer solubility parameter was presented by van Krevelen (Van Krevelen and Te Nijenhuis 2009). In addition, Liu et al also calculated solubility parameters of several polymers for ellipticine delivery (Liu, Xiao et al. 2004). The values obtained by van Krevelen et al and Liu et al are summarized in the table below.

Polymer	δ (J ^{0.5} /cm ^{1.5})	
	From	To
Polyethylene	15.8	17.1
Polypropylene	16.8	18.8
Polyisobutylene	16.0	16.6

Polystyrene	17.4	19.0
Poly(vinyl chloride)	19.2	22.1
Poly(vinyl bromide)	19.4	--
Poly(vinylidene chloride)	20.3	25.0
Poly(tetrafluoroethylene)	12.7	--
Poly(vinyl alcohol)	25.8	29.1
Poly(vinyl acetate)	19.1	22.6
Poly(vinyl propionate)	18.0	--
Poly(methyl acrylate)	19.9	21.3
Poly(ethyl acrylate)	18.8	19.2
Poly(propyl acrylate)	18.5	--
Poly(butyl acrylate)	18.0	18.6
Poly(isobutyl acrylate)	17.8	22.5
Poly(methyl methacrylate)	18.6	26.2
poly(ethyl methacrylate)	18.2	18.7
Poly(butyl methacrylate)	17.8	18.4
Poly(isobutyl methacrylate)	16.8	21.5
Poly(benzyl methacrylate)	20.1	20.5
Polyacrylonitrile	25.6	31.5
Polymethylacrylonitrile	21.9	--
Polybutadiene	16.6	17.6
Polyisoprene	16.2	20.5
Polychloroprene	16.8	18.9
Polyformaldehyde	20.9	22.5
Poly(tetramethylene oxide)	17.0	17.5
Poly(propylene oxide)	15.4	20.3
Poly(ethylene sulphide)	18.4	19.2
Poly(ethylene terephthalate)	19.9	21.9
Poly(8-aminocaprylic acid)	26.0	--
Poly(hexamethylene adipamide)	27.8	--
Poly(lactic-co-glycolic acid)	23.1	--

From the table above, several polymers could be identified as suitable for mixing with kynurenine, including poly(vinylidene chloride), poly(vinyl alcohol), polyacrylonitrile, poly(8-aminocaprylic acid), poly(hexamethylene adipamide), and poly(lactic-co-glycolic acid). However, as the goal in material screening is to select candidate materials to be electrospun into kynurenine-loaded nanofibres, only polymers that can be electrospun and proven in previous

studies will be considered, as a detailed electrospinning feasibility study on a polymer not previously electrospun is outside the scope of this study. Moreover, as kynurenine is only soluble in aqueous solutions containing sodium hydroxide, the candidate polymer matrix must also be soluble in a solvent compatible with water, such as dimethyl sulfoxide and trifluoroethanol. Lastly, the polymer must also be approved by the US Food and Drug Administration (FDA) for use in the human body. Considering the constraints, the most suitable polymer carriers are poly(vinyl alcohol) (PVA) ($\delta_{PVA} = 25.8 - 29.1\sqrt{MJ/m^3}$) and poly(lactic-co-glycolic acid) (PLGA) ($\delta_{PLGA} = 23.1\sqrt{MJ/m^3}$).

With screening results showing PVA and PLGA as compatible with kynurenine, drug-loaded samples were subsequently created using these polymers as carriers. As a negative control, poly(vinyl acetate) (PVAc) ($\delta_{PVAc} = 20\sqrt{MJ/m^3}$) was also chosen to verify the reliability of solubility calculations.

Appendix 2 Determining Closeness of Fit to Empirical Drug Release Models

Background

The first step to estimating the dominant kynurenine release mechanism from nanofibres fabricated is to compare the release data obtained from spectrophotometric measurements to empirical models derived and extensively used in previous work to describe kinetics from different release mechanisms. In this research, four possible release mechanisms were examined including the desorption controlled release described in the work by Srikar et al., diffusion controlled model based on the work by an extensive group of authors such as Higuchi and Crank, the mixed diffusion-swelling model described by Korsmeyer and Peppas, and the matrix degradation-controlled release described by Hopfenberg. Comparison between the closeness of the measured kynurenine release data and the empirical models described would provide a basis for determining the dominant release mechanisms that can be verified through drug-matrix characterizations. In addition, by determining the model that best fits the release data, the coefficients and/or exponents of the model equation could be used to compare between different samples to quantitatively observe the effect of various treatments.

Method

The equations for the four empirical models described above were first rearranged to obtain a linear equation $Y = mX$, in which the term Y would include the fractional release term Mt/M^∞ , and the X would be time t . The original model equation and the rearranged form were presented in Table 2 in the thesis main body, and reproduced below.

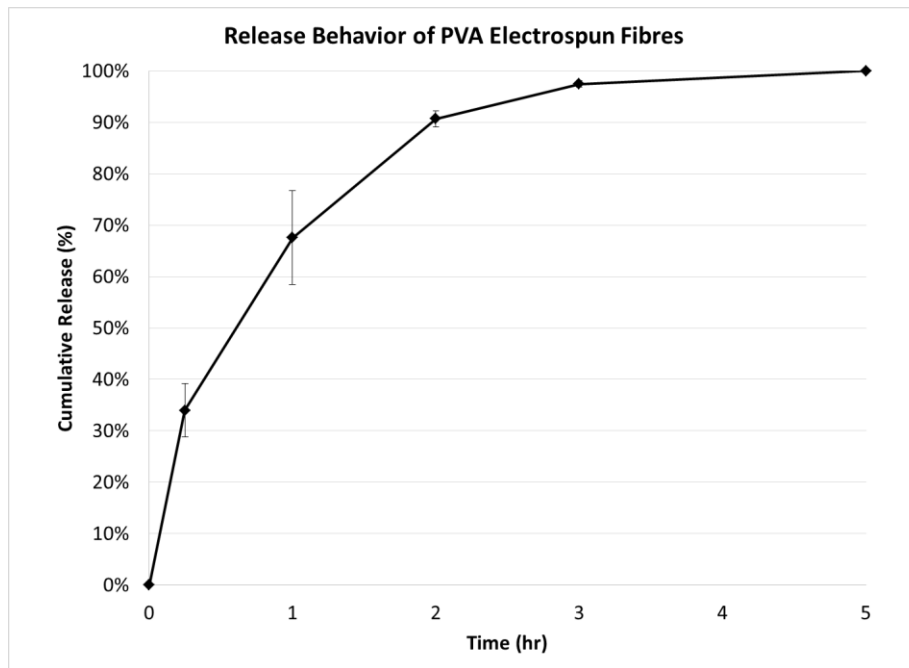
Model	Model Equation	Simplified Straight-line Equation
Surface Desorption	$\frac{M_t}{M_{d0}} = \alpha \left[1 - \exp\left(\frac{-\pi^2 t}{8\tau_r}\right) \right]$	$\ln\left(1 - \frac{1}{\alpha} \frac{M_t}{M_{d0}}\right) = \frac{-\pi^2}{8\tau_r} t$
Diffusion	$\frac{M_t}{M_{\infty}} = K_H \sqrt{t}$	$\frac{M_t}{M_{\infty}} = K_H t^{0.5}$
Mixed Diffusion and Swelling	$\frac{M_t}{M_{\infty}} = K_M t^n$	$\log\left(\frac{1}{K_M} \frac{M_t}{M_{\infty}}\right) = n \log(t)$
Matrix Erosion	$\frac{M_t}{M_{\infty}} = 1 - \left(1 - \frac{k_0 t}{c_0 a}\right)^n$	$\frac{M_t}{M_{\infty}} = \frac{k_0}{c_0 a} t$

To simplify the comparison process, the porosity factor α in the surface desorption equation and the coefficient K_M in the mixed diffusion and swelling equation were assumed to be unity. For the matrix erosion model, the exponent n represents a geometric factor, and for slab-like geometries the factor could be assumed to be unity as well.

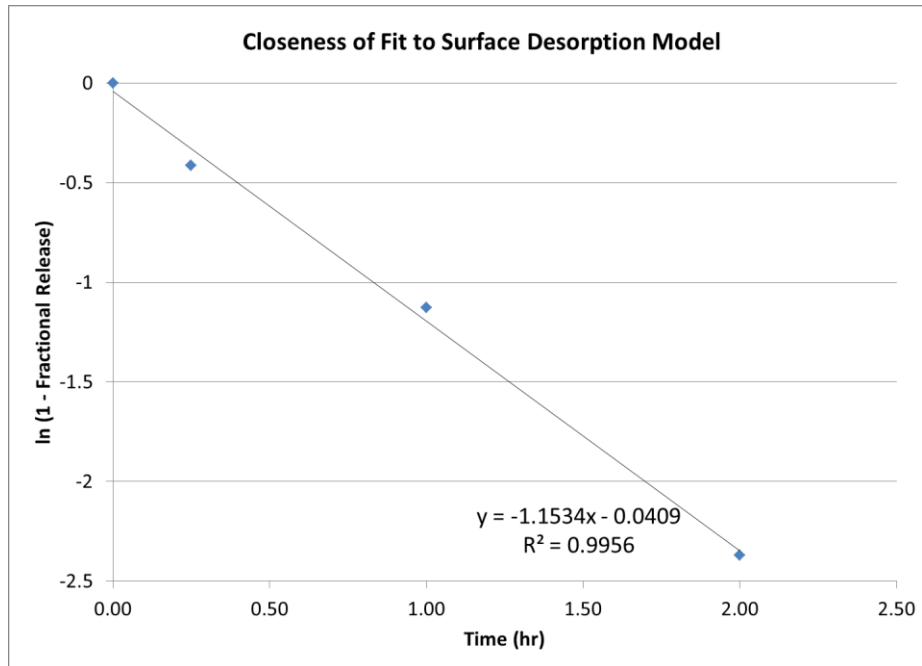
The measured release data for each fibre sample were reported in the form of M_t/M_{∞} vs. t , in which M_t/M_{∞} is the fractional release. These data can be processed into the form $\ln(1 - M_t/M_{\infty})$ vs. t , M_t/M_{∞} vs. $t^{0.5}$, $\log(M_t/M_{\infty})$ vs. $\log(t)$, which could then be plotted. A straight line fit for each of these plots would indicate close fit to the corresponding model. The slopes of the straight line would then represent the model coefficients, such as the $-\pi^2/8\tau_r$ for the surface desorption model and the K_H for the diffusion model.

Sample Calculation

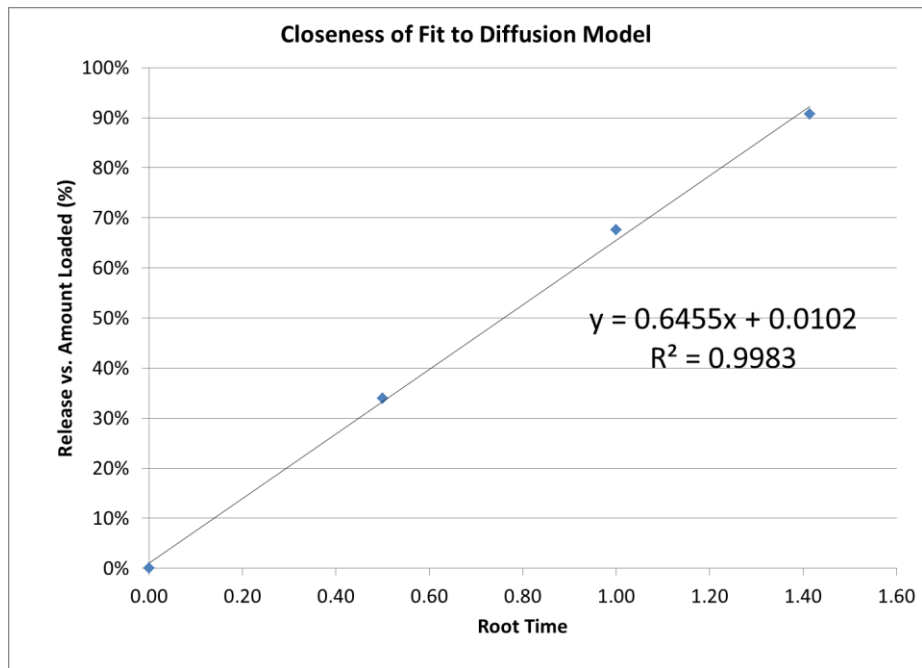
Determination of closeness of fit to the empirical models is demonstrated below using the release data from the 10 wt% PVA 18-88 electrospun fibres containing 2 wt% of kynurenine as an example. The release profile of the sample is shown below.



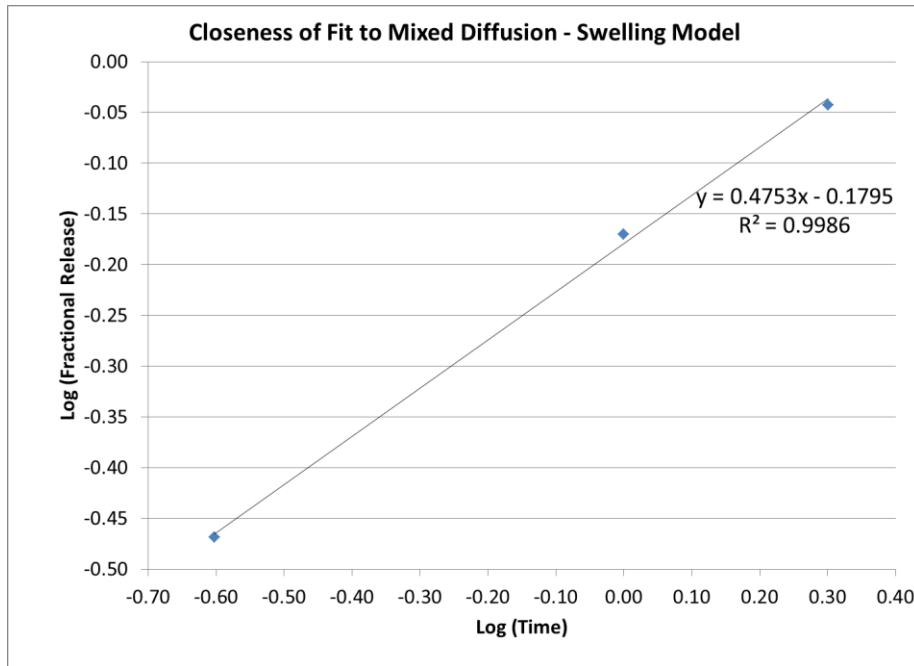
The data was then plotted to determine the fit to the surface desorption model.



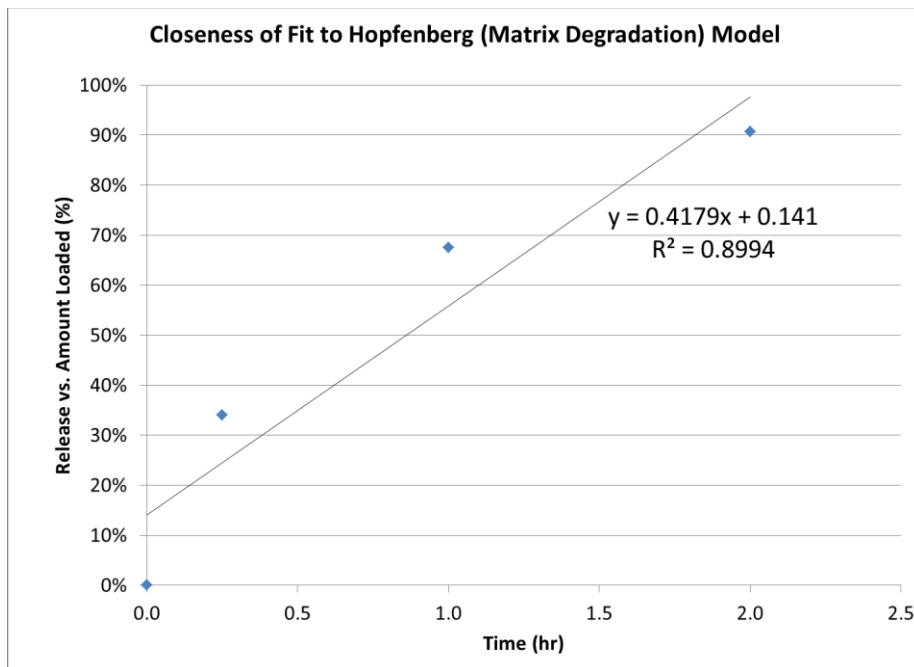
The closeness of fit to the diffusion model is shown below.



From the closes of fit equation, the coefficient K_H could be taken as the slope of the straight line, which is 0.6455. The closeness of fit to the mixed diffusion-swelling model is shown below.



The diffusion exponent in the equation, n , was then taken as the slope of the straight line, which is 0.4753, and would indicate a mainly diffusion-controlled release and less swelling-controlled due to the closeness to 0.5. The comparison to the Hopfenberg model is below.



From the plots, it could be seen that the R^2 value was significantly lower than the other models. In fact, the high R^2 values obtained for the surface desorption, diffusion, and mixed-diffusion models would suggest that all three mechanisms are potentially the dominant one. However, since the closeness of the diffusion exponent n to 0.5 would suggest diffusion-controlled release, the possible dominant release mechanism would be either diffusion or surface desorption. To further investigate, experimental characterization of drug-polymer interaction is required.